Sektion 5.2: Klimadynamik und Landschaftsentwicklung,
Helmholtz-Zentrum Potsdam – Deutsches GeoForschungsZentrum GFZ

Investigations on rainfall variability during the late Quaternary based on geochemical analyses of lake sediments from tropical and subtropical southern Africa

Dissertation
zur Erlangung des akademischen Grades
Doktor der Naturwissenschaften (Dr. rer. nat.)
in der Wissenschaftsdisziplin Geologie

eingereicht an der Mathematisch-Naturwissenschaftlichen Fakultät
der Universität Potsdam

vorgelegt von
Iris Kristen
Februar 2009

Published online at the
Institutional Repository of the University of Potsdam:
URL http://opus.kobv.de/ubp/volltexte/2009/3254/
URN urn:nbn:de:kobv:517-opus-32547
[http://nbn-resolving.org/urn:nbn:de:kobv:517-opus-32547]

Principal supervisor:

Prof. Dr. Gerald H. Haug, Universität Potsdam/ETH Zürich

Co-supervisors:

PD Dr. Hedi Oberhänsli, Sektion 5.2: Klimadynamik und Landschaftsentwicklung, Helmholtz-Zentrum Potsdam – Deutsches GeoForschungsZentrum GFZ

PD Dr. Heinz Wilkes, Sektion 4.3: Organische Geochemie, Helmholtz-Zentrum Potsdam – Deutsches GeoForschungsZentrum GFZ

Prof. Dr. Dirk Verschuren, Research group Limnology, Department of Biology, Ghent University

Table of contents

9. APPENDICES

ABSTRACT

Africa is the biggest landmass in lower latitudes and extends from the tropics over the subtropical desert belts of both hemispheres to the temperate zone of the southern hemisphere. Influence of the westerlies, easterlies and the monsoon are of utmost importance. Accordingly, landscapes, vegetation and living conditions are diverse in Africa. However, all regions share the great vulnerability to gradual as well as abrupt climate change accompanied by a strong demand for research on natural climate variability. This thesis presents investigations on sediments from two African lakes which have been recording changes in their surrounding environmental and climate conditions since more than 200,000 years. Focus of this work is the time of the last Glacial and the Holocene (the last ~100,000 years before present [in the following 100 kyr BP]). One important precondition for this kind of research is a good understanding of the present ecosystems in and around the lakes and of the sediment formation under modern climate conditions. Both studies therefore include investigations on the modern environment (including organisms, soils, rocks, lake water and sediments).

A 90 m long sediment sequence was investigated from Lake Tswaing (north-eastern South Africa) using analyses of the sediment composition, X-ray fluorescence (XRF) scanning and analyses of the organic fraction of the sediments with organic petrology and Rock-Eval pyrolysis. These investigations document alternating periods of high detrital input and low (especially autochthonous) organic matter content and periods of low detrital input, calcareous or evaporitic sedimentation and high autochthonous organic matter content. These alternations are interpreted as changes between relatively humid and arid conditions, respectively. Before c. 75 kyr BP, they seem to follow changes in local insolation whereas afterwards they appear to be acyclic and are probably caused by changes in ocean circulation and/or in the mean position of the Inter-Tropical Convergence Zone (ITCZ). Today, these factors have main influence on precipitation in this area where rainfall occurs almost exclusively during austral summer when the ITCZ reaches its southernmost position and easterly winds carry humidity from the Indian Ocean onto the African continent. Accordingly, the area is covered by Savanna-like vegetation dominated by C4 grasses, and bushes and trees which use the C3 photosynthetic pathway. The lake itself, which is highly alkaline and saline, is dominated by Cyanobacteria and surrounded by *Typha* and *Cyperacea*. All organisms were analysed for their biomarker and bulk organic and compound-specific stable carbon isotope composition. The same investigations on sediments from the modern lake floor document the mixed input of the investigated individual organisms and reveal additional influences by methanotrophic bacteria. A comparison of modern sediment characteristics with those of sediments covering the time 14 to 2 kyr BP shows changes in the productivity of the lake and the surrounding vegetation which are best explained by changes in hydrology. More humid conditions are indicated for times older than 10 kyr BP and younger than 7.5 kyr BP, whereas arid conditions prevailed in between. These observations agree with the results from sediment composition and indications from other climate archives nearby.

Before 7.5 kyr BP, alkenones are detected in the sediments, marking the first report of these compounds from an African lake.

The second lake study deals with Lake Challa, a small, deep crater lake on the foot of Mount Kilimanjaro. In this lake form mm-scale laminated sediments which are most probably varves. With the new technique of micro-XRF scanning, which allows element analyses with 100 µm resolution, it is possible to trace changes in the element composition of individual laminae. By comparing these results with investigations on thin sections, results from ongoing sediment trap studies, meteorological data, and investigations on the surrounding rocks and soils, I develop a model for seasonal variability in the limnology and sedimentation of Lake Challa. The lake appears to be stratified during the warm rain seasons (October – December and March – May) during which detrital material is delivered to the lake and carbonates precipitate. On the lake floor forms a dark lamina with high contents of Fe and Ti and high Ca/Al and low Mn/Fe ratios. Diatoms bloom during the cool and windy season (June – September) when mixing down to c. 60 m depth provides easily bio-available nutrients. Contemporaneously, Fe and Mn-oxides are precipitating which cause high Mn/Fe ratios in the light diatom-rich laminae of the sediments. Trends in the Mn/Fe ratio of the sediments are interpreted to reflect changes in the intensity or duration of seasonal mixing in Lake Challa. This interpretation is supported by parallel changes in the organic matter and biogenic silica content observed in the 22 m long profile recovered from Lake Challa. This covers the time of the last 25 kyr BP. It documents a transition around 16 kyr BP from relatively well-mixed conditions with high detrital input during glacial times to stronger stratified conditions which are probably related to increasing lake levels in Challa and generally more humid conditions in East Africa. Intensified mixing is recorded for the time of the Younger Dryas and the period between 11.4 and 10.7 kyr BP. For these periods, reduced intensity of the SW monsoon and intensified NE monsoon are reported from archives of the Indian-Asian Monsoon region, arguing for the latter as a probable source for wind mixing in Lake Challa. This connection is probably also responsible for contemporaneous events in the Mn/Fe ratios of the Lake Challa sediments and in other records of northern hemisphere monsoon intensity during the Holocene and underlines the close interaction of global low latitude atmospheric circulation.

ZUSAMMENFASSUNG

Afrika ist die größte zusammenhängende Landmasse in niederen Breiten und reicht von den feuchten Tropen über die subtropischen Wüstengürtel beider Hemisphären bis in die von Westwinden geprägte, gemäßigte Klimazone der Südhemisphäre. Entsprechend divers sind Landschaften, Vegetation und Lebensbedingungen in Afrika. Gemeinsam ist jedoch allen Regionen des Kontinents die große Empfindlichkeit für Klimaschwankungen und abrupte Umweltereignisse bei einem gleichzeitig großen Nachholbedarf an wissenschaftlicher Forschung zu natürlicher Klimavariabilität. In dieser Arbeit werden Ergebnisse von Untersuchungen an den Sedimenten zweier afrikanischer Seen vorgestellt, die ein Archiv für Klimaveränderungen über einen Zeitraum von mehr als 200.000 Jahren darstellen. Der Schwerpunkt liegt in dieser Arbeit auf dem letzten Glazial und dem Holozän (ca. 100.000 Jahre vor heute [nachfolgend als 100 kyr BP bezeichnet] bis heute). Grundlegende Voraussetzung für solche Studien ist ein gutes Verständnis der Ökosysteme in und um den See, sowie des gegenwärtigen Sedimentationsgeschehens. Deswegen beinhalten beide Seestudien Untersuchungen der heutigen Organismen, Böden, Gesteine, Wasserchemie und Sedimentablagerungen.

Im Tswaing-See im nordöstlichen Südafrika wurden anhand eines 90 m langen Sedimentprofils Studien zur Sedimentzusammensetzung, Röntgenfluoreszenzanalysen (XRF-Scanning) und Untersuchungen der Zusammensetzung und Qualität des organischen Materials mittels organischer Petrologie und Rock-Eval Pyrolyse durchgeführt. Sie zeigen einen Wechsel zwischen Phasen hohen detritischen Eintrags, während derer v.a. kaum autochthones organisches Material im See erhalten blieb, mit Phasen geringen Eintrags und dafür karbonatischer oder evaporitischer Sedimentation, die hohe Gehalte v.a. autochthonen organischen Materials aufweisen. Diese Phasen werden als relativ feuchte bzw. trockene Perioden interpretiert und folgen bis vor ca. 75 kyr BP Schwankungen der lokalen solaren Einstrahlung. Dieser Einfluss nimmt nach 75 kyr BP ab und azyklische feuchte Phasen werden beobachtet. Mögliche Ursachen sind Veränderungen in der ozeanischen Zirkulation und Verschiebungen in der Lage der Innertropischen Konvergenzzone (ITCZ); beides sind auch heute Haupteinflussfaktoren auf die Niederschläge in der Region. Diese fallen fast ausschließlich im Sommer und bedingen eine Savannenvegetation mit C4-Gräsern sowie Bäumen und Büschen, die C3-Pflanzen sind. Im hoch-alkalischen und -salinen See dominieren Cyanobakterien; entlang der Grundwasserquellen wachsen *Typha* und *Cyperacea* sp. Diese Organismen wurden mittels Analysen der Biomarkerzusammensetzung und der Kohlenstoffisotopie charakterisiert und ihr Einfluss auf die heutigen Seeablagerungen untersucht. Dabei konnten zusätzlich Indikatoren für die Aktivität methanotropher Bakterien nachgewiesen werden. Der Vergleich heutiger Sedimente mit denen des Zeitraumes 14 bis 2 kyr BP zeigt deutliche Veränderungen sowohl in der Zusammensetzung, als auch in der Kohlenstoffisotopie der Biomarker, die mit Veränderungen in der Hydrologie erklärt werden können. Die gefundenen Hinweise auf feuchtere Bedingungen im Zeitraum älter als 10 kyr BP,

für trockenere Verhältnissen zwischen 10 und 7.5 kyr BP und für die nachfolgende Wiederzunahme an Feuchtigkeit werden durch die sedimentologischen Ergebnisse unterstützt. Ein weiteres interessantes Ergebnis dieser Analysen ist der erste Nachweis von Alkenonen in Sedimenten eines afrikanischen Sees.

Objekt der zweiten Seestudie ist der Challa-See am Fuß des Kilimanjaro. Hier werden heute im mm-Maßstab laminierte Sedimente gebildet, bei denen es sich sehr wahrscheinlich um Varven handelt. Mikro-XRF-scanning mit einer Auflösung von 100 µm erlaubt deren Analyse auf Veränderungen in der Elementzusammensetzung. Zusammen mit Untersuchungen der Mikrofazies der Laminae und im Vergleich mit ersten Ergebnissen noch laufender Sedimentfallenstudien, mit meteorologischen Daten und Analysen des Umgebungsgesteins werden die saisonalen Veränderungen in der Temperaturverteilung, der Durchmischungstiefe, dem detritischen Eintrag und der Bioproduktivität des Sees in den Sedimenten nachvollziehbar. Der See ist in den feucht-warmen Perioden von Oktober bis Dezember und von März bis Mai stratifiziert. Während dieser Zeit erfolgt der Eintrag detritischen Materials und Kalziumkarbonat fällt aus; eine dunkle Lage mit hohen Gehalten an Fe und Ti und mit hohen Ca/Al- und niedrigen Mn/Fe-Verhältnissen bildet sich am Boden des Sees. Diatomeen blühen während der kühlen, windigen Periode von Juni bis September, wenn die Durchmischung bis auf etwa 60 m Tiefe Nährstoffe verfügbar macht. Die Ausfällung von Fe- und Mn-oxiden sorgt für hohe Mn/Fe-Verhältnisse; es bildet sich eine helle Lage auf dem Sediment. Trends im Mn/Fe-Verhältnis werden als Signal für Veränderungen in der Intensität oder Dauer der saisonalen Durchmischung interpretiert. Dies wird unterstützt von parallelen Trends in Mn/Fe, dem Anteil an organischem Material und an biogenem Silizium, wie durch Analysen an einem 22 m langen Bohrkern gezeigt werden kann. Nach gut durchmischten und von erhöhtem Eintrag von außen geprägten Verhältnissen während des letzten Glazials erfolgt gegen 16 kyr BP ein Übergang zu stärker stratifizierten Bedingungen. Diese korrespondieren mit einem steigenden Seespiegel und verbreiteten Hinweisen auf feuchte Bedingungen im tropischen Ostafrika. Stärkere Durchmischung herrschte während der Jüngeren Dryas und von 11.4 bis 10.7 kyr BP. Diese Perioden entsprechen Zeiten verringerter Südwest- und vermutlich verstärkter Nordostmonsunintensität im Bereich des Indisch-Asiatischen Monsuns und spiegeln eine global beobachtete südliche Verschiebung der ITCZ wider. Nach einer kurzen stabilen, feuchten Phase im frühen Holozän nimmt die Durchmischung des Sees im Verlauf des Holozän wieder zu. Abrupte Ereignisse während des Holozän scheinen im Challa-See zeitgleich mit Veränderungen der Monsunintensität der Nordhemisphäre aufzutreten und bezeugen die starke klimatische Kopplung der niederen Breiten in globalem Maßstab.

Acknowledgements

First of all, I would like to thank Hedi Oberhänsli and Heinz Wilkes, without whose initiative the project at the South African Lake Tswaing which brought me to Potsdam would not exist, and whose constant support and advice have accompanied me over the years of my PhD. Along with it, I want to acknowledge the Helmholtz-Zentrum Potsdam – Deutsches GeoForschungsZentrum Potsdam GFZ's initial funding of the Tswaing project including the coring campaign, as well as their financial support over the years.

My special thanks go to Professor Gerald H. Haug, former head of Section 3.3 at GFZ, who introduced me to the second project of my PhD on Lake Challa. He always believed in my scientific abilities, strengthened the importance of the global dimensions of my work from the beginning and contributed significantly to the "bigger picture" which underlies the main conclusions of this work.

Leading coordinator of the project on Lake Challa was Dirk Verschuren; I thank him very much for his guidance, his mentoring on tropical limnology and for many helpful comments on my work.

I am very grateful to Klaus Zink. Without his visits in the lab I might not have survived the ceaseless lab work required for organic chemistry. He was a living example of a geologist who succeeded in organic geochemistry and a constant source for fruitful discussions and support.

I thank Brian Horsfield, head of section 4.3, and Achim Brauer, head of section 5.2 (former 3.3) at GFZ; they never let me down when I came to ask for support. I further acknowledge Yannick Garcin from University Potsdam together with Kai Mangelsdorf and many members of the sections 5.2 (former 3.3) and 4.3 at GFZ who always let me participate in their enormous pool of scientific knowledge. I want to especially quote Birgit Plessen, Peter Dulski, Georg Schettler, Andrea Vieth and Rudolf Naumann who significantly contributed to the results presented in this thesis. Many more people helped me with the analytical work: Gabi Arnold, Dieter Berger and Michael Köhler prepared resin blocks and thin sections; Brigitte Richert ran μXRF measurements; Ursula Röhl, Rik Tjallingii and Vera Lukies from University Bremen taught me how to run the XRF scanner; Petra Meier introduced me to elemental analyses; Cornelia Karger and Kristin Günther ran GC and GCMS analyses and together with Anke Sobotta were a constant help in the labs of section 4.3; Doreen Noak and Michael Gabriel ran IRM-GC-MS analyses; Juliane Herwig and Helga Kemnitz introduced me to the SEM facility; Andreas Hendrich and Manuela Dziggel aided with graphical problems and unwilling printers; and Christine Gerschke, secretary of section 5.2 (former 3.3), often helped to master the manifold pitfalls of German bureaucracy.

I thank all people who helped with field work in Kenya and South Africa. I especially acknowledge Tim Partridge and Arnot Venter, who welcomed me in South Africa with a hospitality never experienced before and implanted a true love for this country in my heart.

I am very grateful to Helge Arz; his mere presence in the room made him often the first aim of my attacking questions, and over the years we shared not only the office but many hours of philosophising.

Benjamin, your knowledge and feeling for the English language helped me at least as much as your sense of humour.

A special thank goes to Olga Kwiecien, Susanne Stefer, Christian Wolff, Hans von Suchodoletz, Sebastian Breitenbach and Clara Mangili; we did not only share wonderful and extremely necessary lunch and coffee breaks but also began a wonderful friendship within the walls of the GFZ.

Finally, I want to express my gratitude to all my friends and my family, especially to Kathrin, my parents and my sister Claudia, their imperturbable faith and love were always energy source and a soft pillow for me.

1. Introduction

Over the last few years, global climate change has increasingly become a matter of public awareness and concern. The release of the latest report of the Intergovernmental Panel of Climate Change (ICPP) in 2007 strongly promoted this development. It unmistakably points to the contribution of human activities, especially in form of the release of greenhouse gases, to the recent climate change (http://www.ipcc.ch/). Moreover, latest results from studies on the composition of air trapped in Antarctic ice as deep as 3,200 m below the modern surface reveal that present-day concentrations of methane and carbon dioxide are unprecedented during the last 800,000 years (Brook 2008; Loulergue et al. 2008; Lüthi et al. 2008). Nevertheless, human-induced climate changes are superimposed on natural climate variability which is active on time scales of millions of years to decades. Pioneering studies, especially from marine sediment and polar ice-core records, have documented the global extent of Cenozoic (e.g. Haug and Tiedemann 1998; Zachos et al. 2001), glacial/interglacial (Bond et al. 1993; Grootes et al. 1993; Petit et al. 1999) and millennial-scale (Broecker 2000; Jouzel et al. 2007) climate change. However, the relative importance of different forcing factors and feedback processes as well as their implications for climate history on the continents are still under debate. Besides changes in global insolation and oceanic circulation, variations in the extent of tropical wetlands are a frequently suggested force driving climate change (Loulergue et al. 2008). Therefore, changes in tropical rainfall patterns through time are a valuable object of climate studies. By choosing two lacustrine sediment sequences from tropical and subtropical eastern Africa for climate studies, this thesis aims to contribute to these open questions in providing additional archives of continental climate change from a region where the presumed driving forces interact.

1.1 Modern climate conditions

The investigated lakes, Lake Challa and Lake Tswaing, are situated in relative proximity to the eastern coast of the African landmass, leaving them both under the influence of the dominant easterly wind systems of eastern equatorial Africa (EEA): the north-easterly trade (or NE monsoonal) winds during southern hemisphere summer and the south-easterly trade (or SE monsoonal) winds during southern hemisphere winter months (Fig. 1). Both wind systems are associated with dry conditions in EEA as air masses are thermally stabilised due to (1) their passage over the dry eastern Sahara and Arabia and the adjacent cool waters of the Arabian Sea upwelling region (NE monsoon), or (2) because they lost humidity along the East African coast and Madagascar and, furthermore, experience subsidence due to frictional shear along the SE African coastline (SE monsoon); blockage of moist, unstable westerly flow from the Atlantic Ocean by the highlands of the East African plateau, and the presence of low-level jet streams supposedly contribute further to the observed dryness of the region (Nicholson 1996). Accordingly, despite its equatorial latitude and proximity to warm Indian Ocean waters, EEA is characterised by semi-arid climate conditions and savanna vegetation.

Rainfall in Africa is strongly connected to convection within the zone where the monsoonal wind systems converge, the Inter-Tropical Convergence Zone (ITCZ) (Nicholson 1996). This zone generally follows the zenith of the sun with a delay of about one month, reaching its northern limit around July and its southern limit around January (Fig. 1). Accordingly, inter-tropical sites like Lake Challa experience two rainy seasons (October – December and March – May), whereas sites at sub-tropical latitudes like Lake Tswaing show one seasonal rainfall maximum during the respective summer season (Hastenrath 1991). For southern Africa (South Africa, Namibia, Botswana, Zimbabwe and most of Zambia), the Congo Air Boundary (CAB), a low pressure system connected to the ITCZ, draws in moisture from the Indian Ocean and separates the tropical easterlies from West-African (Atlantic) monsoonal air masses. Only the southernmost Cape Province receives rainfall during winter due to equatorward expansion of the southern hemisphere westerlies (Barry and Chorley 1998; Preston-Whyte and Tyson 1988).

Trade winds and ITCZ form the lower convergent and the ascending branch of the tropical Hadley cells (Fig. 1) which are essential players in the global atmospheric energy and mass balance (Barry and Chorley 1998). Along the top of the cells, air masses diverge and subside again within semi-permanent anticyclones over the North Pacific and the North Atlantic in the northern hemisphere, and the South Atlantic and the Southern Indian Ocean in the southern hemisphere (Hastenrath 1991). During southern hemisphere winter, an intensification and westward shift of the Indian Ocean anticyclone is responsible for pronounced dry conditions over southern Africa, except the Cape Province (Barry and Chorley 1998; Preston-Whyte and Tyson 1988). Associated with the subsidence within the subtropical high-pressure cells, differences in heat capacity between land masses and oceans as well as within oceans and cooler upwelling regions induce an east-west component into the large-scale tropical airflow known as the Walker circulation; it connects the Hadley cells with the monsoonal systems (Barry and Chorley 1998). The strength of the Walker circulation is preferentially described by the Southern Oscillation Index (SOI) which expresses the pressure difference between Tahiti (18°S, 150°W) and Darwin, Australia (12°S, 130°E). Oscillations within the Walker circulation describe low and high phases, also known as El Niño or warm ENSO (El Niño-Southern Oscillation) phases and as La Niña or cold ENSO phases, respectively (Barry and Chorley 1998; Diaz and Markgraf 1992). They represent major reorganisations within the global atmospheric circulation which are found to also influence rainfall in Africa: whereas EEA experiences above-average rainfall especially between October and December during warm ENSO phases (Indeje et al. 2000; Nicholson 2000; Plisnier and Serneels 2000; Schreck and Semazzi 2004), southern Africa experiences drought especially in the mature to late warm phase (Reason et al. 2000; Rouault and Richard 2005). ENSO is further manifested in changes in sea surface temperature (SST) gradients in the Pacific and Indian Ocean (Barry and Chorley 1998; Diaz and Markgraf 1992). In the Indian Ocean, however, it seems to interact with the Indian Ocean Dipole (IOD). This phenomenon was discovered after intensive studies of the strong ENSO event 1997/98 and describes the SST difference between the equatorial eastern and western Indian Ocean (Saji et al. 1999; Webster et al. 1999). Whereas the positive effects of elevated

western Indian Ocean SST on East African rainfall are increasingly documented, their interaction with ENSO and changes in the Pacific SST remain under discussion (Black et al. 2003; Clark et al. 2003; Gadgil et al. 2004; Giannini et al. 2008; Hastenrath et al. 2004; Kabanda and Jury 1999; Lizcano and Todd 2005; Pascal et al. 2007; Reason 2001; Reason 2002; Reason and Rouault 2002; Washington and Preston 2006).

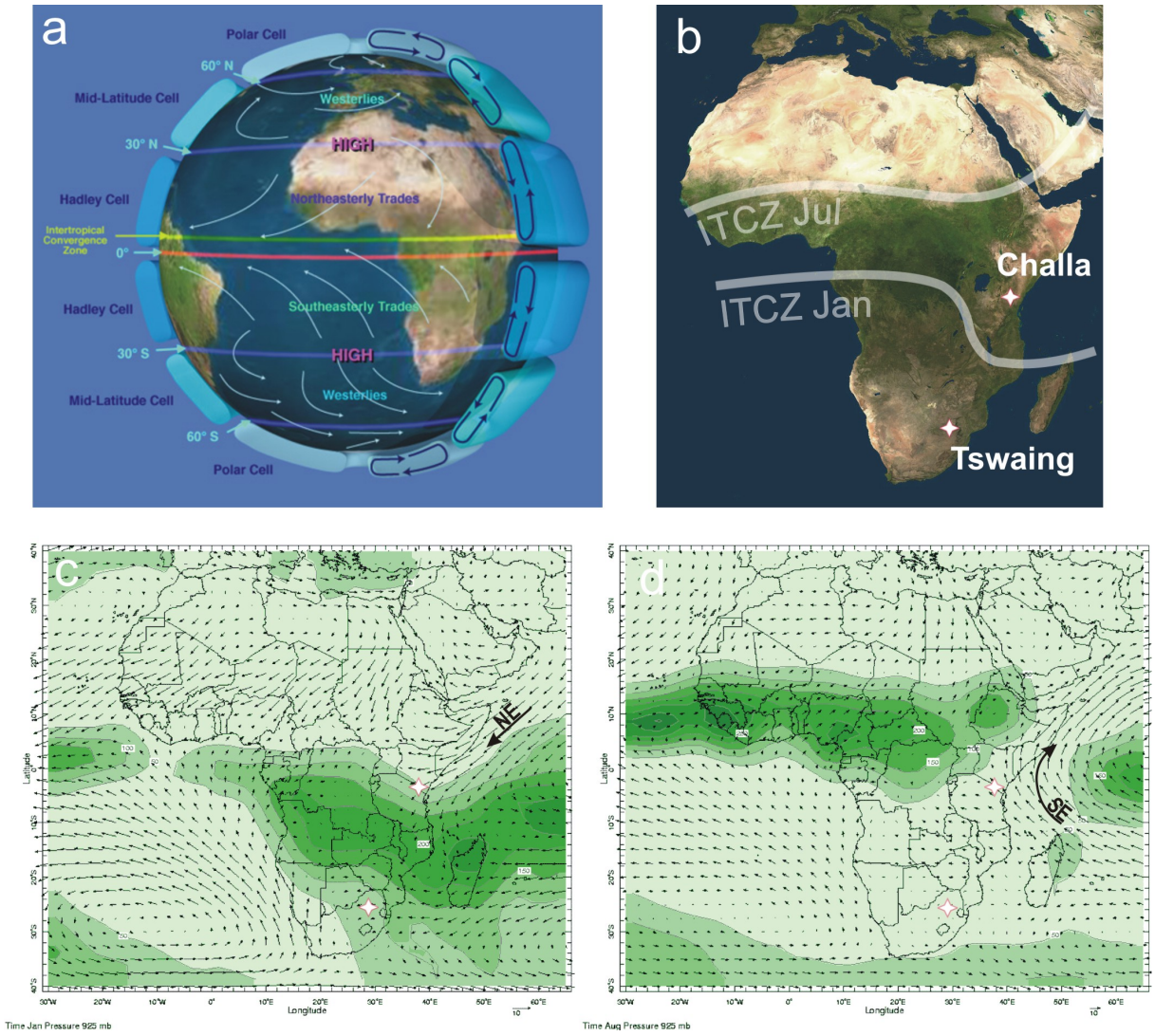

Figure 1: a) Schematic illustration of the main African atmospheric circulation features: Inter-tropical Convergence Zone (ITCZ), north- and south-easterly trade winds, high pressure cells over the northern and southern hemisphere subtropics, and tropical Hadley Cells (source: http://sealevel.jpl.nasa.gov); b) approximate northern and southern limit of seasonal ITCZ migration (modified from NASA); c) + d) seasonal migration of the ITCZ over Eastern Africa, monthly precipitation (shading, mm/month) based on satellite precipitation estimates over ocean areas and rain gauge data over land regions, contours are drawn at 50 mm intervals. Climatological wind vectors for the 925 hPa pressure level indicate wind direction with wind speed proportional to the length of the vectors (source: http://iridl.ldeo.columbia.edu).

1.2 Objectives of this thesis

The main objective of this thesis is to add to our understanding of the geographical patterns and causes of tropical rainfall variability at various time scales. Africa constitutes the largest landmass in the tropics, but to date only few climate studies enlighten our understanding of natural temperature and rainfall variability on long time scales, with sufficient age control and time resolution. Traditional climate archives of temperate regions which fulfil these demands, such as tree rings and ice cores, are rare in tropical Africa. However, in recent years an increasing number of lake studies have demonstrated that, when chosen carefully, lacustrine sediments can be a valuable and comprehensive recorder of climate variability in tropical East-Africa over various time scales (e.g. Gasse et al. 1989; Johnson et al. 2002; Russell et al. 2007; Street-Perrott et al. 2007; Talbot and Lærdal 2000; Verschuren et al. 2000; Wooller et al. 2003).

In this thesis I present new results from analyses of the sedimentary records of two lakes in tropical and subtropical southern Africa: Lake Challa (3°19'S, 37°42'E) which is located close to the equator and probably has been under continuous influence of tropical circulation systems; and Lake Tswaing (25°24'S, 28°04'E) which lies at the southern limit of the region influenced by tropical circulation and should be a sensitive recorder of its southern extent. Both lakes contain sediment records that reach back at least into the last (Lake Challa) and penultimate (Lake Tswaing) glacial period. Comparison of the climate records of these two localities, with a main focus on the last 25,000 years, shall provide new insights into tropical atmospheric dynamics during glacial, interglacial and especially transitional (Termination I) times.

Both lake studies include investigations on the modern lake environment. The idea to use modern conditions to calibrate changes in past ecosystems is long established in particular fields of palaeolimnology (e.g., diatom assemblage studies; Battarbee et al. 2001). It is increasingly regarded a prerequisite for palaeoclimate studies on continental archives, which are influenced not only by global and regional climate phenomena but also by local factors like topography, geology and surrounding vegetation, resulting in individual characteristics for each site. Assuming a certain temporal stability in these factors, investigations on modern ecosystem components like hydrological and element fluxes, biological dynamics, sedimentation processes and diagenetic effects can help interpret palaeorecords, and give a baseline against which to compare observed changes in the past.

In particular, this work addresses the following issues:

- A detailed survey of the modern ecosystem components of the Tswaing Crater and their characterisation with organic geochemical (biomarkers) and bulk organic and compound-specific stable carbon isotope investigations
- Characterisation of the nature of the preserved organic matter and evaluation of the changing biomarker and stable carbon isotope composition of the Lake Tswaing sedimentary record covering the last 200,000 years

- Tracing changes in the elemental composition of the Lake Tswaing sediment record of the last 80,000 years
- Understanding of the formation of laminated sediments in Lake Challa under modern climatic conditions, with a special focus on seasonal element cycling within the lake and its preservation in the sediments
- Tracing changes in the compositional and elemental inventory of the Lake Challa sediment record to evaluate changes in the environment and in tropical climate back to 25,000 years BP

1.3 Structure of the thesis

This thesis is subdivided into seven chapters. With the exception of chapter one, two and seven, all chapters represent manuscripts submitted or to be submitted to peer-reviewed ISI journals.

Chapter one (Introduction) introduces the general issue of climate change and the relevance of this thesis for African palaeoclimatology. It further gives an overview about modern African climate and its main actors.

Chapter two introduces the two locations studied, and gives an overview of general methodological aspects of this thesis.

Chapter three ("Hydrological changes in southern Africa over the last 200 kyr as recorded in lake sediments from the Tswaing impact crater") has been published in *South African Journal of Geology*. It documents the variability in sources and preservation of organic matter in sediments from Lake Tswaing. In combination with geochemical investigations and previous mineralogical studies from this location, a change in rainfall variability from being predominantly precessionally driven to more irregular spacing during the last glacial period is suggested.

Chapter four ("Biomarker and stable carbon isotope analyses of sedimentary organic matter from Lake Tswaing: Evidence for deglacial wetness and early Holocene drought from South Africa") is submitted to *Journal of Paleolimnology*. It demonstrates the applicability of biomarkers and their stable carbon-isotope composition as proxies for changes in the carbon cycle of Lake Tswaing, and the relation of these changes to hydrological variability in subtropical southern Africa.

Chapter five ("Investigations on seasonality in Lake Challa (Kenya/Tanzania) and its sedimentary documentation in recent lake sediments") is to be submitted to *Limnology and Oceanography*. It combines results of investigations on the modern limnology, water chemistry

and very-high-resolution geochemical studies on recent lake sediments from Lake Challa with meteorological data to calibrate the sedimentary record against modern climatic conditions.

Chapter six ("Lake Challa sediments – a geochemical study of a new climate archive at the foothill of Mount Kilimanjaro") is part of a manuscript which summarises major characteristics of the sediment profile recovered in Lake Challa. Several project members contribute to this manuscript which is unfinished, yet. It is planned to be submitted to *Palaeogeography, Palaeoclimatology, Palaeoecology*. The geochemical and palaeomagnetic records of the 21-m long sediment sequence from Lake Challa, which were produced within this thesis, are interpreted, compared with already available records from other project members, and their palaeoclimatic information is evaluated.

Chapter seven (synthesis, conclusion and outlook) represents an extraction of the information on climate variability in tropical and subtropical southern Africa from the two archives presented earlier, and points out open questions for future studies.

The Appendices add details from biomarker studies on sediments from Lake Tswaing. They contain unpublished results from an initial screening of the Lake Tswaing sedimentary organic matter, chromatograms of the investigated samples, and mass spectra and structures of selected compounds. The complete inventory is available on the enclosed CD.

2. Material and methodology

Main subjects of this thesis are lacustrine sediment sequences recovered at two sites: (i) Lake Tswaing and (ii) Lake Challa (for an overview see Fig. 1b).

2.1 Lake Tswaing (25°24'S, 28°04'E)

Lake Tswaing is located about 40 km northwest of Pretoria at an altitude of 1045 m asl (above sea level) on the interior plateau of South Africa. It developed within a meteorite impact crater that formed ~220,000 years BP (Storzer et al. 1993). It still exhibits a clear circular shape with a rim rising 119 m above the central crater floor and ~60 m above the surrounding grounds (Fig. 2.1). Since its formation it accumulated ~120 m of sediment infill; these document its evolution to its present form of a hypersaline and alkaline pan of less than 3 m depth (Partridge 1999b).

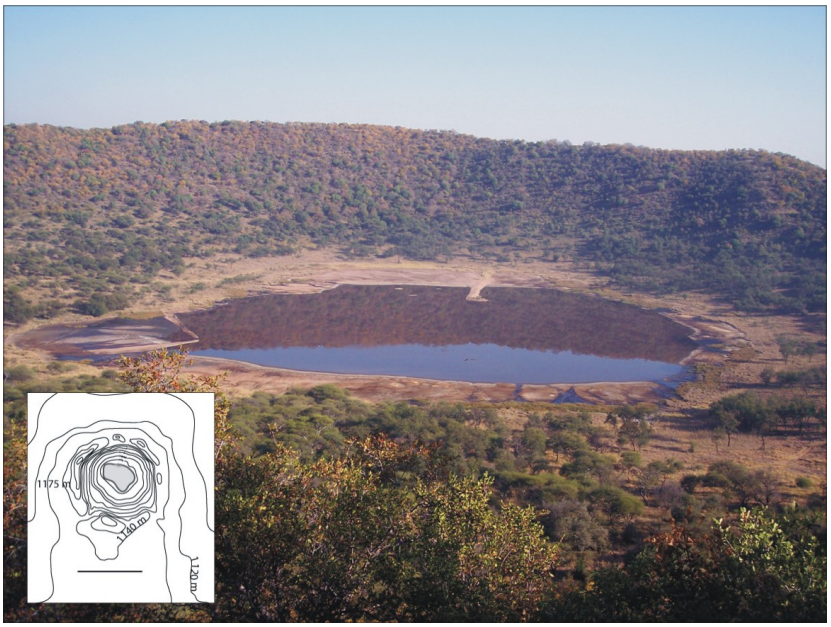

Figure 2.1: The Tswaing Crater during lowstand conditions in May 2005, exposing spring line (right) and left-over structures from its use as a soda mine (left), drilling took place at the end of the promontory (centre) (picture provided by H. Wilkes), inset shows the topography of the Tswaing Crater (bar = 1 km) (after Thorpe 2006).

2.2 Lake Challa (3°19'S, 37°42'E)

Lake Challa is a ~95 m deep freshwater lake located at ~880 m asl on the border between Kenya and Tanzania. It is situated on the lower east slope of Mt. Kilimanjaro, ~35 km from its lower Mawenzi peak (Fig. 2.2); Mombasa on the Indian Ocean coast is ~230 km further to the east. The lake of ~4.2 km² fills a caldera which is Pleistocene in age and located within

volcanic rocks of the Kilimanjaro complex. A detailed seismic survey of the crater infill revealed ~210 m of predominantly horizontally spreading sediments that cover app. the last 250,000 years (Moernaut et al. in prep.).

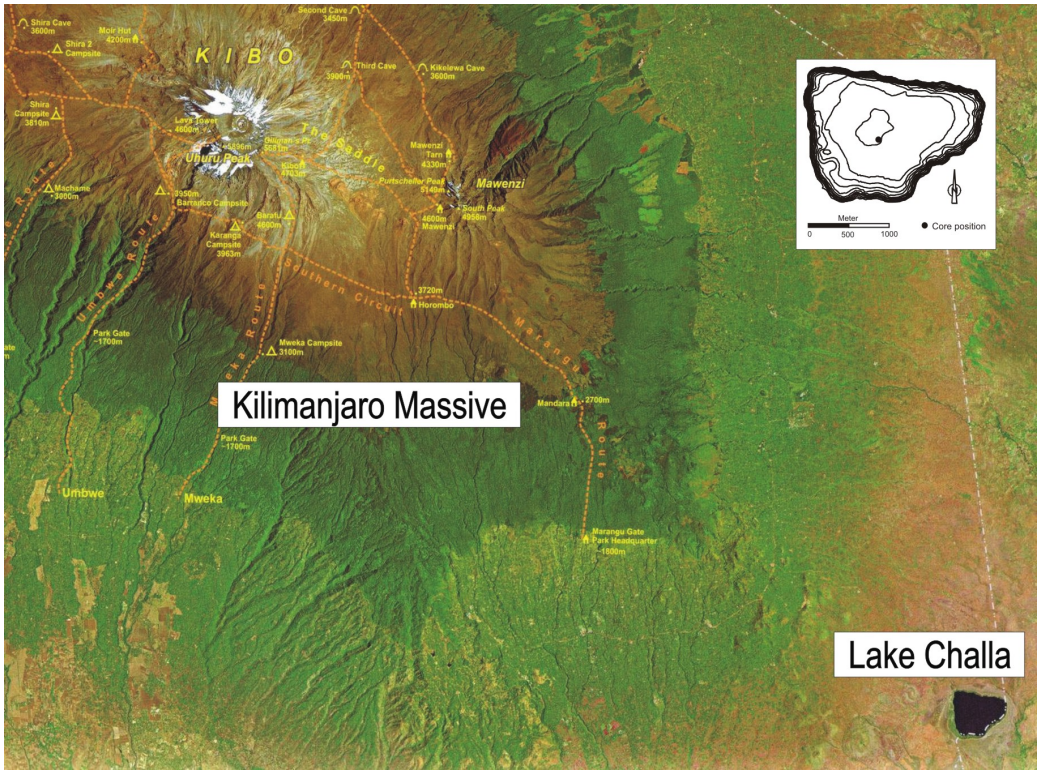

Figure 2.2: Lake Challa on the lower eastern slope of Mount Kilimanjaro (provided by D. Verschuren), colour shading indicates downslope transition from exposed rocks and heathland over the montane forest belt to the sub-montane cultivation and savanna area, inset shows bathymetric map with the central coring position (after Moernaut et al. in prep.).

2.3 Methodology

Both lacustrine sediment sequences are compiled of multiple, parallel cores to assure most complete sediment profiles (Leroy and Colman 2001).

In Lake Tswaing, three cores were obtained between November 2001 and February 2002 by Soiltech (Franki Africa Ltd). The drilling was carried out through the end of a solid promontory (Fig. 2.3), built for salt-production during earlier times. The first core (TSW-1) was obtained using Shelby tube drilling, which provided good quality cores with almost complete sediment recovery and little drilling disturbance down to ~34 m (Fig. 2.3, 2.4). Due to gravel layers, drilling became too difficult in deeper parts. Therefore, a second (TSW-1B) and third (TSW-2) core were recovered using wireline rotary core drilling with a triple-tube core barrel – a method which causes less-complete sediment recovery and more drilling disturbance but allowed to recover material down to ~90 m depth. Thus, the profile covers the complete lacustrine sediment sequence which was identified in an earlier coring project (Partridge 1999a;

Partridge et al. 1993). The construction of the composite profile relies on visual alignment of characteristic laminations between TSW-1 (used between surface and ~34 m uncorrected depth) and TSW-1B (used between ~31 and ~50 m uncorrected depth). The alignment of TSW-1B and TSW-2 was more problematic due to core gaps and less clear lamination. It rests on four visual tie-points between 54.84 and 55.37 m, and the matching of records of percentage water (obtained by weighing samples before and after drying at 105°C overnight) and %LOI 550°C. After aligning of the individual cores, 13 m of intercalated mass flow deposits were subtracted, resulting in a final composite core profile of 78 m length. For description of the sediments see Fig. 2.4 and chapter 3.

Figure 2.3: a) Soiltech drilling device; b) Shelby tube (right) used for recovering TSW 1; c) opened core section of TSW 1.

In Lake Challa, the composite sediment sequence is constructed from cross-correlation of the following cores: three Niederreiter hammer-driven piston cores (CH05-2P, 3P, 4P) of 20 to 22 m length and one gravity core (CH05-1G) of 1 m length covering the sediment-water interface, all recovered in February 2005 with GFZ drilling equipment (Fig. 2.5); and one mini-Kullenberg piston core (CH03-2K) of 2.6 m length, obtained in January 2003 with University of Minnesota drilling equipment. The coring location was set to the central, deepest part of the lake (Fig. 2.1) where a seismic survey revealed uniformly draped lake sediments covering the flat basin floor (Moernaut et al. in prep.). Visual alignment of the individual cores using characteristic laminae and synchronisation of the magnetic susceptibility records where the quality of the lamination did not allow the visual matching resulted in a composite profile of 21.6 m length. After exclusion of five turbiditic intervals, the final lacustrine sediment sequence accounted for 20.6 m of comparatively uniform soft, organic- and diatom-rich mud (for detailed description of the sediments see chapter 6); the main differences in core quality arise from the

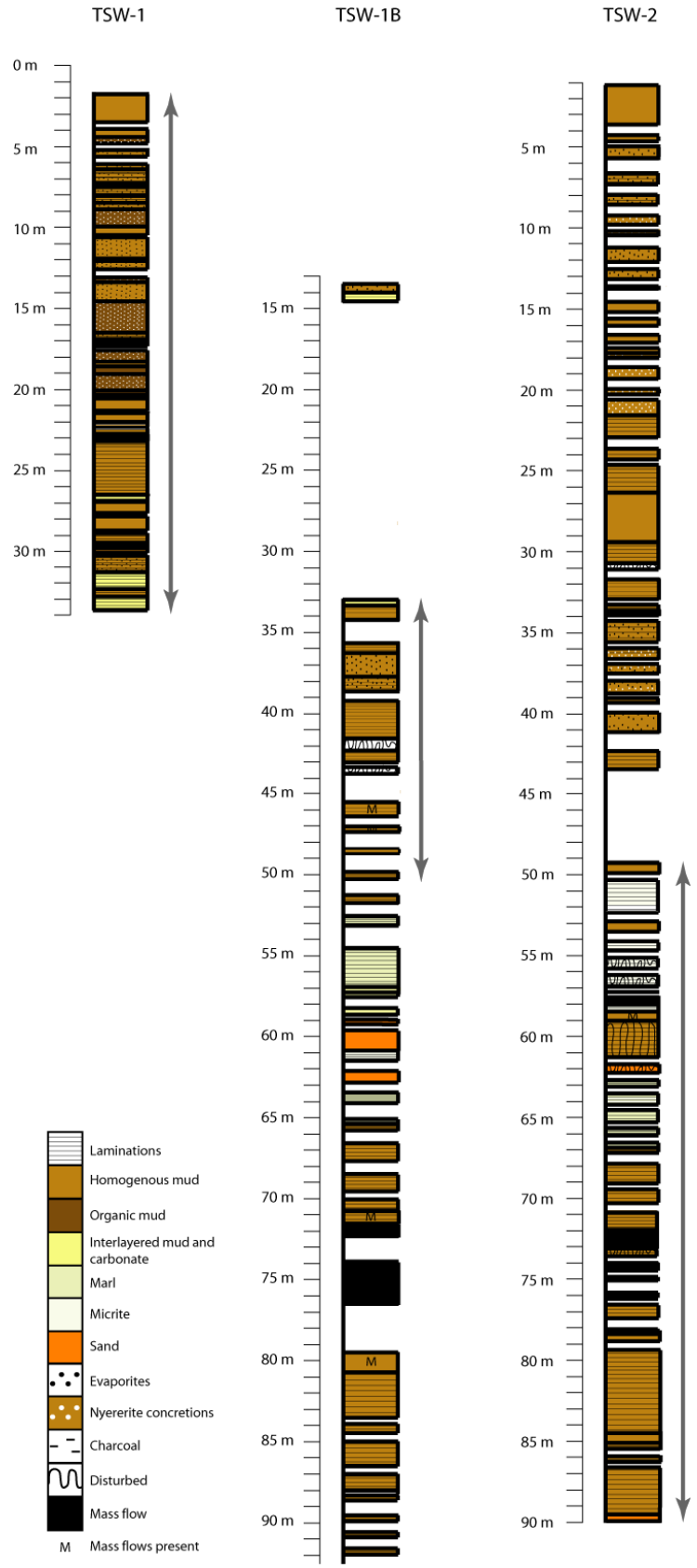

Figure 2.4: Stratigraphy of the sediment cores recovered from Lake Tswaing (after Thorpe 2006), based on sedimentological descriptions by Prof. T.C. Partridge). Thick grey arrows indicate approximate sections of cores used to compile the composite profile.

disturbing effects of the corer's hammering action on and the subsequent transport of sediments with high gas and water content (Fig. 2.6). Collection of three complete parallel sequences allowed construction of a continuous sediment sequence from mostly intact to modestly disturbed core sections. The sometimes strong bending of laminations caused by the coring was taken into account during all sub-sampling operations, by curvilinear cutting of samples along the lamination planes in three dimensions. By convention, composite core depths refer to the uppermost position of laminae and other sedimentary structures, typically in the central area of the cut core surface.

Figure 2.5: Coring platform on Lake Challa in February 2005 (picture provided by D. Verschuren).

The chronologies of both records rest on AMS ^{14}C radiocarbon dating for the time period where those are applicable (<50,000 years). For the Lake Tswaing record, this concerns the upper 20 m of sediments; the chronology of the deeper profile relies on a fission-track date of 220±52 kyr BP from impact glass and tuning of the record of total inorganic carbon content to orbital forcing (for details refer to chapter 3). With reference to Lake Challa, this applies to the complete investigated profile which was dated with very high time resolution (Fig. 2.7). The age model includes 188 AMS ^{14}C dates and ^{210}Pb dating of the most recent sediments. The latter has been transferred from short core CH99-1G (collected by Ghent University) using magnetic susceptibility records; the error this introduced is uncertain, but well within the counting uncertainty of individual ^{14}C dates. Samples from the new, composite core sequence were sent

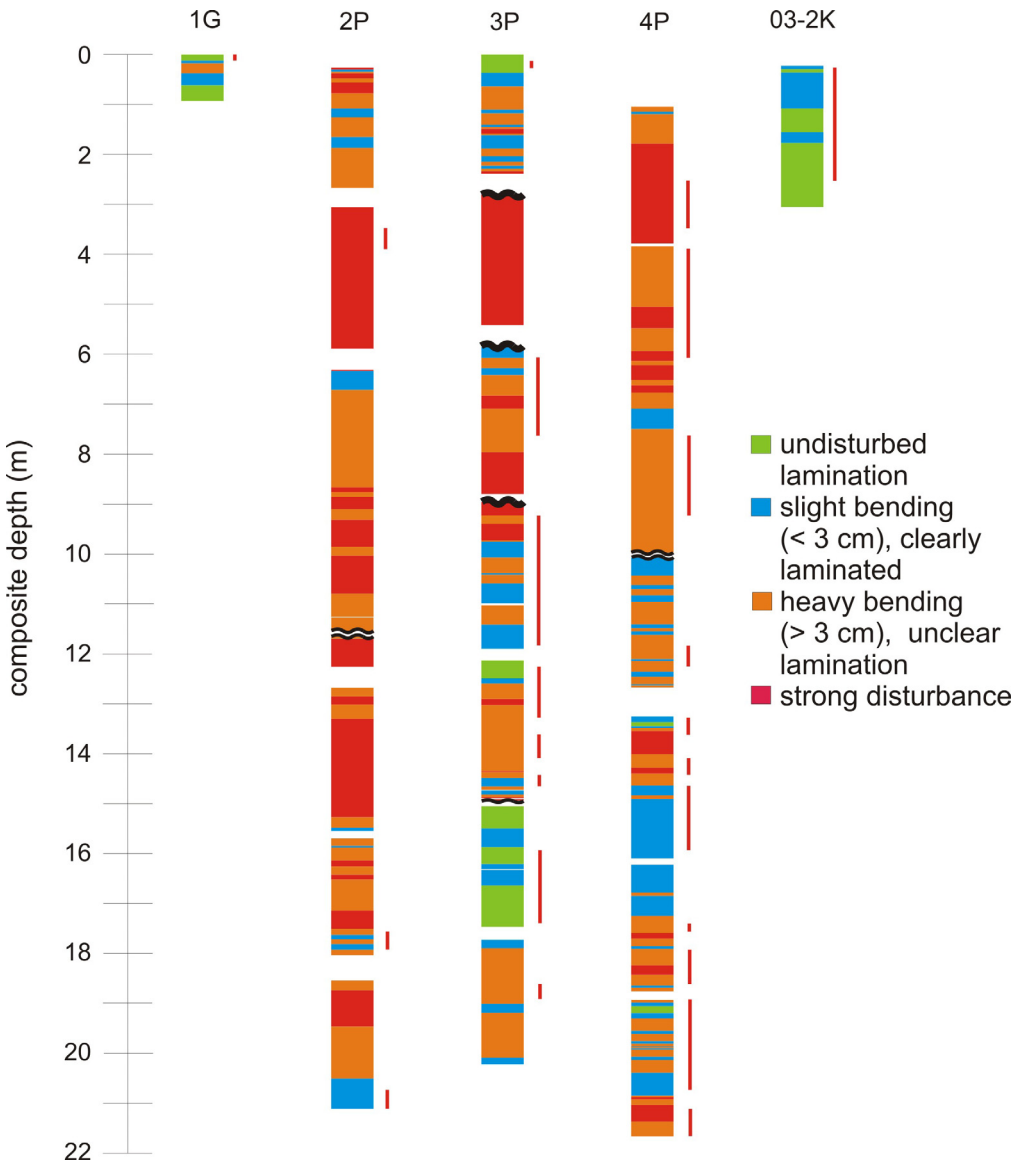

Figure 2.6: Quality of the individual core sections used for construction of the composite profile of Lake Challa sediments from the three parallel drives. Vertical red bars indicate the sections used for construction of the final composite. Wavy lines are shown where the precise size of gaps is uncertain.

for ^{210}Pb and ^{137}Cs dating to Prof. Appleby at the University of Liverpool, but have not yet been processed. Radiocarbon dates on bulk organic matter were corrected for an old-carbon reservoir effect estimated at 17 levels using i) wiggle-match dating of high-density series of bulk organic ^{14}C dates with the ^{14}C calibration curve (IntCal04, Reimer et al. 2004), ii) paired bulk organic ^{14}C dates and ^{210}Pb-derived time markers, and iii) paired bulk organic and grass charcoal ^{14}C dates. Bayesian age-modeling was used for calibration and error-weighted smoothed splines were drawn through the ordered calibrated ranges, resulting in 95% age uncertainties ranging from around 100 years for the Holocene to c. 300-500 years in the glacial section of the record. Details will be published elsewhere (Blaauw et al. in prep.).

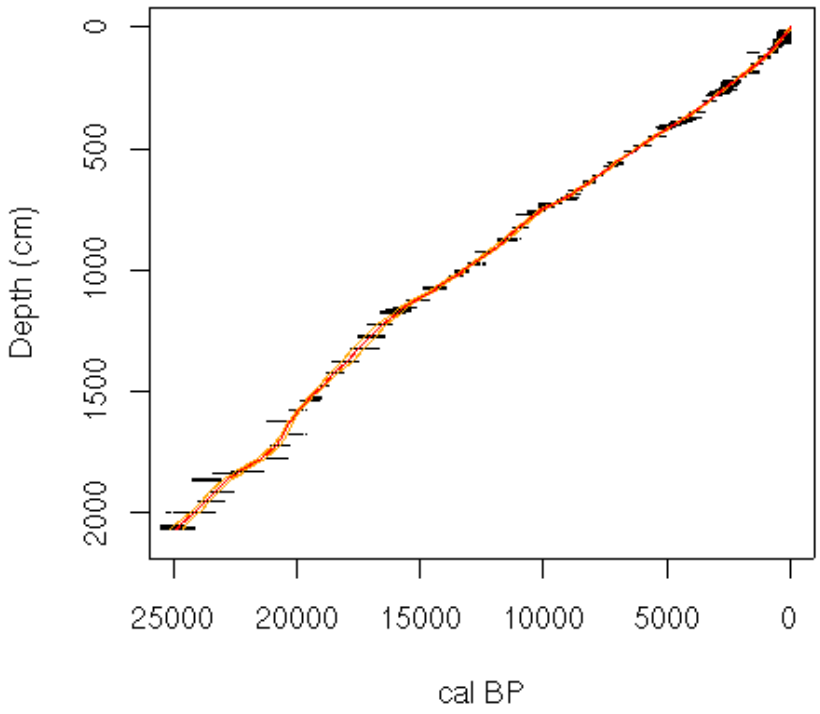

Figure 2.7: Age model of the sediment record from Lake Challa, indicating the depth levels and ranges of individual radiocarbon ages, and the smoothed spline (orange line) with 95% uncertainty ranges (yellow lines).

Both profiles were subject to a multi-proxy approach with this thesis focussing on sedimentological, inorganic and organic geochemical aspects. In both studies I applied the following methods (for details you are referred to the individual manuscripts):

- Magnetic susceptibility measurements
- X-ray fluorescence (XRF) scanning
- Microscopic inspection of 10 cm long thin-section blocks for identification of the nature of sedimentological components and laminations

For Lake Challa additionally:

- Scanning electron microscopy (SEM) in combination with energy-dispersive X-ray analysis of individual sediment fractions (carbonates, diatoms and magnetic extracts)
- XRF and RDA investigations of discrete powdered samples
- High-resolution µXRF scanning of finely laminated sections

For Lake Tswaing additionally:

- Establishing of an improved core chronology based on radiocarbon dating of bulk organic and charcoal material
- Determination of total carbon (TC), total inorganic carbon (TIC) and total nitrogen (TN) contents
- Organic petrology (maceral analysis)
- Rock-Eval pyrolysis
- Biomarker analysis
- Bulk organic and compound-specific stable carbon isotope analyses

3. Hydrological changes in southern Africa over the last 200 kyr as recorded in lake sediments from the Tswaing impact crater

Iris Kristen[1], Andreas Fuhrmann[1,2], Jo Thorpe[3], Ursula Röhl[4], Heinz Wilkes[1], and Hedi Oberhänsli[1]

[1]*GeoForschungsZentrum Potsdam (GFZ Potsdam), Potsdam, Germany*
[2]*now at Saudi Aramco, Dhahran 31311, Saudi Arabia*
[3]*formerly at Department of Geography, University College London, London, Great Britain*
[4]*MARUM - Center for Marine Environmental Research, University of Bremen, Bremen, Germany*

Published in: *South African Journal of Geology* **110,** 311-326

ABSTRACT *Sediments from Lake Tswaing (25°24'30'' S, 28°04'59'' E) document hydrological changes in southern Africa over the last 200 kyr. Using high-resolution XRF-scanning, basic geochemistry (TIC, TOC, TN), organic petrology and Rock-Eval pyrolysis, we identify intervals of decreased carbonate precipitation, increased detrital input, decreased salinity and decreased autochthonous (algal and bacterial) organic matter content that represent periods of less stable water column stratification and increased rainfall. Between 200 and 80 kyr BP, these intervals appear to be contemporaneous with local summer insolation maxima, indicating a strong influence of precessional variability (~23 kyr) on African subtropical climate. This influence weakens during the last glacial period (~80-10 kyr BP), when humid intervals at 73-68 kyr, 54-50 kyr, 37-35 kyr and 15-10 kyr BP are largely out of phase with insolation changes, and presumably reflect southward displacement of the ITCZ (Inter-Tropical Convergence Zone) and/or changes in ocean circulation.*

INTRODUCTION

In order to understand natural climate variability it is important to have long, continuous and well dated climate records from the continents and oceans of both hemispheres, but such records are rare in the southern hemisphere, and especially in southern Africa.

In the last decade, deep coring in Lake Malawi (L in Fig. 3.1) has provided records of lake level-change, diatom composition and temperature over the last 25 to 50 kyr (Finney et al. 1996; Johnson et al. 2002; Powers et al. 2005). Finney et al. (1996) found lake levels 200 to 300 m lower than today for most of the period ~40 to 28 kyr BP and a lake 100 to 150 m shallower than today for the early Holocene. Johnson et al. (2002) and Powers et al. (2005) identified changes in atmospheric circulation and cooler temperatures during the Younger Dryas and the 8.2 kyr-event, indicating a close connection with northern hemisphere climate. Records from stalagmites (e.g. Holmgren et al. 2003; Lee-Thorp et al. 2001; Talma and Vogel 1992) provide precisely dated, high-resolution records of climate variability in South Africa during the

Holocene and the late glacial (last ~30 kyr). According to these studies, temperatures were 5 to 7°C lower than today during the Last Glacial Maximum, then increased in a two step warming at ~17 and 13.5 kyr BP. A similar pattern of warming was found by Gasse (2000) and Partridge et al. (1999) in southern Africa. Records of humidity changes in South Africa are rarer and less clear (Partridge et al. 1999). The available speleothem records (Holmgren et al. 1995; Holmgren et al. 2003; Talma and Vogel 1992) contain hiatuses and do not cover complete glacial/interglacial cycles.

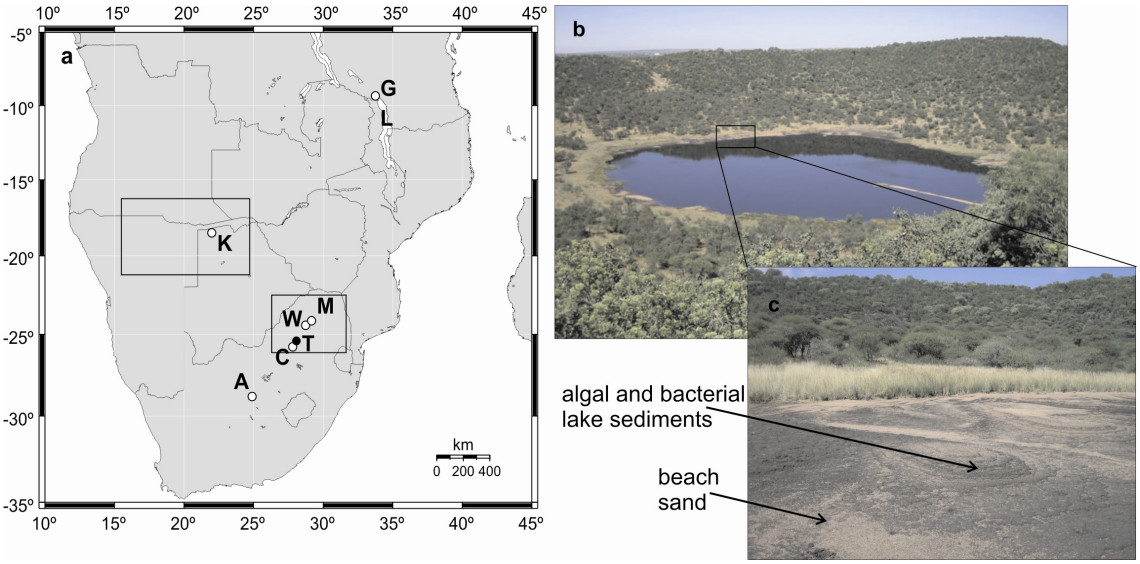

Figure 3.1: a) Map of southern Africa with locations of: Lake Tswaing (T, 25°24'30'' S, 28°04'59'' E), Wonderkrater (W), Makapansgat (M), Gladysvale Cave (C), Tsodilo Hills, northwestern Kalahari (K), Lake Masoko, Tanzania (G), Lake Malawi (L) and Alexandersfontein (A). Dune and cave studies in northern Namibia, Botswana and Zambia are available from Munyikwa (2005); Thomas and Shaw (2002); O'Connor and Thomas (1999); Stokes et al. (1998); Stokes et al. (1997) (left frame), and further cave studies in south-eastern Africa from Brook et al. (1997) (right frame); b) Crater lake Tswaing with present day vegetation: *Acacia* dominating the lower slope, *Spirostachys* and *Combretum* dominating the upper slope, grasses and reeds (*Typha* and *Cyperaceae*) along the shore (T.C. Partridge, pers. comm 2006) and c) close-up of grasses and sandy shore with dried bacterial lake sediments.

The longest and most continuous record of precipitation in South Africa is the sedimentary record from the crater lake Tswaing (formerly "Pretoria Saltpan") (Partridge et al. 1993, Partridge et al. 1997), which covers at least two glacial/interglacial cycles (~200-2 kyr BP). The multidisciplinary study edited by Partridge (1999b) gives a general overview of the origin, geology, sedimentology and limnology of the crater lake. A major finding of this study is the precessional (changes in earth's orbital configuration with ~23,000 year periodicity) control over the mineralogical composition and grain size distribution of the sediments over the last 200 kyr, which weakens during the last glacial period (Partridge 1999a). However, some questions remain about the extent of changes in lake level and the ecosystems over the period of the record, because both pollen and diatoms are absent from parts of the core, and yielded contradictory results in other sections (Scott 1999a; Metcalfe 1999). Here we aim to provide

further insights into changes in the ecosystems in and around the lake on glacial/interglacial time scales. For this purpose, we use organic petrology and Rock-Eval pyrolysis to characterise the composition of the organic matter (OM) in the lake sediments. With this approach, which has been successfully applied to European maar lakes (Fuhrmann et al. 2004) and the North American Great Lakes (Meyers 2003), we can differentiate OM originating from different sources (Meyers and Lallier-Vergès 1999). We interpret these data in the light of high-resolution records of the total inorganic carbon (TIC), total organic carbon (TOC) and total nitrogen (TN) content of the sediments of the complete profile and records of element distributions obtained by XRF scanning from the upper 30 m of the core. Using these data, we attempt to better characterise processes occurring within and around the lake over the period covered by the core and to provide a record of precipitation changes in southern Africa over the past 200 kyr.

GEOGRAPHIC, GEOLOGICAL AND CLIMATOLOGICAL SETTINGS

The 1.13 km-wide crater Tswaing is located approximately 40 km northwest of Pretoria at an altitude of 1045 m asl. The crater was fromed by a meteorite impact, which has been dated at 220±52 kyr BP using fission-track dating (Reimold et al. 1992). The crater is situated in the ~2 Ga old Nebo Granite, the main granite type of the Bushveld complex (Brandt and Reimold 1999). Since its formation, the crater has filled with material eroded from its walls and with autochthonous lacustrine sediments (Partridge et al. 1993). This infilling appears to have been at least partly responsible for a gradual shallowing of the waterbody documented in the mineralogical composition of the sediments (Bühmann and Elsenbroek 1999). The crater walls reach 119 m above the crater floor and 60 m above the adjacent surface. They create an enclosed basin with no surface outflow and a central lake. This lake is today 2 to 3 m deep, alkaline, with a pH value around 10, and hypersaline (up to 250-300 ‰ in bottom waters). Its surface area shrinks by 20-25 % during winter times, causing an average lake level fall of 20 cm below summer high stands (based on a monitoring phase of 28 months; Ashton and Schoeman, 1983). The high salinity causes the water body to be constantly stratified and thus mostly anoxic below 50 cm water depth (Ashton 1999). The high salinity and alkalinity are also responsible for the dominance of bacteria, blue-green algae and protists in the lake water body. A few diatom species inhabit areas where fresh groundwater seeps out of the crater wall. This groundwater inflow, together with rainfall, represents the only natural source of fresh water entering Lake Tswaing. Artesian boreholes that reach down to sandy aquifers below the lacustrine facies provide additional inflow since the 1970s (Ashton and Schoeman 1983; Partridge et al. 1993). The total annual rainfall in this region varies between 400 and 750 mm per year. The rainfall distribution is highly seasonal, with a maximum during the austral summer months (October to April) when the ITCZ reaches its southernmost position (Fig. 3.2). The ITCZ marks the region of the thermal equator where the tropical easterly flows converge and create convective rainfall (Preston-Whyte and Tyson 1988). Annual precipitation is exceeded by an average annual evaporation of 2,375 mm. Monthly mean maximum and

minimum air temperatures in the region range from 14.2 °C to 35.2 °C and 3.6 °C to 15.6 °C, respectively (Ashton 1999). The vegetation around the crater is classified as mixed- and sourish-mixed bushveld assemblages and consists of grassland mixed with deciduous trees and shrubs dominated by *Acacia* and *Combretum* species (Acocks 1953).

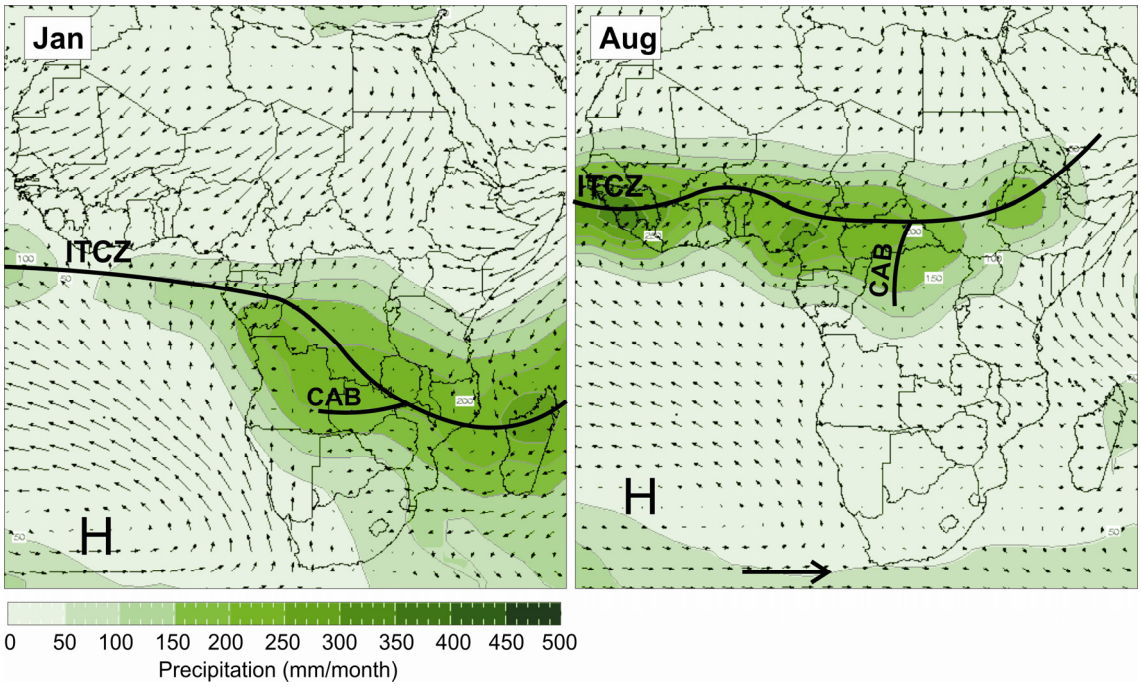

Figure 3.2: Precipitation and wind vectors for the 925 hPa pressure level (small arrows indicate direction, speed is proportional to arrow length) for Africa in January and August (http://iridl.ldeo.columbia.edu, based on NOAA_NCEP data, satellite estimates and rain gauge data), together with main features of atmospheric circulation: Inter Tropical Convergence Zone (ITCZ), Congo Air Boundary (CAB), the subtropical high over the South Atlantic and influence of the westerlies (big arrow) during winter.

MATERIAL AND METHODS

During a coring campaign in 2001/2002, approximately 90 m of sediments were recovered from the lake using Shelby tube drilling for the upper 33 m and wireline rotary core drilling with a triple-tube core barrel for the lower section. The sediments are composed of granitic sands in the lowermost few meters, followed by partly laminated lake sediments (Fig. 3.3). The lake sediments consist of carbonate-dominated marls below ~35 m depth, and halite and fluorite-bearing organic-rich muds in the upper 35 m (Bühmann and Elsenbroek 1999). Mass flows up to 1.5 m thick are intercalated with lacustrine sediments, particularly between depths of 35 and 50 m and 70 and 77 m. These deposits are primarily composed of sand and gravels derived from the crater walls. To create the final composite profile, which is 78 m long (shown in Fig. 3.4, 3.5, 3.6, 3.9 and 3.10, and referred to in the text if not quoted otherwise),

mass flows were excluded, as they are considered abrupt events that disrupt the continuous sequence of sediments (Partridge et al. 1997; Garcin et al. 2006b and references therein).

A total of 217 samples were collected at between 30 and 50 cm resolution and analysed for total carbon (TC), total inorganic carbon (TIC), total organic carbon (TOC) and total nitrogen (TN) content. TIC was determined coulometrically after release of carbon dioxide by reaction with hot phosphoric acid (1:1) (device: Coulomat 702, Ströhlein). The TIC concentrations represent mean values of double measurements. The relative difference between the single measurements was typically below 1%, but for TIC contents below 0.1 % the difference occasionally reached 10%.

TC and TN were analysed using the EuroVector EA3000 Elemental analyzer. Approximately 10 mg of sediment was wrapped in tin and combusted under oxygen flow at >1000 °C. After combustion, CO_2 and N_2 were separated using a GC column and detected using thermal conductivity. The precision for TC was <1 % and for TN <5 %. TOC was determined by calculating the difference between TC and TIC.

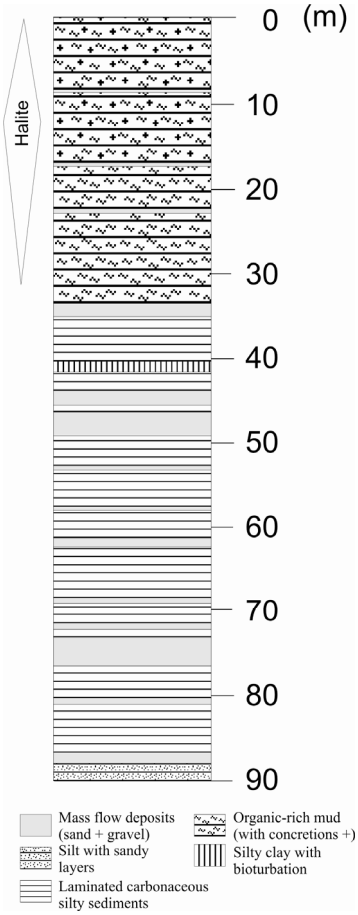

Figure 3.3: Lithology of the sediments recovered from Lake Tswaing in 2001/2002.

Twenty-one samples were collected to characterise the organic material preserved in the sediments using Rock-Eval pyrolysis and maceral analysis. Maceral analysis was carried out by qualitative microscopic inspection of polished blocks using a Zeiss Axioplan microscope in reflected white light and with blue light excitation at 365 nm. Total organic carbon (TOC), hydrogen index (HI) and T_{max} (definition later in this paragraph) were determined using a Rock-

Eval 6 instrument following the procedures described by Espitalié et al. (1977; 1985) and Lafargue et al. (1998). The TOC values from Rock-Eval pyrolysis are very similar to those calculated from the difference between TC and TIC, confirming the validity of the latter approach. The HI corresponds to the yield of volatile organic compounds released by pyrolysis of the macromolecular OM in the sediments and is controlled by the amount of hydrogen in the organic material (kerogen), which is generally higher for algal and bacterial matter than for vascular plants (Meyers and Lallier-Vergès 1999). T_{max} is the temperature at which the greatest amount of volatile organic compounds is released during continuous heating from ~200 to 850 °C. This parameter describes the thermal evolution of organic matter in the sediment. It can be correlated with vitrinite reflectance (e.g. Tissot et al. 1987), which is the most commonly used parameter to describe the changes of microscopic organic constituents during maturation. It is measured using a microscope with incident light and increases with increasing maturity (Taylor et al. 1998). The HI versus T_{max} diagram can be used to evaluate thermal maturity and to classify the kerogen type of OM in the sediments.

The core sections of the upper 31 m were scanned for selected elements at 3 cm resolution using the X-ray fluorescence Core Scanner II at MARUM of the University of Bremen (Germany). A special emphasis was placed on the upper 31 m of the sediments because it is during this time interval (~80 kyr) that previous investigations indicate a change in the controls on climate at the site (Partridge 2002). The XRF core scanner was used to measure major elements (e.g., Al, Si, S, K, Ca, Ti, Cl, and Fe) on split sediment cores as described in Richter et al. (2006), Röhl and Abrams (2000) and Tjallingii et al. (2007). This is a widely accepted, semi-quantitative, non-destructive core logging method that provides records of changing element intensities expressed in “total counts”, reflecting the geochemical composition of the sediments. We excluded intervals rich in mass flow material, evaporitic crusts and concretions because the sediment surface was too rough to perform the scanning in these intervals.

CHRONOSTRATIGRAPHY

The age model for the upper 25 m of the profile is based on nine new radiocarbon ages (Table 3.1 and Fig. 3.4) determined at the Poznan Radiocarbon Laboratory. Three of the dates are on microscopic charcoal fragments, and the others are on bulk OM. A reservoir correction of 1,150 years (the mean age offset of 11 samples from recent lake sediments; Partridge et al., 1997) was applied to the two youngest ages on bulk OM . This correction was applied to these samples because they were taken from intervals where autochthonous material (bacterial and algal) dominates the organic fraction of the sediments (see below). The reservoir effect is assumed to be constant for the last 5,000 yr BP. Beyond this time interval we did not adjust the measured ages, as these samples were obtained from TOC poor intervals where maceral investigation reveals that the OM present is predominantly of terrestrial origin.

The ages show a regular increase with depth, with the exception of one bulk sample (Fig. 3.4). This sample was taken immediately below the charcoal sample from 14.8 m depth, but has a ^{14}C age 10,000 years older; an offset that is probably due to contamination with old OM. This sample is therefore excluded from the age model. For samples younger than 24,000 ^{14}C years, the ages were calibrated using Calib 5.0.2 after McCormac et al. (2004) and Reimer et al. (2004) (calibration curve SHCal04 for samples younger than 11 cal kyr BP and IntCal04 for samples older than 11 cal kyr BP). Ages older than 24,000 ^{14}C years were calibrated using CalPal (calibration curve CalPal2005_SFCP).

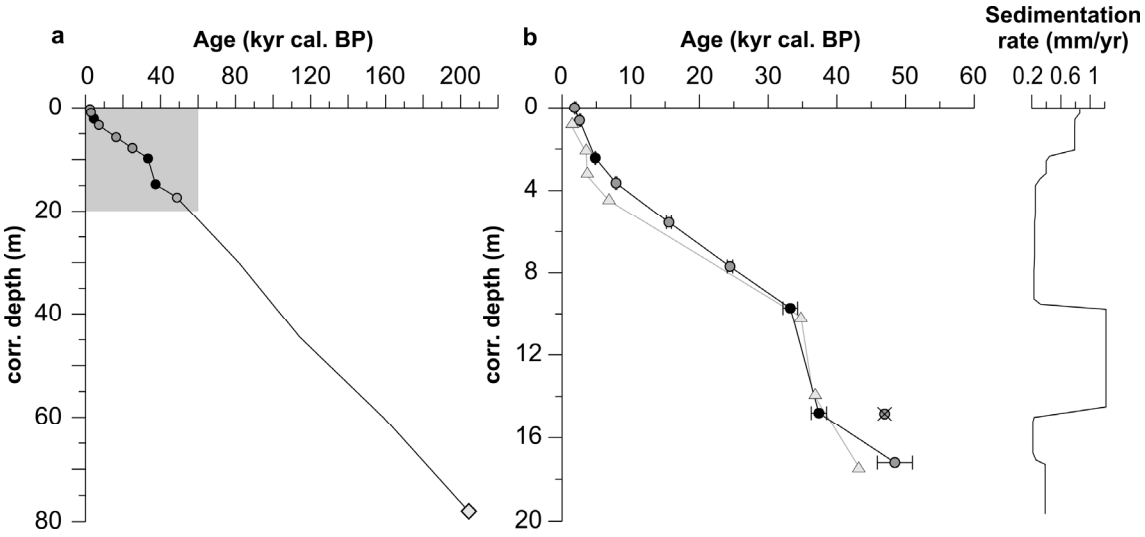

Figure 3.4: a) Age/depth plot for the complete profile, based on radiocarbon ages and the assumed start of lacustrine sedimentation at ~200 kyr BP; the basal age is estimated from the impact age of 220±52 kyr BP (Koeberl et al. 1999), from tuning (for the time window 50–200 kyr BP the age is tuned to local insolation) and from extrapolation of sedimentation rates (for a detailed description of the age model beyond the limit of radiocarbon dating see also Partridge et al. 1997). Filled circles represent radiocarbon ages of charcoal samples, open circles represent radiocarbon ages of bulk OM samples which were both collected from the 2000/2001 core. The two youngest ages include a reservoir correction of 1,150 yrs (Partridge et al. 1997). The depth scale is corrected for mass flows. The grey area delimits the extent of Fig. 3.4 b; b) Age/depth plot and sedimentation rates for the upper 20 m of the Lake Tswaing sediments. The radiocarbon ages of Partridge et al. (1993) are shown in light grey (triangles).

The chronology confirms the previously-published age model based on seven radiocarbon ages from bulk organic material, which was established for a core retrieved in 1988 (Partridge et al. 1993) (Fig. 3.4).

Below the radiocarbon-dated section, the age model rests on the fission-track date of 220±52 kyr BP from impact glass (Koeberl et al. 1999). An attempt to gain a better-constrained age for this material using $^{40}Ar/^{39}Ar$ dating did not provide reliable results due to inherited ^{40}Ar (Jourdan et al. 2007). Furthermore, tests to assess the suitability of quartz grains from the sediments for OSL dating failed (Stephan Woodborne, pers. com. 2006). We therefore constructed an age model for the sediments below 20 m depth using the same procedure as Partridge et al. (1997). This involved tuning our TIC record to the record of January insolation

at 30°S. This approach seems appropriate due to the similarities between the reconstructed palaeo-rainfall record from Partidge et al. (1997), our TIC record, and the record of January insolation. The tuning process results in a maximum deviation of 5,000 years between the tuned age model and an age model constructed by linear interpolation between the last radiocarbon age (48,440 cal. yr BP) and a basal age of 200 kyr BP (allowing ~20,000 years for the deposition of ~15 m of terrigenous sands and gravels that underlay the lacustrine sequence; Partridge et al. 1999) (Fig. 3.4).

Table 3.1: Radiocarbon ages for Lake Tswaing sediments.

original depth (m)	corrected depth (m)	^{14}C age (yr BP)	Std. dev. ±	calibrated age (yr BP)	± 2σ	material
1.595-1.605	0	3095	35	1810*	91	TOC
2.21-2.24	0.61-0.64	3675	35	2538*	175	TOC
4.005-4.065	2.405-2.465	4305	30	4837*	35	charcoal
5.23-5.24	3.63-3.64	7090	50	7850*	115	TOC
7.36-7.38	5.54-5.56	13130	70	15550*	356	TOC
9.785-9.795	7.695-7.705	20410	130	24440*	405	TOC
11.835-11.885	9.705-9.755	28500	600	33220**	1072	charcoal
16.990-17.020	14.790-14.820	31900	800	37390**	1120	charcoal
19.385-19.395	17.195-17.205	44800	2100	48440**	2559	TOC

*Calib 5.0.2 after McCormac et al. (2004) and Reimer et al. (2004)

**CalPal (calibration curve CalPal2005_SFCP)

RESULTS AND DISCUSSION

Basic geochemistry (TIC, TOC, TN) of the complete profile

The records of TIC (range: 0 to 10 %), TOC (0 to 8 %) and TN (0 to 0.4 %) are displayed in Figure 3.5. All datasets show considerable variability. The amplitude of variations in TIC is greatest below 35 m (~93 kyr BP according to the age/depth relationship presented in Table 3.1 and Fig. 3.4), while the amplitude of variations in TOC is greatest above 35 m. This change correlates with the change in the prevailing lithologies (carbonaceous marls vs organic-rich muds; see Fig. 3.3) and presumably documents a shift in the lake system. Below 35 m, higher TIC content appears to reflect stronger evaporation (Partridge et a. 1997), while above 35 m, increased evaporation appears to lead to increased quantities of halite (see next paragraph). This change may be a result of brine evolution (Eugster and Hardie 1978), but it can also be related to the rapid shallowing of the lake by prominent mass flow deposition, and its greater

sensitivity to changes in the precipitation/evaporation ratio after these events. The record of TN shows similar fluctuations to the record of TOC. The TOC/TN ratios are, on average, lower above 30 m depth (19.8 above 30 m compared to 28.4 below 30 m).

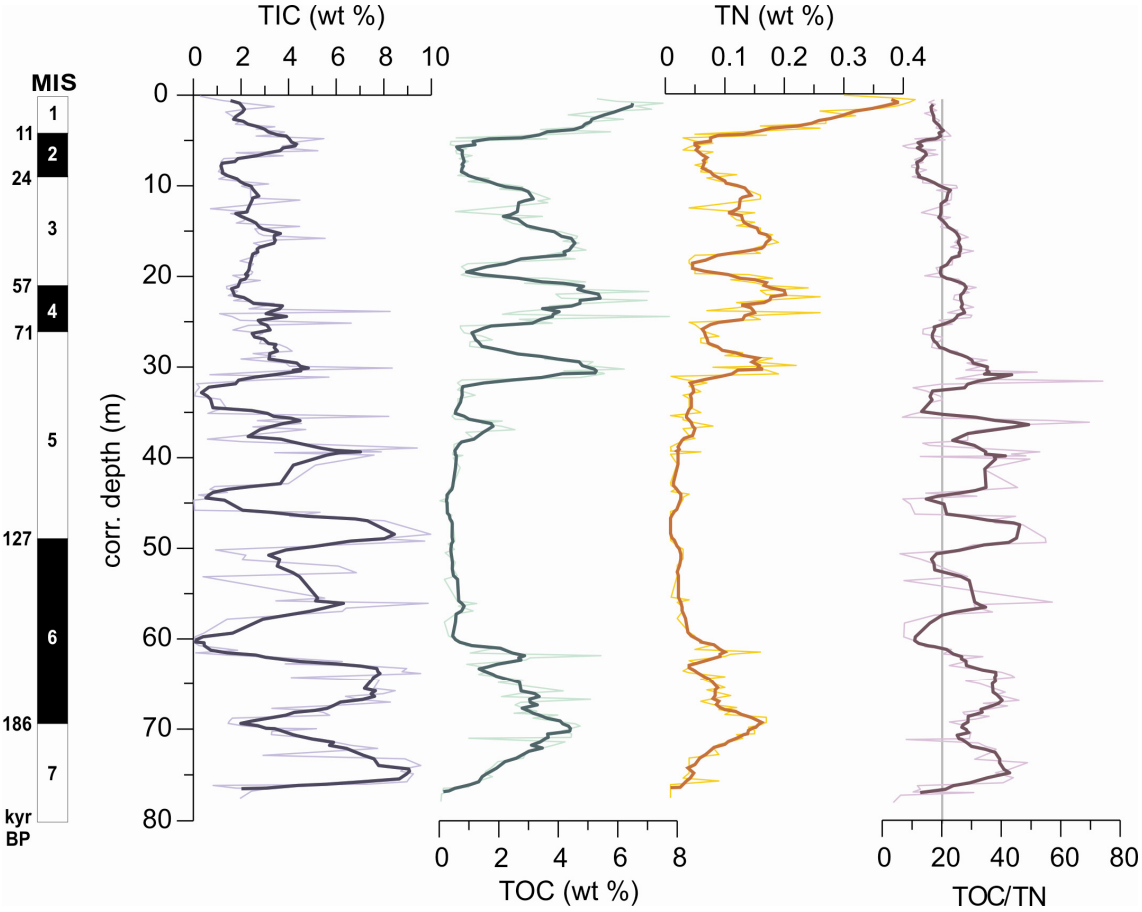

Figure 3.5: Content (wt %) of total inorganic carbon (TIC), total organic carbon (TOC), total nitrogen (TN) and the TOC/TN ratio of the sediments from Lake Tswaing. Thick lines are 5-point running averages of the respective fraction. Left column indicates approximate marine oxygen isotope stages (MIS) according to Bassinot et al. (1994).

Element geochemistry (XRF core scanning)

The XRF scans of our studied cores reveal changes in the importance of selected elements that result from varying detrital input and/or authigenic processes. Element intensities of silica (Si), potassium (K), titanium (Ti), iron (Fe), aluminium (Al), sulphur (S), calcium (Ca) and chlorine (Cl) in the upper 31 m (~84 kyr BP) of organic-rich muds are compared to the mineralogical data of Bühmann and Elsenbroek (1999) (Fig. 3.6). Si, K, Ti and Fe show similar trends, increasing from 4 to 5.5 m, 13 m, 18 to 20 m and from 24.5 to 27 m (~10-15, 35-37, 50-54 and 68-73 kyr BP). Mineralogical and chemical data of the lake sediments revealed that

quartz, feldspars (microcline ($KAlSi_3O_8$) and plagioclase ($(Na,Ca)(Si,Al)_4O_8$)), smectites ($(Na,Ca)Al_4(Si,Al)_8O_{20}(OH)_4 \cdot 2(H_2O)$) and illite ($KAl_2[(OH)_2AlSi_3O_{10}]$) are the major detrital minerals (Bühmann and Elsenbroek 1999). For the studied upper 31 m of the record, the relative amounts of quartz, feldspars and plagioclase co-vary with the intensities of Si, K, Ti and Fe. We therefore infer that these elements reflect detrital, minerogenic input from the shore and the crater wall, which derives from the granitic bedrock that consists of 37-63 % quartz, 10-27 % microcline, 18-54 % plagioclase and < 5 % mica (Bühmann and Elsenbroek 1999). The Al values do not co-vary with the other elements. Similar to the relative abundance of smectites, Al displays a rather smooth trend, which is probably the result of a balance between aeolian inputs and sheetwash, whereas K, Si, Ti and Fe derive only from sheetwash. The amount of Cl reflects the abundance of halite (NaCl), which is a major component of the lake sediments in the uppermost 31 m of the cored sequence (Bühmann and Elsenbroek 1999) and is indicative of saline conditions in the lake. Today it makes up 66 % of the salt deposits that are deposited around the lake during the dry season (Bühmann and Elsenbroek 1999). Contrary to Partridge et al. (1993), who considered the halite in the sediments to be primarily a secondary precipitate from pore water, we interpret it as in-situ product forming in the water column or at least near the sediment surface. This interpretation is based on the anti-correlation of Cl to the detrital elements and its correlation with the TOC content of the sediments.

Sulphur could be related to the occurrence of gypsum, diagenetic components like pyrite or in OM. In some intervals, the abundance of S co-varies with the intensity of Fe, which may reflect the presence of iron sulfides produced by diagenetic processes, but neither pyrite nor gypsum are major components of the sediments (Bühmann and Elsenbroek 1999). Calcium, like S, does not show a clear correlation with other elements. This element is present in plagioclase and smectite, which can occasionally form up to 30 % of the minerogenic fraction, but is also present in autochthonous calcite. The fact that Ca occurs in both detrital and authigenic minerals may explain the low amplitude of variations in the abundance of this element because the relative abundance of detrital and authigenic minerals are anti-correlated. This effect is probably especially important in the upper ~23 m of the profile where calcite comprises, on average, 7 % of the minerogenic fraction compared to 36 % between 23 and 78 m depth (Bühmann and Elsenbroek 1999).

Figure 3.6 (following page): Intensities of major elements (Si, K, Ti, Fe, Al, S, Ca and Cl) from XRF-core scanning of the upper 31 m of sediments from Lake Tswaing. Thick lines show 7-point running averages. The mineralogical composition is redrawn after Bühmann and Elsenbroek (1999). It has been transferred to the new corrected depth scale to facilitate comparison. Abbreviations: halite (Hl), smectites (Sm), quartz (Qz), plagioclase (Plg), microcline (Mkl). Left column indicates approximate marine oxygen isotope stages according to Bassinot et al. (1994). Grey bars highlight humid periods with increased detrital input and reduced precipitation of halite.

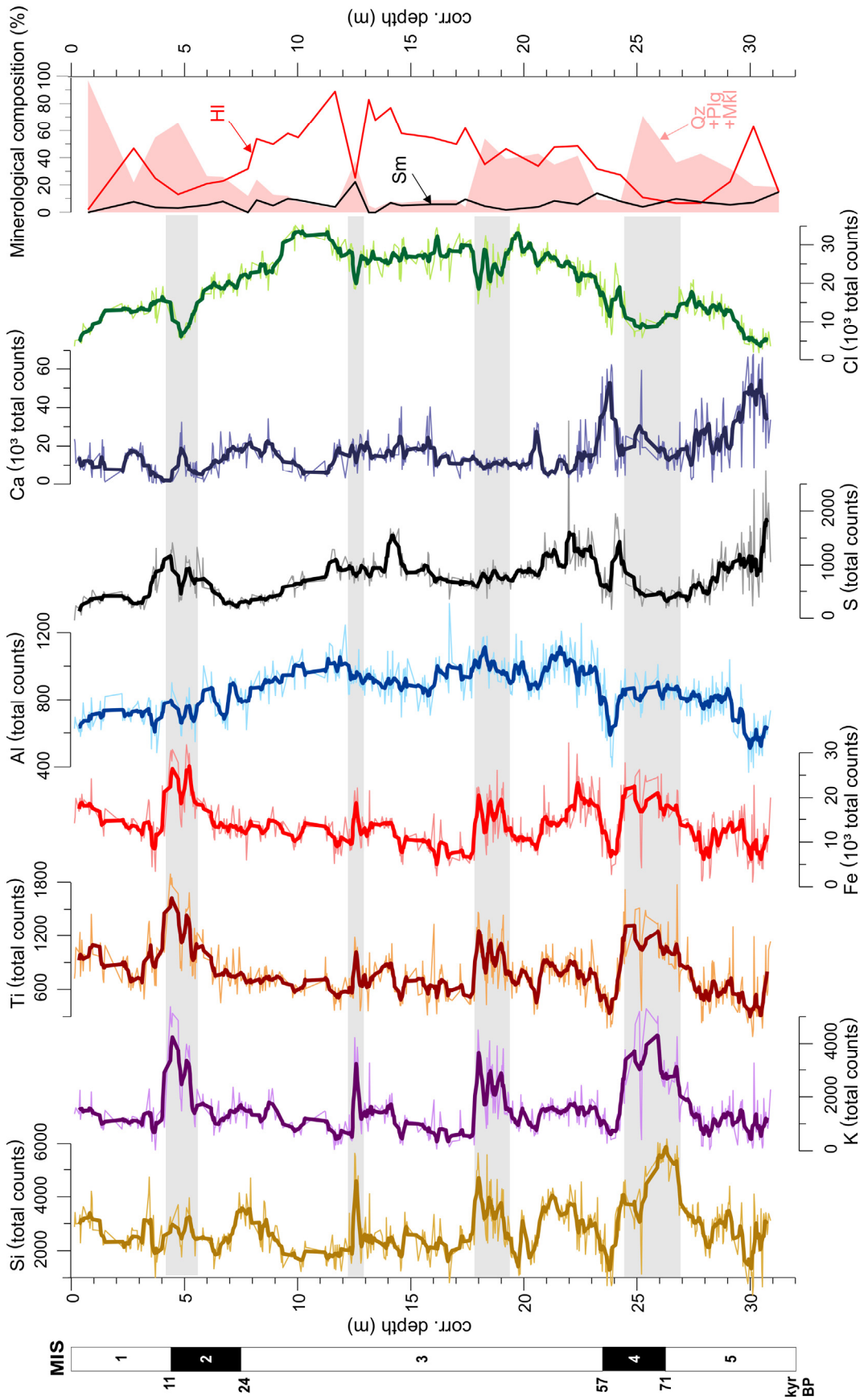
Minerological composition (%)
Hl
Sm
Qz +Plg +Mkl
corr. depth (m)
Ca (10³ total counts)
Cl (10³ total counts)
S (total counts)
Al (total counts)
Fe (10³ total counts)
Ti (total counts)
K (total counts)
Si (total counts)
MIS
1
2
3
4
5
11
24
57
71
kyr BP

Organic petrology and Rock-Eval pyrolysis

Organic petrology using microscopic methods is a useful means of characterising OM in lake sediments in order to reconstruct palaeoclimatic variations (e.g. Fuhrmann et al. 2003; Patience et al. 1996; Sifeddine et al. 1996). Particulate autochthonous OM can be differentiated from ligno-cellulosic allochthonous OM due to its different morphology and fluorescence characteristics. For example, algal OM appears light green, yellowish or orange under blue light excitation, whereas fresh terrestrial plant material appears black or dark brown and often has cellular or fibrous structures (Taylor et al. 1998). High reflectance terrigenous particulate OM (which appears steel-grey under normal white light, Fig. 3.7 c and d) represents input of eroded geologically older OM or oxidised fragments (Fuhrmann et al. 2004). In the investigated profile, samples high in TOC contain frequent layers of autochthonous material in the form of filamentous algae or cyanobacteria (F, Fig. 3.7 a and b), as well as abundant colonies of the colonial green alga *Botryococcus braunii* (B, Fig. 3.7 a). In the deepest 15 m of the core, unknown filamentous algae dominate the autochthonous organic fraction. Pollen grains are rare, but other terrestrial plant material is frequently present in organic-rich samples. It forms dark layers where sediments are laminated (T, Fig. 3.7 b), or is present as single particles with fibrous and cellular structures where sediments are homogenous (Fig. 3.7 e). A considerable proportion of these particles seem to be relatively highly oxidised (Fig. 3.7 c and d). Samples with TOC <0.5 % lack any recognisable autochthonous organic components. Most of the OM in these samples consists of small, oxidised terrigenous particles (Fig. 3.7 c).

Rock-Eval pyrolysis data show that the sediments from Lake Tswaing can be divided into 3 groups according to their HI and T_{max} values (group A, B, C in Fig. 3.8, Table 3.2). Group A has HI values higher than 300 mg HC/g TOC and T_{max} values higher than 400°C. Group B has HI values lower than 300 mg HC/g TOC and T_{max} values higher than 400°C, while the HI values of group C are lower than 300 mg HC/g and the T_{max} values are lower than 380°C. The latter are found in the interval between 35 and 55 m (~40-60 m uncorrected depth in Fig. 3.3, ~93-145 kyr BP). For samples above and below this interval, HI and TOC co-vary and T_{max} remains stable at around 430°C (Fig. 3.8, Table 3.2). As expected for relatively young sediments like those from Lake Tswaing, thermal maturity as assessed by T_{max} is low, with vitrinite reflectance (R_r) mainly below 0.5 % (Fig. 3.8, Taylor et al., 1998). The distribution within the HI-T_{max}-diagram (Fig. 3.8) can be used to identify the kerogen type (Types I, II, III, indicated by dashed lines in Fig. 3.8), and thus indicates the origin of the OM (Meyers and Lallier-Vergès 1999). Type I OM, which is especially rich in hydrogen, predominantly derives from microbial biomass or the waxy coatings of terrestrial plants. Type II OM, which is moderately enriched in hydrogen, typically derives from autochthonous sources, particularly algae. Higher plant debris is primarily Type III OM, which is poor in hydrogen. Samples from group B can be classified as samples containing Type III OM. They are characterised by TOC contents <1%. Samples from group A have TOC values >1% and contain predominantly Type II OM. Generally lower TOC/TN ratios (Fig. 3.5) support the results from Rock-Eval pyrolysis that, particularly in the upper 30 m, autochthonous OM is the main component of TOC (Meyers 2003). The high TOC content of the samples, combined with the presence of well-preserved

land plant debris and the laminated nature of the sediments in some sections, indicate that conditions were anoxic in the hypolimnion and in the sediments of the lake.

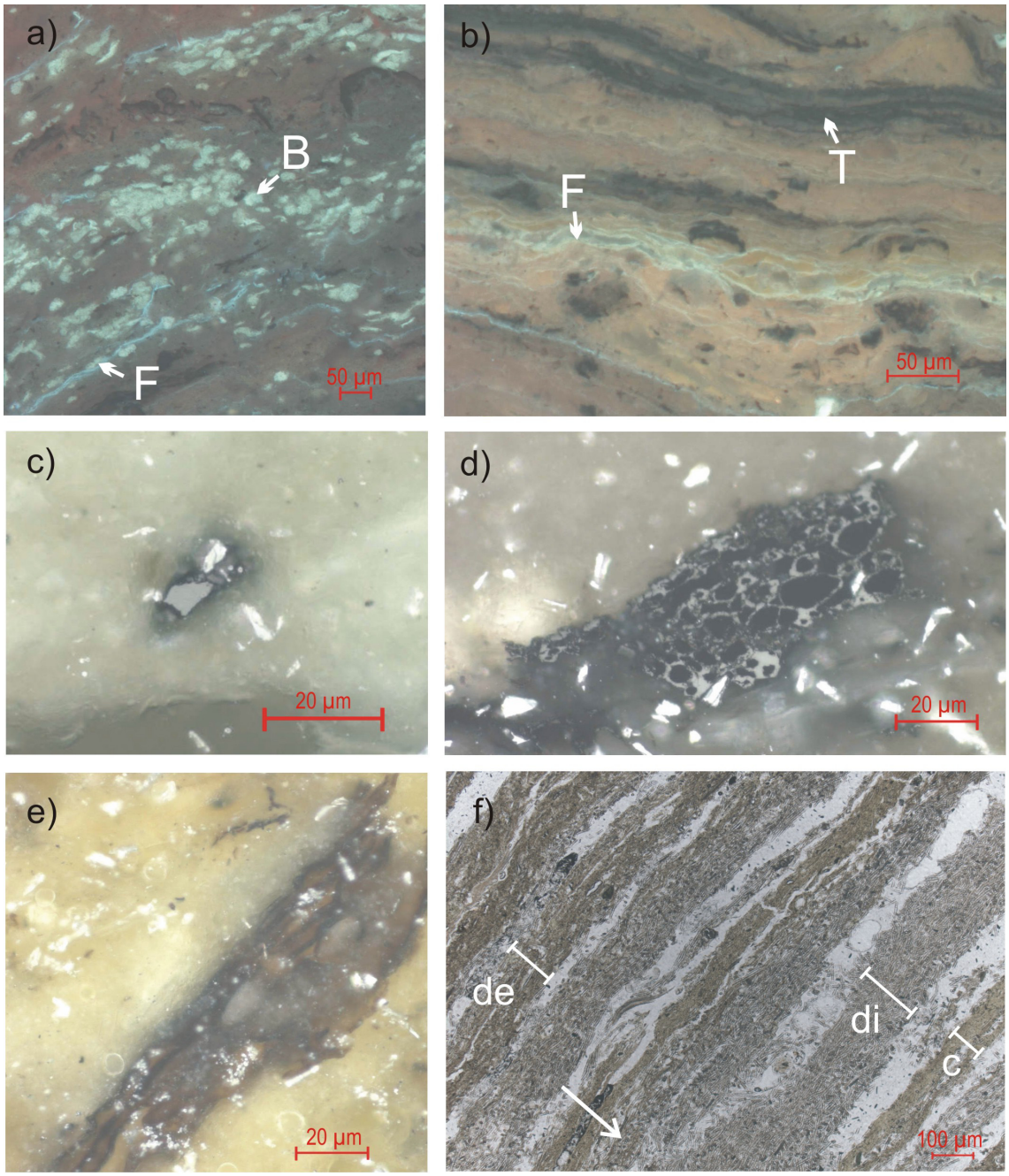

Figure 3.7: a) Laminated sediment from 21.4 m depth (~59 kyr BP), *Botryococcus braunii* colonies (B) and filamentous cyanobacteria or algae (F); b) laminated sediment from 29.5 m depth (~80 kyr BP), rich in filamentous cyanobacteria or algae (F), terrestrial material (T) appears dark and is enriched in distinct layers; c) organic-poor sediment sample from 34.8 m depth (~92 kyr BP), where only small quantities of highly reflecting terrestrial particles are present; d) highly reflecting terrestrial particle (fusinite) from 29.5 m depth; e) fresh organic plant material from 21.4 m depth; f) laminated section (44.7 m depth, ~115 kyr BP) with detrital (de), diatom (di) and carbonate (c) layers (arrow points down). Figure 3.7 a) and b) show photographs taken under blue light excitation, 3.7 c) to e) are taken under reflected white light, 3.7 f) shows a thin section photo taken under normal white light.

Sample	corr. depth (m)	TOC (wt%)	T_{max} (°C)	HI (mg HC/ g TOC)
1	0.6	6.13	426.0	412.0
2	7.5	0.44	428.0	177.0
4	11.1	2.32	427.0	320.0
5	12.5	0.27	422.0	136.0
6	16.3	3.29	434.0	372.0
7	19.2	0.31	427.0	95.0
8	21.4	6.32	431.0	495.0
9	25.2	0.71	440.0	114.0
10	25.4	0.31	430.0	111.0
11	29.5	4.92	429.0	470.0
12	34.8	0.34	357.5	75.0
13	36.6	1.36	449.5	542.0
14	39.2	0.37	325.0	114.5
15	44.7	0.19	315.0	226.0
16	48.4	0.19	373.0	47.5
17	60.1	0.52	426.0	116.0
18	61.5	4.77	433.5	522.0
19	63.3	0.77	435.5	172.5
20	68.8	3.32	434.0	389.5
21	69.4	4.68	433.5	410.0
22	74.9	1.31	433.5	502.5

Table 3.2: Hydrogen Index (HI), total organic carbon content (TOC) and T_{max} values of Lake Tswaing sediments.

The OM in samples from group C, which have very low T_{max} values, can not be classified according to this scheme (Samples 12, 14, 15, 16 in Table 3.2 and Fig. 3.8). Scott (1999a) reported that the interval between 30 and 60 m is barren of pollen and suggested that this was due to oxidation of OM during deposition in a shallow lake environment or during subaerial exposure of the sediments during arid events at the top of this section. Diatom investigations indicate, however, that the lake water was relatively fresh (conductivity generally less than 1000 μScm^{-1}) and moderately alkaline (pH 7.5-8.5) with a trend towards more alkaline conditions at the top of the section (~35 m) (Metcalfe 1999). Between ~40 and 50 m, the diatom assemblage composition indicates that conditions were well mixed. Thin sections indicate that there is inter-annual or seasonal lamination between ~50 and 43 m (~58-50 m in Fig. 3.3), with diatom-rich horizons alternating with carbonaceous and clastic-rich horizons (Fig. 3.7 f). This lamination suggests that benthic organisms were absent, possibly due to anoxic conditions in the hypolimnion, but that there was enough seasonal variation in the epilimnion to allow diatom blooms, calcite precipitation, and sedimentation from sheetwash. Bioturbational structures occur at ~35 m depth (~40 m in Fig. 3.3), indicating that conditions were sufficiently oxygenated to support benthic organisms. In summary, results from the study of diatom assemblages and sedimentology indicate the presence of a freshwater lake that was deep enough to sustain a well mixed epilimnion and an anoxic hypolimnion. Towards the top of the section, at ~35 m, the lake appears to have become shallower, allowing complete mixing of the water body. The reason for

the lack of OM remains uncertain, but is probably due to oxidation of OM in either the epilimnion or in the sediments after deposition.

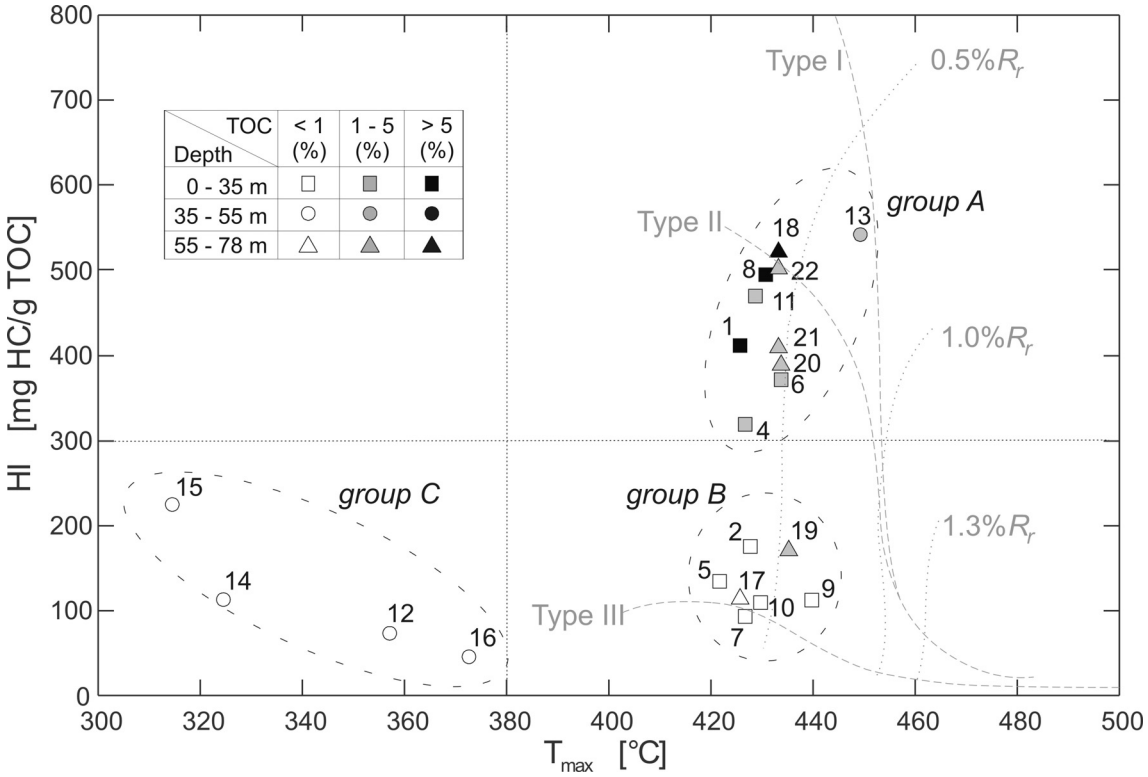

Figure 3.8: HI-T_{max} diagram. Sample labels correspond to sample numbers in Tab. 3.2. For explanation of HI and T_{max}, and of the kerogen types I, II, III see text. R_r indicates reflectance/maturity of the OM (Taylor et al. 1998).

Above ~35 m depth, the combination of results from organic and inorganic geochemistry and XRF shows that TOC content is generally low and predominantly composed of allochthonous material when Cl intensities are low and the intensities of detrital elements (K, Fe, Ti and Si) are high, indicating increased runoff. We interpret these observations as an indication of increasingly oxic conditions in the lake water column due to less stable lake stratification related to increased freshwater inflow which reduces salinity. These conditions are less favourable for the preservation of OM but might also be less favourable for the bacterial and algal community and thereby lead to a decrease in organic productivity. When TOC is high (>4 %), autochthonous bacterial and algal production is increased and organic remains are frequently preserved (Fig. 3.5, 3.7 and 3.8) along with terrestrial plant material. Chlorine intensities are relatively high during these periods, indicating a more saline environment with a stratified lake and anoxic conditions in the hypolimnion.

Palaeoclimatic interpretation

The record of grain size distribution (Partridge 1999a) along with sediment (Bühmann and Elsenbroek 1999), diatom assemblage (Metcalfe 1999) and pollen (Scott 1999a) composition from Tswaing are for the moment the best available records from the site. These data indicate that insolation variability influenced climate in the low latitudes of the southern hemisphere between ~200 and 80 kyr BP. The new records presented in this study confirm this finding (as far as is possible, given the limitations of the age model). Although the uncertainties in the chronology of the sedimentary sequence from Lake Tswaing for the period >48,440 yr BP means that caution is necessary when discussing the timing of palaeoclimatic changes, we will attempt to evaluate our records in the context of other records of palaeoclimatic changes from the subtropics.

For the time period between ~200 and 80 kyr BP, lower amounts of carbonate in the sediments (which we suggest reflects higher summer rainfall) appear to be related to higher summer insolation values at 30°S, which are, in turn, related to precessional maxima (Fig. 3.9 a and b). Analogous to seasonal changes today, increased solar radiation during the southern hemisphere summer season may have increased the intensity of convection associated with the ITCZ in the southern hemisphere, which may have resulted in more intense and/or longer periods of summer rainfall in this area (Tyson 1999). Other records from southern Africa support this interpretation. Brook et al. (1997) presented speleothem records from several caves in Namibia and south-eastern Africa (Fig. 3.1). The records from the caves in south-eastern Africa indicate that conditions were humid 133-131, 111-103, 93-83 and 77-69 kyr BP; periods that correspond reasonably well with intervals of lower TIC content in the sediments of Lake Tswaing, indicating that the climate was relatively wet (Fig. 3.9 a and b). The speleothems from caves in northern Namibia record increased aridity 105-100 and ~60 kyr BP, with maximum aridity between 130 and 112 kyr BP (Fig. 3.9 c). The highest TIC values, which indicate high levels of evaporation, are recorded in the sediments from Lake Tswaing at this time (~46-49 m depth) (Fig. 3.9 a and 3.5). Insolation variability also has a strong influence on local climate in the subtropics of South America, where stalagmites record increases in tropical rainfall during southern hemisphere insolation maxima over the past 210 and 120 kyr (Wang et al. 2004; Cruz et al. 2005). For the northern hemisphere subtropics, precessional influence on monsoonal climates in Africa and Asia is well established (e.g. Clemens et al. 1991; deMenocal et al. 2000; Prell and Campo 1986; Wang et al. 2001). It therefore appears that between 200 and 80 kyr BP changes in precessional parameters affected aridity (as reflected by the amount of carbonate in the sediments) and precipitation (as reflected by the amount of detritus) in southern Africa, as originally proposed by Partridge (1999a).

After 80 kyr BP, the reconstructed rainfall curve, which was based on grain size and the amount of carbonate in the sediments (Partridge 1999a; Fig. 3.9 b), shows lower amplitude changes, in common with the insolation values, although the two records diverge after 60 kyr BP. The rainfall record peaks before the corresponding insolation maximum at ~47 kyr BP is reached, and it is relatively high ~30 kyr BP, when austral summer insolation is at a minimum.

Furthermore, it exhibits a broad minimum from the Last Glacial Maximum until the middle Holocene (~27-5 kyr BP). The latter finding is not corroborated by the XRF-element scans (Fig. 3.6 and 3.9) presented in this study, or by mineralogical investigations (Bühmann and Elsenbroek 1999). These lines of evidence indicate that detrital input from the crater walls due to higher rainfall increased at 73-68, 54-50, 37-35 and 15-10 kyr BP. Studies based on records of dune activity and on lake sediments in the Kalahari also indicate that conditions were relatively humid during these intervals (left frame in Fig. 3.1 and Fig. 3.9 d) (Munyikwa 2005; Thomas et al. 2003; Thomas and Shaw 2002; O'Connor and Thomas 1999; Stokes et al. 1998; Stokes et al. 1997). According to these studies, dunes formed between 36 and 28 kyr BP, indicating that conditions were relatively arid at this time. This is the interval when Cl intensities are highest in the sediments from Tswaing, indicating that this was the most arid period of the last 80 kyr at the site (Fig. 3.6 and 3.9). Arid periods also occurred ~62-58 kyr BP, 50-38 kyr BP, and 28-18 kyr BP. Sediments from Lake Tsodilo (Thomas et al. 2003; K in Fig. 3.1) document lacustrine conditions 40-32 and 18-11 kyr BP, while the lake was dry 32-18 kyr BP. Both the lacustrine intervals correspond with humid phases at Lake Tswaing. In southern Tanzania, recent magnetic susceptibility and pollen data (Garcin et al. 2006a; Garcin et al. 2006b) (G in Fig. 3.1) indicate relatively wet conditions 23-11 kyr BP and relatively dry conditions 45-23 kyr BP. At Alexandersfontein, Butzer et al. (1973) (A in Fig. 3.1) reported that lake levels increased during Termination I, at approximately 16 kyr BP. In caves in south-eastern Africa, Brook et al. (1997) (right frame in Fig. 3.1) identified humid periods with speleothem growth at ~50-43, 36-35, ~23-19 and 14-10 kyr BP (Fig. 3.9 c) and Pickering et al. (in press) (C in Fig. 3.1) dated periods of glacial flowstone growth to 56-42 and 16-10 kyr BP. High resolution stable isotope records from speleothems in Makapansgat Valley, which have good age control for the last 25 kyr BP (Holmgren et al. 2003; M in Fig. 3.1, Fig. 3.10 c, d) and the pollen record from Wonderkrater Spring (Scott and Holmgren 2003; W in Fig. 3.1 and Fig. 3.10 f, g) indicate that conditions were dry and relatively cool 23-22 and 18-17 kyr BP in line with the records from Tswaing. After ~13 kyr BP the Makapansgat record indicates increasingly humid conditions, but a hiatus interrupts the record between 12.5 and 10 kyr BP.

During the early Holocene (10-7 kyr BP), all available southern African archives indicate warm and dry conditions, with peak aridity around 8 kyr BP. During the middle and late Holocene, most of the records indicate gradually more humid conditions (Fig. 3.9 and 3.10). This trend contrasts with that observed in the northern hemisphere subtropics of Africa (e.g. deMenocal et al. 2000; Gasse 2000; Kuper and Kropelin 2006), where conditions appear to have been wet during the early Holocene, with a gradual reduction in rainfall during the middle and late Holocene. These changes are thought to be related to changes in northern hemisphere insolation, which appears to have influenced local climate after Termination I (Gasse 2000; Holmgren et al. 2003 and references therein). Lake Tswaing thus appears to record the synchronous minimum in summer insolation in the southern hemisphere.

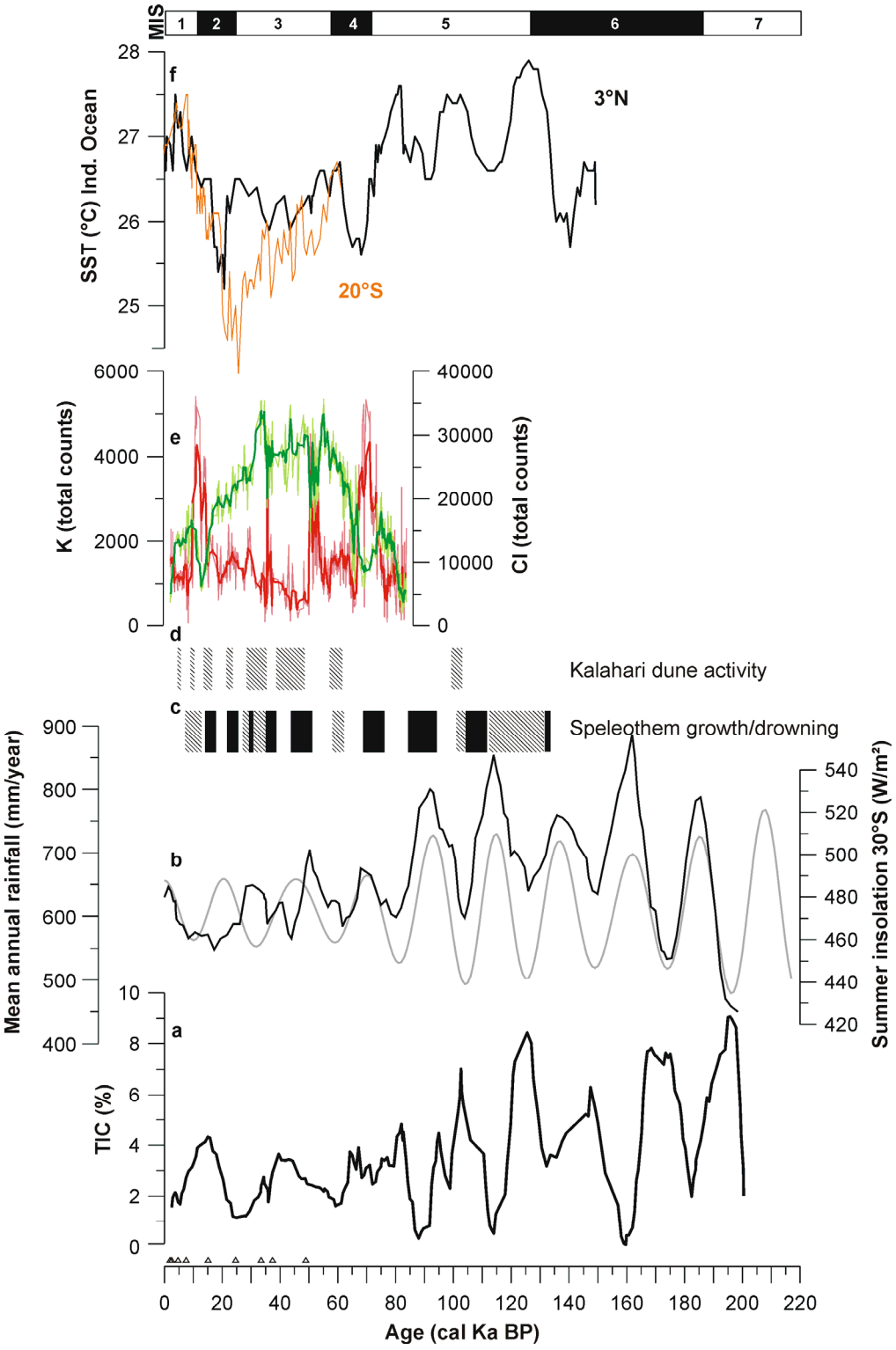

Figure 3.9: Comparison between a) the total inorganic content (TIC, 5-point running average) of the Lake Tswaing sediments for the last 220 kyr BP (this study; triangles indicate calibrated radiocarbon dates); b) reconstructed rainfall for Lake Tswaing (Partridge 1999a) together with local summer insolation (pale grey curve) at 30°S; c) speleothem growth during humid phases in south-east Africa (black) and speleothem growth during more arid phases in presently drowned caves from northern Namibia (striped) (Brook et al. 1997); d) dune activity during arid phases in the northern Kalahari (Munyikwa 2005; O'Connor and Thomas 1999; Thomas and Shaw 2002); e) the Cl (green curve) and K intensities (red curve) of Lake Tswaing sediments (this study); f) the alkenone-derived sea surface temperature (SST) records from the western Indian Ocean cores MD79257 (20°24'S, 36°20'E, orange curve) and MD85674 (3°11'N, 50°26'E, black curve) (Bard et al. 1997). The black and white bar at the top depicts marine oxygen isotope stages (after Bassinot et al. 1994).

The similarities between the record of hydrological change from Lake Tswaing and other records of climate change from southern Africa provide some confidence in our interpretation of the sediment archive and point to similar controls on climate in north-eastern South Africa, the northern Kalahari and southern Tanzania. On a seasonal scale, these areas receive rainfall during southern hemisphere summer, when the ITCZ reaches its southernmost position and easterly winds bring moisture to the subcontinent form the western Indian Ocean (Fig. 3.2) (Tyson 1986; Tyson and Preston-Whyte 2000). It has been shown that Indian Ocean surface temperatures (IOSTs) varied synchronously with northern hemisphere sea and air temeratures over the last 150 kyr BP (Bard et al. 1997) (Fig. 3.9 f and g), indicating that the changes in climate in southern Africa described above, were not caused directly by higher IOSTs. Stokes et al. (1997) proposed that the sea surface temperature (SST) gradient between the western Indian Ocean and the eastern South Atlantic caused wet/dry phases in the Kalahari, suggesting that the Kalahari (and thus Lake Tswaing) experienced wetter conditions when the SST gradient was low. To test this hypothesis, we calculated the SST gradient between the south-eastern Atlantic and the south-western Indian Ocean over the last 21 kyr, using data from Bard et al. (1997) and Kim et al. (2002) (Fig. 3.10 a). The SST gradient decreases substantially between 18 and 17 kyr BP, just before the records of the intensities of elements related to detrital input increase in the sediments from Tswaing, indicating more humid conditions and supporting the hypothesis that changes in the SST gradient may have affected conditions at Tswaing by determining the inland penetration of tropical easterly air masses. The fact that intensities of detrital elements decrease during the Holocene, when the SST gradient is still low, might be explained by low summer insolation during this period. Modelling studies indicate that present day rainfall over south-eastern Africa is sensitive to changing SSTs in the south-western Indian Ocean (Reason 2001; Reason 2002; Washington and Preston 2006), but it is not possible to test whether this connection exists on glacial/interglacial time scales, due to a lack of records from the Indian Ocean.

An alternative explanation, which has been proposed based on palaeoclimatic records from a well-dated core from Lake Masoko in southern Tanzania (G in Fig. 3.1), is that the ITCZ was displaced southward during the Younger Dryas and the Last Glacial Maximum, increasing precipitation at Lake Masoko ~23-19 kyr and ~15-11.7 kyr BP (Garcin et al. 2006a, Garcin et al. 2006b); a phenomenon that has also been described in archives from Central America (Cruz et al. 2005; Haug et al. 2001; Wang et al. 2004) and subtropical Asia (Wang et al. 2001). Modelling results confirm that cold periods in the northern hemisphere that are linked to perturbations in the meridional overturning circulation can induce a southward shift in the position of the ITCZ (Chiang et al. 2003; Zhang and Delworth 2005). The humid period recorded in Lake Tswaing sediments at 15-10 kyr BP might correspond to the humid phase 15-11.7 kyr BP in the Lake Masoko record and may represent a response to the Younger Dryas in the northern hemisphere, but there is no clear response to earlier millennial-scale cooling events such as Heinrich events known from northern hemisphere climate archives (e.g. Hemming 2004).

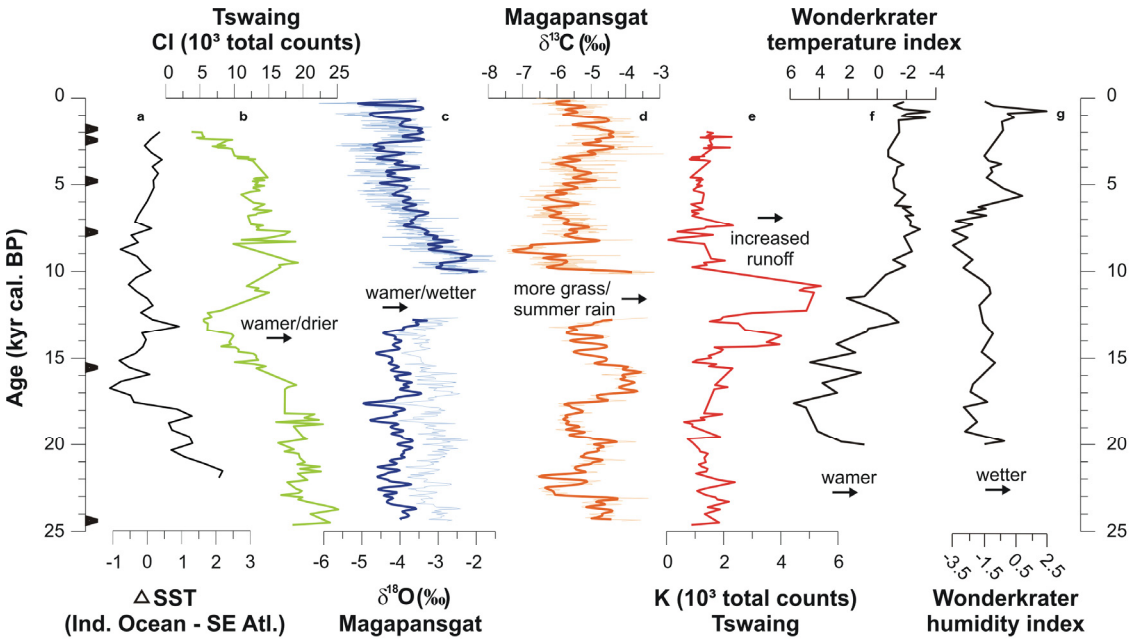

Figure 3.10: Comparison between a) the calculated difference between Indian (Bard et al. 1997) and south-east Atlantic alkenone-derived SSTs (Kim et al. 2002), b) the Cl intensities from Lake Tswaing sediments, c) the $\delta^{18}O$ and the d) $\delta^{13}C$ records from the Makapansgat Valley (24°8.824'S, 29°10.371'E) (Holmgren et al. 2003), e) the K intensities from Lake Tswaing sediments, f) the temperature and g) the humidity indices derived from the Wonderkrater pollen record (24°25.806'S, 28°44.626'E) (Scott and Holmgren 2003) for the last 25 kyr BP. Triangles indicate calibrated radiocarbon ages.

CONCLUSIONS

The study of the organic matter present in the sediments from Lake Tswaing using organic petrology and Rock-Eval pyrolysis, in combination with detailed geochemical analysis of the bulk sediment (TIC, TOC, TN and high-resolution XRF-scanning), provides new insights into changes in this lake system during the last ~200 kyr BP. During periods with higher precipitation and increased detrital input from the catchment, lower water column stability, and oxidising conditions at the lake bottom, the preservation of autochthonous and allochthonous OM decreased. In contrast, when higher Cl intensities indicate more saline conditions, allochthonous and autochthonous OM are well preserved, probably because the lake was stratified for significant periods of time, creating anoxic conditions in the bottom waters. The interpretation of these records in terms of palaeoclimatic change corroborates the findings that precessionally-controlled insolation had an important influence on the hydrological cycle in southern Africa between 200 and 80 kyr BP and the Holocene (Bühmann and Elsenbroek 1999; Partridge 1999a; Scott 1999a). During the last glacial period, however, processes that are presumably linked to changes in the position of the ITCZ and/or changes in ocean circulation appear to dominate over the influence of insolation, leading to more humid conditions at 73-68 kyr, 54-50 kyr, 37-35 kyr and 15-10 kyr BP. To better constrain the underlying processes

responsible for these changes, the chronology of sediments from Lake Tswaing must be improved and high-resolution records from the surrounding oceans are needed.

ACKNOWLEDGEMENTS

We acknowledge the GFZ for funding this work and the coring and Jörg Negendank for the enthusiastic support for this second coring campaign. We further thank Helge Arz, Klaus Zink, Gerald Haug, Brian Horsfield and Maarten de Wit for helpful discussions. Tim Partridge is especially thanked for useful information about the site and the coring as well as for all his support in field trips to and sampling campaigns at Lake Tswaing. We acknowledge Vera Lukies (Bremen) and Rik Tjallingii (now at Kiel University) for technical support and discussion and Dr Stephanie de Villiers and an anonymous reviewer for constructive comments on our manuscript. This is Inkaba yeAfrica contribution 20.

4. Biomarker and stable carbon isotope analyses of sedimentary organic matter from Lake Tswaing: Evidence for deglacial wetness and early Holocene drought from South Africa

Iris Kristen[1], Heinz Wilkes[1], Andrea Vieth[1], Klaus-G. Zink[1,2], Birgit Plessen[1], Jo Thorpe[3], and Hedi Oberhänsli[1]

[1]*GeoForschungsZentrum Potsdam (GFZ Potsdam), Potsdam, Germany*
[2]*now at GNS Science, Lower Hut, New Zealand*
[3]*formerly at Department of Geography, University College London, London, Great Britain*

Accepted for publication in: *Journal of Paleolimnology*

ABSTRACT *Comparing the organic matter (OM) composition of modern and past lake sediments contributes to the understanding of changes in lacustrine environments over time. We investigate modern plant and lake water as well as modern and ancient sediment samples from the Tswaing Crater in South Africa using biomarker and stable carbon isotope analyses (SCIA) on bulk OM and specific biomarker compounds. The characteristic molecular markers for higher land plants (predominantly C3-type deciduous angiosperms) in Lake Tswaing are long-chain n-alkanes (n-$C_{27,29,31,33}$), n-alkanols (n-C_{28+30}), stigmasterol, β-sitosterol, β-amyrin, α-amyrin and lupeol. The C_{17} n-alkane, tetrahymanol, gammaceran-3-one and C_{29} sterols dominate autochthonously produced OM. By comparing SCIA on bulk OM and the characteristic biomarkers, we follow the modern carbon cycle in the crater environment and find indications for methanogenic activity in the lake from isotopically depleted moretene. A comparative study of core sediments reveals changes in the terrestrial (C3 vs. C4) and aquatic bioproductivity and allows insights into the variability of the carbon cycle under the influence of changing climatic conditions for the time from the end of the last glacial (Termination I) to the late Holocene, c. 14,000–2,000 calibrated years before present (yr BP). The most pronounced changes occur in the aquatic realm at c. 10,000 yr BP and 7,500 yr BP when our results imply climate swings from more humid to more arid and to gradually more humid conditions again, which can be related to a shift in the position of the Inter-Tropical Convergence Zone or to changes in the tropical atmosphere-ocean interaction. Long-chain alkenones (LCAs) have been identified in ancient lake sediments from Africa for the first time. They occur in samples older than 7,500 yr BP and their distribution (dominance of C_{38} and of tri- over tetra-unsaturated LCAs) is distinctly different from other published records suggesting a to date unknown source organism.*

INTRODUCTION

The sedimentary record from Lake Tswaing (formerly "Pretoria Saltpan") has been studied for about 20 years. Timothy C. Partridge was the first to discover the potential of this record as a climate archive and initiated the first scientific coring campaign in 1988/1989. The work focused predominantly on inorganic parameters (grain size, mineralogy, geochemistry) and added several new southern African palaeoclimate records (e.g., Partridge 1993; Partridge et al. 1997; Partridge 1999b). Pollen, although absent over wide parts of the profile, was the only investigated organic parameter besides diatoms (Scott 1999a). The analysis of sedimentary organic matter (OM), however, can provide a variety of insights into past ecosystems and environments, e.g., into bioproductivity, circulation conditions, and the composition of the surrounding vegetation (Meyers 1997; Meyers and Lallier-Vergès 1999). In a previous study, organic petrology and Rock-Eval pyrolysis were used to investigate the nature and origin of the OM in Lake Tswaing sediments over the last c. 200,000 yr BP and elucidated intervals of good OM preservation with high input from autochthonous sources (filamentous algae or cyanobacteria and *Botryococcus*) (Kristen et al. 2007).

In this study we report on detailed biomarker analyses of the soluble OM to understand changes in the ecosystem of the Tswaing Crater since the end of the last glacial. The combination of biomarker analyses, analyses of stable carbon isotope ratios of bulk OM, and compound-specific stable carbon isotope ratios of plant and sediment material allow a comprehensive description of the present-day ecosystem of the Tswaing Crater and its carbon cycle. With the subsequent investigation of a sedimentary sequence covering the time c. 14,000–2,000 yr BP, we aim to trace changes in the past ecosystem and the carbon cycle over time and evaluate variations in the light of regional and global climate change.

Similar approaches with a direct comparison of modern and past ecosystems are rare for Africa (e.g., Rommerskirchen et al. 2003; Rommerskirchen et al. 2006). Yet, with increasing numbers of climate studies the number of studies with contradictory results also increases (e.g., Castañeda et al. 2007; Garcin et al. 2006a), highlighting the need for a solid understanding of the investigated parameters and the specific conditions at the investigated site. Organic geochemical studies from Africa to date have focussed predominantly on past vegetation and palaeoclimate changes, on tropical Africa, and on the last glacial/interglacial cycle. Investigations on the lipid content (*n*-alkanes, *n*-alkanols, *n*-alkanoic acids) and the compound-specific or bulk organic stable carbon isotopic composition (Ficken et al. 1998; Ficken et al. 2000; Huang et al. 1999b; Street-Perrott et al. 2004), on lignin phenols (Huang et al. 1999a), combined with investigations on pollen and grass cuticles (Ficken et al. 2002; Wooller et al. 2003) have revealed that during the last glacial period C4 grasses dominated over C3 plants in the neighbourhood of lakes at Mount Kenya (East Africa). Opposite conditions prevailed during the early Holocene. This vegetation change is interpreted as a response to the combination of lower atmospheric CO_2-concentrations and reduced precipitation during glacial times and vice versa during the early Holocene. Similar hydrological conditions are reported from studies on sedimentary OM from the Ethiopian Lake Tilo (only Holocene) (Lamb et al. 2004) and from

Lake Victoria (Talbot and Lærdal 2000). The latter experienced several abrupt lake level changes from the Last Glacial Maximum (LGM), when the lake was desiccated, to more stable Holocene conditions. Similarly, Lake Malawi reveals oxidative conditions in the deeper lake during pronounced lowstands dated to LGM and c. 11,800–10,000 yr BP (Filippi and Talbot 2005). Most of the referred studies on biomarkers assume the general validity of published data to assign specific OM sources, variable OM input and depositional conditions. However, lakes are individual systems with specific geological, limnological, environmental and climatic conditions and responses, which condense in the OM. Accordingly, this paper deals with (1) a detailed study of the present-day ecosystem of the Tswaing Crater and we use this data (2) to evaluate changes recorded in the sedimentary OM covering the time c. 14,000–2,000 yr BP. Special attention is thereby given to the influence of climate on the ecosystem variability.

STUDY SITE

The 1.13 km-wide crater Tswaing is located approximately 40 km northwest of Pretoria at an altitude of 1045 m above sea level (asl). The crater was formed in granitic bedrock by a meteorite impact, which has been dated to 220±52 kyr BP using fission-track dating (Reimold et al. 1992). The crater walls reach 119 m above the crater floor and 60 m above the adjacent surface. They form a closed basin with no surface in- or outflow and a lake in the centre. At present, the lake is 2 to 3 m deep, alkaline, with a pH around 10, and hypersaline (up to 250–300‰ in bottom waters). Located in the austral summer rainfall zone, it receives rainfall and groundwater inflow between October and April (400–750 mm/a) when the Inter-Tropical Convergence Zone (ITCZ) reaches its southernmost position. During winter time the climate is dry and according to monitoring data collected during 28 months the lake shrinks by 20–25% (Ashton and Schoeman 1983). The high salinity causes the water body to be constantly stratified and thus anoxic below 50 cm water depth; during night-time, oxygen-deficiency prevails throughout the whole water column (Ashton 1999). These conditions, together with the high alkalinity of the lake water body, effectuate microbes and cyanobacteria to be the dominant organisms. A few diatom species inhabit areas where fresh groundwater seeps into the lake. This groundwater inflow, together with rainfall, represents the natural source of freshwater. Artesian boreholes that reach down to sandy aquifers below the carbonaceous lacustrine facies provide additional leak inflow since the 1970s (Ashton and Schoeman 1983; Partridge et al. 1993). Monthly mean maximum and minimum air temperatures in the region range from 14.2°C to 35.2°C and 3.6°C to 15.6°C, respectively (Ashton 1999). The vegetation around the crater today is classified as Mixed and Sourish-Mixed Bushveld assemblages and consists of grassland mixed with deciduous trees and shrubs dominated by *Acacia* and *Combretum* species (Acocks 1953) (Fig. 4.1). While trees and bushes are predominantly C3 plants, grasses in this dry, summer-rainfall area are dominated by C4 species (Scott 2002).

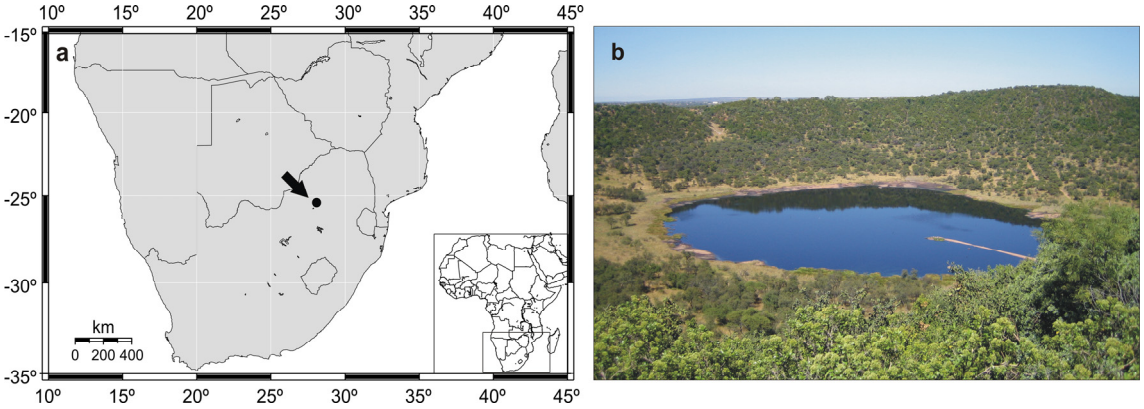

Figure 4.1: a) Map of southern Africa with the location of Lake Tswaing (arrow, 25°24'30'' S, 28°04'59'' E); b) View towards the south across the Tswaing Crater in April 2006 with present-day vegetation. Note the change in the dominant species of trees/bushes app. half way up the slope: *Acacia* species dominate the lower slope, *Spirostachys* and *Combretum* dominate the upper slope, grasses and reeds (*Typha* and *Cyperaceae*) along the shore (T. C. Partridge, pers. commun.).

MATERIAL AND METHODS

Sample preparation, extraction and fraction separation

During May 2005 and April 2006 we sampled the dominant plant species around the crater lake and lake water, bacterial mats and sediments within the lake (list of organisms see Table 4.2). Only leaves were used for the bulk and lipid analyses of the modern plant material. We recovered 14 samples from between 2 and 7 m core depth from a core taken in 2001/2002. The core samples average over 5 to 10 cm intervals to assure similar time coverage for all (c. 150 yr). With exception of the water samples, all samples were freeze-dried, ground and homogenised before extraction. The water samples were extracted using the method of Bligh and Dyer (1959), sediment and plant samples were extracted by accelerated solvent extraction or flow-blending (Radke et al. 1978) using a mixture of dichloromethane and methanol (99/1, v/v) as a solvent. The extracts were separated by medium-pressure liquid chromatography (Radke et al. 1980) into fractions of aliphatic/alicyclic hydrocarbons, aromatic hydrocarbons and nitrogen, sulphur and oxygen (NSO) compounds. Further separation of the NSO compounds into a neutral NSO compound and a more polar fatty acid fraction was achieved following a modified method of McCarthy and Duthie (1962). Trimethylsilylation of the neutral NSO compound fraction was carried out using MSTFA (N-Methyl-N-(trimethylsilyl)trifluoroacetamide).

Gas chromatography (GC-FID), gas chromatography-mass spectrometry (GC-MS) and isotope ratio monitoring-gas chromatography-mass spectrometry (IRM-GC-MS)

Identification and quantification of individual compounds within the aliphatic hydrocarbon and the neutral NSO compound fraction was achieved using GC and GC-MS techniques. GC analysis was performed on an Agilent 6890 Series instrument equipped with a cold injection system and an Ultra 1 methyl siloxane fused silica capillary column (50 m length, 0.2 mm inner diameter (ID), 0.33 µm film thickness (FT)). Helium was used as carrier gas, and the temperature of the GC oven was programmed to an initial temperature of 40°C (hold 2 min), a heating rate of 5°C/min, and a final temperature of 300°C, held isothermal for 65 min. The injector temperature rose from initially 40°C to 300°C (hold 3 min) at a rate of 700°C/min. The MS-coupled GC Thermo GC Ultra was equipped with a Thermo PTV injection system and a SGE BPX5 fused silica capillary column (50 m length, 0.22 mm ID, 0.25 µm FT). Helium was used as carrier gas, and the temperature of the GC oven was programmed from 50°C (hold 1 min) to 310 or 350 °C at a rate of 3°C/min, followed by an isothermal phase of 30 min. The injector temperature was programmed from 50 to 300°C at a rate of 10°C/s. A DSQ Thermo Finnigan Quadrupole MS, operating in the electron impact ionisation mode (EI) at 70 eV, was used for compound identification. Full scan mass spectra were recorded from *m/z* 50 to 600 (hydrocarbons) or 650 (neutral NSO compounds) at a scan rate of 2.5 scans/s. Compound identifications are based on comparison of mass spectra to those reported in the literature, in the NIST mass spectral database, and on comparison with authentic standards.

The carbon isotopic composition of saturated hydrocarbons was measured using IRM-GC-MS. The IRM-GC-MS system consisted of a GC unit (6890N, Agilent Technology, USA) connected to a GC III combustion device coupled via open split to a MAT 253 mass spectrometer (ThermoFisher Scientific, Germany). Three µl of the aliphatic hydrocarbon fraction were injected to the programmable temperature vaporisation inlet (PTV, Agilent Technology, USA) with a septumless head, working in split/splitless mode. The injector was held at a split ratio of 1:1 and an initial temperature of 230°C. With injection, the injector was heated to 300°C at a programmed rate of 700°C/min and held at this temperature for the rest of the analysis time. The aliphatic hydrocarbon fractions were separated on a fused silica capillary column (HP Ultra 1, 50 m length, 0.2 mm ID, 0.33 µm FT, Agilent Technology, Germany). The temperature program started at 40°C and was then increased to 300°C at a rate of 3°C/min, held there for 25 min. Helium, set to a flow rate of 1.0 ml/min, was used as carrier gas. The organic compounds in the GC effluent stream were oxidised to CO_2 in the combustion furnace held at 940°C on a CuO/Ni/Pt catalyst. CO_2 was transferred on line to the mass spectrometer to determine carbon isotope ratios. All samples were measured in triplicate with a standard deviation of ≤0.5‰ for most of the compounds and samples. The isotopic ratios (also $\delta^{13}C_{org}$, see next paragraph) are given in delta notation relative to Vienna PeeDee Belemnite (VPDB).

$$\delta_{sample}(‰) = [(({}^{13}C/{}^{12}C)_{sample} / ({}^{13}C/{}^{12}C)_{standard})-1]*1000$$

Analysis of total organic carbon content (TOC) and stable carbon isotope ratios of bulk organic matter ($\delta^{13}C_{org}$)

Determinations of the TOC and $\delta^{13}C_{org}$ of the sediment were carried out on decalcified samples. Approximately 3 mg of sediment were weighed in Ag-capsules, treated with 20% HCl, heated for 3 h at 75°C, and finally wrapped up in the Ag-capsules. For the plant material analyses, about 2 mg of dried and homogenized material was wrapped up in tin-capsules. The carbon content and $\delta^{13}C$ values were measured using a CarloErba NC2500 elemental analyzer coupled via a ConFlowIII interface with a DELTAplusXL mass spectrometer (ThermoFisher Scientific, Bremen). The samples were combusted under excess oxygen and the released gases were flushed by a helium carrier-gas flow into the IRMS. The isotopic ratios are given in delta notation relative to VPDB. The calibration was performed using isotopic standards (USGS24, CH-7) and proven with a soil reference sample (Boden2). The precision for replicate analyses is 0.2% for TOC and better than 0.2‰ for $\delta^{13}C$.

Chronology

The age model of the profile is based on nine radiocarbon ages determined by the Poznań Radiocarbon Laboratory (Table 4.1). Three of the radiocarbon ages are from microscopic charcoal fragments, and the others are on bulk OM. The ages show a regular increase with depth. For details on the litho- and chronostratigraphy we refer to Kristen et al. (2007).

Table 4.1: Radiocarbon ages for the Lake Tswaing sediment core from 2001/2002.

original depth (m)	corrected depth (m)	Lab no.	^{14}C age (yr BP)	Std. dev. ±	calibrated Age (yr BP)	± 2σ	material
1.595-1.605	0	Poz-15663	3095	35	1810*[1]	91	TOC
2.21-2.24	0.61-0.64	Poz-15669	3675	35	2538*[1]	175	TOC
4.005-4.065	2.405-2.465	Poz-12211	4305	30	4837*	35	charcoal
5.23-5.24	3.63-3.64	Poz-15664	7090	50	7850*	115	TOC
7.36-7.38	5.54-5.56	Poz-15665	13130	70	15550*	356	TOC
9.785-9.795	7.695-7.705	Poz-15667	20410	130	24440*	405	TOC
11.835-11.885	9.705-9.755	Poz-12212	28500	600	33220**	1072	charcoal
16.990-17.020	14.790-14.820	Poz-12213	31900	800	37390**	1120	charcoal
19.385-19.395	17.195-17.205	Poz-15668	44800	2100	48440**	2559	TOC

*Calib 5.0.2 after McCormac et al. (2004) and Reimer et al. (2004)

**CalPal (calibration curve CalPal2005_SFCP; http://www.calpal.de)

[1] including 1,150 yr reservoir correction (mean age offset of recent lake sediments; Partridge *et al.* 1997)

RESULTS AND DISCUSSION

Characterisation of the present-day environment based on biomarkers and stable carbon isotope investigations

Monitoring of modern lake systems is an important prerequisite of lake-based palaeoclimatology as it helps to understand the occurrence and preservation of specific constituents of the OM and the parameters based on their relative abundance in individual lake basins. In the next paragraphs, we present the components of the modern carbon cycle and its imprint on sediments of Lake Tswaing under modern climatic conditions, aiming to provide a solid basis for the interpretation of long-term geochemical records from this site.

Biomarker composition of lake microorganisms

The present-day aquatic ecosystem is dominated by cyanobacteria (Ashton 1999), a typical inhabitant of alkaline lakes (Grimalt et al. 1991). Samples of floating cyanobacterial mats are identified as *Oscillatoria* sp. by marker-pigments oscillaxanthin, myxoxanthophyll und echinenon (S. Fietz, pers. commun.). The aliphatic hydrocarbon fraction of *Oscillatoria* sp. consists predominantly of the C_{17} *n*-alkane with minor contributions of C_{15} and C_{16} *n*-alkanes and C_{17} *n*-alkenes (Fig. 4.2 a, Table 4.2). In the neutral NSO compound fraction of these floating cyanobacterial mats, phytol (II; roman numerals refer to structures of biomarkers given in App. H) is the overall dominant compound (Table 4.2). This observation corroborates earlier studies on cyanobacteria (e.g., Grimalt et al. 1991; Rontani and Volkman 2005; Shiea et al. 1991) and is in agreement with the conclusion of Volkman (2005) that most cyanobacteria are not able to produce sterols.

In the very shallow lake areas, benthic microbial mats reveal an aliphatic hydrocarbon fraction that is dominated by C_{17} *n*-alkane and -alkene similar to the floating cyanobacterial mats. Both lipids have been described as abundant compounds in benthic mat-forming cyanobacteria (Boon et al. 1983; Pearson et al. 2007; Rontani and Volkman 2005; Thiel et al. 1997b). In the neutral NSO compound fraction, the benthic microbial mats differ clearly from the floating cyanobacterial matter. Tetrahymanol (Xb), squalene (I), and phytol dominate a complex mixture of saturated and unsaturated steroidal alcohols with 27 to 29 carbon atoms (Fig. 4.2 f). Tetrahymanol, squalene and phytol also prevail in extracts of water samples from Lake Tswaing from c. 30 cm water depth (Table 4.2). These compounds are therefore interpreted to originate from either benthic microorganisms or microorganisms that thrive in the deeper water column. Phytol arises in most cases from the degradation of chlorophylls (Rontani and Volkman 2003). It is therefore an ubiquitous compound in aquatic environments where it can result from autochthonous and allochthonous OM. Tetrahymanol has been frequently

identified in marine ciliates (Harvey and McManus 1991), but was also found in lake waters (Grimalt et al. 1991; Pearson et al. 2007; Thiel et al. 1997a), in coastal bacterial mats (Rontani and Volkman 2005), and in the phototrophic bacterium *Rhodopseudomonas palustris* (Kleemann et al. 1990). As Harvey and McManus (1991) documented that tetrahymanol is only produced by ciliates when dietary sterol supply is poor or absent, we attribute the presence of tetrahymanol to the activity of the photosynthetic sulphur bacterium *Rhodopseudomonas palustris*, since sterols are abundant in Lake Tswaing. This organism is known to be common in water and soils, and to be metabolically versatile; it is able to thrive in the absence or presence of oxygen and to fix nitrogen (Larimer et al. 2003) – abilities, that possibly favour its growth in Lake Tswaing under the prevailing aquatic conditions. Oxidation of tetrahymanol results in gammaceran-3-one (Xa) (Thiel et al. 1997a), which is present in small amounts in the samples from benthic mats and deeper lake waters, and commonly occurs in the sediments (see below). Squalene is the biosynthetic precursor of steroids in higher organisms (Tchen and Bloch 1957) and of hopanoids in bacteria (Volkman 2005). Boon et al. (1983) observed squalene in cyanobacterial mats from Solar Lake, but it is also reported as a major component in halophilic archaea and methanogens (Rontani and Volkman 2003; Tornabene et al. 1979). We consider it being of predominantly bacterial origin in Lake Tswaing, although neither a contribution of halophilic archaea, nor a contamination of the mat by surrounding higher plants, in which squalene is also present (see next paragraph), can be ruled out. The sterols of the microbial mats show compositional patterns dominated by unsaturated C_{29} compounds (Fig. 4.2 f, Table 4.2). Most of the identified compounds are known from cyanobacterial mats as well as from other microorganisms such as marine phytoplankton (Boon et al. 1983; Grimalt et al. 1991; Volkman 1986 and references therein). They have also been reported from other saline lake sediments (Pearson et al. 2007). Most likely, a multitude of microorganisms contribute to the observed signal, and also input from land plants is likely to occur as indicated by the presence of β-sitosterol (see next paragraph).

Biomarker composition of macrophytes and higher land plants

Macrophytes along the lake shore comprise predominantly *Typha angustifolia* and *Cyperacea* sp. *Typha angustifolia* exhibits a clear odd carbon number preference of the *n*-alkanes maximising at *n*-C_{31} (Fig. 4.2 b, Table 4.2), whereas *Cyperacea* sp. contains very few *n*-alkanes with maxima at *n*-C_{23} and *n*-C_{29} (Table 4.2). The surrounding higher land plant assemblage along the crater wall is dominated by grasses and different species of *Acacia, Combretum, Sclerocarya* and *Zizyphus* (Fig. 4.1). The aliphatic fraction of leaf tissue from these plants contains predominantly C_{27} to C_{33} long-chain *n*-alkanes with a strong odd carbon number preference (Fig. 4.2 a-d, Table 4.2) and accordingly agree with earlier observations from other higher land plant studies (e.g., Eglinton and Hamilton 1963; Meyers 2003). The individual land plant species show differing distribution patterns of *n*-alkanes with *Acacia tortilis* (Fig. 4.2 c), *Acacia karoo*, *Acacia robusta* and *Sclerocarya birrea* maximising at *n*-C_{29}, *Combretum*

apiculatum maximising at *n*-C_{31}, *Zizyphus mucronata* maximising at *n*-C_{27} and grasses exhibiting two maxima at *n*-C_{27} and *n*-C_{33}.

The neutral NSO compound fraction of *Typha angustifolia, Acacia robusta,* and *Acacia karoo* is dominated by α-tocopherol (vitamin E) (III), a compound that is abundant in higher land plants, cyanobacteria, and micro- and macroalgae (Rontani and Volkman 2005). It is present as a major constituent in most of the investigated modern plant and water samples (Fig. 4.2 f-h). Stigmasterol (24-ethylcholesta-5,22-dien-3β-ol) (IXb), β-sitosterol (24-ethylcholest-5-en-3β-ol) (Vc), β-amyrin (olean-12-en-3β-ol) (XIV), α-amyrin (urs-12-en-3β-ol) (XII), lupeol (lup-20(29)-en-3ß-ol) (XVI) and germanicol (olean-18-en-3ß-ol) (XV) are characteristic triterpenoidal alcohols in the investigated higher land plants and macrophytes (Fig. 4.2 g, h; Table 4.2). The occurrence of these compounds corresponds to other studies on lacustrine systems (e.g., Meyers 1997; Pearson et al. 2007; Volkman 2005) where they have been described as typical constituents of vascular plants. Phytol and squalene, major compounds in the autochthonous lake organisms (see above), are also present in the investigated higher land plants and macrophytes. In *Zizyphus mucronata* and *Combretum apiculatum*, squalene is the dominant compound. The C_{28} and C_{30} *n*-alkanols are the only straight-chain alcohols that are abundant in the modern leaf material (Table 4.2).

Biomarker composition of the sediments

The composition of the extractable OM of modern Lake Tswaing sediments corresponds to a mixture of the above described individual sources (lake organisms, macrophytes, and higher land plants). The aliphatic fraction consists predominantly of odd-numbered *n*-alkanes and reveals a bimodal distribution with maximum amounts of *n*-C_{17} and *n*-C_{31}, which reflects the contribution of autochthonous and terrestrial sources, respectively (Fig. 4.2).

Phytane, phytenes and moretene (XIII), identified as additional compounds in the sediments, have not been detected in any of the investigated modern organisms or water samples from the Tswaing Crater. However, the occurrence of phytane and phytenes has been described from other alkaline (Grimalt et al. 1991) and hypersaline (Boon et al. 1983) environments. Phytane and phytenes are often interpreted as products of the phytol side-chain of chlorophyll-*a* that form during early diagenesis in anoxic environments (Tissot and Welte 1984). The frequent occurrence of phytol in modern organisms from the Tswaing Crater together with the prevailing anoxic conditions in the deeper water column would support such an interpretation. However, this pathway has not been proved so far (Grossi et al. 1996; Rontani and Volkman 2003). In methanogenic archaea, phytane and phytenes are unambiguously detected (Tornabene et al. 1979). Additionally, the formation of phytenes and phytadienes has been reported from anaerobic biodegradation of phytol by sulphate-reducing bacteria (Grossi et

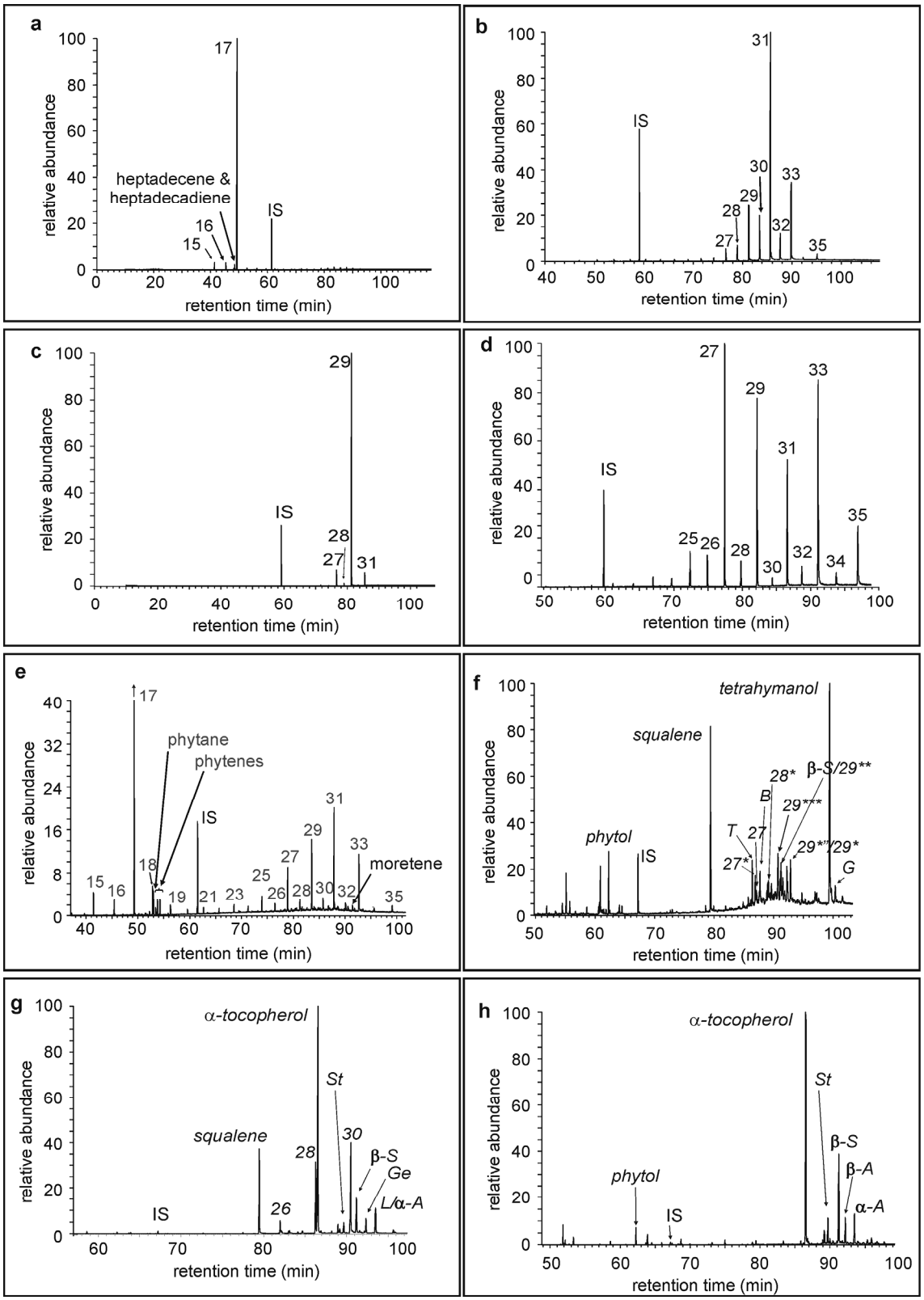

Figure 4.2: TIC chromatograms of modern plant and sediment samples from the Tswaing Crater (IS = internal standard, for other labels see Table 4.2); a) aliphatic hydrocarbon fraction of planktonic cyanobacteria (*Oscillatoria* sp.); b) aliphatic hydrocarbon fraction of *Typha angustifolia*; c) aliphatic hydrocarbon fraction of *Acacia tortilis*; d) aliphatic hydrocarbon fraction of unknown grass; e) aliphatic hydrocarbon fraction of modern lake sediment; f) neutral NSO compound fraction of microbial mat sample; g) neutral NSO compound fraction of *Acacia karoo*; h) neutral NSO compound fraction of *Typha angustifolia.*

Table 4.2: Concentrations of abundant biomarkers identified in modern samples from the Tswaing Crater.

Compounds	abbr. (Fig. 4.2)	structure in App. H	Sample no. [1] [concentrations in µg/g TOC if not quoted otherwise] 1	2	3[2]	4[2]	5	6	7	8	9	10	11	12	13	14
C_{15} *n*-alkane	15		9	n.d.	n.d.	1.1										62
C_{16} *n*-alkane	16		46	n.d.	n.d.	1.0										19
C_{17} *n*-alkene			141	n.d.	n.d.	0.26										5
C_{17} *n*-alkane	17		1741	n.d.	n.d.	20										652
C_{18} *n*-alkane	18		24	n.d.	n.d.	0.9										48
C_{19} *n*-alkane	19		4	n.d.	n.d.	0.35										
C_{25} *n*-alkane	25		6	n.d.	n.d.	0.23	65	8	26		11	11	9	7	58	
C_{27} *n*-alkane	27		9	n.d.	n.d.	0.26	447	25	212	70	25	20	41	7	371	
C_{29} *n*-alkane	29		14	n.d.	n.d.	0.26	1300	85	1666	23	58	50	157	12	282	
C_{31} *n*-alkane	31		14	n.d.	n.d.	0.27	693	64	178		30	287	497		204	
C_{33} *n*-alkane	33		7	n.d.	n.d.		270	16				168	267		439	
C_{35} *n*-alkane	35			n.d.	n.d.										200	
1-Octadecanol			18												n.d.	32
1-Icosanol														71	n.d.	
1-Hexacosanol	*26*							232		147	71				n.d.	
1-Octacosanol	*28*		5		49	0.11	1236	1770	9	1527	418			221	n.d.	
1-Triacontanol	*30*			3	3	0.10		3071	15	2365	731			3014	n.d.	
3,7,11,15-Tetramethyl-hexadecenol (Phytol)		II	261	28	1.3	1.9	144	53		57			184	45	n.d.	1680
Squalene		I	38	87	70	4	92	175		3264	522	1208		65	n.d.	
α-Tocopherol	*T*	III	13	23	9	1.2	497	2735		625	1802	850	3787	578	n.d.	
Cholest-5-en-3β-ol	*27**	Va	18	20		0.53									n.d.	
5α (H)-Cholestan-3β-ol	*27*	IV		5		0.10									n.d.	
24-Methyl-cholesta-5,22-dienol (Brassicasterol)	*B*	IXa		15		0.35									n.d.	
C_{29} Cholestanol				7		0.24									n.d.	
24-Methylcholest-5-en-3b-ol	*28**	Vb		11		0.33		235						496	n.d.	
24-Ethylcholesta-5,22-dien-3β-ol (Stigmasterol)	*St*	IXb		14	8	0.42		479		273	76	52	428	1875	n.d.	
24-Ethyl-cholesta-5,7,22-trien-3β-ol	*29****	VIII		53		3									n.d.	
24-Ethylcholest-5-en-3β-ol (β-Sitosterol)	*β-S*	Vc		13	12	0.54	414	1779		420	288	244	1600	2015	n.d.	
24-Ethylcholesta-7,22-dien-3β-ol	*29***	VII		28		0.48									n.d.	
4,24-Dimethyl-cholest-5-en-3β-ol/ 24-Ethyl-cholest-7-en-3β-ol	*29*"/ 29**	XI VI		32		1.2									n.d.	
Olean-18-en-3β-ol (Germanicol)	*Ge*	XV									115				n.d.	
Olean-12-en-3β-ol (β-Amyrin)	*β-A*	XIV			6								450		n.d.	
Urs-12-en-3β-ol (α-Amyrin)/ Lup-20(29)-en-3β-ol (Lupeol)	*α-A L*	XII XVI			46						232		543		n.d.	
Tetrahymanol		Xb	46	224		12									n.d.	55
Gammaceran-3-one	*G*	Xa				0.64										

[1] 1=bacterial mat (solid), 2=bacterial mat (fluid), 3=water (surface), 4=water (~30cm), 5=*Sclerocarya* ("caffra") *birrea*, 6=*Acacia robusta*, 7= *Acacia tortilis*, 8=*Zizyphus mucronata*, 9=*Acacia karoo*, 10=*Combretum apiculatum*, 11=*Typha angustifolia*, 12=*Cyperaceae*, 13=grass (*Digitaria* sp.), 14=floating cyanobacteria (*Oscillatoria* sp.)

[2] concentration in µg/mg extractable lipids

n.d.=not determined

al. 1998). Both processes can contribute to the phytenes observed in modern anoxic sediments from Lake Tswaing. Sulphate reduction as a prominent process in Lake Tswaing was already proposed by Ashton (1999) who measured a strong gradient in sulphate concentration from 300 mg/l in 25 cm water depth to 0.5 mg/l in 1 m water depth. The strong odour of H_2S from water samples below 0.5 m water depth supports this interpretation. The hopanoid biomarker moretene (17β(H)-moret-22(29)-ene or isohop-22(29)-ene) has been rarely reported in the literature. It is structurally closely related to diploptene which has been more intensively studied. Diploptene has been related to bacterial sources including purple non-sulfur bacteria, acetic acid bacteria, nitrifying/denitrifying bacteria, methylo- and methanotrophic bacteria and also cyanobacteria (Elvert et al. 2001; Ourisson et al. 1987; Sinninghe Damsté et al. 2004). We did not observe diploptene in the modern environment of Lake Tswaing but in deeper parts of the sediment profile (Kristen, unpublished). Moretene was found in sediments especially from acidic lakes in Japan and from Lake Baikal (Ishiwatari et al. 2005; Uemura and Ishiwatari 1995), in early Holocene (limnic) sediments from the Black Sea (Blumenberg et al. 2009) and possibly also in sediments from an alkaline lagoon in Spain ("unknown hopene exhibiting a mass spectrum similar to diploptene but eluting at shorter retention time", Grimalt et al. 1991). Except for lake sediments, moretene was detected in rhizomes of the fern *Davallia mariesii* (Shiojima and Ageta 1990). However, since ferns are absent from the Tswaing Crater, and in agreement with results from compound-specific stable carbon isotope analysis (see section "Stable carbon isotope ratios of organic constituents of the modern ecosystem") we follow indications of Blumenberg et al. (2009) and Uemura and Ishiwatari (1995) and attribute the occurrence of moretene in the sediments of Lake Tswaing to the activity of methanotrophic bacteria. Consequently, a derivation of moretene, phytane and phytenes by a bacterial community including methanotrophic and sulphate-reducing bacteria, and maybe also methanogenic archaea, which thrives in the deeper water column or at the sediment/water interface, is inferred.

The composition of the neutral NSO compounds of the sediments corresponds to the findings in the water and mat samples, except that tetrahymanol is the overall dominant compound; squalene has not been detected in the sediments and phytol and α-tocopherol contents are minor. This observation suggests a rapid oxidative degradation of squalene, phytol, and α-tocopherol, whereas tetrahymanol is either exceptionally abundant in the sediments despite ongoing degradation which is indicated by the higher contents of gammaceran-3-one in the sediments compared to water samples, or it is more resistant to degradation. Both possibilities probably apply as tetrahymanol is a prominent compound in sediments of the core down to 40 m depth (c. 100 kyr BP).

Stable carbon isotope composition of organic constituents of the modern ecosystem

Stable carbon isotope data can be used for addressing processes relevant for the carbon cycle of modern ecosystems. It can provide insight into, for example, the way of carbon

assimilation (C3 vs. C4) of land plants, the carbon source for aquatic organisms (e.g., dissolved CO_2, HCO_3^-, or methane) and influences on the respective carbon source (e.g., changes in atmospheric CO_2 levels, temperature, nutrient availability and bioproductivity, or intensity of recycling) (Leng et al. 2005; Meyers 2003). Accordingly, we have investigated the marker compounds described in the previous section for their stable carbon isotopic composition and compare these results with data available from literature to trace active metabolic processes and their inter-connection in the Lake Tswaing ecosystem (Fig. 4.3).

For bulk floating cyanobacterial matter we observe a $\delta^{13}C_{org}$ of -24.0‰. This value is consistent with a ^{13}C-depletion of c. 22‰ relative to the carbon source observed by Sakata et al. (1997) in laboratory experiments and a $\delta^{13}C_{DIC}$ of -1.7‰ of the modern surface waters. This $\delta^{13}C_{DIC}$ reflects the predominance of bicarbonate and carbonate in the water under a prevalent pH of 9–10. The C_{17} *n*-alkane of floating cyanobacteria is 10.6‰ depleted in ^{13}C relative to the bulk material. This difference is slightly larger compared to earlier investigations from Sakata et al. (1997) with -8.4‰. Microbial mats in the shallow lake area are characterised by a relatively high $\delta^{13}C_{org}$ value of -18‰, which is comparable to published data from hypersaline microbial mats (Schidlowski and Matzigkeit 1984; Schouten et al. 2001).

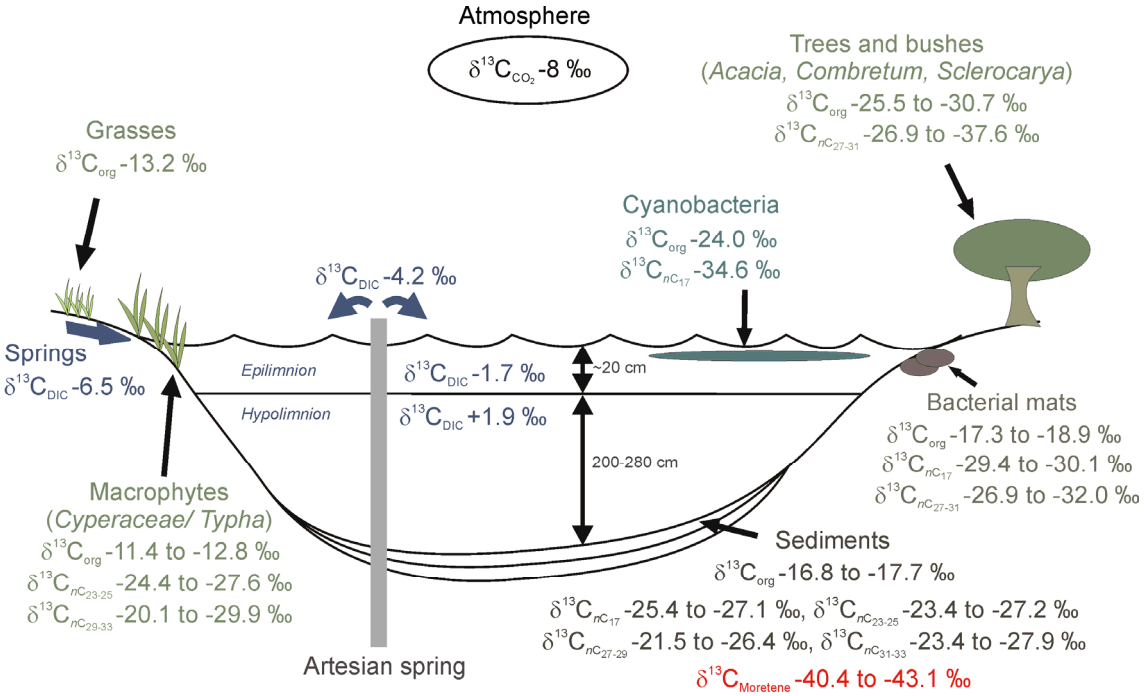

Figure 4.3: Sketch with main components of the modern ecosystem and their relative stable carbon isotopic composition of bulk tissue and selected biomarkers from the aliphatic hydrocarbon fraction.

The investigated trees and bushes (listed in Table 4.2), except the grasses and macrophytes, show $\delta^{13}C_{org}$ values between -25.5 and -30.7‰. These values fall within the range commonly associated with C3 plants (O'Leary 1981). The dominant long-chain *n*-alkanes (*n*-$C_{27,29,31,33}$) have $\delta^{13}C$ values of -26.9 to -37.6‰. Their 1.4–6.9‰ lower signature corresponds to results Collister et al. (1994) reported for *n*-alkanes of C3 plants with 1.6–8.9‰ ^{13}C-depletion. The investigated macrophytes *Typha angustifolia* and *Cyperacea* sp., and the grasses show $\delta^{13}C_{org}$ values of -11.4 to -13.2‰. These signatures fall within the range typically attributed to C4 plants (O'Leary 1981), but *Typha* sp. is jointly classified as C3 plant (Evans, 1975; Fry, 1986; Kao-Kiffin and Balser, 2007) and $\delta^{13}C_{org}$ values of *Typha* have been described in the range of -24.8 to -27.7‰ (Hornibrook et al., 2000; Stern et al., 2007; Wang et al., 2003). Street-Perrott et al. (2004) stated that macrophytes are able to use HCO_3^- as carbon source which would result in higher $\delta^{13}C$ values. Additionally, conditions of a saline habitat can cause a shift in the $\delta^{13}C$ signature of plants to higher values (O'Leary 1988; Wooller et al. 2007). The unusually high $\delta^{13}C$ value of *Typha angustifolia* is interpreted to be a combination of these two effects. The dominant *n*-alkanes *n*-C_{23} and *n*-C_{29} of *Cyperacea* sp. range from -24.9 to -27.2‰, and the dominant *n*-alkanes *n*-C_{27} and *n*-C_{33} of *Typha angustifolia* range from -20.1 to -22.6‰, resulting in a fractionation range of 10 to 15‰ compared to the bulk plant material. This range is consistent with data published by Collister et al. (1994) for C4 plants and larger than observed ranges for C3 plants. This discrepancy for *Typha angustifolia* might again be related to the highly evaporative conditions at the lake site.

Modern sediments from Lake Tswaing are characterized by a $\delta^{13}C_{org}$ signature of -16.8 to -17.7‰. These values are consistent with a mixed input of the components described above. This mixture is also indicated by compound-specific $\delta^{13}C$ signals of the sediment samples. Long-chain *n*-alkane $\delta^{13}C$ values (*n*-$C_{27,29,31,33}$) are intermediate between those of C3 plants and macrophytes (Fig. 4.3). The isotopic composition of mid-chain *n*-alkanes corresponds to values found in modern macrophytes. Only the $\delta^{13}C$ of *n*-C_{17} is higher in the sediments (c. -26‰) than in the sampled floating cyanobacteria (-34.6‰). This discrepancy is interpreted to be associated with seasonal or inter-annual differences in the $\delta^{13}C$ signature of the water column and corresponding cyanobacterial blooms, which are integrated in the top few centimeters of sediment. However, it is also possible that microbial mats from the lake shore contribute to this signal. Noticeable is the $\delta^{13}C$ of moretene which is more than 10‰ lower than the values of any other compound in the sediments. This is interpreted as a contribution of moretene from bacteria (or a bacterial community) living in the deeper water column of Lake Tswaing or at the sediment surface and feeding on a carbon source isotopically depleted in ^{13}C. This carbon source might be a mixture of degraded OM from the photic zone and oxidised methane, or methane directly consumed by methanotrophs as has been discussed previously for moretene (Blumenberg et al. 2009; Uemura and Ishiwatari 1995) and also for the structurally related compound diploptene (Elvert et al. 2001; Spooner et al. 1994). In this context, the detection of an unusually high $\delta^{13}C_{DIC}$ signature at 50 cm water depth (+1.9‰) might confirm that methane generation occurs in Lake Tswaing (Rosenfeld and Silverman 1959) (Fig. 4.3).

Tracing the changing carbon cycle in the Tswaing Crater – a sediment core study (c. 14,000–2,000 yr BP)

We have characterised the modern terrestrial and aquatic environment of the Tswaing Crater using biomarkers and stable carbon isotope ratios of the predominant organisms adapted to the present-day climatic conditions. In the following, we describe changes in the concentrations (in µg/g TOC, if not quoted otherwise) of these biomarkers and in their stable carbon isotopic signatures to trace modifications in the ecosystem of the Tswaing Crater recorded in cored lake sediments which cover the time from the end of the last glacial (Termination I) to the late Holocene (14,000–2,000 yr BP). We infer changes in the lacustrine, near-surface primary (probably predominantly cyanobacterial) productivity from changes in the concentration of the C_{17} *n*-alkane. Changes in the concentration and carbon isotopic composition of moretene are thought to reflect bacterial activity in the bottom-water or at the sediment/water interface. The concentration of tetrahymanol additionally indicates the varying contribution of bacterial biomass in the lake. Changes in the stable carbon isotope composition of the C_{29} *n*-alkane are most probably related to changes in the relative contribution of bushes and trees (C3 plants) versus grasses and macrophytes (C4-type signal). Variable amounts of the sterols which were identified in the modern higher plants further trace changes in the abundance of higher plants around the lake.

The total amount of biomarkers, as TOC content in general, is very low in samples from 14,000–10,000 yr BP with the exception of a short period around 11,300 yr BP (see next paragraph) (Fig. 4.4). This indicates that productivity in and around the lake was reduced due to unfavourable climatic conditions and/or that hydrology did not allow preservation of OM during this time. In a preceding study (Kristen et al. 2007), we compared XRF data from the current profile to mineralogical data from a previously studied core from Tswaing (Bühmann and Elsenbroek 1999) and interpreted the correspondence of high relative proportions of detrital minerals (quartz, mikrokline, plagioclase) with high potassium, aluminium, and iron intensities in combination with low chlorine intensities and TOC contents as indication for increased sheet-wash and reduced lake water salinity and stability. These more humid conditions were observed for the period 15,000–10,000 yr BP (Fig. 4.4 b). Because sedimentation rates were relatively low during this time (c. 0.24 mm/yr, Fig. 4.4 a), reduced lake water salinity and increased turbulence probably favoured microbial activity and OM degradation. Under these conditions, biomarker concentrations are too low to reliably determine compound-specific stable carbon isotope ratios. Results from a pollen and palaeomagnetic study from Lake Masoko (9°20.0'S, 33°45.3'E), however, support our interpretation. Both proxies indicate more humid conditions with a short dry season in the southern hemisphere subtropics for the period 15,000–11,800 yr BP (Garcin et al. 2007). Garcin et al. (2007) relate this observation to a probable southward position of the Inter-Tropical Convergence Zone (ITCZ). However, as this interval further coincides with observations of rising temperatures in the tropical Indian Ocean (Bard et al. 1997; Levi et al. 2007), the humid period may equally be connected to generally higher moisture availability in this region.

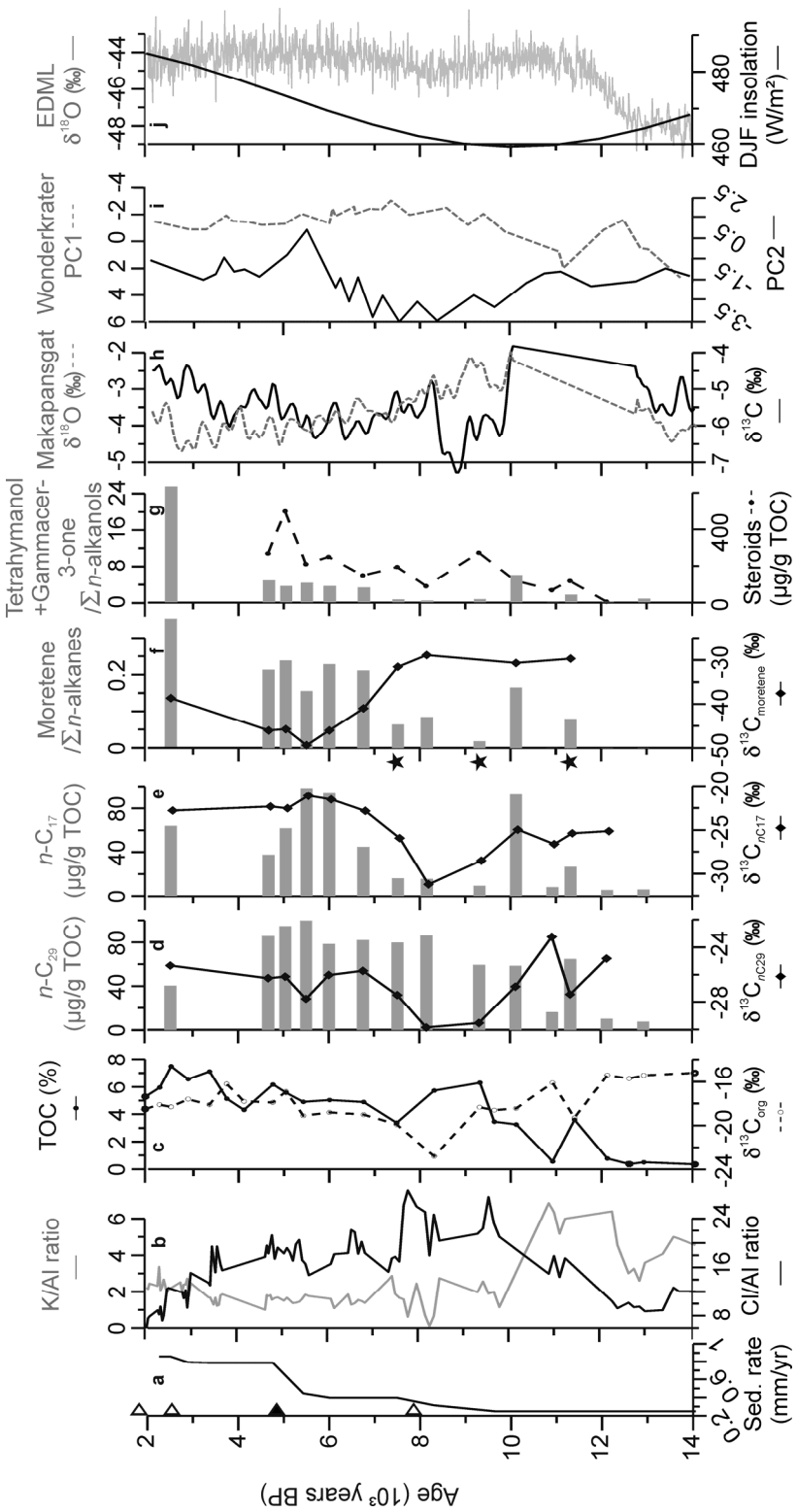

Figure 4.4: Downcore plots of a) sedimentation rate, based on radiocarbon ages from Table 4.1 (open triangles show ^{14}C ages on bulk organic matter, filled triangles on charcoal); b) K/Al (grey) and Cl/Al (black) intensity ratios from XRF-core scanning (modified after Kristen et al. 2007); c) $\delta^{13}C_{org}$ (dashed line) and total organic carbon content (TOC, black line); d-f) $\delta^{13}C$ of selected aliphatic biomarkers (black lines), in comparison with the concentration of the respective biomarkers (grey bars) or the ratio of moretene vs. *n*-alkanes (f, grey bars, stars highlight the samples which contain long-chain alkenones),; g) ratio of tetrahymanol+gammaceran-3-one (diagenetic product of tetrahymanol) vs. *n*-alkanols (grey bars) and concentration of terrestrial steroids (dashed line) of Lake Tswaing sediments; in comparison with h) $\delta^{13}C$ (black line) and $\delta^{18}O$ (dashed line) from a stalagmite from Makapansgat Valley (24°8.824'S, 29°10.371'E) (Holmgren et al. 2003); i) the temperature (PC1, dashed line) and humidity indices (PC2, black line) derived from the Wonderkrater pollen record (24°25.806'S, 28°44.626'E) (Scott and Holmgren 2003); j) $\delta^{18}O$ record from Antarctic ice core from Dronning Maud Land (EDML) (EPICA 2006, grey) and changing summer (mean december, january and february, DJF) insolation at 30°S.

Around 11,300 yr BP, probably only for a short period of a few hundred years, conditions became favourable for preservation of OM and biomarker concentrations increased (Fig. 4.4). This happened while K/Al ratios were elevated, indicating higher run-off from the catchment, and rising Cl/Al ratios point to enhanced evaporation, which was apparently strong enough to allow a stabilisation of the water column and OM preservation. We relate these observations to generally rising temperatures during Termination I, which are also reported from the Wonderkrater pollen sequence (Scott 1999b; Scott and Holmgren 2003) (Fig. 4.4 i). The high variability of the Tswaing record in this time interval 12,500–10,000 yr BP may be a reflection of the global climate oscillations during this period (Younger Dryas, Preboreal Oscillation) and/or relate to changes in the coupling of the tropical atmosphere and ocean circulation at the glacial/interglacial transition as suggested by Levi et al. (2007) based on observations in marine sediments from the Indian Ocean or by Rein et al. (2005) offshore Peru. Yet, reliably dated documentations of these phenomena are scarce in southern Africa, and resolution and uncertainties within the chronology of the sedimentary record presented here preclude more detailed interpretations. The increased OM content of this time slice allows compound-specific isotope analyses and reveals $\delta^{13}C$ values of *n*-C_{17} similar to modern values (-25‰), indicating similar hydrological conditions in the past for photosynthetic organisms in the lake. The $\delta^{13}C$ value of *n*-C_{29} of -27.5‰ is similar to the signal of modern C3 plants, but lower than the modern sedimentary signal (Fig. 4.3). This observation reflects a higher proportion of C3 plants in the surrounding of the lake and/or a lower abundance of grasses and/or macrophytes. Pollen and stable carbon isotope studies from South Africa (Holmgren et al. 2003; Scott 2002) report, in contrast to studies from tropical Africa (Aucour et al. 1994; Huang et al. 1999b; Olago 2001; Wooller et al. 2003), no expansion of C4 grasses under glacial conditions, making major changes in the C3/C4 proportion during Termination I unlikely. Therefore, the shift in $\delta^{13}C$ signatures probably results from a local decrease in input from grasses/macrophytes and/or less evaporative stress for macrophytes during a period with higher rainfall, as inferred from element distribution data (Kristen et al. 2007). Biomarkers typical for bacterial activity are also present around 11,300 yr BP with $\delta^{13}C$ values of moretene c. 10‰ more enriched in ^{13}C than modern values. This data resembles values from terrestrial plant input and are only slightly lower than OM produced in the surface water. We therefore interpret the bacterial signal to result from bacteria degrading this OM.

With the beginning Holocene 10,500–10,000 yr BP, all biomarker concentrations and especially the ones of autochthonously produced compounds rise significantly (Fig. 4.4). TOC contents of the sediments and the amounts of terrestrial biomarkers as *n*-C_{29} remain high from this time on or even show an increasing trend throughout the Holocene as does the contribution of terrestrial steroids. These observations point to continuously favourable conditions for higher plant vegetation in and around the crater, possibly in relation to the post-glacial warming, and continuously good preservation of organic matter in a more saline, stagnant lake (Kristen et al. 2007). The lacustrine near-surface and bottom-lake productivity, however, breaks down again between 10,000 and 7,500 yr BP, when concentrations of *n*-C_{17}, moretene and tetrahymanol decline by more than 85% (comparison 10,100/9,300 yr BP). The contemporaneous decrease in the $\delta^{13}C$ signature of *n*-C_{17} is consistent with reduced productivity in the lake surface waters

(Leng et al. 2005). The $\delta^{13}C$ values of moretene, however, remain stable until c. 7,500 yr BP and imply no change in the bacterial community at the lake bottom during early Holocene times. In parallel, the $\delta^{13}C$ signal of *n*-C_{29} decrease to around -30‰ which indicates a shift to a higher proportion of C3 vegetation around the lake and/or decreasing input from grasses/macrophytes and/or less evaporative stress for macrophytes. The time period 10,000–7,000 yr BP, however, is recorded as the driest period of the last 20,000 years in the Wonderkrater pollen record (Scott and Holmgren 2003). Elevated chlorine and low potassium intensities in the Tswaing sediments during this time interval further point to arid conditions at the site (Kristen et al. 2007) (Fig. 4.4 b). The period 10,000–7,000 yr BP coincides with times of dune formation in western Zambia (O'Connor and Thomas 1999), and with an exceptionally white interval in a stalagmite of the Makapansgat Valley that exhibits the lowest $\delta^{13}C$ values of the whole record (Holmgren et al. 2003) (Fig. 4.4 h). The latter is interpreted as a period with reduced vegetation cover, especially reduced grass abundance. Combining the evidences from surrounding locations and from the Lake Tswaing record, the period 10,000–7,500 yr BP appears to be a generally drier period, where the expansion of grasses and probably also macrophytes was reduced and the productivity of photosynthetic organisms in the lake was diminished. An orbitally induced northward shift of the ITCZ accompanied by a shortening of the rainy season (as suggested earlier by Garcin et al. (2007) and references therein) can provide a possible mechanism, affecting particularly shallow rooting grasses. The consequential reduction in ground water inflow could have led to a shrinking of the lake area and the surrounding swamps as well as to reduced nutrient inflow into the lake, which in sum resulted in the observed decrease in primary productivity and $\delta^{13}C$ signals of the OM. The increased aridity for the southern subtropics appears to be linked to a northward expansion of the area influenced by the ITCZ according to observations from tropical and subtropical northern Africa (e.g., Felton et al. 2007; Ficken et al. 2002; Gasse 2000; Lamb et al. 2004; Lamb et al. 2007; Stager et al. 2003; Talbot and Lærdal 2000) where this interval represents a humid period.

After c. 7,500 yr BP, the amount of autochthonously produced OM increases again accompanied by a shift to higher $\delta^{13}C$ values of *n*-C_{17}, *n*-C_{29} and TOC. These changes indicate a restart of near-surface lacustrine productivity and an increasing proportion of plants with a C4-type signal around the lake. Following this line of reasoning, the aforementioned trend can be interpreted as an increase of grasses and/or macrophytes around the lake and increased nutrient supply under more humid conditions. This trend continues until c. 5,500 yr BP and is complemented by the Wonderkrater pollen record that implies gradually more humid conditions maximising at c. 5,500 yr BP (Scott and Holmgren 2003) (Fig. 4.4 i). Climate archives from northern subtropical and tropical Africa display increasing aridity and/or stronger seasonality during the same period (e.g., Gasse 2000; Johnson 1996; Lamb et al. 2004; Talbot and Lærdal 2000; Tiercelin et al. 2008). This anti-phase behaviour of northern and southern hemisphere subtropics in response to precessional forcing has been frequently reported from climate archives of the African and American continents (e.g., Cruz et al. 2005; Fleitmann et al. 2003; Partridge et al. 1997). In parallel, the $\delta^{13}C$ signal of moretene decreases by 20‰ to a value of -50‰ at c. 5,500 yr BP. This value falls within a range typical for methane produced in freshwater environments (Whiticar et al. 1986). The shift in the $\delta^{13}C$ signature of moretene is

interpreted as a shift in the bacterial community towards a higher proportion of methanotrophic bacteria similar to assemblages present in the modern lake (see section "Stable carbon isotope ratios of organic constituents of the modern ecosystem").

Occurrence of long-chain alkenones in core sediments

Long-chain di-, tri-, and tetra-unsaturated alkenones (LCAs) with chain lengths ranging from C_{37} to C_{38} were detected in three samples from the early to mid Holocene (marked with stars in Fig. 4.4). LCAs are ubiquitous in marine sediments (e.g., de Leeuw et al. 1980; Marlowe et al. 1984; Rosell-Mele et al. 2002), and are increasingly found in lacustrine environments at high and low latitudes (Cranwell 1985; D'Andrea and Huang 2005; Li et al. 1996; Pearson et al. 2007; Theissen et al. 2005; Thiel et al. 1997a; Volkman et al. 1988; Zink et al. 2001). Source organisms for LCAs are predominantly members of Prymnesiophyceae, but other groups are discussed (e.g., Li et al. 1996; Marlowe et al. 1984; Zink et al. 2001). The degree of influence of environmental conditions like water temperature and salinity or alkalinity and differences in source organisms on distribution patterns of LCAs is still not fully understood. In contrast to previous studies (Cranwell 1985; D'Andrea and Huang 2005; Li et al. 1996; Pearson et al. 2007; Theissen et al. 2005; Thiel et al. 1997a; Volkman et al. 1988; Zink et al. 2001), we do not observe a decrease in concentration with increasing chain length of LCAs. Furthermore, the tetra-unsaturated compounds are very low in concentration compared to the tri-unsaturated ketones (Fig. 4.5). Similar observations are, to our knowledge, only documented from other shallow, saline lakes in Spain, where Pearson et al. (2007) found LCAs dominated by tri-unsaturated C_{38} alkenones. The low concentrations of tetra-unsaturated LCAs are in agreement with results of a cultivation study by Sun et al. (2007), who described a decrease in concentrations of tetra-unsaturated LCAs with increasing growth temperatures for *Chrysotila lamellosa*, a non-calcifying haptophyte that was shown to be an important alkenone producer especially in brackish water (Marlowe et al. 1984; Sun et al. 2007). However, the dominance of C_{38} over C_{37} alkenones could not be proved from their studies. Thus, it seems plausible that in the very shallow, warm, alkaline and hypersaline environment of Lake Tswaing alkenones were produced by an organism similar or identical to the one detected in Spanish lakes which, however, remains unidentified up to now.

In Lake Tswaing sediments, LCAs are only present in samples older than 7,500 years BP. These samples have TOC concentrations above 0.5% but low concentrations of tetrahymanol and moretene (Fig. 4.4) and relatively high $\delta^{13}C$ values for moretene. Likewise, Thiel et al. (1997a) found high amounts of LCAs in samples with low concentrations of tetrahymanol/gammaceran-3-one in a sediment sequence from the highly alkaline Lake Van in Turkey which covers the last 15,000 years. They interpreted this negative correlation to reflect changes in water stratification with higher concentrations of LCAs during periods of increased convection and nutrient availability. In sediments from Lake Tswaing, LCAs are observed in one sample from the presumably more arid period 10,000–7,500 yr BP, when lake productivity

was diminished due to nutrient scarcity, and also in the sample from c. 11,300 yr BP, when nutrient availability allowed higher lake productivity (see sections above). We therefore tentatively conclude that the presence/absence of LCAs in sediments from Lake Tswaing depends on changes within the microbial community of the lake. As indicated by the $\delta^{13}C$ signature of moretene, the establishment of methanotrophic organisms after c. 7,500 yr BP may have displaced LCA producing organisms that were present until then.

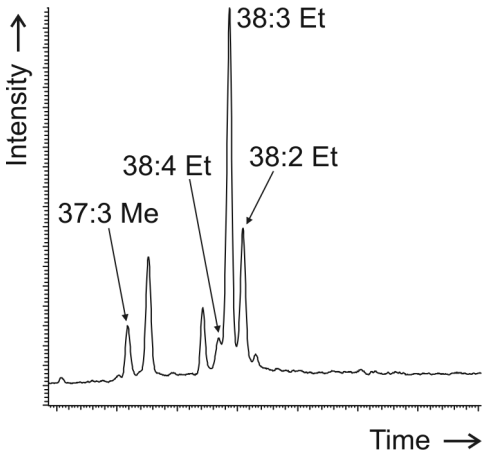

Figure 4.5: Gas chromatogram showing the long-chain alkenone (di-, tri- and tetra-unsaturated methyl and ethyl ketones with 37 and 38 carbon atoms) distribution in a sediment sample from Lake Tswaing (3.5 m depth, 7,500 yr BP).

CONCLUSIONS

In this study we have characterised the modern organisms of the Lake Tswaing environment using several key biomarkers. The presently abundant higher-plant species characteristically produce odd-numbered long-chain *n*-alkanes (*n*-$C_{27,29,31,33}$), stigmasterol, β-sitosterol, β-amyrin, α-amyrin, lupeol and germanicol, as well as even-numbered long-chain alcohols (*n*-C_{28+30}). The floating cyanobacteria and microbial mats contain predominantly the C_{17} *n*-alkane, tetrahymanol and several C_{29} sterols. In the modern lake sediments, a mixture of theses compounds is detected, together with phytane, phytenes and the rare biomarker moretene, which point to an active bacterial community in the deeper lake or surface sediments. Bulk and compound-specific stable carbon isotope analyses give a more detailed picture of the modern carbon cycle of the Tswaing ecosystem, to which C3 and C4 plants and aquatic organisms contribute. Moretene thereby shows a distinctly lower isotopic composition than the other biomarkers, indicating the presence of methanotrophic bacteria.

The $\delta^{13}C$ signature of biomarkers identified in the modern ecosystem and their relative contribution to a 7 m long core sequence reveal changes in the ecosystem of the Tswaing Crater between 14,000 and 2,000 yr BP. Under more humid conditions during Termination I (c. 14,000–10,000 yr BP), OM was almost absent in the sediments and was probably oxidised, whereas it was well-preserved in a stagnant, saline lake environment afterwards. After a period

of increased aquatic productivity at the beginning of the Holocene, surface and bottom-water bioproductivity broke down between 10,000 and 7,500 yr BP. This interval is interpreted to represent an arid period or a period with a long dry season, during which grasses and macrophytes were reduced around the lake and diminished nutrient input limited the aquatic bioproductivity. We propose a northward shift of the ITCZ to be the underlying forcing factor, which is in agreement with other African climate studies. After c. 7,500 yr BP, input from aquatic organisms increased with increasing humidity, reaching a maximum c. 5,500 yr BP. Microbial activity in particular was higher after c. 7,500 yr BP when methanotrophic bacteria seem to become an abundant constituent of the microbial lake community.

For the first time, to our knowledge, long-chain alkenones (LCAs) were identified in African lake sediments. All samples containing LCAs are older than c. 7,500 yr BP and the occurrence of LCAs appears to reflect a different microbial community within the lake, further indicated by up to 20‰ higher $\delta^{13}C$ values of moretene during that time period. Due to the unusual dominance of C_{38} LCAs and of tri- over tetra-unsaturated compounds, different source organisms than those described to date from other lake sites must be considered for Lake Tswaing.

ACKNOWLEDGEMENTS

We acknowledge the GFZ for funding this work and for the financial support for the coring campaign in 2001/2002. We especially thank Susanne Fietz for investigating pigments in the cyanobacterial samples and Kai Mangelsdorf, Philippe Schaeffer, and Yannick Garcin for fruitful discussions. Tim Partridge provided useful information about the site and data relevant for the coring; we kindly acknowledge his support during field trips and sampling campaigns at Lake Tswaing. Carsten Löser is thanked for his help in botanical issues. We are grateful to Anke Sobotta, Cornelia Karger, Kristin Günther, Jenny Wunger und Michael Gabriel for technical help in the laboratories.

5. Investigations on seasonality in Lake Challa (Kenya/Tanzania) and its sedimentary documentation in recent lake sediments

Iris Kristen[1], Christian Wolff[1], Dirk Verschuren[2], Georg Schettler[1], Rudolf Naumann[1], Peter Dulski[1], Isla Milne[3], Gerald H. Haug[1,4]

[1]*Helmholtz Centre Potsdam GFZ – German Research Centre for Geosciences, Potsdam, Germany*
[2]*Limnology Unit, Department of Biology, Ghent University, Belgium*
[3]*Department of Biology, Queen's University Kingston, Ontario, Canada*
[4]*Geological Institute, ETH Zürich, Switzerland*

To be submitted to: *Limnology and Oceanography*

ABSTRACT *By combining limnological investigations carried out in Lake Challa on seven occasions between September 1999 and December 2007, we have developed a picture of seasonal variability in physical and chemical conditions. The lake is stratified during the two warm wet seasons (October – December, March – May) and the epilimnion restricted to about 20 m water depth. During the windy dry seasons (January – February, June – September) the epilimnion deepens, reaching maximum extension of app. 50 – 60 m during cool southern hemisphere winter months. Sediment-trap collections indicate that this seasonal variability in limnology is reflected in the input of allochthonous detritus, authigenic calcium carbonate and the relative importance of diatom vs. non-diatom algal detritus. Highest diatom abundance occurs from June to September when deep mixing provides easily bio-available nutrients. In parallel, redox-sensitive elements (Fe/Mn) are precipitating. During the warm, wet seasons of water-column stratification, non-diatomaceous organic and detrital input is accompanied by formation of endogenic calcite in the epilimnion, and presumably by Fe-sulphide formation at the lake bottom. High-resolution μXRF analyses and microscopic inspection of thin-sectioned sediments representing the last ~65 years of mid-lake sediment deposition suggest a direct transfer to and preservation of the seasonal signal in lake-floor sediments, supporting their utility as a high-resolution climate archive for equatorial East Africa.*

INTRODUCTION

In discussions of the impact of global warming on hydrology and human water resources, archives of past hydrological variability in tropical regions and especially tropical Africa are attracting increasing attention (Cullen et al. 2006; Mölg et al. 2005). Understanding the sensitivity of natural ecosystems to climate variability and human impact is a vital prerequisite to predict their functioning under increasingly disturbed conditions. Such an

understanding relies on natural archives of past environmental change, as instrumental records and historical documentation in many regions cover only a few decades to one century, and therefore fail to capture the full range of natural ecosystem dynamics at the relevant time scales. Traditional climate archives of temperate regions, such as tree rings and ice cores are rare in tropical Africa. In recent years an increasing number of lake studies have been carried out which aim to elucidate East African climate variability over various time scales (e.g., Gasse et al. 1989; Johnson et al. 2002; Russell et al. 2007; Street-Perrott et al. 2007; Talbot and Lærdal 2000; Verschuren et al. 2000; Wooller et al. 2003). However, the lake-derived reconstruction of climate in eastern Africa suffers from first-order inconsistencies. For example, Lakes Masoko and Malawi, which are less than 100 km apart, indicate qualitatively very different hydrologic conditions for the Younger Dryas period (11.7-12.8 kyr BP) (Brown et al. 2007; Garcin et al. 2006). Incongruent interpretations, especially of older records, may partly be caused by low temporal resolution and improper age control. More often, however, the discrepancy originates in a seemingly conflicting palaeoclimatic interpretation of particular sedimentary parameters (proxies). In this regard, the monitoring of modern lake systems is an important prerequisite of lake-based palaeoclimatology, as it ground-truths the hypothesised causal links between the sediment record, lake functioning, and climate. With this study we aim to understand the genesis of laminated sediments in Lake Challa, a freshwater crater lake near Mt. Kilimanjaro (Kenya/Tanzania), under present-day climatic conditions in order to provide a mechanistic basis for palaeoclimatic interpretation of long-term geochemical records from this site.

STUDY SITE AND MODERN CLIMATE CONDITIONS

Lake Challa (3°19'S, 37°42'E) is a freshwater crater lake with a surface area of 4.2 km² and an inter-annually varying maximum depth of 92-98 m (range of observations 1999-2007). It is located at ~880 m asl on the lower east slope of Mt. Kilimanjaro (Fig. 5.1) within igneous rocks (predominantly trachy-basalts) of the tertiary Kilimanjaro complex (Bear 1955). These basalts are covered by "calcareous tuffaceous grits", a calcite-cemented tuffaceous breccia that is probably related to the formation of the Challa crater (Downie and Wilkinson 1972). The volcanic complex is underlain by metamorphic basement rocks (predominantly gneisses) which outcrop east- and southward of Lake Challa and dominate the south-eastern Kenya lowlands to the Indian Ocean coast (Petters 1991). Seismic surveys detected ~210 m of sediment infill in the crater, which cover the last ~250,000 years (Moernaut et al. in prep.). The water budget of the lake is controlled by sub-surface in- and outflow, and the local precipitation/evaporation balance of ~600 mm/yr rainfall and ~1700 mm/yr lake-surface evaporation (Payne 1970). Steep crater walls, which reach up to 170 m above the lake surface, restrict the lake's catchment area to little more than the direct lake surface and keep surface inflow by direct runoff very limited. One small, ~300-m-long creek breaching the NW corner of the caldera enlarges the catchment marginally and has only been active during years of exceptionally heavy rainfall (information from local fishermen). The sub-surface inflow to Lake Challa derives most probably from percolation of precipitation falling in or above the forest zone on the upper slopes of Mt.

Kilimanjaro. Within this lake basin form laminated sediments of autochthonous character which are predominantly composed of biogenic silica, organic matter, and endogenic calcite.

Figure 5.1: Location of Lake Challa (C, 3°19'S, 37°42'E) and bathymetric map (right panel, depth contours at 10 m intervals; Moernaut et al. in prep.). Black outline in the left panel indicates coverage of Figure 5.2.

Climatic conditions in tropical East Africa and therefore at Lake Challa are controlled by the seasonal passage of the Inter-Tropical Convergence Zone (ITCZ) (Fig. 5.2), associated with the changing zenith position of the sun. Following its crossing over the equator during the equinoxes, rainfall occurs predominantly from October to December and from March to May (Fig. 5.3). These two rain seasons are referred to as the "long rains" and "short rains", respectively. The former usually bring the major amount of rainfall to East Africa, but the latter are reported to show stronger inter-annual variability, presumably in response to changes in Indian Ocean surface temperatures and related atmospheric circulation (Black et al. 2003; Clark et al. 2003; Hastenrath et al. 2004; Kabanda and Jury 1999; Schreck and Semazzi 2004). Temperatures in this region just south of the Equator are lowest during northern hemisphere summer (June – August) and highest during northern hemisphere winter (November – March). Wind speeds show the opposite pattern with strong winds from May to October that are related

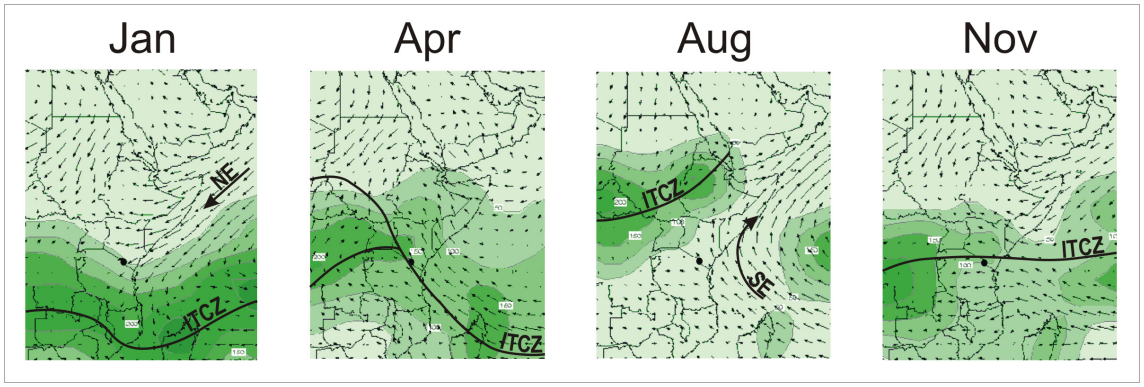

Figure 5.2: Seasonal migration of the ITCZ over East Africa. Monthly precipitation (shading, mm/month) is based on satellite precipitation estimates over ocean areas, and rain gauge data over land; contours drawn at 50-mm intervals. Climatological wind vectors for the 925 hPa pressure level indicate wind direction with wind speed proportional to the length of the vectors. Source: http://iridl.ldeo.columbia.edu.

to the south-easterly trade winds during the period of a northward displaced ITCZ (Fig. 5.2) and generally weaker winds from November to April. The north-easterly trade winds during January and February are less eminent and more variable.

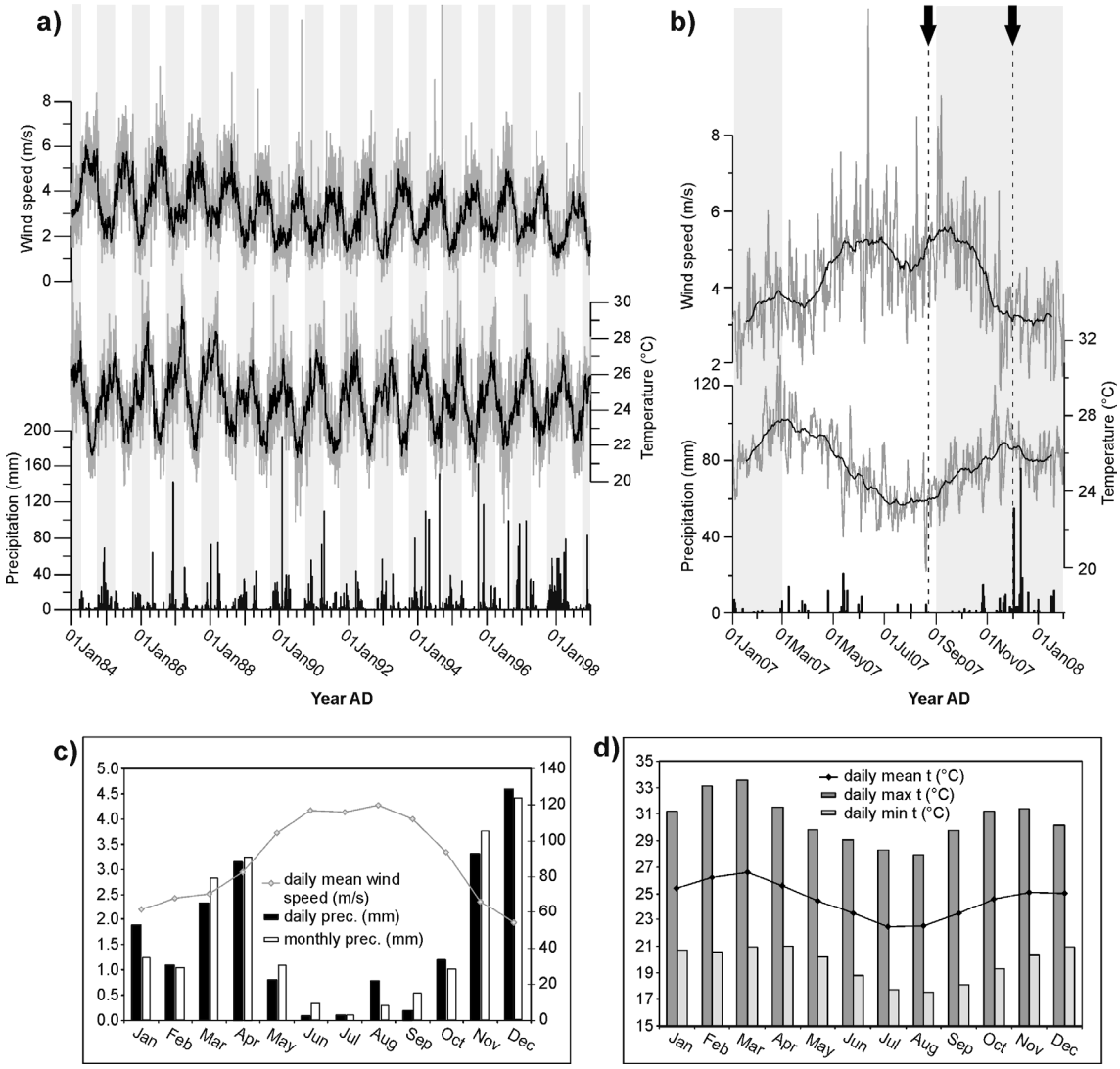

Figure 5.3: a) + b) Daily meteorological data from Voi, Kenya (~100 km E of Lake Challa), covering the time periods 1984 - 1999 (a), and 1 January 2007 - 1 February 2008 (b) (periods between 1 September and 1 March are shaded, black line in (a) is 11-day running average, black line in (b) is 31-day running average (~monthly mean), days of sampling lake-water chemistry are marked by arrows in (b). Source: http://hurricane.ncdc.noaa.gov/CDO/, global surface summary of day data of the federal climate complex; c) daily precipitation and wind data (left axis) averaged per month (1984-1999), and monthly precipitation data (right axis) from Voi (1904-1990). Source: NOAA NCDC GCPS monthly station data. d) daily maximum, minimum and mean temperature data from Voi, averaged per month (1984-1999).

LAKE WATER SAMPLING AND LABORATORY ANALYSES

Lake water sampling for chemical analyses was accomplished along vertical profiles in the centre of the lake on 23 August 2007, in the late afternoon, and on 01 December 2007, at

noon. Samples were taken every 5 m between 0 and 20 m water depth, and every 10 m between 20 and 80 m water depth in August 2007; in December 2007 samples were taken at 0, 5, 10, 20, 40 and 60 m depth. Within six hours, the water samples (100 ml each) were filtered through 0.2 µm, 25 mm diameter Whatman GD/X PP syringe filters, and 50 ml of the samples were acidified with concentrated HNO_3 to a pH of ~2 for analyses of cations. The samples were stored at 4 °C until processing. Analyses of the individual compounds followed the analytical procedures given in Eggermont et al. (2007). Temperature, pH, specific conductance (includes normalisation to a temperature of 25 °C) and dissolved oxygen were measured using a Hydrolab Quanta CTD profiler for profiles down to 50 m, and a multi-parameter water quality meter (YSI model: 600XL-B-D) for profiles down to the lake bottom in February 2005 and September 2006. In September 1999, a WTW multiprobe was used down to 15 m water depth; for measurements below this depth, water samples were brought up with a Hydrobios water sampler. Measurements were achieved every 1 m down to 21 m water depth and every 2 m down to 50 m water depth in November 2006 and August 2007, every 1 m down to 30 m water depth and every 2 m down to 100 m water depth in September 2006, every 0.5 m down to 15.5 m water depth and every 10 m from 20 m downward in September 1999, every 1 m over the whole 50-m profile in January 2003 and every 2 m in February 2005. Due to technical problems no oxygen measurements could be made in December 2007.

One sediment-trap was installed in November 2006 at 35 m water depth in the centre of the lake. The trap was emptied and redeployed every ~4 weeks, providing 11 monthly samples between mid-November 2006 and December 2007 (November and December 2006 are not separated). No means of preservation (i. e. poisoning with $HgCl_2$) was added to the trap. After retrieval, samples were allowed to settle for one or two days, decanted and stored frozen until transfer to GFZ laboratories, where they were filtered (Schleicher&Schnell RC-L 60, 1µm, 50 mm), and the filter residue freeze-dried. Individual particulate compounds were studied in smear slides, which were prepared with Merck Kaiser's glycerol gelatine for microscopy (molten at 40 °C). Further investigations were done by scanning electron microscopy (SEM). Detailed analytical results regarding the sediment-trap material will be published elsewhere (Wolff et al. unpublished data).

One gravity core (CH05-1G; 49 cm long) taken at the centre of the lake (~94 m water depth) in February 2005 was dedicated to the study of sediment lamination. The sediment surface was undisturbed according to observation of clear bottom water upon retrieval, and comparison with other short cores collected over the years, all showing the same set of recent lamination at the surface. Changes in the composition of sediments deposited over the past ~2000 years were studied under the microscope on thin sections from 10-cm long resin-impregnated blocks, and by micro X-ray fluorescence (µXRF) scanning of the resin-block surface. Micro XRF scanning is a semi-quantitative, non-destructive logging method that provides records of changing element intensities for major and minor elements (Al, Si, K, Ca, Ti, Mn, Fe and Sr). Scanning was performed under vacuum, using an EAGLE III XL µXRF spectrometer (Röntgenanalytik, Germany) at GFZ Potsdam, applying 40 kV tube voltage, 300 µA tube current, 123 µm spot size and 100 µm step size. Further, selected samples of powdered rocks and soils from the lake catchment were fused in Li tetraborate-metaborate flux

(FLUXANA, FX-X65) and analysed by wavelength-dispersive XRF spectrometry using a Panalytical Axios Advanced XRF spectrometer. Quantification of element concentrations was achieved using calibration curves generated from multiple certified reference samples.

In this study we compare ratios of element intensities (cps) achieved by µXRF scanning of resin blocks with ratios of element concentrations (wt% on the basis of oxides) obtained by wavelength-dispersive XRF spectrometry. Due to the element dependence of µXRF sensitivity (the cps to wt% ratio), which ranges from ca. 7 for Al to 300 for Fe using the above described experimental parameters, intensity ratios are not identical to concentration ratios. To convert element intensity ratios into concentration ratios, we prepared the same rock and soil samples from the catchment of Lake Challa which were analysed by wavelength-dispersive XRF as pressed pellets (grain size < 63 µm) for analysis by µXRF. The established conversion factors for selected element pairs, expressed as concentration ratio/intensity ratio, are 1.1±0.1 for Mn/Fe, 0.50±0.02 for Si/Al and 0.072±0.008 for Ca/Al (Dulski, unpublished data). These values show that, for example, the Mn/Fe ratios derived from µXRF scanning of powdered soil/rock samples are in a comparable range as the ratio from wavelength-dispersive XRF spectrometry (Table 5.2), whereas Ca/Al ratios differ by more than one order of magnitude. The converted ratios are referred to as Mn/Fe*, Si/Al* and Ca/Al*. For the interpretation of µXRF scanning results, we assume Ti and Al intensities to trace allochthonous mineral input to the sediments. Both elements are frequently applied in this way in geochemical and palaeoclimate studies from various marine and lake sediment archives (e.g., Brown et al. 2007; Haberzettl et al. 2007; Haug et al. 2001; Johnson et al. 2002). We furthermore show that Ti concentrations are high in local igneous rocks (Table 5.2), therefore Ti intensities should be a valuable tracer for erosional input from within the catchment. Aluminium concentrations in local and regional rocks and soils are more similar to each other (Table 5.2), thus aluminium intensities should trace more general detrital input by both erosion and dust.

RESULTS AND DISCUSSION

Water chemistry

Results from water chemistry analyses in August and December 2007 characterise Lake Challa as a tropical hard-water lake with dissolved inorganic carbon (DIC = HCO_3^- + CO_3^{2-}) as the dominant anion, followed by Cl^- and SO_4^{2-} (Table 5.1 a, b). According to Talling and Talling (1965), this is the dominant type of lake water in Africa, but it also agrees with the high input of dissolved carbonate from weathering of the surrounding calcite-bearing tuffaceous breccia ("grits", reflected in the decrease of CO_2 from unweathered to weathered grits in Table 5.2). Sulfate concentrations in Lake Challa are generally low and decrease below detection limit in anoxic bottom waters (Fig. 5.4 f). Soluble reactive phosphorus (SRP) was not detected in the upper 40 m of the water column in either season (Fig. 5.4 d, j), indicating that it is readily

consumed by lake organisms or co-precipitated with Fe^{3+}- and Mn^{4+}-oxides and -hydroxides (Fe(Mn)OOH) or with carbonates (Wetzel 1983). In any case, SRP availability is probably a limiting factor for lake productivity. Increase of SRP below 50 m water depth indicates release from settling particles and reflux from the anoxic sediment surface. Similar trends are observed for NH_4^+, where increasing concentration towards the lake bottom in August 2007 indicate release of NH_4^+ from organic matter degradation within anoxic sediments and bottom waters. Its absence down to 60 m water depth in December 2007 indicates oxygen injection to at least 60 m between 23 August and 1 December 2007 (Fig. 5.4 e, k). Additionally, the release of free ammonia (NH_3) due to the increasing pH in surface waters (see section "Thermal regime, water column stratification and primary productivity") probably contributes to the pronounced trend in NH_4^+. Nitrate (NO_3^-) is very low in the top 20 m (August 2007) to 40 m (December 2007), respectively, where it is consumed by primary producers. Detection of NO_3^- in 20–30 m and 50–70 m water depth in August 2007 (Fig. 5.4 e) and at 60 m in December 2007 argues for organic matter degradation and microbially induced nitrification reactions under sub-oxic conditions. However, as other element distributions (SRP, NH_4^+, and next paragraph) and O_2-profiles (see section "Thermal regime, water column stratification and primary productivity") argue for anoxic conditions below 50 m water depth during the sampling campaign in August, the presence of NO_3^- at these greater depths may be also a relict of an earlier, deeper O_2 injection and related nitrifying activity. The presence of NO_3^- and SRP at 60 m water depth in December 2007 could also be an indication for groundwater inflow, but the absence of parallel increasing concentrations of Mg, Na and K argue against this proposition (see next paragraph).

Sodium, Mg and Ca are the dominant cations in Lake Challa waters and occur in similar concentrations (Table 5.1 a, b). Calcium - and to a lesser extent also Mg - concentrations are lower in the mixolimnion (i.e., epilimnion and at least seasonally mixed middle water column) than in the lower hypolimnion (Fig. 5.4 a) under stratified conditions in August 2007, exhibiting a similar trend as DIC (Fig. 5.4 f). These trends can be attributed to precipitation of low-Mg calcite in surface waters (see also section "Thermal regime, water column stratification and primary productivity") and its dissolution at greater depth with increasing free CO_2 (H_2CO_3*, Table 5.1) and accordingly lowered pH (Fig. 5.5 c). These processes are further underlined by the downward increasing trend of water column Ca/Sr (Fig. 5.4 b). Biogenic calcification seems to play a minor role in Lake Challa as mollusc (mostly *Melanoides tuberculata*) and ostracod shell fragments are observed in relevant amounts only in littoral sediments, and in rare turbidite horizons interbedded between profundal sediments (Kristen et al. in prep.). Corrosion of calcite crystals in recent sediments, observed by SEM (Fig. 5.6), also argues for partial dissolution of the endogenic carbonates in CO_2-rich bottom or pore waters. Si concentrations are generally high in Lake Challa (> 20 mg/l), and probably well above the lower limit for diatom growth (Talling and Talling 1965) at any time during the year. Even higher Si concentrations below 50 m water depth (Fig. 5.4 d, j) reflect diatom (and probably some sponge spicule and plant phytolith) dissolution in the anoxic water column, and reflux from the sediments. Dissolved Fe and Mn concentrations are <0.05 mg/l down to 40 m water depth (Fig. 5.4 c, h), reflecting its effective removal via precipitation of Fe(Mn)OOH in oxygenated water. Increasing

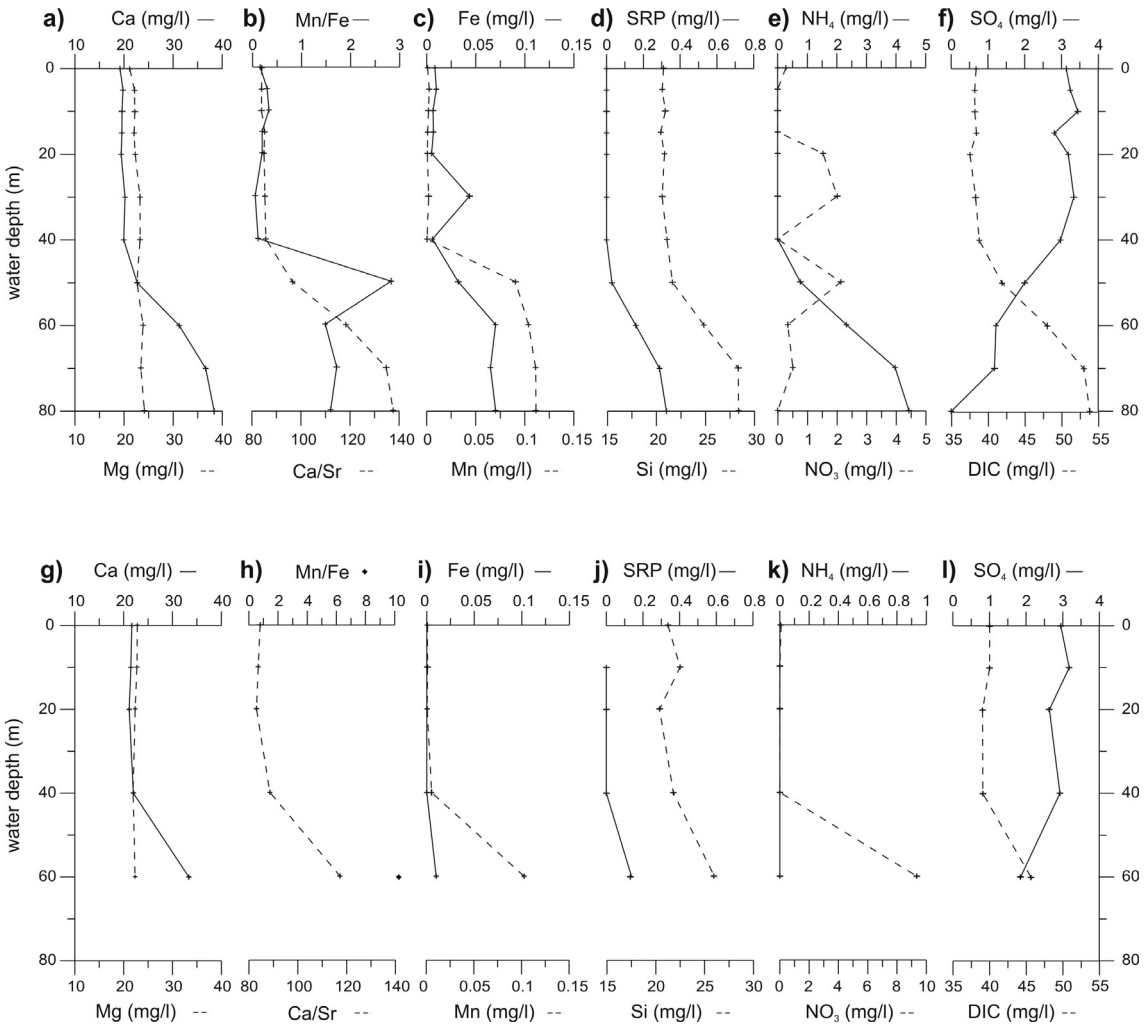

Figure 5.4: Selected profiles of chemical lake-water characteristics of Lake Challa: (a – f) were recovered on 23 August 2007 (late afternoon), (g – l) were recovered on 1 December 2007 (noon). For the complete water chemistry data sets see Table 5.1 a and b.

concentrations downward from the top of the hypolimnion in August 2007 document the rapid (probably microbially mediated) reduction of reactive Fe(Mn)OOH during settling, and at the sediment surface. The steeper downward increase of Mn in comparison to Fe, and therefore peak Mn/Fe ratios at ~50 m water depth (Fig. 5.4 b), reflect the faster rate of reduction of Mn-oxides and -hydroxides in comparison to Fe-oxides and -hydroxides (Balistrieri et al. 1994; Davison 1993; Wetzel 1983). Compared to other stratified lakes (e.g., Davison 1993; Schettler and Albéric 2008; Talling 1966; Talling and Talling 1965), Fe concentrations in the anoxic hypolimnion of Lake Challa (in August 2007) are relatively low. Considering the Fe-rich rocks in the surrounding of the caldera (Table 5.2) this could be an indication for fairly frequent complete mixing of the water column, and related precipitation of Fe-oxides and -hydroxides. On the other hand, Stauffer (1987) reported Fe concentrations below detection limit in the anoxic bottom waters of calcareous hard-water lakes where high amounts of sulphide can build up due to higher pH, and lead to precipitation of Fe-sulphide. The higher concentrations of dissolved Mn compared to Fe in the hypolimnion, parallel decreasing sulphate concentrations,

general Fe/S ratios <<1 (Stauffer 1987) and the occurrence of Fe-sulphides in the sediments (Fig. 5.6) indicate that this process is probably active in Lake Challa bottom waters and sediments and continuously decreases dissolved Fe concentrations.

Table 5.1: Hydrochemical data set from Lake Challa, a) 23 August 2007, b) 1 December 2007 (all concentrations are given in mg/l).

a)

depth (m)	Na	K	Ca	Mg	Fe	Mn	Sr	Ba	F	Cl
0	19.3	5.8	19.2	21.2	0.008	0.001	0.228	0.006	0.20	9.9
5	20.2	6.4	19.8	22.2	0.010	0.003	0.235	0.007	0.27	9.8
10	19.8	6.2	19.6	22.3	0.006	0.002	0.233	0.006	0.31	9.8
15	19.5	6.1	19.5	22.1	0.007	0.001	0.229	0.006	0.30	9.7
20	19.4	5.9	19.4	22.3	0.005	0.001	0.228	0.006	0.27	9.9
30	20.0	6.1	20.2	23.3	0.044	0.002	0.236	0.008	0.28	9.8
40	19.6	5.8	19.9	23.3	0.006	0.001	0.232	0.006	0.27	9.8
50	19.0	6.1	22.7	22.7	0.032	0.091	0.235	0.009	0.23	9.6
60	19.2	5.9	31.3	23.9	0.070	0.104	0.264	0.010	0.32	9.1
70	18.8	6.2	36.7	23.5	0.065	0.111	0.272	0.011	0.26	9.3
80	18.7	5.7	38.4	24.2	0.070	0.112	0.279	0.011	0.25	8.8

depth (m)	DIC	H_2CO_3*	HCO_3	CO_3	SO_4	SRP	NPOC	NH_4	NO_3	Si	TDS
0	38.4	0.25	37.55	0.559	3.1	<0.005	6.7	<0.025	0.28	20.7	138.3
5	38.2	0.25	37.37	0.556	3.2	<0.005	3.9	<0.025	<0.2	20.6	140.8
10	38.2	0.26	37.40	0.532	3.4	<0.005	3.0	<0.025	<0.2	20.9	140.9
15	38.4	0.28	37.63	0.511	2.8	<0.005	2.8	<0.025	<0.2	20.5	139.2
20	37.5	0.41	36.80	0.332	3.2	<0.005	2.8	<0.025	1.5	20.8	140.5
30	38.3	0.47	37.54	0.302	3.3	<0.005	1.8	<0.025	2.0	20.6	144.2
40	38.8	0.62	37.95	0.238	3.0	<0.005	1.5	<0.025	<0.2	21.1	141.9
50	41.9	1.91	39.91	0.087	2.0	0.029	1.5	0.77	2.1	21.6	149.2
60	48.0	4.36	43.64	0.048	1.2	0.160	1.6	2.32	0.34	24.9	167.0
70	53.0	5.92	47.06	0.042	1.2	0.288	1.8	3.97	0.51	28.4	182.4
80	53.8	7.36	46.43	0.034	<0.3	0.325	1.7	4.43	<0.2	28.4	183.5

b)

depth (m)	Na	K	Ca	Mg	Fe	Mn	Sr	Ba	F	Cl
0	22.4	6.7	21.7	22.8	<0.01	0.001	0.256	0.005	0.25	10.3
10	22.2	6.6	21.5	22.7	<0.01	0.001	0.256	0.005	0.31	10.4
20	21.4	6.4	21.1	22.3	<0.01	0.001	0.254	0.005	0.31	10.1
40	21.0	6.3	22.0	21.9	<0.01	0.006	0.248	0.006	0.28	9.4
60	20.8	6.5	33.4	22.3	0.01	0.103	0.284	0.010	0.30	9.2

depth (m)	DIC	H_2CO_3*	HCO_3	CO_3	SO_4	SRP	NH_4	NO_3	Si	TDS
0	40.0	0.06	37.71	2.224	2.9	n.a.	<0.025	0.09	21.2	148.7
10	40.0	0.06	37.51	2.426	3.2	<0.005	<0.025	<0.2	22.5	149.6
20	39.0	0.09	37.38	1.562	2.6	<0.005	<0.025	<0.2	20.4	144.0
40	39.1	0.53	38.27	0.281	2.9	<0.005	<0.025	<0.2	21.8	145.0
60	45.7	1.71	43.84	0.117	1.8	0.138	<0.025	9.3	26.0	175.8

n.a. = not analysed

DIC = dissolved organic carbon, SRP = soluble reactive phosphor, NPOC = non-particulate organic carbon, TDS = total dissolved solids

With total dissolved solid (TDS) concentrations below 200 mg/l (Table 5.1), Lake Challa waters are in general relatively dilute (Talling and Talling 1965). The similarity of specific conductance profiles between September 1999 and December 2007 indicate that seasonal and inter-annual variability is of low amplitude. Judging from a comparison of profiles from September and November 2006, and from August and December 2007 (Fig. 5.5 d), the difference between dry- and rain-season surface-water conductivity is probably on the order of 20–30 µS/cm.

Thermal regime, water column stratification and primary production

However unevenly distributed over the year, the limnological surveys we conducted between September 1999 and December 2007 together with meteorological data from Voi (Fig. 5.3, ~100 km to the East of Lake Challa) and preliminary data from the sediment traps (Wolff et al., unpublished) allow to establish a preliminary model of seasonal changes in the thermal regime and water-column stratification of Lake Challa. Surface warming during southern hemisphere spring and summer (October–May) is associated with the development of a shallow epilimnion. Air temperatures at Voi station (Fig. 5.3 b, d) and surface-water temperatures of Lake Challa (Fig. 5.5 a) both increase from ~23 to ~27 °C. Generally low wind stress during the first few months (Fig. 5.3 a, b, c) allows establishment of thermal stratification with a well defined thermocline between 15 and 20 m water depth (Fig. 5.5 a). From January–February, when usually dry north-easterly trade winds pick up after the southward passage of the ITCZ (Fig. 5.2), the main thermocline is displaced to below 20 m depth (Fig. 5.5 a). Observed differences in the depth of the main thermocline between January 2003 and February 2005 indicate that the intensity of mixing during this season varies between different years (Fig. 5.5 a). This difference is also clearly visible in the meteorological data from Voi, where a secondary seasonal wind maximum occurs e.g., in January 1989, 1991 and 1993 but not in January 1987, 1988 and 1998 (Fig. 5.3 a). The deepest seasonal mixing of the lake, however, occurs during southern hemisphere winter months (June–September), when air temperatures are the lowest of the year (Fig. 5.3). These are also the driest and most windy months of the year during which intense south-easterly trade winds prevail (Fig. 5.2). Within this period, the temperature gradient between surface and bottom waters is reduced to less than 1°C (Fig. 5.5 a), and specific conductance and O_2 profiles imply a mixing of the water column down to between 45 and 60 m water depth depending on the year (Fig. 5.5 b, d). The variable maximum depth of turbidity-diffusive downward O_2 flux thereby reflects the intensity of mixing due to the combination of cooling and wind stress (compare September 1999, September 2006 and August 2007 in Fig. 5.5 b), whereas the deepwater O_2 concentration partly reflects the frequency and duration of such deep-mixing events during the most recent mixing season; both the maximum depth and concentration of deepwater O_2 also depend on the amount of O_2 consumption due to organic matter degradation since that deep-mixing period. This influence can be evaluated by comparing O_2 concentrations below the thermocline in September and November 2006 (Fig. 5.5 b). The persistent increase in specific conductance (~TDS, or salinity) at ~45–60 m depth in all profiles

suggests a limit to seasonal mixing to around this depth due to density stratification (Fig. 5.5 d). Profiles of O_2 (Fig. 5.5 b) and the finely laminated nature of surface sediments (Fig. 5.6, 7) both indicate that the lake bottom and lower water column are predominantly anoxic. However, the degree of stability of tropical lakes can change rapidly (Lewis 1987) and complete mixing of the lake can occur swiftly and irregularly. Accordingly, a deeper mixing event between August and December 2007 as indicated by lake water chemistry (see above) can not be excluded. Meteorological data from Voi would underline this idea by documenting relatively windy conditions throughout September and October 2007 with especially windy days in the beginning of September 2007 (Fig. 5.3 b).

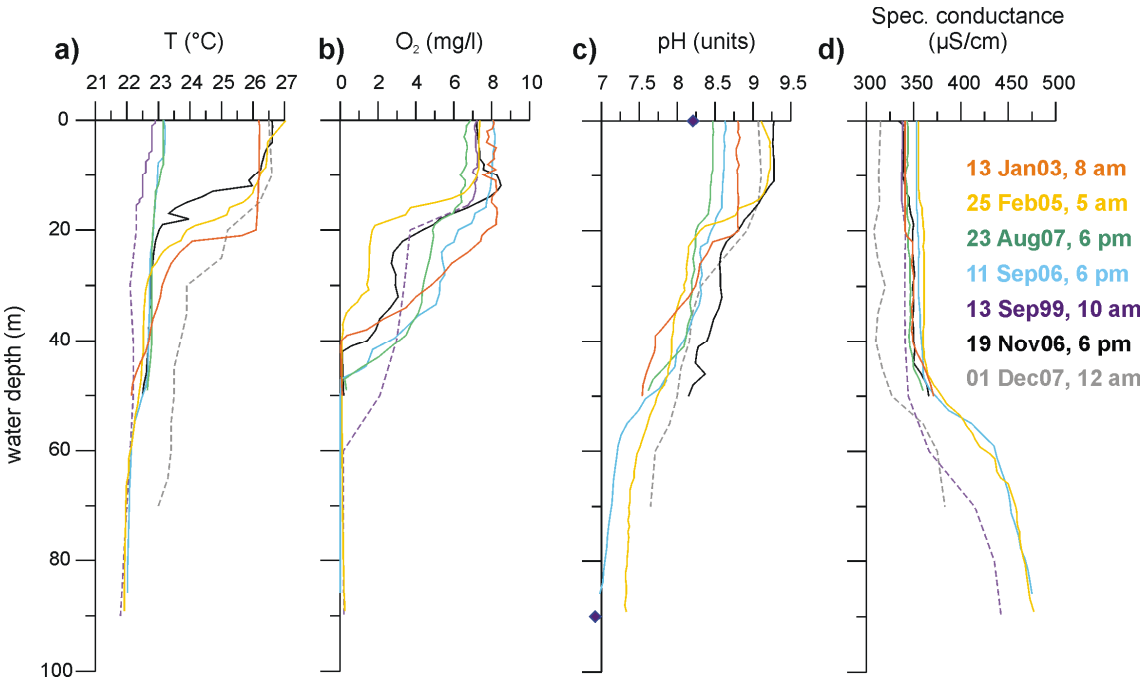

Figure 5.5: Profiles of physical lake-water characteristics of Lake Challa, measured between September 1999 and December 2007. Comparability of profiles from December 2007 and September 1999 (> 15 m) (dashed lines) with the rest of the profiles is ambiguous as those measurements were performed after bringing up the samples to the surface.

The O_2 profile from November 2006 exhibits peak O_2 concentration at ~10–15 m water depth, whereas in all other profiles O_2 concentrations within the upper ~15 m are relatively constant or decrease with depth (Fig. 5.5 a). Such a positive heterograde O_2 profile frequently develops in stratified lakes, reflecting high photosynthetic activity at depth relative to O_2 consumption by heterotrophs (Wetzel 1983). With measured Secchi depths varying between 5 and 7 m (Verschuren, unpublished), surface waters of Lake Challa are sufficiently transparent to support photosynthetic activity to 10-15 m depth. Based on the available sample of O_2 profiles, this seasonal peak in photosynthesis occurs within the short rain season, when surface temperatures are increasing, wind stress is at a seasonal minimum (Fig. 5.3 a), and the developing thermocline is still relatively shallow (Fig. 5.5 a). Together with fresh nutrient input from rainwater and runoff, conditions appear favourable for the otherwise P-limited primary producers. This high primary productivity and high surface-water temperatures are in turn

responsible for the precipitation of endogenic carbonate at that time (Wolff et al., unpublished). High amounts of idiomorphic calcite crystals in sediment-trap samples from November 2006 to February 2007, and surface pH values exceeding 9.0 in November 2006 and February 2005 (Fig. 5.5 c) are indicative for this process. Laminae of calcite crystals are also identified in the sediments (see below, Fig. 5.6). Peak photosynthesis at that time is not due to diatoms, which in Challa are most abundant between June and September, the cool, dry and most windy season of the year (Milne et al. in prep.). Since silica is not limiting for diatom growth in Lake Challa, their main occurrence during periods of deep mixing is probably linked to the input of easily bio-available nutrients from the hypolimnion creating a favourable Si/P ratio (Pilskaln 2004; Talling 1986).

With the described limnological characteristics Lake Challa agrees well with other tropical African lakes. In general, gradual thickening of the mixed layer and reduction in stability resulting from heat loss during the season with minimum temperatures has been described by Lewis (1987) as a typical feature of deep tropical lakes. Kling (1988), for example, reported for 26 out of 31 small crater lakes in Cameroon some degree of stratification, whereby all lakes deeper than 18 m showed pronounced (seasonal) stratification. Also the seasonal temperature variation of 22–27 °C is similar for Cameroon lakes and Lake Challa. Furthermore, similar to Lake Challa, the mixing/upwelling season in large lakes of the East African rift system (e.g., Lake Malawi, Lake Tanganyika) is associated with the cool and windy months of southern hemisphere winter, whereas thermal stratification persists during rather calm and warm southern hemisphere summer months (Pilskaln 2004; Plisnier et al. 1999; Talling 1986).

Formation of laminated sediments in Lake Challa

Recent sediments recovered from Lake Challa comprise predominantly diatomaceous gyttja with between 26 and 68 % biogenic SiO_2 (in the upper 10 cm), varying amounts of organic matter (15–19 %), carbonates (8–18 %) and mineral detritus (0–43 %) (Kristen et al. in prep.). The sediments are characterised by alternating light and dark laminae (Fig. 5.7). High-resolution microfacies and µXRF analyses reveals the nature of this lamination, and allows to link its formation to regional geology and to the seasonally changing limnological conditions of the lake basin.

Microfacies analyses show that light-coloured laminae predominantly consist of diatom skeletons (Fig. 5.6). Corresponding to this high input of (amorphous) SiO_2, light laminae are characterised by elevated Si/Al* values (> 20, Fig. 5.7), significantly higher than Si/Al values of local and regional rock and soil samples (Table 5.2). Following our data on physical limnology (this study) and seasonal phytoplankton dynamics (Milne et al. in prep.), these laminae represent periods of relatively deep water-column mixing, and regeneration of hypolimnetic nutrient stocks during southern hemisphere winter (June–September). Dark laminae are

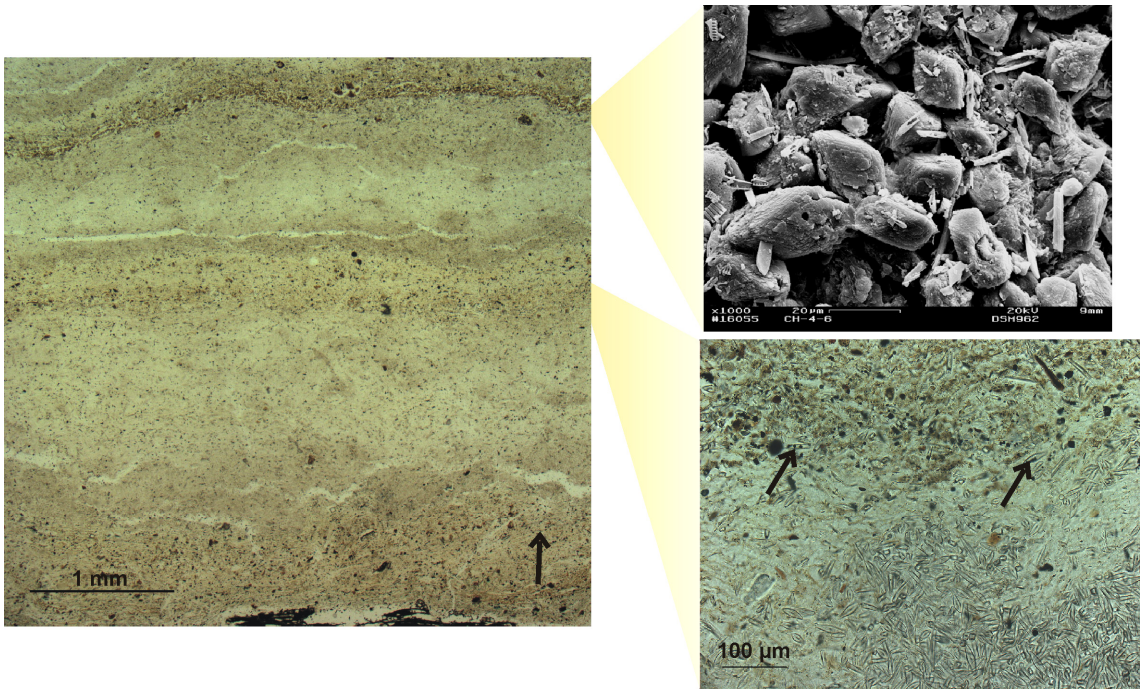

Figure 5.6: Thin section photograph of laminated sediments of CH05-1G (1 cm depth) under normal white light (left panel, arrow points up), showing alternating light (diatom) and dark (detrital, calcite) laminae. Upper right close-up shows SEM photograph of calcite crystals from Lake Challa sediments (scale 20 µm). Lower right close-up shows the transition from light diatom-rich lamina to dark lamina, rich in amorphous organic and detrital material. Note the Fe-sulphides frequently occurring inside diatom frustules within the dark laminae (arrows).

characterised by high intensities of Ti, Fe and S (Fig. 5.7), arguing for increased input of siliciclastics from local (soil and rock) and/or remote (dust) sources during these times. Thin-section analysis shows high amounts of amorphous (non-diatom aquatic) and particulate (mainly terrestrial) organic matter (Fig. 5.6). Complementary to the light laminae, dark laminae are deposited during the southern hemisphere spring and summer, when the two rain seasons (October–December and March–May) enhance runoff and soil erosion within the crater catchment. To what degree wash-out of dust brought from the wider region is contributing to this signal can not be decided here, but it may also play a role. Higher S intensities in these laminae can be related to organic-bound S, or, alternatively, to Fe-sulphide formation. The latter is favoured during times of high reactive Fe availability and enhanced organic matter input (Holmer and Storkholm 2001), which supports reducing conditions in the hypolimnion due to active remineralisation processes especially during the stratified season when no renewed O_2 injection occurs. Both sources presumably contribute simultaneously to the observed S signal in dark laminae (Fig. 5.7), with the significance of the second process corroborated by observations of framboidal Fe-sulphides and Fe-sulphides within diatom frustules (Fig. 5.6). The Fe-sulphides probably also contribute to low (< 0.03) Mn/Fe* values, a further characteristic of dark laminae (Fig. 5.7). Stronger influence on this ratio, however, is expected to derive from the different input of detrital versus autochthonous Fe(Mn)OOH. All possible sources of detrital input (local rocks and soils, and regional dust) have a relatively constant

Mn/Fe value of ~0.015 (Table 5.2). This is because due to predominant easterly winds, wind-blown dust can be expected to have a composition similar to that of the investigated local soils on metamorphic rocks. Light laminae, on the contrary, are characterised by Mn/Fe* values between about three and ten times higher (~0.05–0.1), which we interpret to derive from autochthonously precipitated hydroxides that form due to downward O_2 flux during periods of deep water-column mixing. As anoxic bottom water has Mn/Fe values between 1.5 and 3 (Fig. 5.4 b), Fe(Mn)OOH precipitating from this source water is expected to show relatively high Mn/Fe values.

Dark laminae are further characterised by relatively high Ca intensities (not shown), which can either reflect detrital input from the catchment (calcite-cemented tuffaceaous grits), or autochthonous calcite precipitation. Endogenic calcite is clearly identified in thin-sections and by SEM (Fig. 5.6). To differentiate between these sources with µXRF techniques, we apply a normalisation of Ca versus Al (Fig. 5.7). Peak Ca/Al* values are usually >5 (Fig. 5.7) and unequivocally higher than the Ca/Al value of detrital sources (< 2.5, Table 5.2). They are related to dark laminae and reflect autochthonously precipitated calcite, further confirming observations from sediment-traps (Wolff et al., unpublished) and lake monitoring that calcite forms during warm southern hemisphere summer months (November – March).

CONCLUSIONS

Intermittent limnological surveys conducted on Lake Challa between September 1999 and December 2007 document seasonal variability in lake hydrology consistent with regional meteorological observations. During southern hemisphere spring and summer months (October–May), stable water-column stratification develops and nutrient inflow associated with runoff supports peak photosynthetic activity in the deeper epilimnion of the lake. During winter (June–September), the temperature gradient within the water column is strongly reduced and south-easterly trade winds erode the thermocline to produce a pronounced thickening of the mixed layer. A secondary (less intense) mixing season sometimes occurs in January and February but appears to be variable from year to year. Based on meteorological conditions, water-chemistry analyses and geochemical investigations on the laminated modern-day sediments we develop a model for the formation and preservation of seasonal sediment laminae in Lake Challa. We show that light-coloured laminae dominated by diatoms are related to deep lake mixing, and reflected in relatively high Mn/Fe* values. Dark laminae are characterised by higher detrital influx and therefore high Fe, Ti and S intensities. Low Mn/Fe* ratios and observations of Fe-sulphides within dark laminae suggest reducing conditions in the lower water column during water-column stratification. Simultaneously, high Ca/Al* ratios document calcite precipitation during the warm summer months.

The hydrological investigations presented in this study document distinct seasonality in the Lake Challa system. Sedimentological and geochemical investigations of recent sediments

show that this signal is preserved in the sedimentary record, and results from ongoing lake monitoring will probably allow even finer differentiation of seasonal signals. While more ground-truthing work is planned, including ^{210}Pb-dating of the shallow sediments, the results reported here indicate that the Lake Challa sediment archive is a promising target for high-resolution palaeoclimate studies in East Africa.

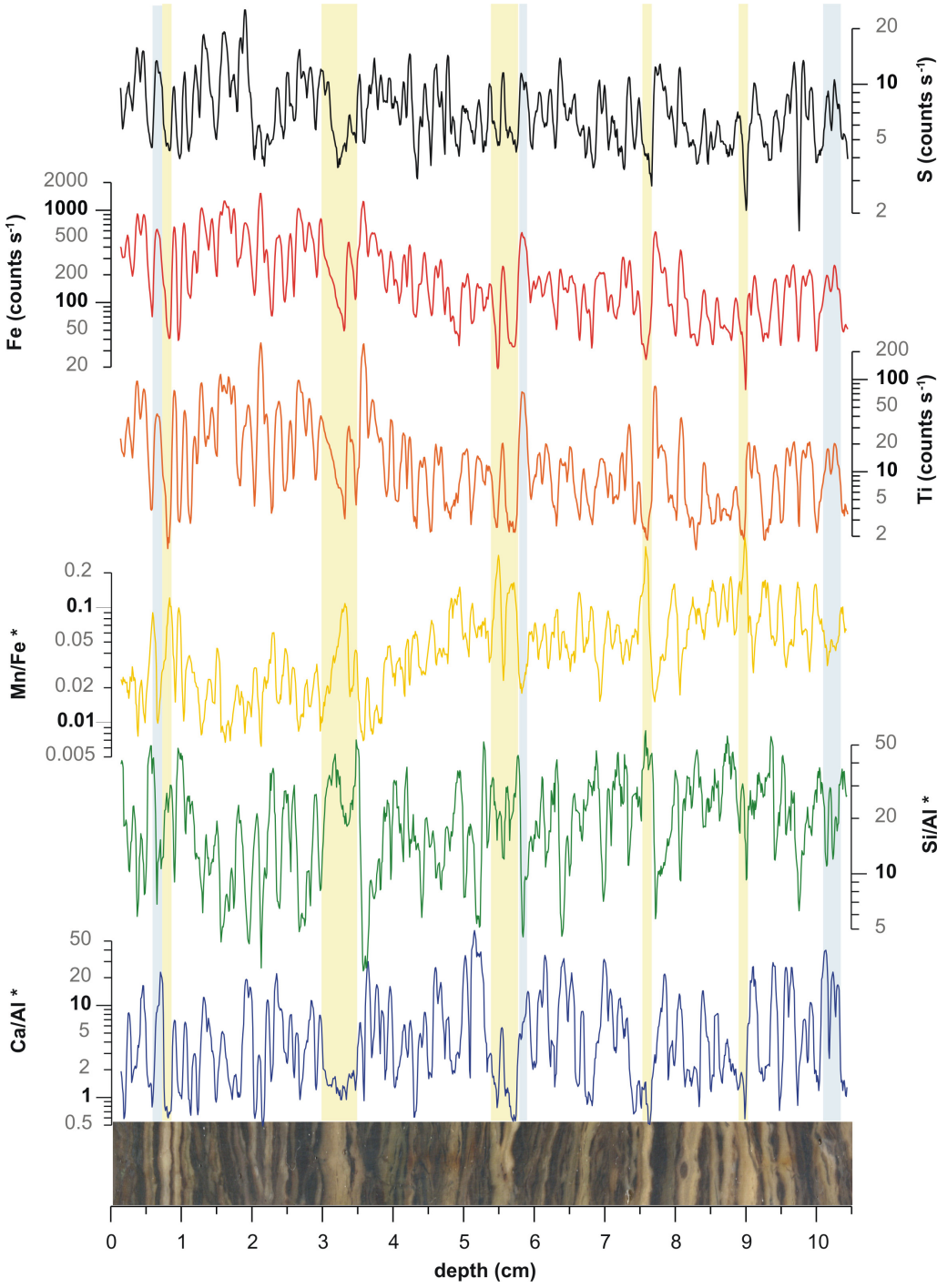

Figure 5.7: Selected µXRF scanning profiles and converted intensity ratios of an exemplary thin section block from short core CH05-1G (0–10 cm below lake floor, corresponding to the last ~65 years). Curves represent 5-point running averages of measurments at 100 µm resolution; yellow bars mark prominent diatom laminae, blue bars prominent organic/detrital laminae.

Table 5.2: Results from XRF analyses of selected source rocks and corresponding soil samples (all collected within 30 km around Lake Challa). Element ratios refer to mass ratios calculated from the oxide content (wt%/wt%).

sample description	CO_2	H_2O	P_2O_5	K_2O	Na_2O	CaO	MgO	MnO	Fe_2O_3	Al_2O_3	TiO_2	SiO_2	Σ	Ca/Al	Si/Al	Mn/Fe
unweathered grits (foot of Challa)	4.68	2.74	0.93	0.68	1.50	15.9	8.53	0.21	14.2	9.70	4.04	35.9	99.1	2.22	3.27	0.017
weathered grits (caldera rim)	0.72	3.55	1.14	2.12	1.41	11.0	8.51	0.23	15.5	11.0	4.29	39.9	99.4	1.36	3.21	0.017
soil on grits (caldera rim)	3.99	5.97	0.84	1.13	0.35	11.3	8.28	0.21	14.0	11.0	4.21	38.1	99.4	1.40	3.07	0.016
local lava (caldera rim)	0.63	2.23	0.63	0.71	1.77	13.0	12.2	0.19	12.9	11.1	3.26	40.7	99.3	1.58	3.24	0.016
soil on lava (caldera rim)	2.31	3.55	0.93	1.83	1.94	9.88	7.22	0.22	14.7	11.7	4.03	41.2	99.4	1.14	3.11	0.016
pumice peaces (caldera rim)	0.54	3.18	0.56	0.48	0.57	13.5	12.5	0.20	13.4	11.8	3.32	39.4	99.5	1.55	2.95	0.017
soil on pumice (caldera rim)	4.60	5.28	0.64	0.79	0.75	9.80	10.5	0.20	13.5	11.2	3.81	38.3	99.4	1.18	3.02	0.016
unweathered basalt (caldera rim)	0.23	1.79	0.69	1.74	3.29	8.28	5.31	0.19	14.1	15.2	3.77	44.9	99.5	0.74	2.62	0.015
unweathered basalt (Rombo Series, foot of Challa)	0.15	1.29	0.84	1.53	3.27	8.69	4.56	0.19	13.6	16.1	3.79	45.5	99.5	0.73	2.50	0.015
soil on basalt	1.30	3.11	0.73	1.40	1.74	8.19	7.66	0.24	17.2	13.1	4.32	40.5	99.4	0.84	2.73	0.015
sand of pool in rivine*	7.82	9.03	0.87	0.81	0.27	4.49	3.26	0.25	17.9	16.1	4.71	34.0	99.5	0.38	1.87	0.016
sand/clay from dry river bed (foot of Challa)	5.54	10.1	0.51	0.25	0.09	1.62	2.78	0.30	22.1	17.6	5.38	33.2	99.5	0.12	1.66	0.015
fsp rich gneiss (Reata Mt.)	0.15	0.73	0.03	5.77	2.04	0.86	0.15	0.07	1.74	12.6	0.14	75.4	99.7	0.09	5.27	0.046
soil on fsp rich gneiss	5.56	3.06	0.18	3.30	1.90	2.53	1.05	0.11	6.91	13.4	1.59	60.0	99.6	0.26	3.97	0.017
banded gneiss (Reata Mt.)	0.05	0.66	0.02	4.84	3.24	0.60	0.01	0.00	0.70	12.4	0.05	77.3	99.9	0.07	5.49	0.002
soil on banded gneiss	1.49	3.15	0.19	2.15	2.58	3.13	1.00	0.15	8.78	17.2	1.73	58.0	99.5	0.25	2.98	0.019
soil from Challa irigation project	5.15	7.12	0.71	1.22	0.71	7.16	3.20	0.24	15.8	16.7	4.24	37.2	99.5	0.58	1.97	0.017
soil from Challa village	3.83	8.28	0.67	1.09	0.21	4.07	3.03	0.25	15.5	17.3	3.97	41.2	99.5	0.32	2.10	0.018

ACKNOWLEDGEMENTS

We acknowledge the Deutsche ForschungsGemeinschaft (DFG) and FWO-Vlaanderen (Belgium) for funding of this work within the framework of the CHALLACEA project in the European Science Foundation EUROCORES Programme EUROCLIMATE (contract No. ERAS-CT-2003-980409). We further acknowledge Matthias Vuille (University of Massachusetts, USA) for providing meteorological data, Jasper Moernaut (Ghent University, Belgium) for the bathymetric map, and Ursula Kegel (GFZ) for laboratory support. Caxton Mukhwana Oluseno is especially thanked for unfailing work in lake monitoring and finally all the Kenya crew members without whose assistance in transport, surveillance and accommodation this project could not be handled.

6. Lake Challa sediments – a geochemical study of a new climate archive at the foothill of Mount Kilimanjaro

Iris Kristen[1] with contributions from
Christian Wolff[1], Birgit Plessen[1]: geochemistry (TC, TIC, TOC)
Daniel Conley[2]: biogenic silica
Maureen Fagot[3]: sampling, loss-on-ignition
Rudolf Naumann[1]: X-ray diffractometry
Norbert Nowaczyk[1]: supervision magnetic susceptibility
Stephan Opitz[1]: magnetic susceptibility of short cores
Ursula Röhl[4]: supervision X-ray fluorescence scanning
Gerald Haug[1,5], Dirk Verschuren[3]: project leaders

[1]*Helmholtz Centre Potsdam GFZ – German Research Centre for Geosciences, Potsdam, Germany*
[2]*GeoBiosphereScienceCentre, QuaternarySciences, Lund University, Sweden*
[3]*Limnology Unit, Department of Biology, Ghent University, Belgium*
[4] *MARUM - Center for Marine Environmental Research, University of Bremen, Germany*
[5]*Geological Institute, ETH Zürich, Switzerland*

Part of a manuscript for submission to: *Palaeogeography, Palaeoclimatology, Palaeoecology*

STUDY SITE AND MODERN-DAY CLIMATE

Lake Challa (3°19'S, 37°42'E) is located at ~880 m asl on the lower east slope of Mt. Kilimanjaro (Fig. 5.1) and fills a volcanic caldera within igneous rocks (predominantly trachy-basalts) of the tertiary Kilimanjaro complex (Bear 1955). These basalts are covered by "calcareous tuffaceous grits", a calcite-cemented tuffaceous breccia that is probably related to the formation of the Challa crater (Downie and Wilkinson 1972). The volcanic complex is underlain by metamorphic basement rocks (predominantly gneisses) which outcrop east- and southward of Lake Challa and dominate the area up to the coast (Petters 1991). Up to 170 m high, the surrounding steep crater walls confine the lake's catchment area and limit freshwater input to sub-surface inflow from groundwater, precipitation (c. 600 mm/yr), run-off from the walls and inflow from one small creek of c. 300 m length. The latter is only active during seasons of exceptionally heavy rainfall (information from local fishermen) and thereby enlarges the catchment by c. 0.2 km² at the NW corner of the caldera. Groundwater inflow derives most probably from percolation of precipitation falling in and above the forest zone on the upper slopes of Mt. Kilimanjaro. Sub-surface outflow and evaporation (1700 mm/yr, Payne 1970) dominate the negative side of the water balance of Lake Challa. The lake surface area covers c. 4.2 km² and its maximum depth varies inter-annually between 92 and 98 m (range of observations 1999-2007). Within this lake basin form laminated sediments of autochthonous character which are predominantly composed of biogenic silica, organic matter, and endogenic

calcite. A seismic survey estimates the sediment infill to comprise ~210 m and cover the last ~250,000 years (Moernaut et al. in prep.).

The climate of tropical Eastern Africa is controlled by the seasonal passage of the Inter-Tropical Convergence Zone (ITCZ; Fig. 5.2) which is connected to the zenith of the sun. Following its crossing over the equator during the equinoxes, rainfall occurs predominantly from October to December and March to May (Fig. 5.3). These two rain seasons are referred to as the "long rains" (Mar–May) and the "short rains" (Oct–Dec). The former are usually associated with the major amount of rainfall of the year in East Africa. Yet, the latter are reported to show stronger inter-annual variability and presumably respond to changes in Indian Ocean surface temperatures and related atmospheric circulation (Black et al. 2003; Clark et al. 2003; Hastenrath et al. 2004; Kabanda and Jury 1999; Schreck and Semazzi 2004). Temperatures in this region are lowest during southern hemisphere winter (Jun–Aug, ~23°C at Voi station, c. 100 km east of Lake Challa, source: http://www.ncdc.noaa.gov) and highest during southern hemisphere summer (~26°C, Nov–Mar). Wind speeds show the inverse pattern. They are generally weaker from November to April and stronger between May and October, which is related to the prevalent south-easterly trade winds during the period of a northward displaced ITCZ (Fig. 5.2). The north-easterly trade winds during January and February are less prominent and more variable, but occasionally form a secondary maximum in the annual course of the wind speed (based on daily observations at Voi 1976-2007, http://www.ncdc.noaa.gov).

MATERIAL, METHODS AND CORE CHRONOLOGY

Several cores were recovered in Lake Challa during coring campaigns between September 1999 and August 2007. To investigate lateral changes within the sediment composition and lamination, seven gravity cores of 25.5 to 35.5 cm length were taken in September 2006 along a horizontal transect from the centre of the lake (98 m water depth) to the periphery part (65 m water depth) of the north-eastern slope of the caldera. For the construction of a long, continuous composite profile we rely on three Niederreiter piston cores (CH05-2P, 3P, 4P) and one gravity core (CH05-1G) recovered in February 2005, and on one mini-Kullenberg core (03-2K) recovered in January 2003. These cores were recovered in the centre of the lake (Fig. 5.1) where sediments are uniformly draped across the lake bottom (Moernaut et al. in prep.). The composite profile of 21.6 m length was obtained by visual alignment of individual marker laminae, and synchronisation of the magnetic susceptibility records where the quality of the lamination did not allow visual cross-correlation. Quality of the lamination suffered primarily from disturbing effects of the corer's hammering action on and the subsequent transport of sediments with high gas and water content. Based on characteristic sediment features (e.g., high magnetic susceptibility values; see below) and close-interval ^{14}C dating, we identified five turbidite horizons together adding up to 0.92 m. They are considered as instantaneous events and excluded from the composite profile to obtain a continuous record of purely lacustrine, mid-lake sedimentation. Magnetic susceptibility was measured every 1 mm

at a precision of 10-6 SI with a Bartington MS2E spot-reading sensor mounted to a fully automatic (GFZ-developed) core-logging system. The drift of the sensor was monitored by readings in air after every 10th reading on the sediments, and was subsequently subtracted from these data by linear interpolation (e.g., Nowaczyk 2001).

Sampling of the composite profile for analysis of total carbon (TC), total organic carbon (TOC), total inorganic carbon (TIC), total nitrogen (TN) and biogenic silica (bSi) was conducted continuously at 2 cm resolution. For all sub-sampling operations, curvilinear cutting of samples along the lamination planes in three dimensions was applied. After freeze-drying and grinding, samples for TOC analysis were decalcified with 20 % HCl and heated for 3 hours at 75 °C. About 20 mg of sediment were loaded in tin capsules (for TC, TN) and c. 3 mg of sediment were packed into silver capsules (for TOC), respectively, and combusted under oxygen flow at >1000 °C. After combustion, CO_2 and N_2 were separated using a GC column and detected using thermal conductivity. The analyses were performed using an elemental analyser (NC25000 Carlo Erba) at the GeoForschungsZentrum Potsdam. The results were referenced against lab-internal soil standards and a reference sample (Urea). The reproducibility for replicate analyses is better than 0.2 % for all analyses. TIC was determined as the difference between TC and TOC, and carbonate content is stoichiometrically calculated from TIC (factor 8.33). The amount of organic matter (OM) was estimated to be 1.0077*TOC+7.198, based on ~130 paired analyses of TOC and weight loss on ignition (Dean 1974) in the upper 2.60 m of the cored sequence. Biogenic silica was extracted with 1 % $NaCO_3$ at 85°C. Five percent of the samples were extracted using the traditional 5 hour extraction with sub-samples removed at 3, 4 and 5 hours (Conley and Schelske 2001). However, no significant increases in slope were observed. Therefore, all samples were extracted in duplicate using a 3 hour extraction to determine bSi concentrations.

The dry bulk density (DBD, g cm^{-3}) was calculated as the dry mass of a sample divided by its initial bulk (wet) volume (Avnimelech et al. 2001). The water content (%) was calculated as the mass of water to the total wet mass.

Changes in the element composition of the sediment profile were studied by means of X-ray fluorescence (XRF) scanning. This is a semi-quantitative, non-destructive logging method that provides records of changing element intensities for major and minor elements with atom weights between 27 and 138 (Al, Si, K, Ca, Ti, Mn, Fe, Zr, Nb and Sr). XRF scanning of split sediment cores in 1 cm resolution was done as described in Richter et al. (2006), Röhl and Abrams (2000) and Tjallingii et al. (2007). The measurements were performed using the X-ray fluorescence Core Scanner II at MARUM, University of Bremen (Germany).

Powder X-ray patterns were achieved from magnetic extracts of samples from 0 m, 0.6 m, 5 m, 7 m, 8 m, 12.3 m and 19.6 m (all sediment depths are given in m composite depth if not stated otherwise). Magnetic grains were extracted using a magnetic needle (70 mT) plunged in c. 10 cm^3 of sediment suspended in an aqueous solution of sodiumpyrophosphate (50 g/l) and ethanol (1/1 v/v) in an ultrasonic bath. Powder X-ray patterns were collected using a Siemens D5000 θ -2 θ powder diffractometer with Cu Kα radiation, automatic divergent and anti-scatter

slits and a secondary graphite monochromator with scintillations counter. The diffraction data were recorded from 4 to 75° 2θ with a step width of 0.02° and a counting time of 4 s per step. The generator was set for 40 kV and 30 mA.

The age model of the composite profile is based on 188 AMS ^{14}C datings, corrected for a lake-carbon reservoir age and calibrated using Intcal04. The magnitude of the reservoir effect at any given time was estimated from i) wiggle-matching high-density series of bulk organic ^{14}C dates with the ^{14}C calibration curve (IntCal04, Reimer et al. 2004), ii) ^{210}Pb-derived time markers for most recent sediments, and iii) paired bulk organic and grass charcoal ^{14}C dates. The screened series of ^{14}C dates were calibrated simultaneously using Bayesian age-modelling, taking into account their stratigraphical order. Error-weighted smoothed splines were drawn through the ordered calibrated ranges, resulting in 95 % age uncertainties ranging from around 100 years for the Holocene to maximally 300-500 years in the glacial section of the record. According to this procedure, the 20.7 m long sediment sequence covers the last c. 25,000 years before present (in the following kyr BP) which corresponds to a mean sedimentation rate of c. 0.8 mm yr^{-1}. Sedimentation rates are approximately constant over the profile except for the last c. 1 kyr and between c. 16 and 20.5 kyr BP where they are up to c. 1.3 times higher. For details of the age model we refer to Blaauw et al. (in prep.).

RESULTS AND DISCUSSION

General sediment characteristics

The sediments recovered from Lake Challa comprise predominantly finely laminated, diatomaceous gyttia with varying amounts of OM, bSi and carbonates (Fig. 6.1). Total organic carbon content (TOC) varies between c. 1 and 22 %, and reach maximum values between 7.5 and 8.5 m sediment depth. Carbonates are virtually absent below 5.3 m and show maximum values up to 40 % in the top 1.5 m. Biogenic silica contents range from 10 to 75 % with average values around 37 %. For most of the top 5 m, biogenic compounds (bSi, OM) and carbonates add up to 60–90 % of the sediments; by subtraction, the residual clastic mineral fraction amounts to a modest 10–40% of total dry mass. Dry bulk density (DBD) decreases from an average value of 0.25 g/cm³ to 0.18 g/cm³ when low-density, biogenic and carbonaceous components are abundant. Water content, on the contrary, is high coincident with high TOC and bSi contents. Potassium (K), titanium (Ti) and iron (Fe) intensities follow the opposite trend, probably reflecting their proportionality to the clastic sediment fraction (Fig. 6.2). All three elements are frequently interpreted in this way (e.g., Bahr et al. 2005; Haug et al. 2001; Lamy et al. 2004). Magnetic susceptibility (MS) values of the sediments above 12 m which are predominantly around or below zero further underline the low minerogenic content of these core sections (Maher and Thompson 1999).

High MS, DBD, K, Fe and Ti intensities and low bSi and water contents characterise distinct homogenous horizons at 4.87–5.13 m, 6.77–7.09 m, 18.99–19.04 m, 19.18–19.24 m and 20.24–20.39 m, as well as mm- to cm-scale sandy layers at 2.3 m, 7.7 m, 13.2 m and 19.4 m, and the core section from 1.2 to 0.5 m (Fig. 6.1 and 6.2). With the exception of the interval 1.2–0.5 m, investigations in thin sections identify these horizons as either reworked ("turbidite") horizons, or ash layers.

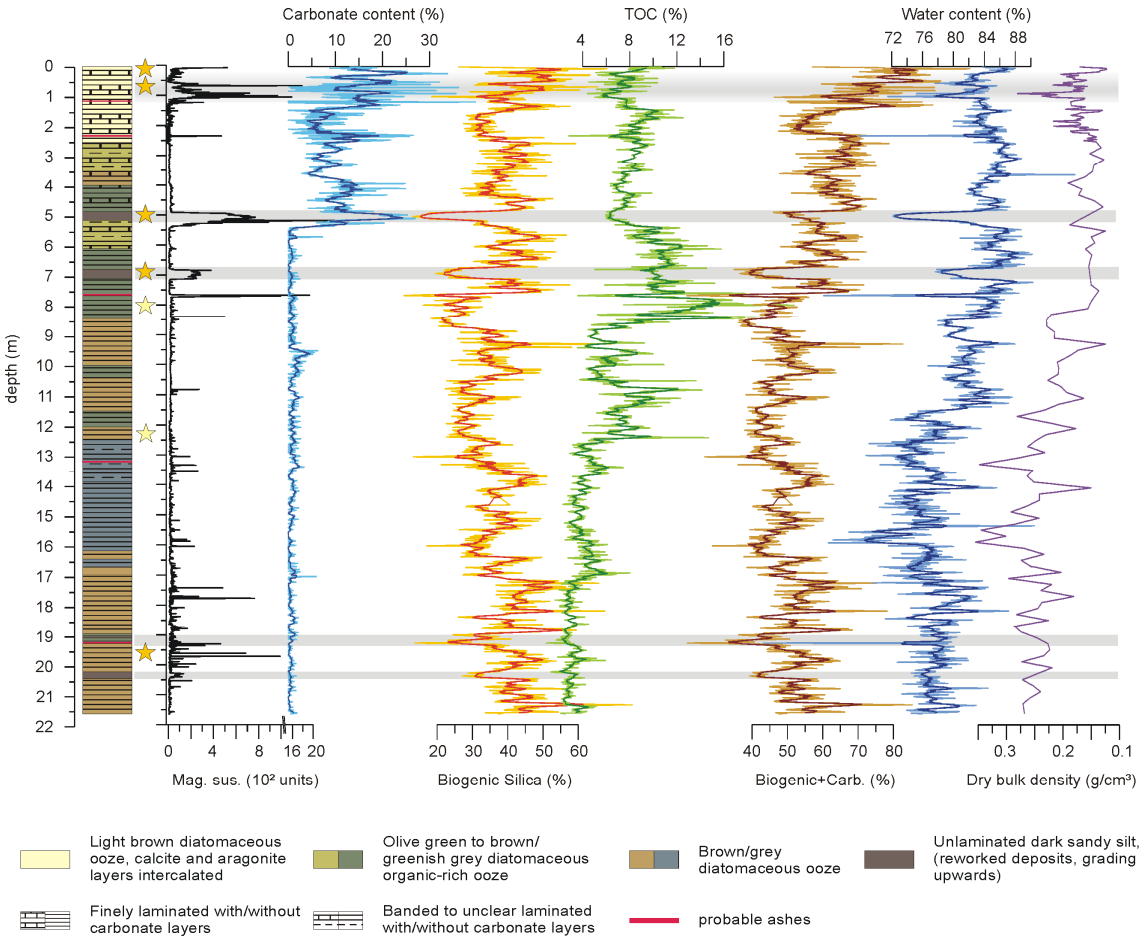

Figure 6.1: Down-core sedimentary profiles of magnetic susceptibility (Mag. Sus.) and selected geochemical parameters from Lake Challa: carbonate content, biogenic silica content, total organic carbon content (TOC), the sum of biogenic (bSi, OM) and carbonaceous components (bSi and OM calculated as quoted in "Material and methods and core chronology"), water content (all in wt-%, thick lines are 5-point running averages), and dry bulk density (note the reversed scale). Stars indicate levels of X-ray diffractometric analyses of magnetic extracts, dark (light) yellow colour show those levels where titanomagnetites were (not) recovered. Grey bars highlight turbidite layers and the interval 1.2-0.5 m.

Turbidite horizons

The sedimentology of the reworked ("turbidite") horizons is distinctly different from the rest of the sediment sequence (Fig. 6.3 a). They show a characteristic sandy bottom layer rich in mineral and volcanic rock fragments (Fig. 6.3 b), grading into a homogenous body that

contains high amounts of littoral components such as mollusc (mostly *Melanoides tuberculata*) and ostracod shell fragments, terrestrial plant OM, and sponge spicules (Fig. 6.3 c). Their light-coloured top almost exclusively consists of diatoms (Fig. 6.3 d, e). MS is generally high within the turbiditic horizons (Fig. 6.1) and reflects the higher fraction of local volcanic rock material, which contains high amounts of titanomagnetites (TM) (Fig. 6.6, for further discussion see below).

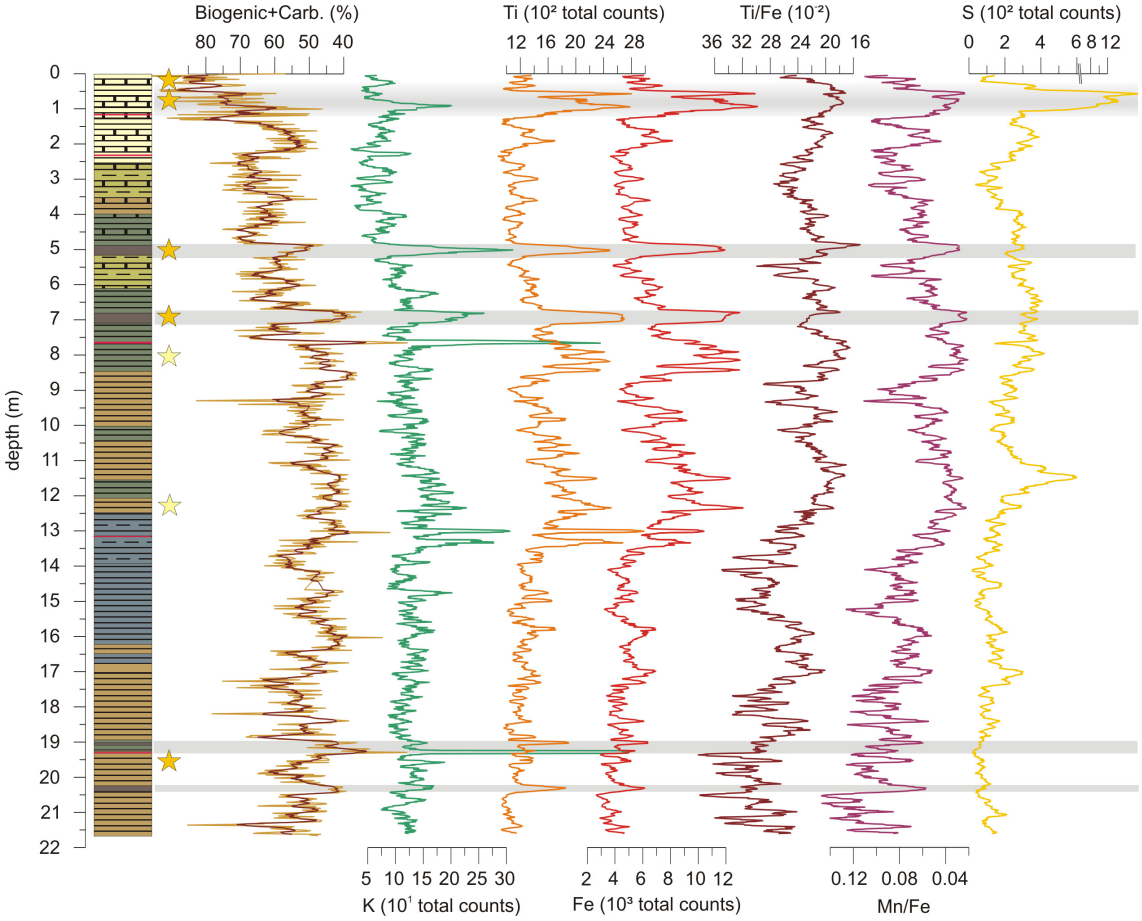

Figure 6.2: Selected down-core profiles of XRF intensities (9-point running averages) compared with the sum of biogenic (bSi and OM) and carbonaceous components (note the reversed scale). For legend of the sediment profile see Fig. 6.1.

Ash layers

Ash layers appear often as light, slightly violet to steel-grey, sandy layers in the sediment profile. They contain translucent to slightly brownish volcanic glass fragments (Fig. 6.4) and are almost always characterised by high intensities of K and high MS (Fig. 6.1 and 6.2); exceptional is the ash layer at 13.2 m. Two prominent ash layers are identified at 7.7 and 19.3 m (c. 8.7 and 22.4 kyr BP). The younger layer is characterised by especially high niobium (Nb), zirconium (Zr) and strontium (Sr) intensities (not shown) and moderately high K

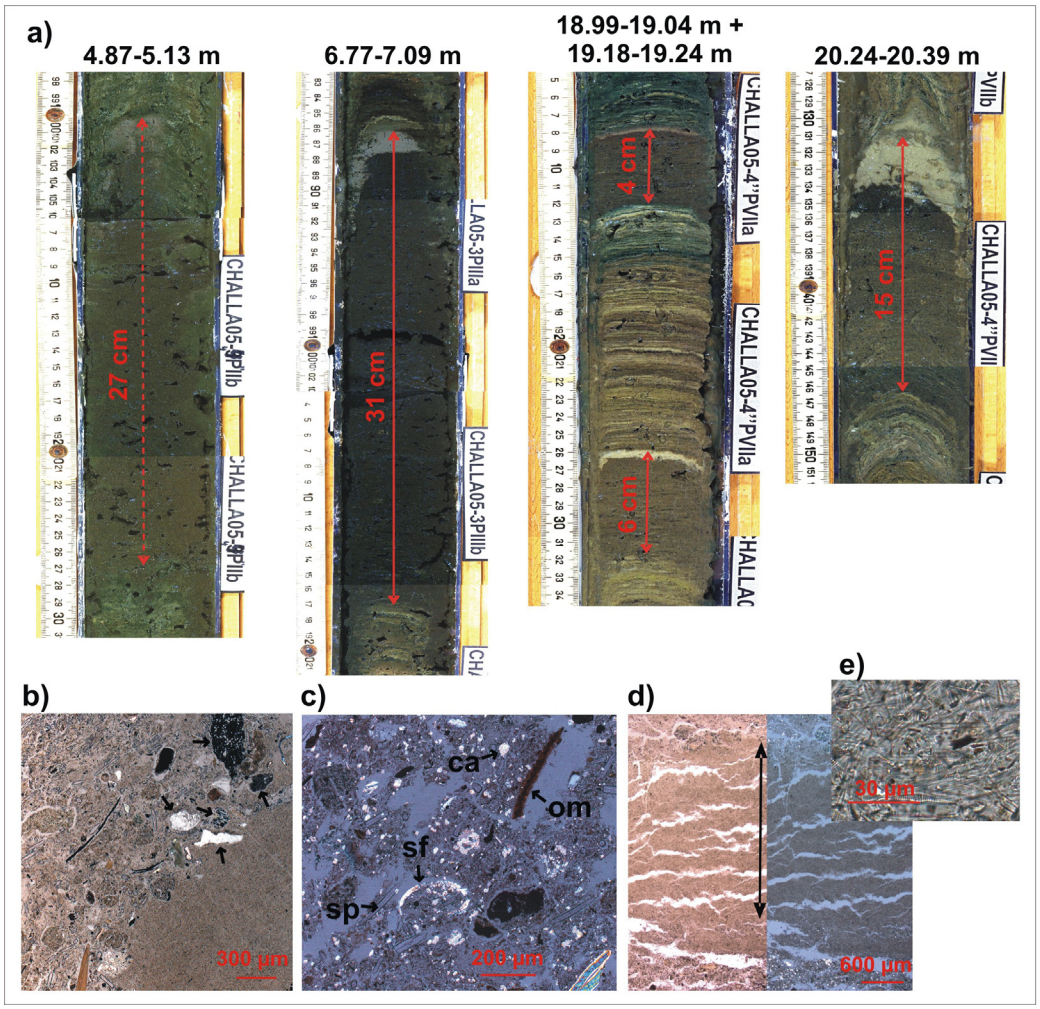

Figure 6.3: a) Core sections with turbidite horizons from Lake Challa sediments. All are characterised by a coarse sandy layer at the base, a homogenous body rich in littoral components (shells, terrestrial organic matter, sponge spicules; carbonates are only present in the turbiditic horizon ~5 m), and a light diatom layer at the top; b) to e) thin section photographs from the turbiditic horizons: b) the coarse base ~7 m with volcanic rock fragments (arrows); c) the homogenous body ~5 m contains shell fragments (sf), terrestrial organic matter (om), carbonates (ca), and sponge spicules (sp); d) the light top layer ~5 m (arrow), which almost exclusively consists of diatoms; e) close-up of diatom-rich top ~5 m. b), c) and right half of d) are taken under polarised light, d) left half and e) are taken under normal white light.

intensities. On the contrary, the older layer shows an especially prominent peak in K, whereas Zr and Sr are less prominent. The high K and Sr contents are presumably related to the widespread alkaline nature of volcanism in East-Africa (Wilkinson et al. 1986; Williams 1970). Zirconium and Nb are incompatible elements often associated with volcanic ashes and have been used in lake sediments from the East-African rift to characterise ash layers (Brown et al. 2007; Johnson et al. 2002). The ratio of Zr and Nb is reported to be source-specific (Scott and Skilling 1999), therefore indicating a different volcanic origin of both ash layers. One probable source for ashes in Lake Challa sediments is Mount Meru, a fluoride-rich nephelinitic volcano located c. 100 km to the west. It was especially active during the last 300,000 years, and the most recent reported eruption dates from 26 October 1910 (http://www.volcano.si.edu, Pyle 1999; Wilkinson et al. 1986). The most prominent eruption during the last 25,000 years

presumably was the formation of the Mt. Meru caldera, which is associated with massive lahar deposits spreading over c. 1,500 km² eastward of the volcano. It took place during the early Holocene as radiocarbon dating of bulk OM from lake sediments within the lahar deposits indicate (oldest date 5845±115 ^{14}C yr [~6660 cal yr BP], Hecky 1971). This event has been suggested to be a prominent Holocene marker horizon in East Africa (Pyle 1999), and could be responsible for the younger prominent ash layer in Lake Challa sediments. The observation of an ash layer of similar age in sediments from northern Lake Malawi (8350±250 yr BP, Barry et al. 2002) corroborates this argument. It may even be recorded in the Mount Kilimanjaro ice core, where especially high concentrations of fluoride, K and Na are reported from ice 8.2–8.4 kyr BP old (Thompson et al. 2002). However, quaternary tephrochronology is poorly developed in eastern Africa due to difficulties in identifying unequivocal chemical signatures (Pyle 1999; Scott and Skilling 1999; Wilkinson et al. 1986). This precludes more definite assignments on the origin of individual tephra layers in the Challa sequence at this point.

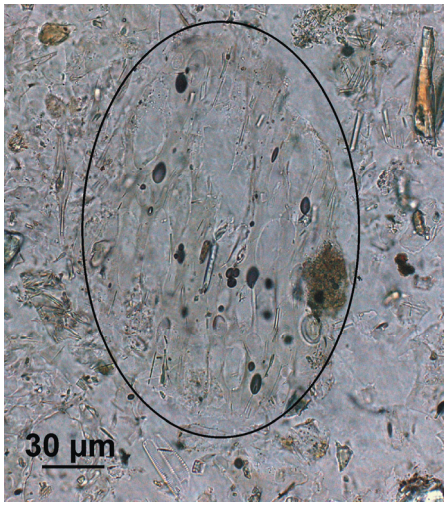

Figure 6.4: Thin section photograph of volcanic glass fragment (almost translucent and rich in vesicles, enclosed in circle) from the ash layer at 19.3 m, under normal white light.

Sources and processes of clastic sediment input

As expected for Lake Challa with its steep crater walls and a very small catchment area, sediments in the lake basin comprise a dominant proportion of autochthonous components. Nevertheless, investigations on the clastic sediment fraction, its mineral and elemental composition, can yield valuable information about sediment input and diagenesis (Boyle 2001). For appropriate application of element intensity ratios from XRF scanning, it is particularly essential to study the origin and underlying processes of the clastic sediment delivery.

Input of clastic material can happen by erosion and run-off from the catchment or by aeolian input of dust from remote areas. In the case of Lake Challa the igneous rocks in the local catchment are distinct from the basement metamorphic rocks (primarily gneisses) predominating to the south-east and east of the crater (Bear 1955) where – due to the predominance of easterly winds in this area (Hastenrath 2001; Thompson et al. 2002) – the main

aeolian source areas are expected. The differences in mineralogical composition of the two source areas can be observed in thin sections, XRD and XRF analyses of representative rock samples (Table 6.1, Fig. 6.5). Prominent differences arise, for example, in the relative amounts of Ti, Fe and K: local basalts, lavas and grits exhibit 6 to 10 times higher Fe and Ti concentrations than the investigated gneisses, whereas the latter show 3 to 4 times higher relative K concentrations than local rocks. Thin-section analyses illustrate the high abundance of titanomagnetite (TM) in the basalts, lavas, and grits that form the caldera (Fig. 6.5), and XRD analyses and scanning electron microscopy (SEM) in combination with energy-dispersive X-ray analyses of magnetic extracts of core top sediments (3-cm increment) show the presence of TM at the central coring location (Fig. 6.6 a). Both observations underscore a local origin of the clastic sediment fraction.

Titanomagnetite is probably also the main source for the magnetic signal of Lake Challa sediments as it is characterised by very high MS (when present in appropriate concentrations) compared to the low positive (negative) susceptibilities of paramagnetic (diamagnetic) minerals of the autochthonous sedimentation (e.g., Maher and Thompson 1999). Comparison of MS records of short cores along a transect from the periphery to profundal lake regions reveals decreasing MS with increasing lake depth and increasing distance to the shore (Fig. 6.7). This observation further favours a local source for Ti-rich minerals in the lake sediments.

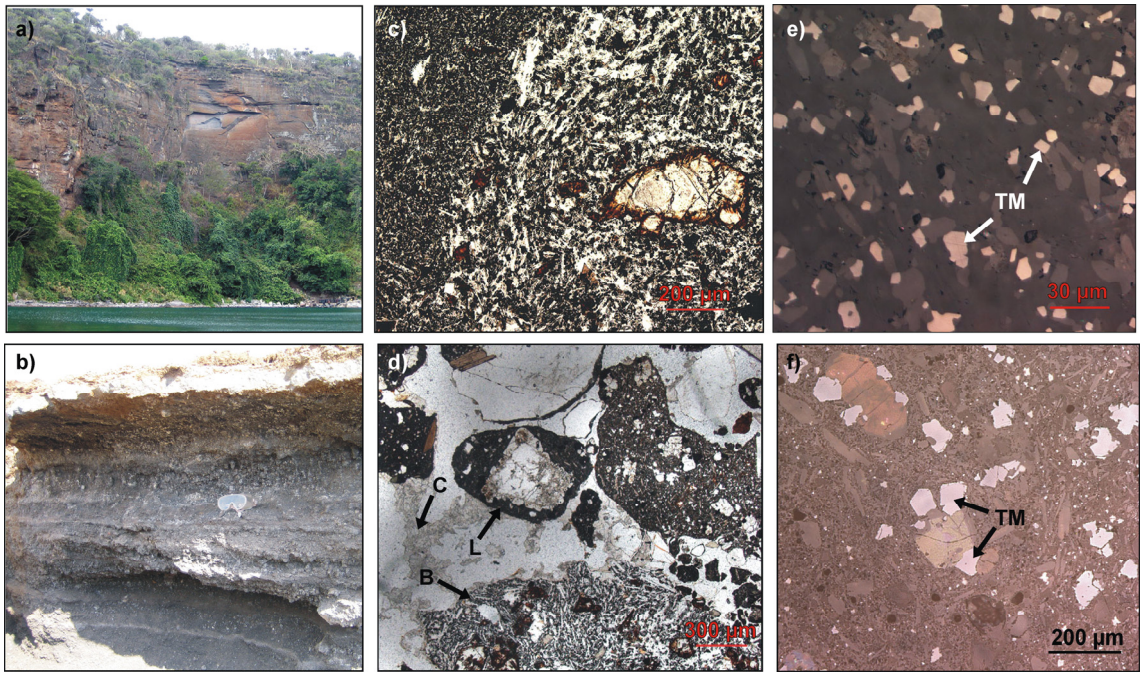

Figure 6.5: Basalts of the Kilimanjaro complex that form the main parts of the crater walls (a) and "calcareous grits" that form the south-eastern crater walls of the Challa crater (b); thin section photographs of basalt (c), dominated by oxides (opaque) and plagioclase (white), and "calcareous grits" (d) (C = calcitic cement, B = basaltic fragment, L = lava fragment with high proportion of opaque glas) under normal white light; thin section photographs of basalt (e) and "calcareous grits" (f) under reflected white light (TM = titanomagnetites, slight colour differences within TM crystals result from maghemitisation process).

However, under the prevailing tropical climatic conditions not rocks but soils are expected to be the main source for transport by wind and erosion. Soils from the different source areas are very similar in elemental composition (Table 6.1) and probably preclude a definite source attribution for individual elements. This is underlined by similar trends in the K and Ti records of the down-core profile (Fig. 6.2). XRD analyses in six discrete horizons of the core demonstrate the presence of TM deeper down the sediment profile but only in intervals which are characterised by relatively high Ti and Fe intensity as well as high MS (at 0.7 m, 5.0 m, 7.0 m and 19.6 m, indicated by dark yellow stars in Fig. 6.1 and 6.2), whereas no TM was detected in core sections with high Ti and Fe intensities but low MS (at 8.0 m and 12.3 m, light yellow stars in Fig. 6.1 and 6.2). This indicates a second non-magnetic source for Ti and Fe, for example clay minerals from soils. In summary, our investigations do not allow a more specific attribution of Ti, Fe or K to a local or remote origin, but MS appears to be a suitable proxy for the input of TM from local rocks to the lake sediments. Similarly, MS was used as a tracer for sediment input from the catchment in a study at Lake Masoko (southern Tanzania) (Garcin et al. 2006b). Following an extensive investigation on the transportation and sedimentation behaviour of multi-domain Ti-rich magnetite in and around that tropical maar lake, these authors were able to demonstrate that the most effective transportation of this material from the exposed lake shore into the lake occurs during periods of high-amplitude lake-level fluctuations combined with drier conditions and high wind stress. Similar processes can be active in Lake Challa and responsible for transportation of local detrital material into profundal sediments. However, dilution by autochthonous components, which plays a minor role in the oligotrophic Lake Masoko, and diagenetic effects are expected to have a stronger influence in the deep, productive and stratified Lake Challa in comparison to Lake Masoko, and may obliterate the original source information contained in MS (see next section).

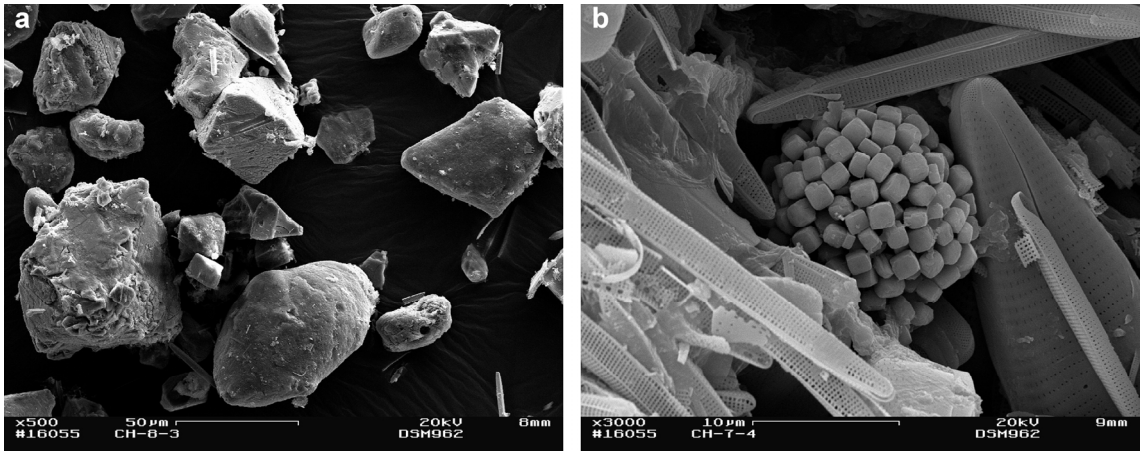

Figure 6.6: SEM images of a) titanomagnetites extracted from Lake Challa surface sediments: ideomorph crystals show clear signs of maghemitisation ("cracks"); b) pyrite framboid embedded in diatom-rich sediment (0.32 m core depth).

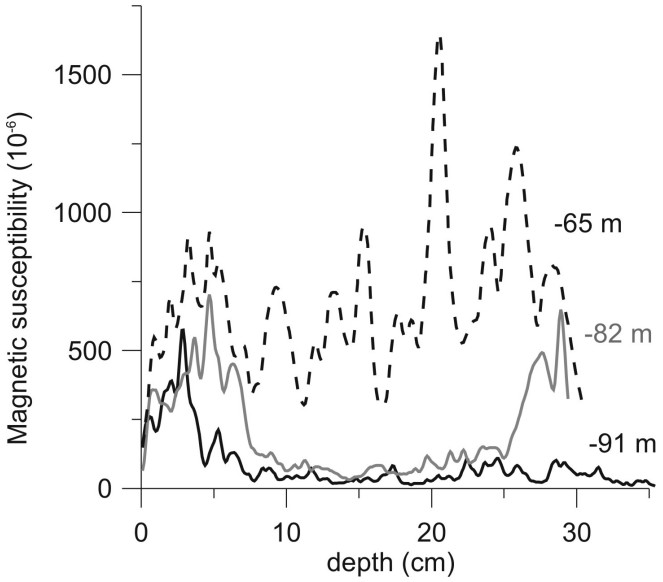

Figure 6.7: Magnetic susceptibility records of three short cores taken at 65, 81 and 98 m water depth.

Influence of diagenesis and changing redox conditions on Lake Challa sediments

Diagenetic processes can alter the element distribution patterns and, on longer time scales, also the magnetic signal of lake sediments (Maher and Thompson 1999; Wersin et al. 1991). Most important are interactions with the sulphur cycle in combination with changing (seasonal or inter-annual) oxygenation of the water column (Holmer and Storkholm 2001). In this context, changing redox conditions are known to especially influence the Fe and manganese (Mn) cycles in lake waters and sediments, whereas Ti-bearing minerals are usually considered to be more conservative in geochemical reactions (Davison 1993; Demory et al. 2005; Wersin et al. 1991; Wetzel 1983). As Mn is mobilised from bottom sediments more rapidly than Fe when redox conditions are deteriorating (trend towards lower pE), ratios between Mn, Fe and Ti retained in the sediment are frequently applied to study changes in the redox state of lakes (Boyle 2001; Demory et al. 2005; Granina et al. 2004; Haberzettl et al. 2007; Wersin et al. 1991).

For Lake Challa sediments, strong correlation between Fe and Ti intensities (r=0.88; Fig. 6.8 a) demonstrates that detrital input is the principal process and source for both elements, and diagenetic remobilisation and influx of dissolved Fe are of relatively minor importance. Similar ranges of Ti/Fe values in lake sediments (0.16-0.36, Fig. 6.9) and in the probable detrital source material (0.16-0.26 excluding fresh metamorphic rocks, Table 6.1) support this hypothesis. Nevertheless, the following observations suggest some influence of changing redox conditions on the Fe and Mn content of Lake Challa sediments:

1) Ti/Fe values show a reasonable correlation (Fig. 6.8 b, r=0.66) with S intensities (except for the interval 1.2–0.5 m), indicating the influence of secondary processes on Fe precipitates in comparison to Ti-bearing mineral phases;

2) Mn/Fe values reach >0.1 only for TOC concentrations <12 % and S intensities <400, and stay below 0.05 for higher TOC concentrations and S intensities, respectively. The linear

correlation is lower here (Fig. 6.8 c, r=0.52) because of the exponential relationship between them, indicating non-linear dependencies for these parameters;

3) In a high-resolution study on modern sediments we observe parallel increasing S and Fe intensities within dark, mm-scale laminae together with framboidal Fe-sulphides (Fig. 6.6) and low Mn/Fe values (Kristen et al. in prep.). This coherence can be detected in other finely laminated intervals of the core profile down to 16 m core depth, thereby corroborating the observation of Wersin et al. (1991) that the Mn/Fe value of lacustrine sediments preserves information on the redox conditions that prevailed at the lake bottom during sediment formation.

Accordingly, we apply Mn/Fe and Ti/Fe intensity ratios to trace changes in redox conditions in Lake Challa since the last glacial period (Fig. 6.9).

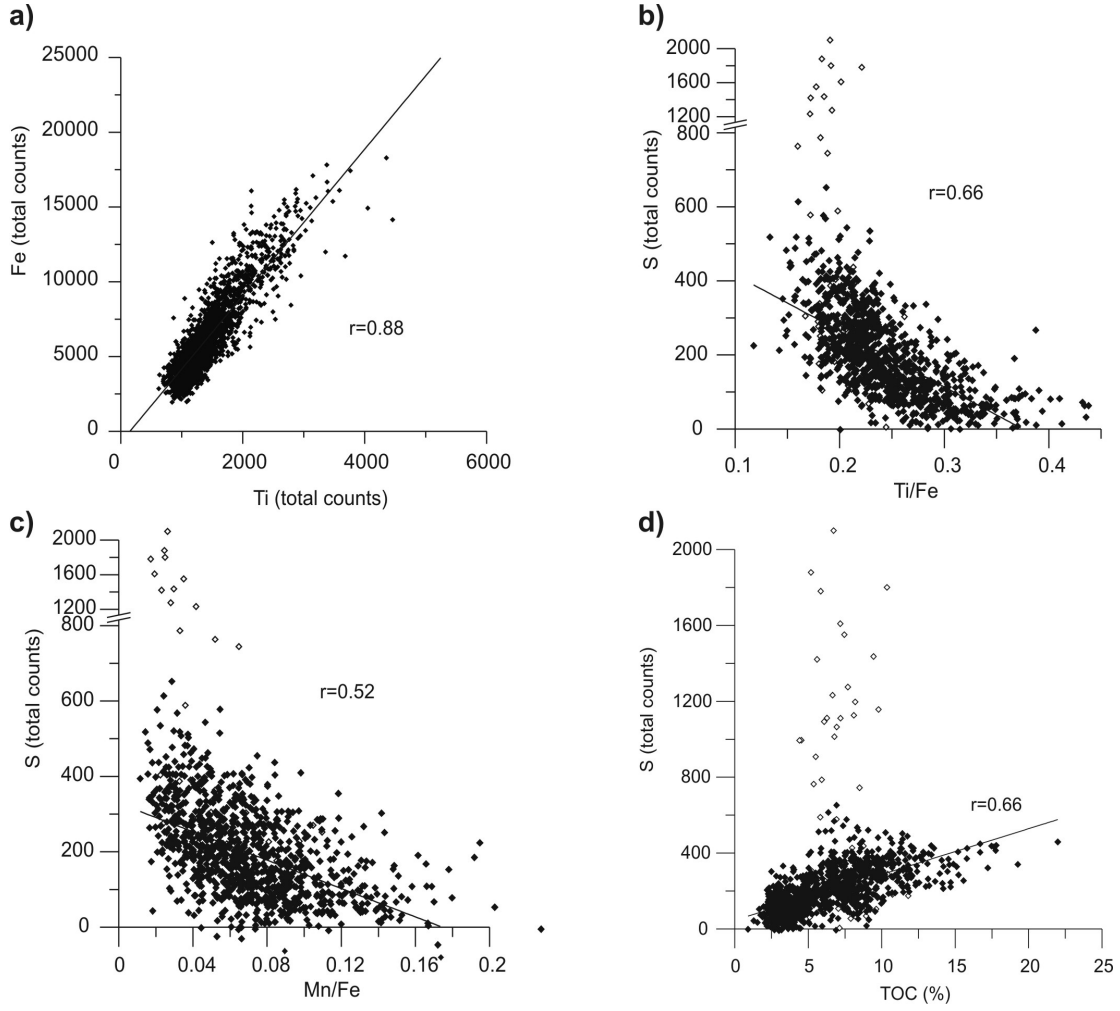

Figure 6.8: Correlation between selected element intensities, element intensity ratios (both derived from XRF scanning), and total organic carbon content (TOC, in wt%), respectively, measured on the sediment core from Lake Challa. Open symbols represent the interval 1.2–0.5 m (passive data points in these plots).

Diagenetic imprint on the magnetic signal of sediments occurs predominantly in the form of dissolution of magnetic minerals (Florindo et al. 2003, and references therein).

Dissolution of magnetite is reported from soils (Grimley and Arruda 2007), anoxic lake sediments (Demory et al. 2005; Williamson et al. 1998) and from marine sediments with high organic carbon and bSi content, and high sulphide concentrations (Canfield and Berner 1987; Florindo et al. 2003). In sediments from Lake Challa, MS is very low over large portions of the cored sequence; it is especially low or even negative when TOC concentrations are high (e.g., between ~12.5 and 1.5 m, Fig. 6.1). This inverse relationship could result from (i) reduced input of TM due to increased distance from the source and/or reduced transport capacity due to decreased run-off or diminished wave activity, (ii) from dilution of the clastic fraction by autochthonously produced biogenic and carbonaceous components, or (iii) from dissolution of the TM in anoxic environments. An increased distance to the source area can be excluded, as due to the basin morphology the lake area would not be significantly diminished by lower lake levels (unless a lowering of >65 m occurs). The sediment composition with high amounts of bSi, OM and carbonates certainly results in severe dilution of the minerogenic fraction, but it also creates ideal preconditions for dissolution of the magnetic sediment fraction. Considering all mentioned influences, the interpretation of the MS signal as a tracer for local clastic input to Lake Challa is ambiguous. Several factors can contribute to low MS; high MS, however, can be related to the activation of local sediment sources and indicates well-mixed conditions within the lake water body, which – besides contributing to transportation by wave-activity – positively influence the preservation of the signal.

Palaeolimnological interpretation

In the previous sections, we discussed the applicability of different sediment characteristics as proxies for detrital input and changes in lake-bottom redox conditions. Accordingly, elevated Mn/Fe ratios represent periods of less intense reducing conditions, and deeper or more prolonged seasonal mixing in relation to higher wind stress and/or lower lake level. High MS indicates periods of active erosion in the catchment, caused by increased precipitation or reduced vegetation cover; wave activity and wind stress must have been strong enough to transport the magnetic particles (probably predominantly TM) and for seasonal or more exceptional deep-mixing events to limit dilution of the MS signal by autochthonous biogenic components. The Ti/Fe ratio probably integrates the processes of detrital input and changing redox conditions. These interpretations are backed with geochemical (TOC, bSi, TN) data. Higher amounts of TOC are mainly attributed to a better preservation of OM under more stable water conditions, whereas increasing amounts of bSi are interpreted to reflect higher nutrient availability in response to stronger mixing (Kristen et al. in prep.); elevated TOC/TN values are interpreted to reflect a higher proportion of terrestrial plant material relative to authigenically produced OM from phytoplankton. These interpretations are in agreement with many lake studies (e.g., Lamb et al. 2004; Meyers 2003; Talbot and Lærdal 2000; Tierney and Russell 2007) and with the other presented parameters. Mutual dilution may have some effect on TOC and bSi variability, but changes in TOC in the range of 2 to 8 % are unlikely to be the only cause for bSi changes of 10 to 20 %; high diatom production and high total algal

productivity need not be correlated. High TOC concentrations additionally tend to be accompanied by high S intensities (Fig. 6.2, 6.8 d), underlining the anoxic conditions which promote preservation of organic-rich sediments. By combining interpretation of Mn/Fe, Ti/Fe and MS with bSi, carbonate and TOC concentrations as well as TOC/TN ratios, we develop a picture of changing limnological conditions in Lake Challa since the last glacial period (25–2 kyr BP) and evaluate its potential as a new palaeoclimate archive for tropical East-Africa.

At the beginning of the record under full-glacial conditions, Mn/Fe and Ti/Fe rise (note the reversed scale in Fig. 6.9) to a maximum, whereas TOC content and TOC/TN values fall to minimum values, between 25 and ~24.5–23.5 kyr BP. At the same time, bSi content is relatively high, carbonates are absent, and MS is low. These observations point to an evolution towards well-mixed lake conditions during a period of reduced detrital input. Carbonates are ether not preserved or were not precipitating during this time. In modern Lake Challa, the formation of endogenic calcite is related to the activity of photosynthetic organisms during the warm and rainy southern hemisphere spring and summer months when the lake is stratified and nutrients are delivered by run-off from the catchment (Kristen et al. in prep.). Accordingly, a reduction in nutrient input, in the length of the stratified season or in temperature are possible explanations for the observed changes in sediment composition. Within the error of the age model this period is contemporaneous with Heinrich event 2, a period of cool temperatures over Greenland (Grootes et al. 1993), especially cool and dry conditions (Allen et al. 1999; Combourieu Nebout et al. 2002; Kwiecien et al. 2009) and probably intensified atmospheric circulation (Cacho et al. 2001) in Europe, and generally cooler and more windy conditions reported from other East African archives (e.g., Brown et al. 2007; Felton et al. 2007; Ficken et al. 2002; Gasse 2000; Johnson et al. 2002).

Between 23.5 and 22.3 kyr BP, increased MS, TOC/TN and Ti/Fe consistently indicate higher input from the catchment. The importance of sediment delivery and new nutrient input from the catchment is further underlined by high BIT indices during this period (Verschuren et al. submitted; Sinninghe Damsté in prep.) and by fossil diatom studies on Lake Challa sediments showing relatively high total biovolume values (Milne 2007). Whether high erosion rates were caused by increased run-off or decreased vegetation cover can not be decided here; ongoing pollen studies may resolve this ambiguity.

Between 22.3 and 22.0 kyr BP, one ash layer and two modest mass flow events (turbidite horizons) are recorded, the latter possibly concluding this period of intense sediment load on the slopes. In the following period (22.0–20.6 kyr BP), reduced TOC/TN, Ti/Fe and MS indicate less allochthonous input. Whereas steadily decreasing Mn/Fe ratios argue for an increasingly stable water column, (seasonal?) mixing was still strong enough to sustain high diatom productivity and promote OM decomposition.

Between 20.6 and 19 kyr BP, variability and values of Mn/Fe and Ti/Fe are generally lower, MS and bSi are reduced, whereas TOC and TOC/TN are relatively high. Following the argumentation above, these observations indicate a decrease in mixing, thereby decreasing

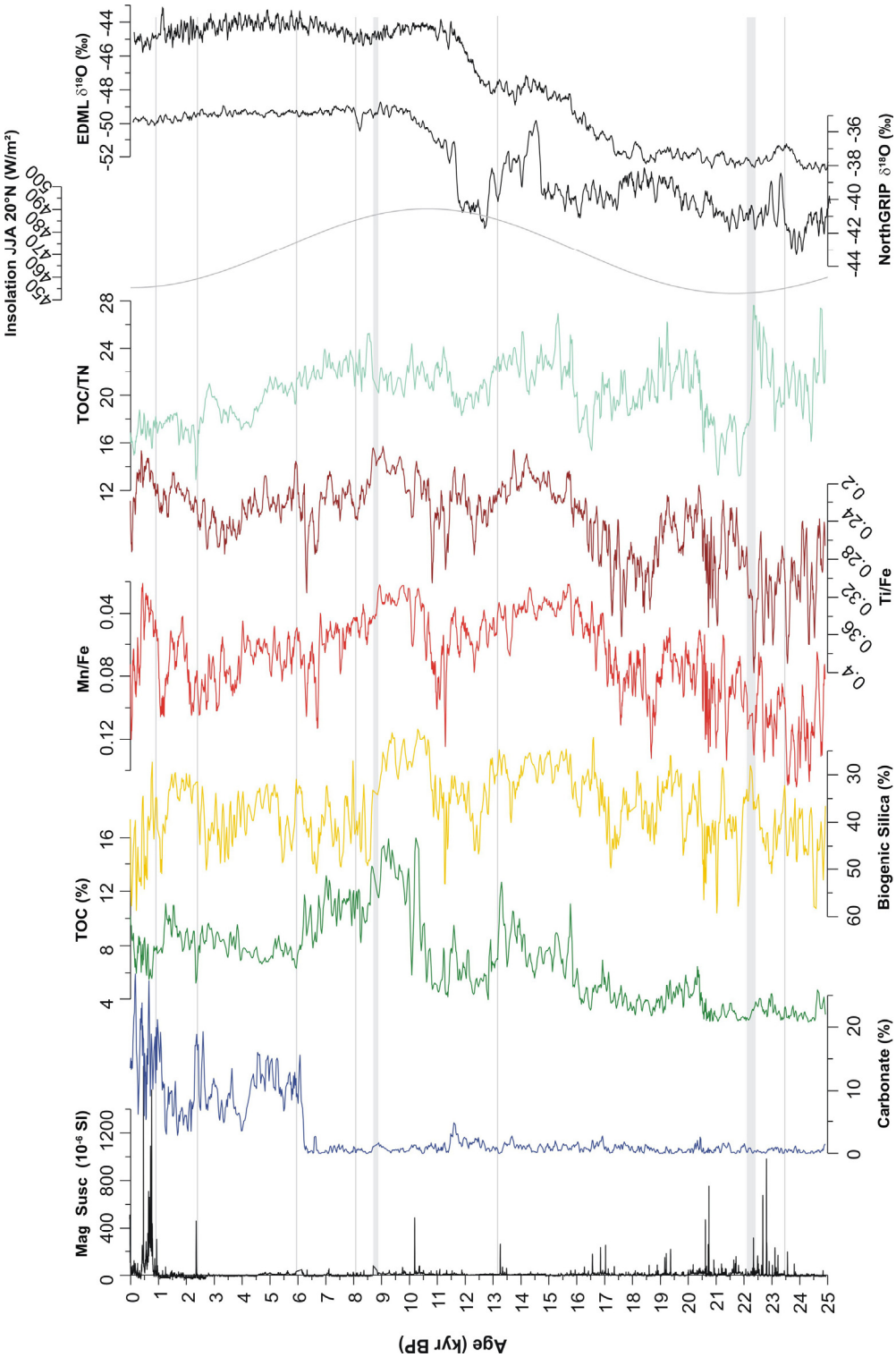

Fig. 6.9: Comparison of selected geochemical records from Lake Challa with the oxygen isotope record ($\delta^{18}O$) of the NorthGRIP ice core, Greenland, based on the GICC05 chronology (Rasmussen 2006; Vinther et al. 2006) and $\delta^{18}O$ of the Dronning Maud Land ice core, Antarctica, based on EDML1/EDC3 age scale (EPICA 2006). Grey lines mark levels of reworked or ash deposits which were excluded from the profile but may have some influences on the following sedimentation.

diatom productivity and increasing OM preservation. Lower MS might be caused by stronger dilution of the clastic component or lowered preservation potential for TM. Fe-sulphide formation was probably enhanced, as indicated by low Mn/Fe and Ti/Fe and increased S intensities (Fig. 6.2). As TOC/TN values are relatively high, this stabilisation was possibly caused by higher lake levels during a humid period with enhanced input of allochthonous organic matter.

An abrupt return to more turbulent and oxidising conditions occurred around 19 kyr BP which lasted until ~17 kyr BP. This period coincides with indications for lower lake levels from seismic-reflection data (Moernaut et al. in prep.), decreased BIT (Sinninghe Damsté in prep.) and decreased concentrations of littoral diatom species (Milne 2007). Reported paleosols from Lake Victoria (Stager et al. 2002; Talbot and Lærdal 2000) and Lake Albert (Williams et al. 2006) as well as other indications for generally dry conditions in tropical East Africa (Gasse 2000) support the conclusion that drier conditions and lower lake levels caused generally less stratified conditions in Lake Challa, which favoured diatom productivity and Mn absorption, reduced OM preservation and Fe-sulphide formation.

From ~17 to 15.8 kyr BP, decreasing Mn/Fe and Ti/Fe ratios, decreasing bSi and partly increasing TOC concentrations point to the establishment of a more stable lake stratification, culminating in a phase of enhanced OM preservation, and probably sulphide precipitation as well, from ~15.8 to 13.3 kyr BP. This period broadly coincides with the onset of the "African Humid Period" (deMenocal et al. 2000) and generally more humid conditions documented in many archives of tropical and subtropical Africa (Gasse 2000). The Nile river system was reactivated after improved regional moisture balance brought its feeding lakes Victoria, Albert and Tana at overflow levels (Beuning et al. 1997; Lamb et al. 2007; Williams et al. 2006). Around lakes on Mount Kenya, humidity rose abruptly after ~14.3 kyr BP (Street-Perrott et al. 2007). Lower δD values of leaf waxes found in Lake Tanganyika document increased precipitation after ~15.1 kyr BP (Tierney et al. 2008). At Lake Masoko the development of semi-deciduous forest indicates increasingly humid conditions (Garcin et al. 2007), and in Lake Malawi the proportion of C4 plants decreased (Castaneda et al. 2007). In western tropical Africa, increases in river discharge are reported from the Niger (Weldeab et al. 2007) and the Congo delta fans (Schefuß et al. 2005). The generally more humid conditions and resulting higher lake levels in Lake Challa probably favoured more intense reducing conditions at the lake bottom. It also fostered vegetation growth around the lake, which may have diminished soil erosion and input of allochthonous materials, as indicated by decreasing TOC/TN and low MS.

Between 13.3 and 12.8 kyr BP, TOC content in sediments from Lake Challa decreases in two steps. Simultaneously, bSi, Mn/Fe and Ti/Fe rise, indicating a destabilisation of the water column with reduced OM preservation and higher diatom productivity due to more intense or longer mixing seasons. These conditions prevailed until ~10.7 kyr BP, but seem to be composed of two main phases from ~12.8 to 11.7 kyr BP and from ~11.4 to 10.7 kyr BP. The former interval corresponds to the Younger Dryas (YD) period which is in many locations from tropical Africa associated with an abrupt reduction in humidity (Gasse et al. 2008; Talbot et al. 2007; Weldeab et al. 2005; Williams et al. 2006) and with indications for stronger winds or

changes in the dominance of north- vs. southeasterly monsoonal winds (Filippi and Talbot 2005; Gasse et al. 2008; Johnson et al. 2002; Talbot et al. 2007). Seismic-reflection and BIT data indicate more arid conditions around Lake Challa (Verschuren et al. submitted). In summary, reported observations seem to indicate a general reorganisation of atmospheric circulation during the YD period which appears to be recorded as increased mixing in Lake Challa. The second, apparently even more pronounced mixing period in Lake Challa ~11.4 to 10.7 kyr BP occurs contemporaneously with a period of increased high-latitude temperature variability, including the 'Preboreal Oscillation' (Fig 6.9) (Lowe et al. 2008; Walker et al. 1999). With the exception of one geochemical record from Lake Tanganyika reporting a coincident deepening of the oxycline there between ~12 and 10 kyr BP (Felton et al. 2007), no other tropical East African climate record shows evidence for especially dry or windy conditions in the earliest Holocene. However, indications for a delayed onset of early Holocene humid conditions associated with the intensification of the Indian South-West Monsoon are reported from north-eastern subtropical Africa (Garcin et al. 2007; Hoelzmann et al. 2004), from cave deposits in Oman (Fleitmann et al. 2003) and from sediment profiles of the Arabian Sea (Ivanochko et al. 2005; Schulz et al. 1998). Also records from the Asian and American Monsoon regions show strong variability between ~11.4 and 10.7 kyr BP with similar, though usually less pronounced, conditions as during the YD period: a weakened South-West Monsoon (Wang et al. 2005; Wang et al. 2001) and intensified North-East Monsoon (Haug et al. 2001; Hughen et al. 1996; Yancheva et al. 2007). These observations argue for a global perturbation of the (northern hemisphere) monsoon system between ~11.4 and 10.7 kyr BP.

After ~10.7 kyr BP, conditions in Lake Challa stabilised until ~8.8 kyr BP: TOC contents reach maximum values; in parallel, Mn/Fe and Ti/Fe ratios are at a minimum as are bSi concentrations; TOC/TN level off around 22. These observations indicate more intense or a longer season of stratified lake water conditions which probably resulted from more humid conditions with higher lake levels and now fully interglacial temperatures around Challa (Verschuren et al. submitted). The onset of these conditions occurs (within the error of the age models) contemporaneously with beginning stalagmite formation in a cave in Oman (Fleitmann et al. 2003) and maybe also with the formation of the ice cap on Mount Kilimanjaro (Thompson et al. 2002, considering that its basal age of ~11.7 kyr BP was assumed by comparison with a stalagmite from Soreq Cave/Israel). Observed humid conditions at Challa are further in agreement with recordings of a humid early Holocene in Lake Tanganyika (Felton et al. 2007; Tierney et al., 2008) and Lake Victoria (Stager et al. 2003; Talbot and Lærdal 2000), as well as in other North- (Gasse 2000; Tiercelin et al. 2008) and West-African (Weldeab et al. 2005) records, documenting the widespread moisture increase in tropical and subtropical northern Africa in response to increased northern hemisphere insolation after the end of the last glacial period.

After ~8.8 kyr BP, Mn/Fe ratios show a generally increasing trend until ~2.2 kyr BP. This trend is accompanied by slightly increasing Ti/Fe ratios, decreasing TOC concentrations, decreasing TOC/TN, generally high bSi concentrations and generally low MS, indicating a continued destabilisation of the Lake Challa water column over the course of the Holocene. This development is consistent with records from Asia (Wang et al. 2005; Yancheva et al. 2007;

Yuan et al. 2004), NE Africa/Arabia (Fleitmann et al. 2003; Kuper and Kröpelin 2006) and the south American subtropics (Haug et al. 2001) which show a decline of the summer/increase of the winter monsoon intensity (Fig. 6.10). A southward shift in the mean position of the ITCZ in response to decreasing northern hemisphere insolation (Fig. 6.9) is a probable forcing mechanism (Yancheva et al. 2007, and references therein). Noteworthy, however, is the early start of destabilisation in Lake Challa ~8.8 kyr BP when compared with the records mentioned above (Fig. 6.10). This may be a specific equatorial characteristic as Lake Challa is the most southern location of the cited monsoon records. The general Holocene trend is overlain by several abrupt events or shifts to inferred increased water-column mixing ~8.8–8.2 kyr BP, 6.6–6.3 kyr BP, 4.0 kyr BP, 2.2 kyr BP and 1.2–1.0 kyr BP. These events have been described from many climate and historical archives as periods of low monsoonal rainfall (Fleitmann et al. 2003; Gupta et al. 2003; Haug et al. 2003; Haug et al. 2001; Thompson et al. 2002; Wang et al. 2005; Yancheva et al. 2007). Their global expression, origin and link to changes in the North-Atlantic and in solar variability are currently under discussion (Morrill et al. 2003).

The interval 1.2 to 0.5 m (~1100 to 350 yr BP)

The short interval 1.2 to 0.5 m is in many aspects different from the majority of the investigated profile. These differences appear very prominent in correlation patterns (Fig. 6.8), where coherences found for the rest of the profile break down. The interval is characterised by especially high S intensities but relatively low TOC contents, high Ti and Fe intensities, relatively low Mn/Fe and Ti/Fe ratios, as well as high MS (Fig. 6.1 and 6.2). Titanomagnetites are detected in the magnetic extract, but also framboidal Fe-sulphides are frequently observed in thin sections of this interval (Fig. 6.6 b). The high MS is probably caused by TM, but if the Fe-sulphides occur in the form of greigite, both minerals could be equally responsible for it (Maher and Thompson 1999). All observations argue for a period of increased detrital input from the catchment area and, at the same time, for increased precipitation of Fe-sulphides within anoxic waters at the sediment-water interface. Both may be achieved under humid climate conditions where increased rainfall causes intense erosion from the catchment and high lake levels with constantly anoxic bottom waters. However, thin section analyses reveal the presence of distinct aragonite layers in this finely laminated core section. High Sr/Ca ratios (not shown) and XRD analyses underline the aragonitic nature of these carbonates and investigations with SEM show their autochthonous habit (Wolff et al. unpublished). The occurrence of aragonite is often associated with increased salinity and therefore lower lake levels and more arid environmental conditions (e.g. Talbot and Kelts 1986). Aridity can be responsible for reduced vegetation cover and increased erosion in the catchment area. However, lower lake levels usually counteract intense reducing conditions at the lake bottom and therefore the accumulation of Fe-sulphides, unless salinity increases enough to strengthen density stratification of the water column. Summarising all the evidences here considered, this interval possibly reflects an exceptionally dry period with extremely low lake levels, or a period with exceptionally strong seasonality.

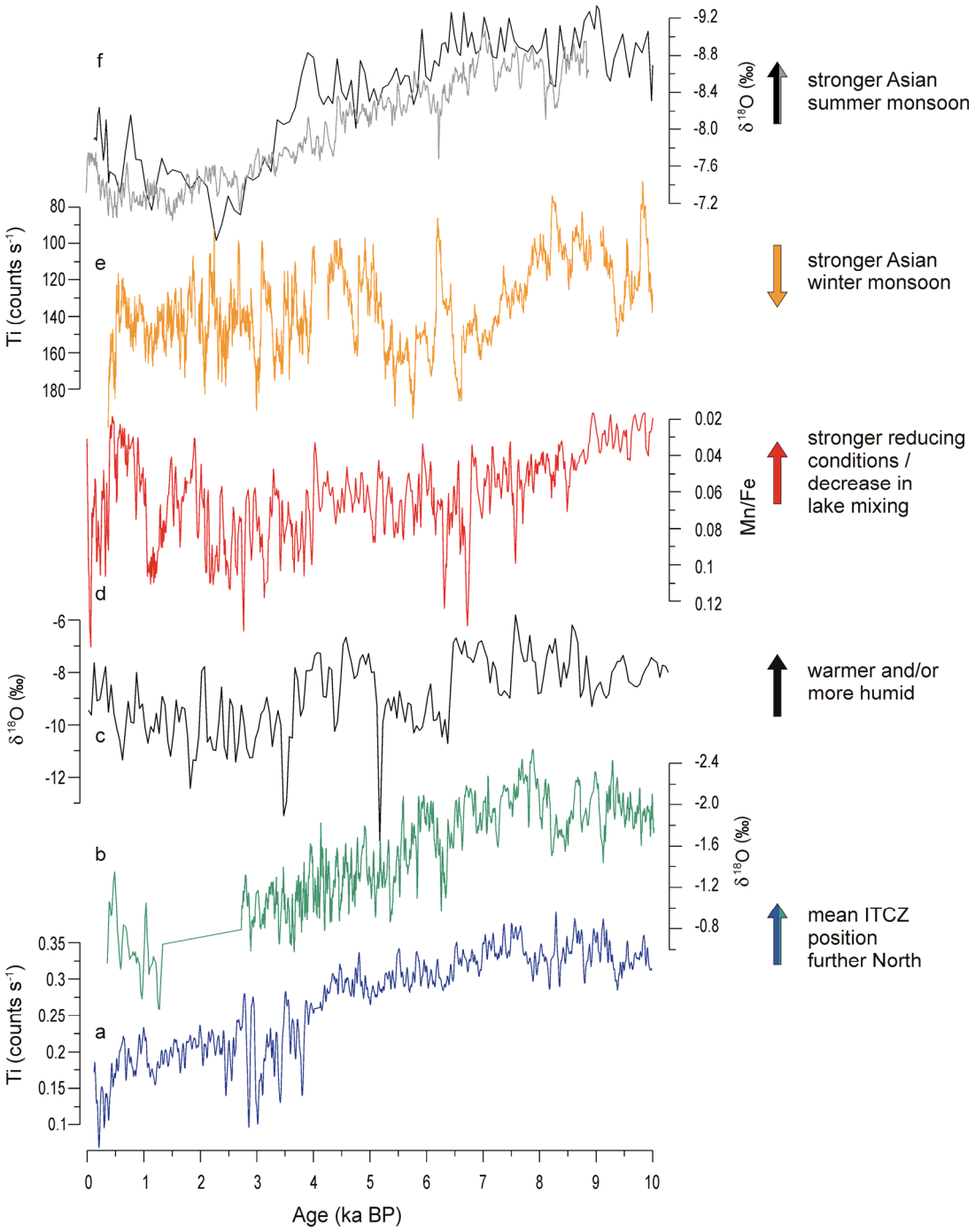

Fig. 6.10: Comparison of different monsoon records: (a) the Ti intensity record of a core from Cariaco basin (10°42' N, 65°10' W) (5-point running average) (Haug et al. 2001); (b) stable oxygen isotope record from a stalagmite from Qunf Cave, southern Oman (17°10 N, 54°18 E, 3-point running average) (Fleitmann et al. 2003); (c) the stable oxygen isotope record from Mount Kilimanjaro ice core KNIF3 (3°04.6 S; 37°21.2 E; 5893 m above sea level) (Thompson et al. 2002); (d) the Mn/Fe ratio of sediments from Lake Challa (3-point running average); (e) the Ti intensity record of sediments from Lake Huguang-Maar, China (21°9'N, 110°17'E) (Yancheva et al. 2007); (f) and two stable oxygen isotope records of stalagmites from Dongge Cave, China (25°17'N, 108°5'E) (grey line represents a 7-point running average after Wang et al. (2005), black after Yuan et al. (2004)).

Furthermore, we can not exclude anthropogenic influence for this period of time. Archaeological sites from early iron-using communities have been found around Mt. Kilimanjaro (e.g. Rombo, Taita) and are dated to the first centuries AD (Kiriama 1993). Widgren (2004) reports intensive banana cultivation for the Kilimanjaro area to occur for over 1,000 years. As those settlements are usually attended by intensive forest clearing, they may have altered erosion rates, inflow and chemistry of the groundwater feeding Lake Challa and may therefore be equally responsible for increased detrital input, changes in carbonate precipitation, eutrophication and Fe-sulphide precipitation.

Table 6.1: Results from XRF analyses of selected source rocks and corresponding soil samples (all collected within 30 km around Lake Challa). Element ratios refer to mass ratios calculated from the oxide content (wt%/wt%).

sample description	SiO_2	TiO_2	Al_2O_3	Fe_2O_3	MnO	MgO	CaO	Na_2O	K_2O	P_2O_5	H_2O	CO_2	Σ	Mn/Fe	Ti/Fe
unweathered grits (foot of Challa)	35.9	4.04	9.70	14.2	0.21	8.53	15.9	1.50	0.68	0.93	2.74	4.68	99.1	0.017	0.24
weathered grits (caldera rim)	39.9	4.29	11.0	15.5	0.23	8.51	11.0	1.41	2.12	1.14	3.55	0.72	99.4	0.017	0.24
soil on grits (caldera rim)	38.1	4.21	11.0	14.0	0.21	8.28	11.3	0.35	1.13	0.84	5.97	3.99	99.4	0.016	0.26
local lava (caldera rim)	40.7	3.26	11.1	12.9	0.19	12.2	13.0	1.77	0.71	0.63	2.23	0.63	99.3	0.016	0.22
soil on lava (caldera rim)	41.2	4.03	11.7	14.7	0.22	7.22	9.88	1.94	1.83	0.93	3.55	2.31	99.4	0.016	0.24
pumice peaces (caldera rim)	39.4	3.32	11.8	13.4	0.20	12.5	13.5	0.57	0.48	0.56	3.18	0.54	99.5	0.017	0.21
soil on pumice (caldera rim)	38.3	3.81	11.2	13.5	0.20	10.5	9.80	0.75	0.79	0.64	5.28	4.60	99.4	0.016	0.24
unweathered basalt (caldera rim)	44.9	3.77	15.2	14.1	0.19	5.31	8.28	3.29	1.74	0.69	1.79	0.23	99.5	0.015	0.23
unweathered basalt (Rombo Series, foot of Challa)	45.5	3.79	16.1	13.6	0.19	4.56	8.69	3.27	1.53	0.84	1.29	0.15	99.5	0.015	0.24
soil on basalt	40.5	4.32	13.1	17.2	0.24	7.66	8.19	1.74	1.40	0.73	3.11	1.30	99.4	0.015	0.22
sand of pool in rivine*	34.0	4.71	16.1	17.9	0.25	3.26	4.49	0.27	0.81	0.87	9.03	7.82	99.5	0.016	0.23
sand/clay from dry river bed (foot of Challa)	33.2	5.38	17.6	22.1	0.30	2.78	1.62	0.09	0.25	0.51	10.1	5.54	99.5	0.015	0.21
fsp rich gneiss (Reata Mt.)	75.4	0.14	12.6	1.74	0.07	0.15	0.86	2.04	5.77	0.03	0.73	0.15	99.7	0.046	0.07
soil on fsp rich gneiss	60.0	1.59	13.4	6.91	0.11	1.05	2.53	1.90	3.30	0.18	3.06	5.56	99.6	0.017	0.20
banded gneiss (Reata Mt.)	77.3	0.05	12.4	0.70	0.00	0.01	0.60	3.24	4.84	0.02	0.66	0.05	99.9	0.002	0.06
soil on banded gneiss	58.0	1.73	17.2	8.78	0.15	1.00	3.13	2.58	2.15	0.19	3.15	1.49	99.5	0.019	0.17
soil from Challa irigation project	37.2	4.24	16.7	15.8	0.24	3.20	7.16	0.71	1.22	0.71	7.12	5.15	99.5	0.017	0.23
soil from Challa village	41.2	3.97	17.3	15.5	0.25	3.03	4.07	0.21	1.09	0.67	8.28	3.83	99.5	0.018	0.22

* rivine (~300 m long) enters Lake Challa in NW corner of the caldera and is according to information from local fishermen only active during years with exceptionally heavy rainfall

7. Summary

7.1 Synthesis

This thesis covers a wide range of methods that are frequently used in palaeolimnology; here I applied them to the sediments of the African subtropical Lake Tswaing and the tropical Lake Challa. The data acquired with methods from inorganic and organic geochemistry document compositional and element characteristics of the sediments, changes in their magnetic properties and in the composition, quality and isotope chemistry of the organic fraction. This multi-proxy approach helps to elucidate different aspects of the investigated lake ecosystems, such as the characterisation of and differentiation between allochthonous and autochthonous sediment and organic matter sources or lake internal element cycles. However, the principal aim of this thesis is the synergetic application of these methods to understand past climatic influences on the lake ecosystems with a special focus on changes in the hydrological cycle. Such an approach ultimately leads to the discussion of changes in African atmospheric circulation based on a comparison of the observations from the subtropical and the tropical lake sites. In the following, I present a summary of the most important results of this work, with a special emphasis on the climatological aspect. Focus are the time windows of (i) the last glacial period (c. 100 – 20 kyr BP), and (ii) the Last Glacial Maximum through Holocene (25 – 0 kyr BP).

(i) The last glacial period (100 – 20 kyr BP) in subtropical southern Africa

In the sediments of Lake Tswaing, periods with humid climate conditions are reflected in decreased organic matter and increased detrital minerogenic content, and with high potassium and iron XRF intensities. More arid periods, in contrast, resulted in more saline conditions with pronounced stratification in the lake. This is reflected in sediments by high total inorganic and organic carbon content and high chlorine XRF intensities. Between ~200 kyr and 75 kyr BP, the lake appears to have been generally relatively fresh with cycles of alternating more humid/arid conditions closely following changes in orbitally-forced solar radiation intensity with a pacing of ~23 kyr (precession), and precipitation of calcium carbonate during more arid periods (chapter 3). With the decreasing amplitude of precessional forcing along with the decrease in earth eccentricity (Fig. 7.1 d) and the establishment of glacial boundary conditions such as cooler Indian Ocean sea surface temperatures (IOSSTs) after ~75 kyr (Bard et al. 1997), the lake changed into a hyper-saline environment with salt precipitation during arid periods and alternating humid/arid conditions following a different pacemaker: humid periods are recorded at 73–68, 54–50, 37–35, and 15–10 kyr BP; arid conditions at ~60–55 kyr, 48–40 kyr, 35–32 kyr, and 10–7.5 kyr BP. With the exception of the youngest intervals, these humid/arid periods occurred while the polar ice caps were enlarged as documented, for example, in increased delivery of ice rafted debris (IRD) to the North Atlantic (Grousset et al. 1993) and to marine sites north of the present winter sea ice extent around Antarctica (Fig. 7.1 a) (Kanfoush et al.

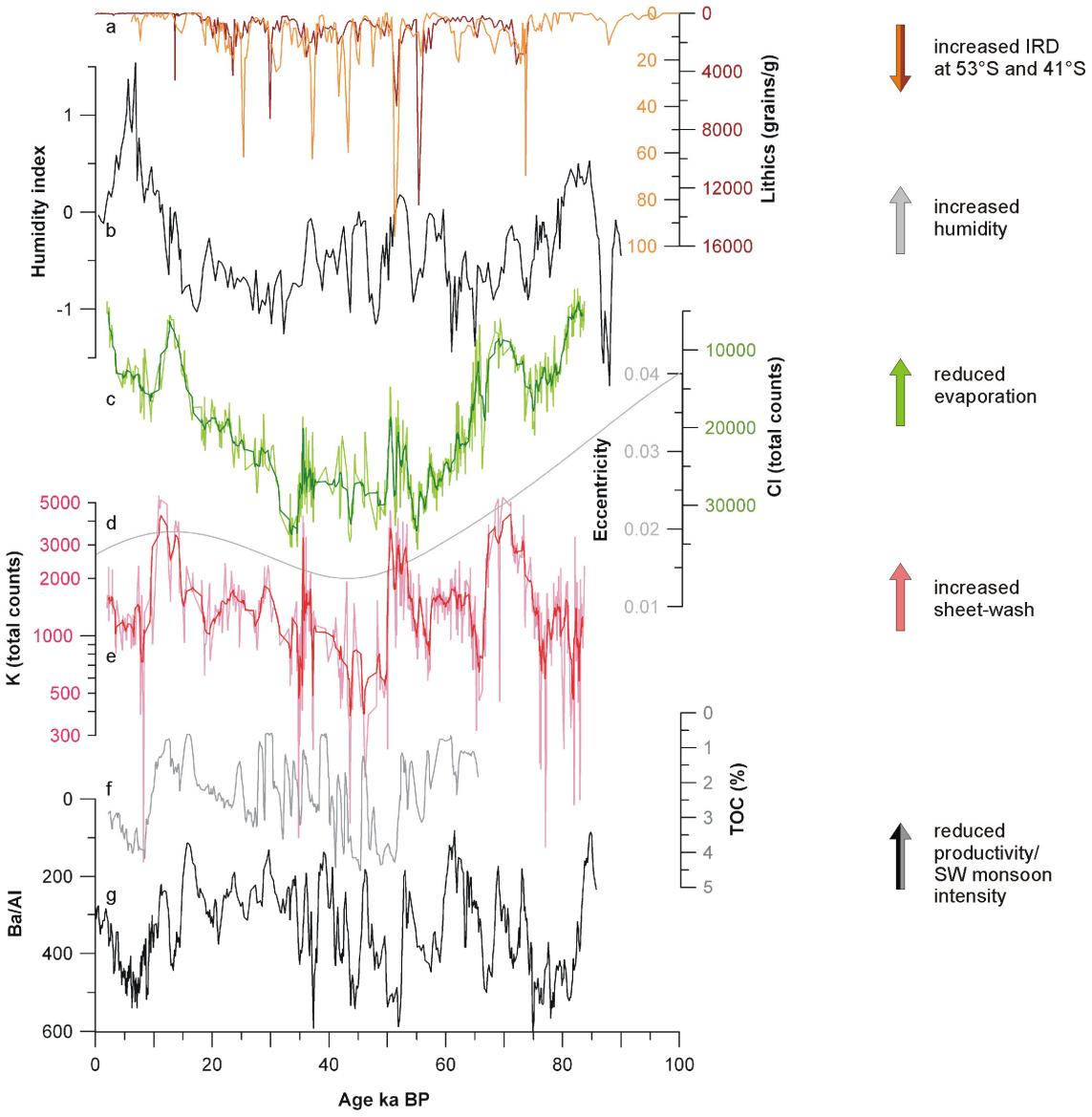

Figure 7.1: Comparison of proxies for palaeohydrology from northern and southern hemisphere subtropical Africa with proxies for Antarctic sea ice extent. (a) counted lithics (grains/g) in two marine sediment profiles from the South Atlantic Ocean polar frontal zone (IRD at 53°S (brown) and 41°S (orange), Kanfoush et al. 2002); (b) reconstructed north-African humidity index from the grain-size spectrum of a marine core (20°45'N, 18°34'W) (Tjallingii et al. 2008); (c) Cl intensity of sediments from Lake Tswaing; (d) variability of earth eccentricity; (e) K intensity of sediments from Lake Tswaing; (f) total organic carbon content (TOC) of a marine core offshore Pakistan (23°07'N, 66°30'E) (Schulz et al. 1998), and (g) Ba/Al ratio (ppm/%) of a marine core offshore Somalia (10.46°N, 51.57°E) (Ivanochko et al. 2005), both tracing upwelling intensity in response to the Indian SW monsoon.

2000; Kanfoush et al. 2002). Those conditions are thought to have caused an equatorward shift of oceanic and atmospheric circulation systems (Holmgren et al. 2003; Tyson 1999). A northward shift of the southern hemisphere westerly wind belt with Antarctic cooling is recorded by many records from southern hemisphere mid-latitudes (Kaiser et al. 2008; Lamy et al. 2004; Stuut and Lamy 2004). The equatorward contraction of the area influenced by tropical rainfall (ITCZ) is suggested to have caused generally more arid conditions in the North-African subtropics between ~75 and 20 kyr BP (Fig. 7.1 b) (Tjallingii et al. 2008). Similar processes probably acted in the South African subtropics and are reflected in generally more arid

conditions recorded in the sediments of Lake Tswaing after ~75 kyr BP. However, also cooler IOSSTs after ~75 kyr BP (Bard et al. 1997) can play a role as the Indian Ocean is the principle moisture source for eastern South Africa (Preston-Whyte and Tyson 1988). The question of the exact timing of abrupt shifts in the hydrology of Lake Tswaing within this period has to be handled with care due to uncertainties in the age model (considering the error of radiocarbon dating of 1.000 – 2.270 years for ages between 33 and 48 kyr BP, and possible but unknown changes in reservoir effect which is 1.150 years under modern conditions, see chapter 3). However, these strong fluctuations in Lake Tswaing hydrology occurred during a period of strong millennial-scale changes in the high-latitudes (Kanfoush et al. 2000; NGRIP-Members 2004) as well as in the African tropics and subtropics (Adegbie et al. 2003; Ivanochko et al. 2005; Schulz et al. 1998; Tierney et al. 2008; Tjallingii et al. 2008). More humid conditions in Lake Tswaing thereby seem to correspond to periods of reduced upwelling and monsoon intensity in the Arabian Sea (Fig. 7.1) and to intervals of atmospheric cooling in high northern latitudes (Dansgaard et al. 1993; NGRIP-Members 2004). This observation concurs with observations from South America and Asia of millennial-scale anti-phasing of northern and southern hemisphere monsoonal systems during the last glacial period (Baker et al. 2001; Hodell et al. 2008; Peterson et al. 2000; Wang et al. 2001), and, furthermore, adds to the evidence for a tight coupling between climate changes in high- and low latitudes (deMenocal 2008). It disagrees, however, with proposed super-ENSO conditions during northern high-latitude cooling (Stott et al. 2002), as modern El Niño years are associated with drier than normal conditions in south-eastern Africa (Cook 2000; Nicholson 2000; Nicholson and Kim 1997).

(ii) Last Glacial Maximum through Holocene (25 – 0 kyr BP)

The transition from the last glacial period into the present interglacial is documented in both investigated sediment profiles (Fig. 7.2). Sediments from Lake Tswaing record a transition to humid conditions after ~16 kyr BP, an abrupt change to more arid conditions ~10 kyr BP, and subsequently more humid conditions after ~7.5 kyr BP (Fig. 7.2 c). These shifts are well documented in biomarker concentrations and compound-specific stable carbon isotope ratios which indicate a higher (lower) productivity within and around the lake during more humid (arid) periods (chapter 4). The manganese to iron (Mn/Fe) XRF ratio in sediments from Lake Challa indicates increasingly reducing conditions in the deeper water column from ~17 to 16 kyr BP, a transition from intense to less intense reducing conditions (or from more pronounced stratification to deeper and/or longer mixing) after ~14 kyr BP and a reversal again after ~10.7 kyr BP (Fig. 7.2 b). These changes in redox conditions and therefore mixing within the lake water body can be a response to lake-level fluctuation and/or changing wind stress and/or temperatures. The interpretation of Mn/Fe ratios in these terms is supported by parallel changes in total organic carbon and biogenic silica concentrations (chapter 6), and further rests on investigations of the modern lake water and sediment chemistry where higher Mn/Fe ratios are recorded in sediments deposited during the cool, dry and windy months of the year

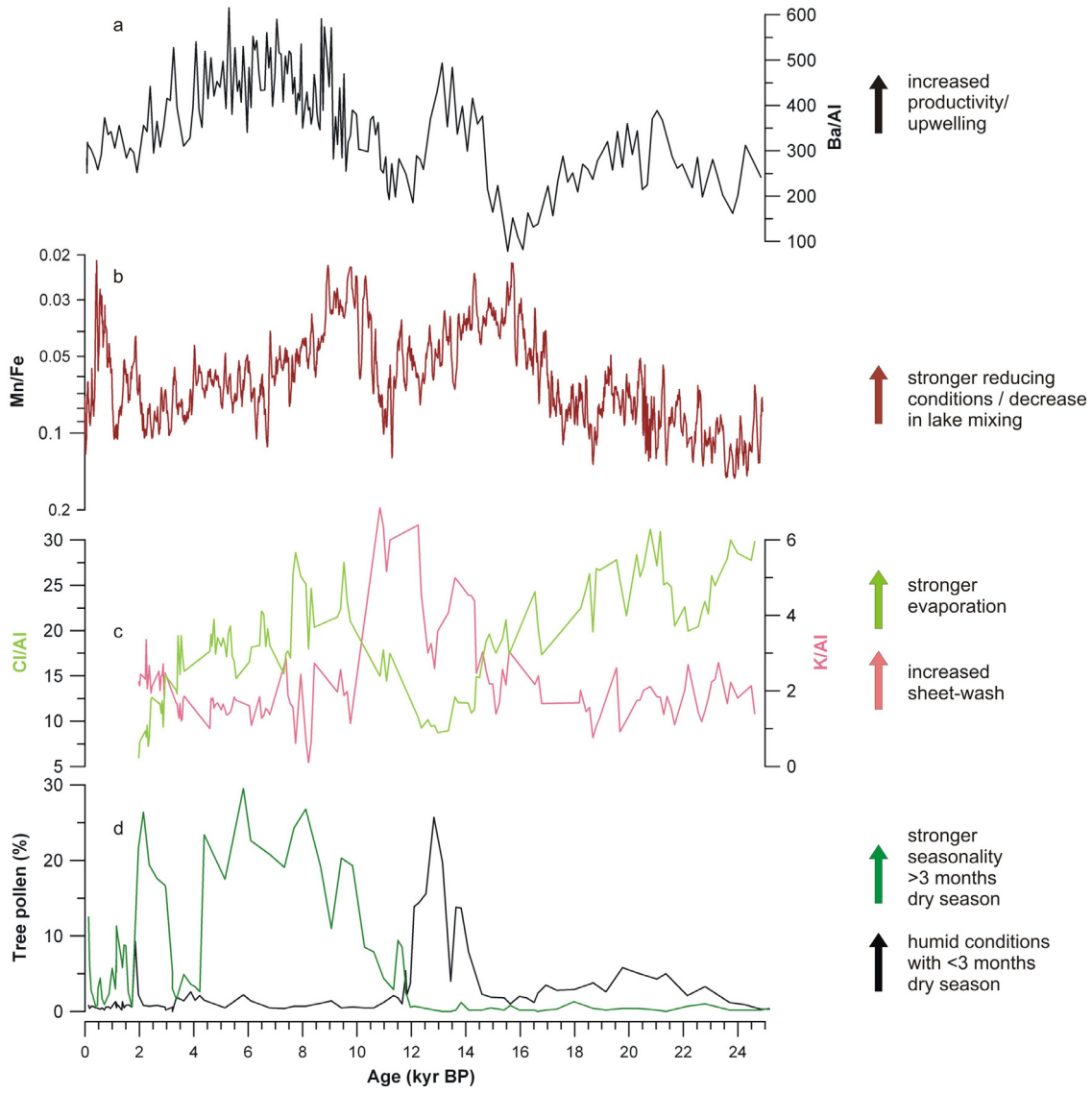

Figure 7.2: Comparison of monsoon records from eastern Africa. (a) Ba/Al ratio (ppm/%) of a marine core offshore Somalia (10.46°N, 51.57°E) (Ivanochko et al. 2005); (b) Mn/Fe intensity ratio of sediments from Lake Challa (7-point running average); (c) Cl and K intensity of sediments from Lake Tswaing; (d) percentage of tree pollen in sediments from Lake Masoko (9°20.0'S, 33°45.3'E), black curve indicates percentage of *Macaranga* which requires a short dry season, green curve indicates the percentage of *Uapaca* which suggests strong seasonality at the site with a dry season (Garcin et al. 2006a).

accompanied by deep seasonal mixing (chapter 5). The intense reducing conditions ~16–14 kyr BP can be interpreted to relate to high lake levels during the early phase of the "African Humid Period" (deMenocal et al. 2000), but may also be influenced by steadily increasing lake surface-water temperatures between ~19 and 14 kyr BP as documented by the Lake Challa TEX_{86} record (Verschuren et al. submitted). The subsequent increase in mixing culminates at ~12.5–12.0 kyr BP and again at ~11.4–10.7 kyr BP. The earlier interval roughly corresponds to the Younger Dryas (YD) period for which other investigated parameters from Lake Challa (BIT index, seismics, Verschuren et al. submitted) argue for reduced freshwater inflow and lower lake levels. To the south, records from Lake Tswaing and Lake Masoko (Garcin et al. 2006a)

indicate wetter conditions during the YD period (Fig. 7.2 c and d). The observations from these three lakes are in accordance with observations from Central America (Haug et al. 2001; Wang et al. 2007) and Asia (Wang et al. 2001; Yancheva et al. 2007; Yuan et al. 2004) and can be interpreted to document a generally southward displacement of the ITCZ during the YD period, as it has also been suggested by climate modelling (Broccoli et al. 2006). The period ~11.4–10.7 kyr BP, which appears even drier/windier than the YD in the Lake Challa record, has in its extent no counterpart on other continents. The records from Central America and Asia mentioned above document only slight decreases in monsoon intensity. However, climate archives from southern Arabia and those areas in north-eastern Africa influenced by the Indian Monsoon system indicate strong aridity for the time between the end of the YD and 10 kyr BP. Gaps occur in stalagmite records from Oman and Socotra Island (Fig. 7.3 e) (Fleitmann et al. 2003; Shakun et al. 2007), aeolian dust influx to the Arabian Sea is at a maximum while upwelling intensity continues to be reduced after the YD (Ivanochko et al. 2005) (Fig. 7.2 a), and the widespread increase in humidity recorded in climate archives from northern subtropical Africa often did not take place before ~10.8 kyr BP (Garcin et al. 2007; Hoelzmann et al. 2004). These observations document a strong response of the African and Indian Monsoon system which is probably also reflected in Lake Challa sediments. About the underlying forcing factors I can only speculate but possible influences are (1) enhanced NE monsoon winds in response to only slowly retreating glaciers on the Tibetan plateau (Overpeck et al. 1996), (2) strong climate fluctuations in northern and southern high-latitudes known as “Preboreal” period that may have changed global temperature gradients and monsoon strength (Hughen et al. 1996), (3) changes in solar radiation, which shows characteristic minima at ~11.2–11.5 kyr BP and ~10.9 kyr BP, known to affect SW monsoon intensity elsewhere (Bond et al. 2001; Gupta et al. 2003), and (4) changes in IOSSTs and in the tropical atmosphere ocean circulation. The latter may include changes in the El Niño Southern Oscillation (ENSO) analogous to observations by Rein et al. (2005), who describe pronounced La Niña-like conditions offshore Peru at ~11 kyr BP (Fig. 7.3 a). Strong coupling between ENSO and IOSSTs has been frequently observed on both modern and historical time scales, though it strongly interacts with an Indian Ocean internal oscillation (IOD) (Ashok et al. 2001; Behera et al. 2006; Black et al. 2003; Chang et al. 2006; Charles et al. 2003; Charles et al. 1997; Cole et al. 2000; Saji et al. 1999; Webster et al. 1999). Strong influences of El Niño/La Niña and IOD events on rainfall variability in tropical and southern East Africa have been documented by many authors (Black et al. 2003; Cook 2000; Giannini et al. 2008; Indeje et al. 2000; Nicholson and Kim 1997; Saji and Yamagata 2003; Washington and Preston 2006). Accordingly, El Niño/positive IOD-events cause a more intense and prolonged “short rain season” (regularly October–December) in tropical East Africa, thereby strongly restricting the subsequent short dry season connected to the NE monsoon winds (January–February) (Fig. 7.4); the summer rainfall zone of eastern South Africa experiences lower than average rainfall during this season (January–March) (opposite conditions in both regions prevail during La Niña/negative IOD-events). A comparison of high- resolution µXRF measurements of the top ~23 cm of the Challa sediment record with historical western IOSSTs strongly implies a link between IOSSTs, global tropical atmosphere and ocean circulation changes and climatic conditions recorded in the Mn/Fe ratio of sediments from Lake Challa

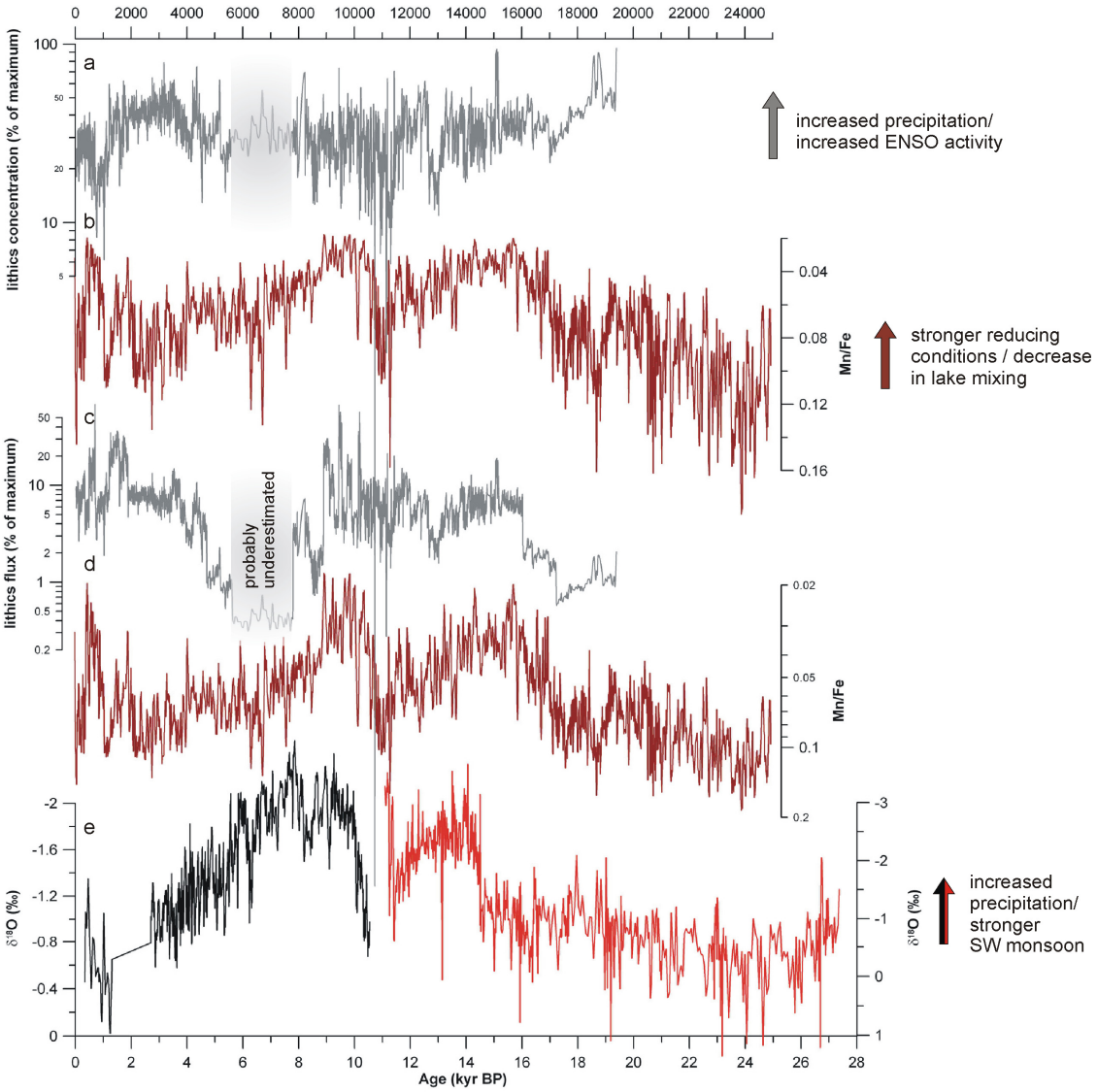

Figure 7.3: Comparison of tropical climate records from the Pacific and Indian Ocean realm. Lithics concentration (a) (5-point running average) and flux (c) (3-point running average) from a marine sediment core offshore Peru (12°03'S, 77°39.8'W) (Rein et al. 2005); Mn/Fe intensity ratio (b+d) (3-point running averages) of sediments from Lake Challa; (e) stable oxygen isotope record from stalagmites from Qunf Cave, southern Oman (17°10 N, 54°18 E, black curve, 3-point running average) (Fleitmann et al. 2003) and from Moomi Cave, Socotra Island, Yemen (12º30'N, 54ºE, red curve) (Shakun et al. 2007).

(Fig. 7.5). Supposing analogous behaviour on decadal and millennial time scales and a period of prolonged La Niña-like conditions ~11.4–10.7 kyr BP, the transfer of the modern scenario for tropical East and South Africa would explain the parallel increase in mixing observed in Lake Challa and the contemporaneous increase in sheet-wash observed in Lake Tswaing (Fig. 7.2 c). The same line of evidence could be applied to describe the observed opposite trends in Lake Challa and Lake Tswaing during the early Holocene. However, records about ENSO variability during the early Holocene are contradictory (Moy et al. 2002; Rein et al. 2005). More often and in accordance with model results (e.g., Kutzbach and Street-Perrott 1985), a northward shift of the ITCZ in response to the orbital configuration with maximum insolation in the northern

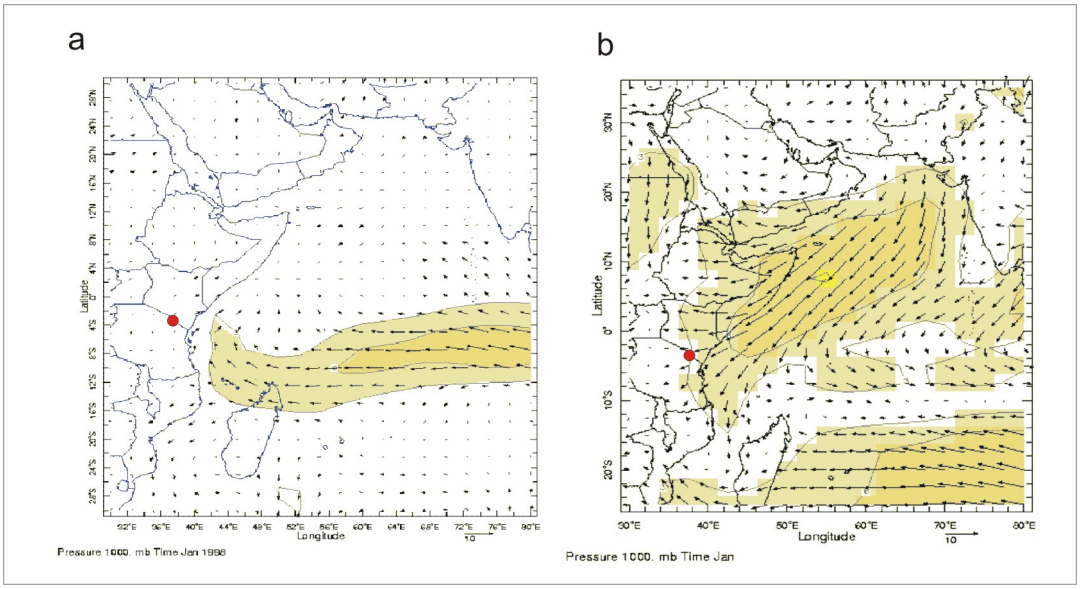

Figure 7.4: Wind vectors for the 1000 hPa pressure level (a) during the strong El Niño/positive IOD event in January 1998, (b) as climatological mean of Jan 1971 to Jan 2000. Arrows indicate wind direction with wind speed proportional to the length of the vectors. Contour lines are drawn at intervals of 3 m/s. Source: http://iridl.ldeo.columbia.edu.

hemisphere is quoted to explain the early Holocene maximum in humidity and of SW monsoon strength in northern hemisphere subtropics (see also chapter 4). Intriguing are, though, the similarities between high-frequency ENSO variability observed offshore Peru (Rein et al. 2005) from 10.3 to 8.9 kyr BP, the changes in Mn/Fe of Lake Challa sediments, and high-resolution monsoonal records from southern Arabia (Fig. 7.3) which underline a strong connection between these low-latitude regions with ENSO as a probable mediator.

The middle and later Holocene saw the re-establishment of aquatic macrophytes and grasses and the flourishing of the microbial community of Lake Tswaing, in accordance with evidence for more humid conditions from other regional climate archives of southern Africa. This swing in hydrology seems to follow predominantly a change in insolation, which regained stronger influence after the minimum in eccentricity and local insolation and after the abolition of glacial boundary conditions. The abruptness of the observed increase in humidity after ~7.5 kyr BP compared to the more gradual changes in insolation indicates involvement of non-linear hydrological responses or unknown feedback processes; non-linearity of climate response to orbital forcing has often been described for northern hemisphere African subtropics (e.g. Claussen et al. 2006; Tierney et al. 2008; Tjallingii et al. 2008) and might be system-inherent or characteristic for individual archives and sensitivity thresholds (Fleitmann et al. 2007; Kröpelin et al. 2008; Liu et al. 2007).

Sediments from Lake Challa are characterised by generally increasing Mn/Fe ratios during the middle to late Holocene, indicating intensified/prolonged seasonal mixing within the lake water body. This observation corresponds to indications for lake level lowering in the

Challa basin from seismic and the BIT index data (Verschuren et al. subm.). Similar trends and events can be observed in records of monsoon intensity from the Asian (Wang et al. 2005; Yancheva et al. 2007; Yuan et al. 2004), the NE African/Arabian (Fleitmann et al. 2003; Kuper and Kröpelin 2006) and the South American subtropics (Haug et al. 2001) (Fig. 6.10 and 7.5). Intensified mixing in Lake Challa accordingly corresponds to periods of weaker SW monsoon and intensified NE monsoon, suggesting the latter to be the dominant mixing control during the Holocene. Distinct, abrupt shifts occur synchronously (within uncertainties of the chronologies) ~8.8–8.2 kyr BP, 6.6–6.2 kyr BP, 4.0 kyr BP, 2.2 kyr BP, 1.2–1.0 kyr BP and 0.5–0.4 kyr BP (precision of the youngest is hampered in the Challa record by uncertainties within the ^{210}Pb dating (see chapter 1)), and underline the close connection of global monsoon regions.

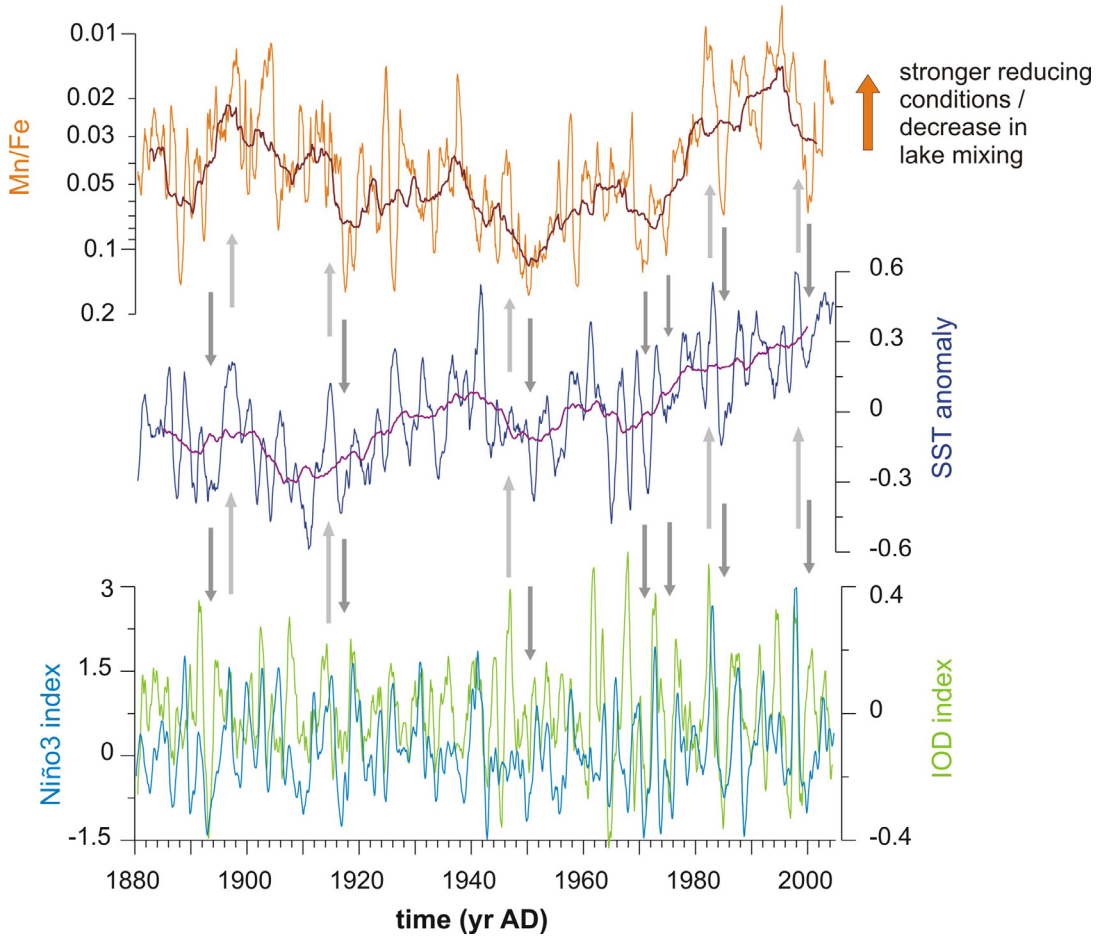

Figure 7.5: Comparison of (a) the Mn/Fe intensity ratios from high-resolution µXRF measurements on sediments from Lake Challa (orange line represents 17-point running average); (b) changes in western Indian Ocean sea surface temperatures (blue line represents 1-year running average) (Kaplan et al. 1998); (c) the Niño3 index (Kaplan et al. 1998) and the Indian Ocean Dipole (IOD) index (Saji et al. 1999) over the last 125 years. The age scale of Mn/Fe is based on varve counting (est. error ±4 yr, Wolff unpublished). Grey arrows indicate tentatively parallel events.

As suggested earlier (Wang et al. 2005; Yancheva et al. 2007), shifts in the mean annual ITCZ position may be the underlying forcing factor, ultimately driven by solar variability. This inter-relation has also been stressed to explain the observed coherence between the Arabian Sea monsoonal region and high-latitude North Atlantic (Bond et al. 2001; Gupta et al. 2003).

Over the last 2,000 years, in many of the presented records appear similar patterns with only slight differences in timing (compare Fig. 7.3 and 6.10). These differences in timing may be real, but can also be related to anthropogenic influences or difficulties in age modelling (see also chapter 6). Due to these uncertainties, detailed investigations of this time interval are left open for future studies.

7.2 Conclusion

The investigated lake ecosystems and sedimentary archives from the Tswaing and Challa crater basins provide for their region highly significant records of a new quality:

- The geochemical and element intensity data from Lake Tswaing sediments yield one of the longest and of the very few continuous (at present till the end of the last interglacial period as a minimum) terrestrial climate records from the South-African summer rainfall zone
- With parallel investigations on modern and past organic carbon sources we are able to comprehensively describe the specific ecosystem of the Tswaing crater lake, of its surrounding landscape and of their evolution over the last ~200,000 years
- The combination of lake monitoring, meteorological data and high-resolution measurements on recent sediments from Lake Challa deliver insights into the formation of laminated sediments in the tropics
- The high-resolution and extremely well-dated sediment record from Lake Challa documents gradual as well as abrupt changes in the East African monsoon system since the Last Glacial Maximum (25,000 years BP)

Both archives add valuable information about past climate change in eastern Africa. They document the close connection between African low-latitude regions and northern and southern high-latitude regions, especially during glacial and deglacial times. Both records document the strong imprint of orbitally induced changes in insolation especially during times of reduced high-latitude ice extent, but besides, call for additional influences which are probably related to the evolution of the tropical atmosphere-ocean circulation.

The investigations of both climate archives are based on detailed investigations of the modern conditions at the sites. This approach fosters a more solid understanding of the presently active processes and their imprint on the sediment records. Although the interaction of a multitude of forcing mechanisms is difficult to decipher, both records, and in particular the

high-resolution record from Lake Challa, provide a valuable test for modelling studies which are equally necessary to improve our understanding of earth's climate evolution.

7.3 Potential of the studied sites: An outlook

The studies on the climate archives of Lake Tswaing (South Africa) and Lake Challa (Kenya/Tanzania) provide valuable new information about modern and past environmental conditions at both sites, but also point out the potential for future studies.

With the new coring campaign at Tswaing in 2001/2002 and the recovery of three overlapping cores, the quality of the recovered material improved already substantially in comparison to older available sediments. Nevertheless, it was not possible to compose a complete profile and gaps remained frequently between ~33 and 80 m depth (compare Fig. 2.4). Fluid-supported rotary drilling for sediments below 30 m depth caused heavy disturbance and core loss. Another drawback associated with the sediment archive of Lake Tswaing is the core chronology. The new ^{14}C AMS radiocarbon ages on charcoal material prepared within this thesis consolidated the chronology for the sediments of the last 50,000 years (~20 m depth). Nevertheless, paired dating of charcoal and bulk organic material should be aspired to estimate past changes in the reservoir effect. No improvement could be achieved for the chronology of the remaining 70 m of the sediment profile as tests for U/Th series dating by Jo Thorpe from UCL London gave completely unexpected results and need further verification. Climate interpretations will remain tentative as long as the stratigraphy rests on the available fission-track date and tuning (compare chapter 3). Therefore, future studies should aim to tackle this problem and to, e.g., get a statistically better confined fission-track age for the impact event, or to test further techniques like exposure dating, especially when considering the good quality of finely laminated sections between c. 80 and 90 m depth. A professional future scientific coring campaign may help to erase some of the principle uncertainties associated with this archive.

This thesis presents first investigations on the organic fraction of the sediments from Lake Tswaing (leaving aside pollen which were investigated earlier). The work concentrates on organic matter characterisation with organic petrology and Rock-Eval pyrolysis beside analyses of the saturated hydrocarbon and the alcohol fraction of the extractable organic matter and demonstrates the ecological peculiarity of this lake archive. Initial screening of the complete extractable organic matter with GC-MS revealed an overabundance of compounds including previously undescribed compounds (see Appendix A). The fatty acid fraction was left unexplored as initial screening showed that fatty acids are completely bound within the sediments (presumably due to the alkaline environment) and require different extraction techniques. Test analyses further revealed the presence of tetraether lipids which may allow the application/evaluation of new proxy indices like BIT, CBT and MBT (TEX_{86} is more unlikely due to the dominance of branched vs. cyclic compounds). The now at the GFZ well-established analytical equipment for measuring deuterium isotopes (δD) on individual organic compounds should be used in a future study. It has been suggested that comparing δD of aquatic lipids with

those from leaf waxes of higher plants are the potentially best possible tool to reconstruct the hydrological cycle of lakes especially in arid environments (Hou et al. 2008). The Tswaing crater would be an ideal site to test this hypothesis. Moreover, the biomarker study presented in chapter 4 demonstrates the benefit of high-resolution investigations of selected time-slices. A similar approach can be used for other time periods. Considering this wealth of potential information from the organic fraction, the available sediments from Lake Tswaing definitely deserve further investigation. But also important processes in the modern environment such as weathering of soils are waiting to be analysed. A chance for more regular monitoring of the site may arise with the establishment of a new museum at the potential World Heritage site Tswaing.

Contrary to Lake Tswaing, the composite sediment profile from Lake Challa is complete and shows no gaps. Nevertheless, core quality suffered over many parts from intense bending caused by the coring and disturbance due to gas and fluid movements (see Fig. 2.6). Initiation of a new coring campaign with available improved technology promises cores of higher quality and can also serve to extend the investigated time frame as seismic data indicate the presence of undisturbed sediments down to ~210 m (~250,000 years). Sediments with continuously high quality may also allow varve counting for age control over longer intervals than presently feasible (with the available material counting is in progress for the upper 2.7 m and the deepest ~3 m of the profile). This method can improve the control of the reservoir age effect but also allows high precision dating for long µXRF scanning records. Currently, further $^{210}Pb/^{137}Cs$ dating of the top 36 cm of the sediments are on the way. They will improve the anchoring of the ^{14}C chronology. Another to date unexplored possibility for anchoring of the age model derives from the identified ashes. Establishing a tephrochronology for the Quaternary in East Africa would provide valuable time horizons for many lacustrine climate archives in the region. High-resolution µXRF scanning of the upper finely laminated section gave already valuable knowledge about changing element composition of the youngest sediments at app. monthly scale (chapter 5). The application of this method to older sediments promises insights into seasonality at Lake Challa during times of different climate boundary conditions (early Holocene, last Glacial). Data of this quality will also be the basis for comparison with modelling studies which, in my opinion, are necessary to understand the interaction of the different climatological and hydrological processes that are active at this lake site. Valuable addition to improve process understanding comes from the monitoring campaign at the lake that started in November 2006 and is currently running. It will give insights into seasonality of lake productivity, carbonate precipitation, detrital input and isotope geochemistry, and will improve the understanding of inter-annual events. In this context, a comprehensive study of source waters for Lake Challa and a better understanding of the groundwater hydrology in the Kilimanjaro area in general are urgently needed.

The studies at Lake Tswaing and at Lake Challa can be considered as some kind of pilot investigation. As research in both projects is in progress or planned to be continued in the near future, the results presented in the framework of this thesis provide a solid basis for future work. That future investigations on climate variability and the underlying processes are needed, also and especially for Africa, can be followed in the media and politics, but it is also demonstrated

in the scientific community, e.g., by ongoing discussions about the causes of observed abrupt events as known from archives of African monsoon intensity: are they related to feedback processes or abrupt climate change itself (Chang et al. 2008; Fleitmann et al. 2007; Kröpelin et al. 2008; Liu et al. 2007)? Further modelling studies will help to gain better knowledge about theses issues; however, they will always need the frame provided by proxy information from palaeo climate archives.

8. References

Acocks, J. P. H. (1953). Veld types of South Africa. Government Printer, Pretoria, pp. 192.

Adegbie, A. T., Schneider, R. R., Röhl, U., and Wefer, G. (2003). Glacial millennial-scale fluctuations in central African precipitation recorded in terrigenous sediment supply and freshwater signals offshore Cameroon. *Palaeogeography, Palaeoclimatology, Palaeoecology* **197,** 323-333.

Albro, P. W. (1976). Bacterial waxes. *In* Chemistry and Biochemistry of Natural Waxes. (P. E. Kolattukudy, Ed.), pp. 419-450. Elsevier, Amsterdam.

Allen, J. R. M., Brandt, U., Brauer, A., Hubberten, H.-W., Huntley, B., Keller, J., Kraml, M., Mackensen, A., Mingram, J., Negendank, J. F. W., Nowaczyk, N. R., Oberhansli, H., Watts, W. A., Wulf, S., and Zolitschka, B. (1999). Rapid environmental changes in southern Europe during the last glacial period. *Nature* **400,** 740-743.

Ashok, K., Guan, Z., and Yamagata, T. (2001). Impact of the Indian Ocean Dipole on the relationship between the Indian Ocean Monsoon Rainfall and ENSO. *Geophysical Research Letters* **28,** 4499-4502.

Ashton, P. J. (1999). Limnology of the Pretoria Saltpan crater lake. *In* Tswaing, investigations into the origin, age and palaeoenvironments of the Pretoria Saltpan. (T. C. Partridge, Ed.), pp. 72-90, Council of Geoscience (Geological Survey of South Africa), Pretoria.

Ashton, P. J., and Schoeman, F. R. (1983). Limnological studies on the Pretoria Salt Pan, a hypersaline maar lake. *Hydrobiologia* **99,** 61-73.

Aucour, A.-M., Hillaire-Marcel, C., and Bonnefille, R. (1994). Late Quaternary Biomass Changes from ^{13}C Measurements in a Highland Peatbog from Equatorial Africa (Burundi). *Quaternary Research* **41,** 225-233.

Avnimelech, Y., Ritvo, G., Meijer, L. E., and Kochba, M. (2001). Water content, organic carbon and dry bulk density in flooded sediments. *Aquacultural Engineering* **25,** 25-33.

Bahr, A., Lamy, F., Arz, H., Kuhlmann, H., and Wefer, G. (2005). Late glacial to Holocene climate and sedimentation history in the NW Black Sea. *Marine Geology* **214,** 309-322.

Baker, P. A., Rigsby, C. A., Seltzer, G. O., Fritz, S. C., Lowenstein, T. K., Bacher, N. P., and Veliz, C. (2001). Tropical climate changes at millennial and orbital timescales on the Bolivian Altiplano. *Nature* **409,** 698-701.

Balistrieri, L. S., Murray, J. W., and Paul, B. (1994). The geochemical cycling of trace elements in a biogenic meromictic lake. *Geochimica et Cosmochimica Acta* **58,** 3993-4008.

Bard, E., Rostek, F., and Sonzogni, C. (1997). Interhemispheric synchrony of the last deglaciation inferred from alkenone palaeothermometry. *Nature* **385,** 707-710.

Barry, R. G., and Chorley, R. J. (1998). Atmosphere, weather and climate. Routledge, London, pp. 409.

Barry, S., Filippi, M., Talbot, M. R., and Johnson, T. C. (2002). Sedimentology and geochronology of late Pleistocene and Holocene sediments from northern Lake Malawi. *In* The East African Great Lakes: Limnology, Palaeolimnology and Biodiversity. (E. O. Odada, and D. O. Olago, Eds.), pp. 369-392. Kluwer Academic Publishers, Dordrecht.

Bassinot, F. C., Labeyrie, L. D., Vincent, E., Quidelleur, X., Shackleton, N. J., and Lancelot, Y. (1994). The astronomical theory of climate and the age of the Brunhes-Matuyama magnetic reversal. *Earth and Planetary Science Letters* **126,** 91-108.

Battarbee, R. W., Jones, V. J., Flower, R. J., Cameron, N. G., and Bennion, H. (2001). Diatoms. *In* Tracking Environmental Change Using Lake Sediments. (J. P. Smol, H. J. B. Birks, and W. M. Last, Eds.), pp. 155-202. Kluwer Academic Publishers, Dordrecht.

Bear, L. M. (1955). Geology of the Taveta Area, Explanation of Degree Sheet 64 N.E. and 64 S.E. Report No. 32. (Geological Survey of Kenya, Ed.). Government Printer, Nairobi, pp. 48.

Behera, S. K., Luo, J. J., Masson, S., Rao, S. A., Sakuma, H., and Yamagata, T. (2006). A CGCM Study on the Interaction between IOD and ENSO. *Journal of Climate* **19,** 1688-1705.

Beuning, K. R. M., Talbot, M. R., and Kelts, K. (1997). A revised 30,000-year paleoclimatic and paleohydrologic history of Lake Albert, East Africa. *Palaeogeography, Palaeoclimatology, Palaeoecology* **136,** 259-279.

Black, E., Slingo, J., and Sperber, K. R. (2003). An Observational Study of the Relationship between Excessively Strong Short Rains in Coastal East Africa and Indian Ocean SST. *Monthly Weather Review* **131,** 74-94.

Blaauw, M., Verschuren, D., van Geel, B., van der Plicht, J., Kristen, I., and Lyaruu, A. (in prep.). A centennial-scale chronology over the last 25,000 years for Lake Challa (Mt. Kenya, eastern equatorial Africa).

Bligh, E. G., and Dyer, W. J. (1959). A rapid method for total lipid extraction and purification. *Canadian Journal of Biochemistry and Physiology* **37,** 911-917.

Blumenberg, M., Seifert, R., Kasten, S., Bahlmann, E., and Michaelis, W. (2009). Euphotic zone bacterioplankton sources major sedimentary bacteriohopanepolyols in the Holocene Black Sea. *Geochimica et Cosmochimica Acta* **73,** 750-766.

Bond, G., Broecker, W. S., Johnsen, S. J., McManus, J. F., Labeyrie, L., Jouzel, J., and Bonani, G. (1993). Correlations between climate records from North Atlantic sediments and Greenland ice. *Nature* **365,** 143-147.

Bond, G., Kromer, B., Beer, J., Muscheler, R., Evans, M. N., Showers, W., Hoffmann, S., Lotti-Bond, R., Hajdas, I., and Bonani, G. (2001). Persistent Solar Influence on North Atlantic Climate During the Holocene. *Science* **294,** 2130-2136.

Boon, J. P., Hines, H., Burlingame, A. L., Klok, J., Rijpstra, W. I. C., De Leeuw, J. W., Edmunds, K. E., and Eglinton, G. (1983). Organic geochemical studies of Solar Lake laminated cyanobacterial mats. *In* Advances in Organic Geochemistry 1981. (M. Bjoroy, P. Albrecht, C. Cornford, K. D. Groot, G. Eglinton, E. Galimov, D. Leythaeuser, R. Pelet, J. Rullkotter, and G. Speers, Eds.), pp. 207-227. Wiley, Chichester.

Boyle, J. F. (2001). Inorganic geochemical methods in palaeolimnology. *In* Tracking environmental change using lake sediments. (W. M. Last, and J. P. Smol, Eds.), pp. 83-141. Kluwer Academic Publishers, Dordrecht.

Brandt, D., and Reimold, W. U. (1999). The Geology and Geophysical Signature of the Pretoria Saltpan (Tswaing) Impact Structure. *In* Tswaing, investigations into the origin, age and palaeoenvironments of the Pretoria Saltpan. (T. C. Partridge, Ed.), pp. 6-34, Council of Geoscience (Geological Survey of South Africa), Pretoria.

Broccoli, A. J., Dahl, K. A., and Stouffer, R. J. (2006). Response of the ITCZ to Northern Hemisphere cooling. *Geophysical Research Letters* **33,** doi:10.1029/2005GL024546.

Broecker, W. S. (2000). Abrupt climate change: causal constraints provided by the paleoclimate record. *Earth-Science Reviews* **51,** 137-154.

Brook, E. (2008). Palaeoclimate: Windows on the greenhouse. *Nature* **453,** 291-292.

Brook, G. A., Cowart, J. B., Brandt, S. A., and Scott, L. (1997). Quaternary climatic change in southern and eastern Africa during the last 300 ka: the evidence from caves in Somalia and the Transvaal region of South Africa. *Zeitschrift für Geomorphologie* Supplementband **108,** 15-48.

Brown, E. T., Johnson, T. C., Scholz, C. A., Cohen, A. S., and King, J. W. (2007). Abrupt change in tropical African climate linked to the bipolar seesaw over the past 55,000 years. *Geophysical Research Letters* **34,** doi:10.1029/2007GL031240.

Bühmann, D., and Elsenbroek, J. H. (1999). Mineralogy and geochemistry of the Pretoria Saltpan borehole core. *In* Tswaing, investigations into the origin, age and palaeoenvironments of the Pretoria Saltpan. (T. C. Partridge, Ed.), pp. 91-117. Council of Geoscience (Geological Survey of South Africa), Pretoria.

Butzer, K. W., Fock, G. J., Stuckenrath, R., Zilch, A. (1973). Palaeohydrology of Late Pleistocene Lake, Alexandersfontein, Kimberley, South Africa. *Nature* **243**, 328-330.

Cacho, I., Grimalt, J. O., Canals, M., Sbaffi, L., Shackleton, N. J., Schönfeld, J., and Zahn, R. (2001). Variability of the western Mediterranean Sea surface temperature during the last 25,000 years and its connection with the Northern Hemisphere climatic changes. *Paleoceanography* **16,** 40-52.

Canfield, D. E., and Berner, R. A. (1987). Dissolution and pyritization of magnetite in anoxie marine sediments. *Geochimica et Cosmochimica Acta* **51,** 645-659.

Castaneda, I. S., Werne, J. P., and Johnson, T. C. (2007). Wet and arid phases in the southeast African tropics since the Last Glacial Maximum. *Geology* **35,** 823-826.

Chang, P., Yamagata, T., Schopf, P., Behera, S. K., Carton, J., Kessler, W. S., Meyers, G., Qu, T., Schott, F., Shetye, S., and Xie, S. P. (2006). Climate Fluctuations of Tropical Coupled Systems - The Role of Ocean Dynamics. *Journal of Climate* **19,** 5122-5174.

Chang, P., Zhang, R., Hazeleger, W., Wen, C., Wan, X., Ji, L., Haarsma, R. J., Breugem, W.-P., and Seidel, H. (2008). Oceanic link between abrupt changes in the North Atlantic Ocean and the African monsoon. *Nature Geoscience* **1,** 444-448.

Charles, C. D., Cobb, K., Moore, M. D., and Fairbanks, R. G. (2003). Monsoon-tropical ocean interaction in a network of coral records spanning the 20th century. *Marine Geology* **201,** 207-222.

Charles, C. D., Hunter, D. E., and Fairbanks, R. G. (1997). Interaction Between the ENSO and the Asian Monsoon in a Coral Record of Tropical Climate. *Science* **277,** 925-928.

Chiang, J. C. H., Biasutti, M., and Battisti, D. S. (2003). Sensitivity of the Atlantic Intertropical Convergence Zone to Last Glacial Maximum boundary conditions. *Paleoceanography* **18**(4), 1094, doi:10.1029/2003PA000916**.**

Clark, C. O., Webster, P. J., and Cole, J. E. (2003). Interdecadal Variability of the Relationship between the Indian Ocean Zonal Mode and East African Coastal Rainfall Anomalies. *Journal of Climate* **16,** 548-554.

Claussen, M., Fohlmeister, J., Ganopolski, A., and Brovkin, V. (2006). Vegetation dynamics amplifies precessional forcing. *Geophysical Research Letters* **33**.

Clemens, S. C., Prell, W. L., Murray, D., Shimmield, G. B., and Weedon, G. (1991). Forcing mechanisms of the Indian Ocean monsoon. *Nature* **353,** 720-725.

Cole, J. E., Dunbar, R. B., McClanahan, T. R., and Muthiga, N. A. (2000). Tropical Pacific Forcing of Decadal SST Variability in the Western Indian Ocean over the Past Two Centuries. *Science* **287,** 617-619.

Collister, J. W., Rieley, G., Stern, B., Eglinton, G., and Fry, B. (1994). Compound-specific d13C analyses of leaf lipids from plants with differing carbon dioxide metabolisms. *Organic Geochemistry* **21,** 619-627.

Combourieu Nebout, N., Turon, J. L., Zahn, R., Capotondi, L., Londeix, L., and Pahnke, K. (2002). Enhanced aridity and atmospheric high-pressure stability over the western Mediterranean during the North Atlantic cold events of the past 50 k.y. *Geology* **30,** 863-866.

Conley, D. J., and Schelske, C. L. (2001). Biogenic Silica. *In* Tracking Environmental Change Using Lake Sediments. Volume 3: Terrestrial, Algal, and Siliceous Indicators. (J. P. Smol, H. J. B. Birks, and W. M. Last, Eds.), pp. 281-293. Kluwer Academic Publishers, Dordrecht.

Cook, K. H. (2000). The South Indian Convergence Zone and Interannual Rainfall Variability over Southern Africa. *Journal of Climate* **13,** 3789-3804.

Cranwell, P. A. (1985). Long-chain unsaturated ketones in recent lacustrine sediments. *Geochimica et Cosmochimica Acta* **49,** 1545-1551.

Cruz, F. W., Jr., Burns, S. J., Karmann, I., Sharp, W. D., Vuille, M., Cardoso, A. O., Ferrari, J. A., Silva Dias, P. L., and Viana, O., Jr. (2005). Insolation-driven changes in atmospheric circulation over the past 116,000 years in subtropical Brazil. *Nature* **434,** 63-66.

Cullen, N. J., Mölg, T., Kaser, G., Hussein, K., Steffen, K., and Hardy, D. R. (2006). Kilimanjaro Glaciers: Recent areal extent from satellite data and new interpretation of observed 20th century retreat rates. *Geophysical Research Letters* **33**.

D'Andrea, W. J., and Huang, Y. (2005). Long chain alkenones in Greenland lake sediments: Low d13C values and exceptional abundance. *Organic Geochemistry* **36,** 1234-1241.

Dansgaard, W., Johnsen, S. J., Clausen, H. B., Dahl-Jensen, D., Gundestrup, N. S., Hammer, C. U., Hvidberg, C. S., Steffensen, J. P., Sveinbjornsdottir, A. E., Jouzel, J., and Bond, G. (1993). Evidence for general instability of past climate from a 250-kyr ice-core record. *Nature* **364,** 218-220.

Davison, W. (1993). Iron and manganese in lakes. *Earth-Science Reviews* **34,** 119-163.

De Leeuw, J. W., v. d. Meer, F. W., Rijpstra, I. C., and Schenck, P. A. (1980). On the occurrence and structural identification of long chain unsaturated ketones and hydrocarbons in sediments. *In* Advances in Organic Geochemistry. (A. C. Douglas, and J. R. Maxwell, Eds.), pp. 211-217. Pergamon Press, Oxford.

Dean, W. E. (1974). Determination of carbonate and organic matter in calcareous sediments and sedimentary rocks by loss on ignition: comparison with other methods. *Journal of Sedimentary Petrology* **44,** 242-248.

DeMenocal, P. B. (2008). Palaeoclimate: Africa on the edge. *Nature Geoscience* **1,** 650-651.

DeMenocal, P. B., Ortiz, J., Guilderson, T., Adkins, J., Sarnthein, M., Baker, L., and Yarusinsky, M. (2000). Abrupt onset and termination of the African Humid Period: rapid climate responses to gradual insolation forcing. *Quaternary Science Reviews* **19,** 347-361.

Demory, F., Oberhänsli, H., Nowaczyk, N. R., Gottschalk, M., Wirth, R., and Naumann, R. (2005). Detrital input and early diagenesis in sediments from Lake Baikal revealed by rock magnetism. *Global and Planetary Change* **46,** 145-166.

Diaz, H. F., and Markgraf, V. (1992). El Nino - Historical and Paleoclimatic Aspects of the Southern Oscillation. Cambridge University Press, Cambridge, pp.476.

Downie, C., and Wilkinson, P. (1972). The Geology of Kilimanjaro. The Department of Geology, The University of Sheffield, Sheffield, pp.253.

Eggermont, H., Russell, J., Schettler, G., Van Damme, K., Bessems, I., and Verschuren, D. (2007). Physical and chemical limnology of alpine lakes and pools in the Rwenzori Mountains (Uganda–DR Congo). *Hydrobiologia* **592,** 151-173.

Eglinton, G., and Hamilton, J. E. (1963). The distribution of alkanes. *In* Chemical Plant Taxonomy. (T. Swaine, Ed.), pp. 187-217. Academic Press, New York.

Elvert, M., Whiticar, M. J., and Suess, E. (2001). Diploptene in varved sediments of Saanich Inlet: indicator of increasing bacterial activity under anaerobic conditions during the Holocene. *Marine Geology* **174,** 371-383.

EPICA Community Members (2006). One-to-one coupling of glacial climate variability in Greenland and Antarctica. *Nature* **444,** 195-198.

Espitalié, J., Deroo, G., Marquis, F. (1985). La pyrolyse Rock-Eval et ses applications (1ère partie). *Revue de l'Institut Francais du Pétrole* **40**, 563-579.

Espitalié, J., Laporte, J. L., Madec, M., Marquis, F., Leplat, P., Paulet, J., and Boutefeu, A. (1977). Méthode rapide de caractérisation des roches méres, de leur potential pétrolier et de leur degré d'évolution. *Revue de l'Institut Francais Pétrole* **32,** 23-42.

Eugster, H. P., and Hardie, L. A. (1978). Saline Lakes. *In* Lakes: Chemistry, Geology, Physics. (A. Lerman, Ed.), pp. 237-293. Springer-Verlag, New York - Heidelberg - Berlin.

Evans, L. T. (1975). Crop physiology: some case histories. Cambridge University Press, Cambridge, pp. 374.

Felton, A. A., Russell, J. M., Cohen, A. S., Baker, M. E., Chesley, J. T., Lezzar, K. E., McGlue, M. M., Pigati, J. S., Quade, J., Curt Stager, J., and Tiercelin, J. J. (2007). Paleolimnological evidence for the onset and termination of glacial aridity from Lake

Tanganyika, Tropical East Africa. *Palaeogeography, Palaeoclimatology, Palaeoecology* **252,** 405-423.

Ficken, K. J., Li, B., Swain, D. L., and Eglinton, G. (2000). An *n*-alkane proxy for the sedimentary input of submerged/floating freshwater aquatic macrophytes. *Organic Geochemistry* **31,** 745-749.

Ficken, K. J., Street-Perrott, F. A., Perrott, R. A., Swain, D. L., Olago, D. O., and Eglinton, G. (1998). Glacial/interglacial variations in carbon cycling revealed by molecular and isotope stratigraphy of Lake Nkunga, Mt. Kenya, East Africa. *Organic Geochemistry* **29,** 1701.

Ficken, K. J., Wooller, M. J., Swain, D. L., Street-Perrott, F. A., and Eglinton, G. (2002). Reconstruction of a subalpine grass-dominated ecosystem, Lake Rutundu, Mount Kenya: a novel multi-proxy approach. *Palaeogeography, Palaeoclimatology, Palaeoecology* **177,** 137-149.

Filippi, M. L., and Talbot, M. R. (2005). The palaeolimnology of northern Lake Malawi over the last 25 ka based upon the elemental and stable isotopic composition of sedimentary organic matter. *Quaternary Science Reviews* **24,** 1303-1328.

Finney, B. P., Scholz, C. A., Johnson, T. C., and Trumbore, S. (1996). Late Quaternary Lake-level Changes of Lake Malawi. *In* The Limnology, Climatology and Paleoclimatology of the East African Lakes. (T. C. Johnson, and E. O. Odada, Eds.), pp. 495-521. Gordon and Breach Publishers, Amsterdam.

Fleitmann, D., Burns, S. J., Mangini, A., Mudelsee, M., Kramers, J., Villa, I., Neff, U., Al-Subbary, A. A., Buettner, A., Hippler, D., and Matter, A. (2007). Holocene ITCZ and Indian monsoon dynamics recorded in stalagmites from Oman and Yemen (Socotra). *Quaternary Science Reviews* **26,** 170-188.

Fleitmann, D., Burns, S. J., Mudelsee, M., Neff, U., Kramers, J., Mangini, A., and Matter, A. (2003). Holocene Forcing of the Indian Monsoon Recorded in a Stalagmite from Southern Oman. *Science* **300,** 1737-1739.

Florindo, F., Roberts, A. P., and Palmer, M. R. (2003). Magnetite dissolution in siliceous sediments. *Geochemistry, Geophysics, Geosystems* **4,** 1053, doi:10.1029/2003GC000516.

Fry, B. (1986). Sources of carbon and sulfur nutrition for consumers in three meromictic lakes of New York State. *Limnology and Oceanography* **31,** 79-88.

Fuhrmann, A., Fischer, T., Lücke, A., Brauer, A., Zolitschka, B., Horsfield, B., Negendank, J. F. W., Schleser, G. H., and Wilkes, H. (2004). Late Quaternary environmental and climatic changes in central Europe as inferred from the composition of organic matter in annually laminated maar lake sediments. *Geochemistry, Geophysics, Geosystems* **5,** Q11015.

Fuhrmann, A., Mingram, J., Lücke, A., Houyuan, L., Horsfield, B., Jiaqi, L., Negendank, J. F. W., Schleser, G. H., and Wilkes, H. (2003). Variations in organic matter composition in sediments from Lake Huguang Maar (Huguangyan), south China during the last 68 ka: implications for environmental and climatic change. *Organic Geochemistry* **34,** 1497-1515.

Gadgil, S., Vinayachandran, P. N., Francis, P. A., and Gadgil, S. (2004). Extremes of the Indian summer monsoon rainfall, ENSO and equatorial Indian Ocean oscillation. *Geophysical Research Letters* **31,** doi:10.1029/2004GL019733.

Garcin, Y., Vincens, A., Williamson, D., Buchet, G., and Guiot, J. (2007). Abrupt resumption of the African Monsoon at the Younger Dryas--Holocene climatic transition. *Quaternary Science Reviews* **26,** 690-704.

Garcin, Y., Vincens, A., Williamson, D., Guiot, J., and Buchet, G. (2006a). Wet phases in tropical southern Africa during the last glacial period. *Geophysical Research Letters* **33**(L07703).

Garcin, Y., Williamson, D., Taieb, M., Vincens, A., Mathé, P.-E., and Majule, A. (2006b). Centennial to millennial changes in maar-lake deposition during the last 45,000 years in tropical Southern Africa (Lake Masoko, Tanzania). *Palaeogeography, Palaeoclimatology, Palaeoecology* **239**(3-4), 334-354.

Gasse, F. (2000). Hydrological changes in the African tropics since the Last Glacial Maximum. *Quaternary Science Reviews* **19,** 189-211.

Gasse, F., Chalié, F., Vincens, A., Williams, M. A. J., and Williamson, D. (2008). Climatic patterns in equatorial and southern Africa from 30,000 to 10,000 years ago reconstructed from terrestrial and near-shore proxy data. *Quaternary Science Reviews* **27,** 2316-2340.

Gasse, F., Lédée, V., Massault, M., and Fontes, J.-C. (1989). Water-level fluctuations of Lake Tanganyika in phase with oceanic changes during the last glaciation and deglaciation. *Nature* **342**.

Giannini, A., Biasutti, M., Held, I., and Sobel, A. (2008). A global perspective on African climate. *Climatic Change* **90,** 359-383.

Goad, L. J., and Withers, N. (1982). Identification of 27-Nor-(24R)-24-methylcholesta-5,22-dien-3β-ol and Brassicasterol as the major sterols of the marine dinoflagellate *Gymnodinium simplex*. *Lipids* **17,** 853-858.

Granina, L., Muller, B., and Wehrli, B. (2004). Origin and dynamics of Fe and Mn sedimentary layers in Lake Baikal. *Chemical Geology* **205,** 55-72.

Grimalt, J. O., Yruela, I., Saiz-Jimenez, C., Toja, J., de Leeuw, J. W., and Albaiges, J. (1991). Sedimentary lipid biogeochemistry of an hypereutrophic alkaline lagoon. *Geochimica et Cosmochimica Acta* **55,** 2555-2577.

Grimley, D. A., and Arruda, N. K. (2007). Observations of magnetite dissolution in poorly drained soils. *Soil Science* **172,** 968-982.

Grootes, P., Stuvier, M., White, J. W. C., Johnsen, S. J., and Jouzel, J. (1993). Comparison of oxygen isotope records from the GISP2 and GRIP Greeenland ice cores. *Nature* **366,** 552-554.

Grossi, V., Baas, M., Schogt, N., Klein Breteler, W. C. M., De Leeuw, J. W., and Rontani, J. F. (1996). Formation of phytadienes in the water column: myth or reality? *Organic Geochemistry* **24,** 833-839.

Grossi, V., Hirschler, A., Raphel, D., Rontani, J. F., De Leeuw, J. W., and Bertrand, J. C. (1998). Biotransformation pathways of phytol in recent anoxic sediments. *Organic Geochemistry* **29,** 845-861.

Grousset, F. E., Labeyrie, L., Sinko, J. A., Cremer, M., Bond, G., Duprat, J., Cortijo, E., and Huon, S. (1993). Patterns of Ice-Rafted Detritus in the Glacial North Atlantic (40-55°N). *Paleoceanography* **8,** 175–192.

Gupta, A. K., Anderson, D. M., and Overpeck, J. T. (2003). Abrupt changes in the Asian southwest monsoon during the Holocene and their links to the North Atlantic Ocean. *Nature* **421,** 354-357.

Haberzettl, T., Corbella, H., Fey, M., Janssen, S., Lucke, A., Mayr, C., Ohlendorf, C., Schabitz, F., Schleser, G. H., Wille, M., Wulf, S., and Zolitschka, B. (2007). Lateglacial and Holocene wet--dry cycles in southern Patagonia: chronology, sedimentology and geochemistry of a lacustrine record from Laguna Potrok Aike, Argentina. *The Holocene* **17,** 297-310.

Hanisch, S., Ariztegui, D., and Püttmann, W. (2003). The biomarker record of Lake Albano, central Italy - implications for Holocene system response to environmental change. *Organic Geochemistry* **34,** 1223-1235.

Harvey, H. R., and McManus, G. B. (1991). Marine ciliates as a widespread source of tetrahymanol and hopan-3β-ol in sediments. *Geochimica et Cosmochimica Acta* **55,** 3387-3390.

Hastenrath, S. (1991). Climate Dynamics of the Tropics. Kluwer Academic Publishing, Dordrecht, pp.488.

Hastenrath, S. (2001). Variations of East African Climate during the past two centuries. *Climatic Change* **50,** 209-217.

Hastenrath, S., Polzin, D., and Camberlin, P. (2004). Exploring the Predictability of the 'Short Rains' at the Coast of East Africa. *International Journal of Climatology* **24,** 1333-1343.

Haug, G. H., and Tiedemann, R. (1998). Effect of the formation of the Isthmus of Panama on Atlantic Ocean thermohaline circulation. *Nature* **393,** 673 - 676.

Haug, G. H., Günther, D., Peterson, L. C., Sigman, D. M., Hughen, K. A., and Aeschlimann, B. (2003). Climate and the Collapse of Maya Civilization. *Science* **299,** 1731 - 1735.

Haug, G. H., Hughen, K. A., Sigman, D. M., Peterson, L. C., and Röhl, U. (2001). Southward Migration of the Intertropical Convergence Zone Through the Holocene. *Science* **293,** 1304-1308.

Hecky, R. E. (1971). The Paleolimnology of the Alkaline, Saline Lakes on the Mt. Meru Lahar. PhD thesis, Duke University, pp. 209.

Hemming, S. R. (2004). Heinrich events: Massive late Pleistocene detritus layers of the north Atlantic and their global climate imprint. *Review of Geophysics* **42**, doi:10.1029/2003RG000128.

Hodell, D. A., Anselmetti, F. S., Ariztegui, D., Brenner, M., Curtis, J. H., Gilli, A., Grzesik, D. A., Guilderson, T. J., Müller, A. D., Bush, M. B., Correa-Metrio, A., Escobar, J., and Kutterolf, S. (2008). An 85-ka record of climate change in lowland Central America. *Quaternary Science Reviews* **27,** 1152-1165.

Hoelzmann, P., Gasse, F., Dupont, L. M., Salzmann, U., Staubwasser, M., Leuschner, D. C., and Sirocko, F. (2004). Palaeoenvironmental changes in the arid and subarid belt (Sahara-Sahel-Arabian Peninsula) from 150 kyr to present. *In* Past Climate Variability through Europe and Africa. (R. W. Battarbee, Ed.), pp. 219-256. Springer, Dordrecht, The Netherlands.

Holmer, M., and Storkholm, P. (2001). Sulphate reduction and sulphur cycling in lake sediments: a review. *Freshwater Biology* **46,** 431-451.

Holmgren, K., Karlen, W., and Shaw, P. A. (1995). Paleoclimatic Significance of the Stable Isotopic Composition and Petrology of a Late Pleistocene Stalagmite from Botswana. *Quaternary Research* **43,** 320-328.

Holmgren, K., Lee-Thorp, J. A., Cooper, G. R. J., Lundblad, K., Partridge, T. C., Scott, L., Sithaldeen, R., Siep Talma, A., and Tyson, P. D. (2003). Persistent millennial-scale climatic variability over the past 25,000 years in Southern Africa. *Quaternary Science Reviews* **22,** 2311-2326.

Hornibrook, E. R. C., Longstaffe, F. J., Fyfe, W. S., and Bloom, Y. (2000). Carbon-isotope ratios and carbon, nitrogen and sulfur abundances in flora and soil organic matter from a temperate-zone bog and marsh. *Geochemical Journal* **34,** 237-245.

Hou, J., D'Andrea, W. J., and Huang, Y. (2008). Can sedimentary leaf waxes record D/H ratios of continental precipitation? Field, model, and experimental assessments. *Geochimica et Cosmochimica Acta* **72,** 3503-3517.

Huang, Y., Freeman, K. H., Eglinton, T. I., and Street-Perrott, F. A. (1999a). delta 13 C analyses of individual lignin phenols in Quaternary lake sediments; a novel proxy for deciphering past terrestrial vegetation changes. *Geology* **27,** 471-474.

Huang, Y., Street-Perrott, F. A., Perrott, R. A., Metzger, P., and Eglinton, G. (1999b). Glacial-interglacial environmental changes inferred from molecular and compound-specific [delta]13C analyses of sediments from Sacred Lake, Mt. Kenya. *Geochimica et Cosmochimica Acta* **63,** 1383-1404.

Hughen, K. A., Overpeck, J. T., Peterson, L. C., and Trumbore, S. (1996). Rapid climate changes in the tropical Atlantic region during the last deglaciation. *Nature* **380,** 51-54.

Indeje, M., Semazzi, F. H. M., and Ogallo, L. J. (2000). ENSO signals in East African rainfall seasons. *International Journal of Climatology* **20,** 19-46.

Ishiwatari, R., Yamamoto, S., and Uemura, H. (2005). Lipid and lignin/cutin compounds in Lake Baikal sediments over the last 37 kyr: implications for glacial-interglacial palaeoenvironmental change. *Organic Geochemistry* **36**, 327-347.

Ivanochko, T. S., Ganeshram, R. S., Brummer, G.-J. A., Ganssen, G., Jung, S. J. A., Moreton, S. G., and Kroon, D. (2005). Variations in tropical convection as an amplifier of global climate change at the millennial scale. *Earth and Planetary Science Letters* **235,** 302-314.

Jaffé, R., and Hausmann, K. B. (1995). Origin and early diagenesis of arborinone/isoarborinol in sediments of a highly productive freshwater lake. *Organic Geochemistry* **22,** 231-235.

Johnson, T. C. (1996). Sedimentary Processes and Signals of Past Climatic Change in the Large Lakes of the East African Rift Valley. *In* The Limnology, Climatology and Paleoclimatology of the East African Lakes. (T. C. Johnson, and E. O. Odada, Eds.), pp.367-412. Gordon and Breach Publishers, Amsterdam.

Johnson, T. C., Brown, E. T., McManus, J., Barry, S., Barker, P., and Gasse, F. (2002). A High-Resolution Paleoclimate Record Spanning the Past 25,000 Years in Southern East Africa. *Science* **296,** 113-132.

Jourdan, F., Renne, P. R., and Reimold, W. U. (2007). The problem of inherited $^{40}Ar^{*}$ in dating impact glass by the $^{40}Ar/^{39}Ar$ method: Evidence from the Tswaing impact crater (South Africa). *Geochimica et Cosmochimica Acta* **71**, 1214-1231.

Jouzel, J., Masson-Delmotte, V., Cattani, O., Dreyfus, G., Falourd, S., Hoffmann, G., Minster, B., Nouet, J., Barnola, J. M., Chappellaz, J., Fischer, H., Gallet, J. C., Johnsen, S., Leuenberger, M., Loulergue, L., Luethi, D., Oerter, H., Parrenin, F., Raisbeck, G., Raynaud, D., Schilt, A., Schwander, J., Selmo, E., Souchez, R., Spahni, R., Stauffer, B., Steffensen, J. P., Stenni, B., Stocker, T. F., Tison, J. L., Werner, M., and Wolff, E. W. (2007). Orbital and Millennial Antarctic Climate Variability over the Past 800,000 Years. *Science* **317,** 793-796.

Kabanda, T. A., and Jury, M. R. (1999). Inter-annual variability of short rains over northern Tanzania. *Climate Research* **13,** 231-241.

Kaiser, J., Schefuß, E., Lamy, F., Mohtadi, M., and Hebbeln, D. (2008). Glacial to Holocene changes in sea surface temperature and coastal vegetation in north central Chile: high versus low latitude forcing. *Quaternary Science Reviews* **27,** 2064-2075.

Kanfoush, S. L., Hodell, D. A., Charles, C. D., Guilderson, T. P., Mortyn, P. G., and Ninnemann, U. S. (2000). Millennial-Scale Instability of the Antarctic Ice Sheet During the Last Glaciation. *Science* **288,** 1815-1819.

Kanfoush, S. L., Hodell, D. A., Charles, C. D., Janecek, T. R., and Rack, F. R. (2002). Comparison of ice-rafted debris and physical properties in ODP Site 1094 (South Atlantic) with the Vostok ice core over the last four climatic cycles. *Palaeogeography, Palaeoclimatology, Palaeoecology* **182,** 329-349.

Kao-Kiffin, J., and Balser, T. C. (2007). Elevated CO2 differentially alters belowground plant and soil microbial community structure in reed canary grass-invaded experimental wetlands. *Soil Biology & Biochemistry* **39,** 517-525.

Kaplan, A., Cane, M., Kushnir, Y., Clement, A., Blumenthal, M., and Rajagopalan, B. (1998). Analyses of global sea surface temperature 1856-1991. *Journal of Geophysical Research* **103,** 18567-18589.

Kim, J.-H., Schneider, R. R., Muller, P. J., and Wefer, G. (2002). Interhemispheric comparison of deglacial sea-surface temperature patterns in Atlantic eastern boundary currents. *Earth and Planetary Science Letters* **194,** 383-393.

Kiriama, H. O. (1993). The iron-using communities in Kenya. *In* The Archaeology of Africa. (T. Shaw, P. Sinclair, B. Andah, and A. Okpoko, Eds.), pp. 485-498. Routledge, London.

Kleemann, G., Poralla, K., Englert, G., Kjosen, H., Liaaen-Jensen, S., Neunlist, S., and Rohmer, M. (1990). Tetrahymanol from the phototrophic bacterium *Rhodopseudomonas palustris*: first report of a gammacerane triterpene from a prokaryote. *Journal of General Microbiology* **136,** 2551-2553.

Kling, G. W. (1988). Comparative transparency, depth of mixing, and stability of stratification in lakes of Cameroon, West Africa. *Limnology and Oceanography* **33,** 27-40.

Koeberl, C., Shirey, S. B., and Reimold, W. U. (1999). The origin of the Pretoria Saltpan crater. *In* Tswaing, investigations into the origin, age and palaeoenvironments of the Pretoria Saltpan. (T. C. Partridge, Ed.), pp. 55-63, Council of Geoscience (Geological Survey of South Africa), Pretoria.

Kristen, I., Fuhrmann, A., Thorpe, J., Röhl, U., Wilkes, H., and Oberhänsli, H. (2007). Hydrological changes in southern Africa over the last 200 Ka as recorded in lake sediments from the Tswaing impact crater. *South African Journal of Geology* **110,** 311-326.

Kröpelin, S., Verschuren, D., Lezine, A. M., Eggermont, H., Cocquyt, C., Francus, P., Cazet, J. P., Fagot, M., Rumes, B., Russell, J. M., Darius, F., Conley, D. J., Schuster, M., von Suchodoletz, H., and Engstrom, D. R. (2008). Climate-Driven Ecosystem Succession in the Sahara: The Past 6000 Years. *Science* **320,** 765-768.

Kuper, R., and Kröpelin, S. (2006). Climate-Controlled Holocene Occupation in the Sahara: Motor of Africa's Evolution. *Science* **313,** 803-807.

Kutzbach, J. E., and Street-Perrott, F. A. (1985). Milankovitch forcing of fluctuations in the level of tropical lakes from 18 to 0 kyr BP. *Nature* **317,** 130-134.

Kwiecien, O., Arz, H. W., Lamy, F., Plessen, B., Bahr, A., and Haug, G. H. (2009). North Atlantic control on precipitation pattern in the eastern Mediterranean/Black Sea region during the last glacial. *Quaternary Research* **in press**.

Lafargue, E., Marquis, F., and Pillot, D. (1998). Rock-Eval 6 applications in hydrocarbon exploration, production and soil contamination studies. *Revue de l'Institut Francais du Pétrole* **53,** 421-437.

Lamb, A. L., Leng, M. J., Umer Mohammed, M., and Lamb, H. F. (2004). Holocene climate and vegetation change in the Main Ethiopian Rift Valley, inferred from the composition (C/N and δ13C) of lacustrine organic matter. *Quaternary Science Reviews* **23,** 881-891.

Lamb, H. F., Bates, C. R., Coombes, P. V., Marshall, M. H., Umer, M., Davies, S. J., and Dejen, E. (2007). Late Pleistocene desiccation of Lake Tana, source of the Blue Nile. *Quaternary Science Reviews* **26,** 287-299.

Lamb, H. F., Leng, M. J., Telford, R. J., Ayenew, T., and Umer, M. (2007). Oxygen and carbon isotope composition of authigenic carbonate from an Ethiopian lake: a climate record of the last 2000 years. *The Holocene* **17,** 517-526.

Lamy, F., Kaiser, J., Ninnemann, U., Hebbeln, D., Arz, H. W., and Stoner, J. (2004). Antarctic Timing of Surface Water Changes off Chile and Patagonian Ice Sheet Response. *Science* **304,** 1959-1962.

Larimer, F. W., Chain, P., Hauser, L., Lamerdin, J., Malfatti, S., Do, L., Land, M. L., Pelletier, D. A., Beatty, J. T., Lang, A. S., Tabita, F. R., Gibson, J. L., Hanson, T. E., Bobst, C., Torres, J. L. T. y., Peres, C., Harrison, F. H., Gibson, J., and Harwood, C. S. (2003). Complete genome sequence of the metabolically versatile photosynthetic bacterium Rhodopseudomonas palustris. *Nature Biotechnology* **22,** 55-61.

Lee-Thorp, J. A., Holmgren, K., Lauritzen, S. E., Linge, H., Moberg, A., Partridge, T. C., Stevenson, C., and Tyson, P. D. (2001). Rapid climate shifts in the southern African interior throughout the mid to late Holocene. *Geophysical Research Letters* **28,** 4507-4510.

Leng, M. J., Lamb, A. L., Heaton, T. H. E., Marshall, J. D., Wolfe, B. B., Jones, M. D., Holmes, J., and Arrowsmith, C. (2005). Isotopes in lake sediments. *In* Isotopes in Palaeoenvironmental Research. (M. J. Leng, Ed.), pp. 147-184. Springer, Dordrecht, The Netherlands.

Leroy, S. A. G., and Colman, S. M. (2001). Coring and drilling equipment and procedures for recovery of long lacustrine sequences. *In* Tracking Environmental Change Using Lake Sediments. (J. P. Smol, H. J. B. Birks, and W. M. Last, Eds.), pp.107-135. Kluwer Academic Publishers, Dordrecht.

Levi, C., Labeyrie, L., Bassinot, F., Guichard, F., Cortijo, E., Waelbroeck, C., Caillon, N., Duprat, J., de Garidel-Thoron, T., and Elderfield, H. (2007). Low-latitude hydrological cycle and rapid climate changes during the last deglaciation. *Geochemistry Geophysics Geosystems* **8,** doi:10.1029/2006GC001514.

Lewis, W. M. J. (1987). Tropical Limnology. *Annual Review of Ecology and Systematics* **18,** 159-184.

Li, J., Philp, R. P., Pu, F., and Allen, J. (1996). Long-chain alkenones in Qinghai Lake sediments. *Geochimica et Cosmochimica Acta* **60,** 235-241.

Liu, Z., Wang, Y., Gallimore, R., Gasse, F., Johnson, T., deMenocal, P., Adkins, J., Notaro, M., Prentice, I. C., Kutzbach, J., Jacob, R., Behling, P., Wang, L., and Ong, E. (2007). Simulating the transient evolution and abrupt change of Northern Africa atmosphere-ocean-terrestrial ecosystem in the Holocene. *Quaternary Science Reviews* **26,** 1818-1837.

Lizcano, G., and Todd, M. (2005). Non-ENSO control on southern Africa precipitation variability. *Philosophical Transactions of the Royal Society A* **363,** 61-62.

Loulergue, L., Schilt, A., Spahni, R., Masson-Delmotte, V., Blunier, T., Lemieux, B., Barnola, J.-M., Raynaud, D., Stocker, T. F., and Chappellaz, J. (2008). Orbital and millennial-scale features of atmospheric CH4 over the past 800,000 years. *Nature* **453,** 383-386.

Lowe, J. J., Rasmussen, S. O., Björck, S., Hoek, W. Z., Steffensen, J. P., Walker, M. J. C., and Yu, Z. C. (2008). Synchronisation of palaeoenvironmental events in the North Atlantic region during the Last Termination: a revised protocol recommended by the INTIMATE group. *Quaternary Science Reviews* **27,** 6-17.

Lüthi, D., Le Floch, M., Bereiter, B., Blunier, T., Barnola, J.-M., Siegenthaler, U., Raynaud, D., Jouzel, J., Fischer, H., Kawamura, K., and Stocker, T. F. (2008). High-resolution carbon dioxide concentration record 650,000-800,000 years before present. *Nature* **453,** 379-382.

Maher, B. A., and Thompson, R. (1999). Quaternary Climates, Environments and Magnetism. Cambridge University Press, Cambridge, pp. 390.

Marlowe, I. T., Brassell, S. C., Eglinton, G., and Green, J. C. (1984). Long chain unsaturated ketones and esters in living algae and marine sediments. *Organic Geochemistry* **6,** 135-141.

McCarthy, R. D., and Duthie, A. P. (1962). Rapid quantitative method for separation of free fatty acids from other lipids. *Journal of Lipid Research* **3,** 117-119.

McCormac, F. G., Hogg, A. G., Blackwell, P. G., Buck, C. E., Higham, T. F. G., and Reimer, P. J. (2004). SHCal04 Southern Hemisphere Calibration 0 - 11.0 cal kyr BP. *Radiocarbon* **46,** 1087-1092.

Metcalfe, S. E. (1999). Diatoms from the Pretoria Saltpan - a record of lake evolution and environmental change. *In* Tswaing, investigations into the origin, age and palaeoenvironments of the Pretoria Saltpan. (T. C. Partridge, Ed.), pp. 172-192, Council of Geoscience (Geological Survey of South Africa), Pretoria.

Meyers, P. A. (1997). Organic geochemical proxies of paleoceanographic, paleolimnologic, and paleoclimatic processes. *Organic Geochemistry* **27,** 213-250.

Meyers, P. A. (2003). Applications of organic geochemistry to paleolimnological reconstructions: a summary of examples from the Laurentian Great Lakes. *Organic Geochemistry* **34,** 261-289.

Meyers, P. A., and Lallier-Vergès, E. (1999). Lacustrine Sedimentary Organic Matter Records of Late Quaternary Paleoclimates. *Journal of Paleolimnology* **21,** 345-372.

Milne, I. (2007). Climate and environmental change inferred from diatom communities in Lake Challa (Kenya-Tanzania). PhD thesis, Queen's University, pp. 100.

Moernaut, J., Verschuren, D., Charlet, F., Kristen, I., Fagot, M., Van der Plicht, M., and De Batist, M. (in prep.). Seismic-stratigraphic record of lake-level fluctuations in Lake Challa (equatorial East-Africa): climate stability and change over the last 140 ka.

Mölg, T., Hardy, D. R., Cullen, N. J., and Kaser, G. (2005). Tropical glaciers in the context of climate change and society: Focus on Kilimanjaro (East Africa). *In* Contribution to Wengen 2004 Workshop: Mountain Glaciers and Society, pp. 28.

Morrill, C., Overpeck, J. T., and Cole, J. E. (2003). A synthesis of abrupt changes in the Asian summer monsoon since the last deglaciation. *The Holocene* **13,** 465-476.

Moy, C. M., Seltzer, G. O., Rodbell, D. T., and Anderson, D. M. (2002). Variability of El Nino/Southern Oscillation activity at millennial timescales during the Holocene epoch. *Nature* **420,** 162-165.

Munyikwa, K. (2005). Synchrony of Southern Hemisphere Late Pleistocene arid episodes: A review of luminescence chronologies from arid aeolian landscapes south of the Equator. *Quaternary Science Reviews* **24,** 2555-2583.

NGRIP-Members. (2004). High-resolution record of Northern Hemisphere climate extending into the last interglacial period. *Nature* **431,** 147-151.

Nicholson, S. E. (1996). A Review of Climate Dynamics and Climate Variability in Eastern Africa. *In* The Limnology, Climatology and Paleoclimatology of the East African Lakes. (T. C. Johnson, and E. O. Odada, Eds.), pp. 25-56. Gordon and Breach Publishers, Amsterdam.

Nicholson, S. E. (2000). The nature of rainfall variability over Africa on time scales of decades to millenia. *Global and Planetary Change* **26,** 137-158.

Nicholson, S. E., and Kim, J. (1997). The relationship of the El Nino-Southern Oscillation to African rainfall. *International Journal of Climatology* **17,** 117-135.

Nowaczyk, N. R. (2001). Logging of magnetic susceptibility. *In* Tracking environmental change using lake sediments. (W. M. Last, and J. P. Smol, Eds.), pp. 155-170. Kluwer Academic Publishers, Dordrecht.

O'Connor, P. W., and Thomas, D. S. G. (1999). The Timing and Environmental Significance of Late Quaternary Linear Dune Development in Western Zambia. *Quaternary Research* **52,** 44-55.

Olago, D. O. (2001). Vegetation changes over palaeo-time scales in Africa. *Climate Research* **17,** 105-121.

O'Leary, M. H. (1981). Carbon isotope fractionation in plants. *Phytochemistry* **20,** 553-567.

O'Leary, M. H. (1988). Carbon isotopes in photosynthesis: fractionation techniques may reveal new aspects of carbon dynamics in plants. *Bioscience* **38,** 328-336.

Ourisson, G., Rohmer, M., and Poralla, K. (1987). Prokaryotic hopanoids and other polyterpenoid sterol surrogates. *Annual Review of Microbiology* **41**, 301-333.

Overpeck, J., Anderson, D., Trumbore, S., and Prell, W. (1996). The southwest Indian Monsoon over the last 18 000 years. *Climate Dynamics* **12,** 213-225.

Partridge, T. C. (1999a). The sedimentary record and its implications for rainfall fluctuations in the past. *In* Tswaing, investigations into the origin, age and palaeoenvironments of the Pretoria Saltpan. (T. C. Partridge, Ed.), pp. 127-142, Council of Geoscience (Geological Survey of South Africa), Pretoria.

Partridge, T. C. (1999b). Tswaing, investigations into the origin, age and palaeoenvironments of the Pretoria Saltpan. Council for Geosciences, Geological Survey of South Africa, Pretoria, pp. 198.

Partridge, T. C. (2002). Were Heinrich events forced from the southern hemisphere? *South African Journal of Science* **98,** 43-46.

Partridge, T. C., DeMenocal, P. B., Lorentz, S. A., Paiker, M. J., and Vogel, J. C. (1997). Orbital forcing of climate over South Africa: a 200,000-year rainfall record from the Pretoria Saltpan. *Quaternary Science Reviews* **16,** 1125-1133.

Partridge, T. C., Kerr, S. J., Metcalfe, S. E., Scott, L., Talma, A. S., and Vogel, J. C. (1993). The Pretoria Saltpan: a 200,000 year Southern African lacustrine sequence. *Palaeogeography,Palaeoclimatology,Palaeoecology* **101,** 317 - 337.

Partridge, T. C., Scott, L., and Hamilton, J. E. (1999). Synthetic reconstructions of southern African environments during the Last Glacial Maximum (21-18 kyr) and the Holocene Altithermal (8-6 kyr). *Quaternary International* **57/58,** 207-214.

Pascal, T., Fabrice, C., and Hervé, D. (2007). Impact of southeast Indian Ocean sea surface temperature anomalies on monsoon-ENSO-dipole variability in a coupled ocean–atmosphere model. *Climate Dynamics* **28,** 553-580.

Patience, A. J., Lallier-Verges, E., Alberic, P., Desprairies, A., and Tribovillard, N. (1996). Relationships between organo-mineral supply and early diagenesis in the lacustrine environment: A study of surficial sediments from the Lac du Bouchet (Haute Loire, France). *Quaternary Science Reviews* **15,** 213.

Payne, B. R. (1970). Water balance of Lake Chala and its relation to groundwater from tritium and stable isotope data. *Journal of Hydrology* **11,** 47-58.

Pearson, E. J., Farrimond, P., and Juggins, S. (2007). Lipid geochemistry of lake sediments from semi-arid Spain: Relationships with source inputs and environmental factors. *Organic Geochemistry* **38,** 1169-1195.

Peterson, L. C., Haug, G. H., Hughen, K. A., and Röhl, U. (2000). Rapid Changes in the Hydrologic Cycle of the Tropical Atlantic During the Last Glacial. *Science* **290,** 1947 - 1951.

Petit, J. R., Jouzel, J., Raynaud, D., Barkov, N. I., Barnola, J. M., Basile, I., Bender, M., Chappellaz, J., Davis, M., Delaygue, G., Delmotte, M., Kotlyakov, V. M., Legrand, M., Lipenkov, V. Y., Lorius, C., Pepin, L., Ritz, C., Saltzman, E., and Stievenard, M. (1999). Climate and atmospheric history of the past 420,000 years from the Vostok ice core, Antarctica. *Nature* **399,** 429-436.

Petters, S. W. (1991). Regional Geology of Africa. Springer-Verlag, Berlin – Heidelberg, pp.722.

Pickering, R., Hancox, P. J., Lee-Thorp, J. A., Grün, R., Mortimer, G. E., McCulloch, M. T., and Berger, L. R. (in press). Stratigraphy, U-Th chronology, and paleoenvironments at Gladysvale Cave: insights into the climatic control of South African hominin bearing cave deposits. *Journal of Human Evolution*.

Pilskaln, C. H. (2004). Seasonal and interannual particle export in an African rift valley lake: A 5-yr record from Lake Malawi, southern East Africa. *Limnology and Oceanography* **49,** 964-977.

Plisnier, P. D., Chitamwebwa, D., Mwape, L., Tshibangu, K., Langenberg, V., and Coenen, E. (1999). Limnological annual cycle inferred from physical-chemical fluctuations at three stations of Lake Tanganyika. *Hydrobiologia* **407,** 45-58.

Plisnier, P.-D., and Serneels, S. (2000). Impact of ENSO on East African ecosystems: a multivariate analysis based on climate and remote sensing data. *Global Ecology and Biogeography* **9,** 481-497.

Powers, L. A., Johnson, T. C., Werne, J. P., and Castaneda, I. S. (2005). Large temperature variability in the southern African tropics since the Last Glacial Maximum. *Geophysical Research Letters* **32,** L08706 1-4.

Prell, W. L., and Campo, E. V. (1986). Coherent response of Arabian Sea upwelling and pollen transport to late Quaternary monsoonal winds. *Nature* **323,** 526-528.

Preston-Whyte, R. A., and Tyson, P. D. (1988). The Atmosphere and Weather of Southern Africa. Oxford University Press, Cape Town, pp. 375.

Pyle, D. M. (1999). Widely dispersed Quaternary tephra in Africa. *Global and Planetary Change* **21,** 95-112.

Radke, M., Sittard, H. G., and Welte, D. H. (1978). Removal of soluble organic matter from rock samples with a flow-through extraction cell. *Analytical Chemistry* **50,** 663-665.

Radke, M., Wilsch, H., and Welte, D. H. (1980). Preparative hydrocarbon group type determination by automated medium pressure liquid chromatography. *Analytical Chemistry* **52,** 406-411.

Rampen, S. W., Schouten, S., Abbas, B., Elda Panoto, F., Muyzer, G., Campbell, C. N., Fehling, J., Sinninghe, D., and S., J. (2007). On the origin of 24-norcholestanes and their use as age-diagnostic biomarkers. *Geology* **35,** 419-422.

Rasmussen, S. O. (2006). A new Greenland ice core chronology for the last glacial termination. *J. Geophys. Res.* **111,** D06102.

Reason, C. J. C. (2001). Subtropical Indian Ocean SST dipole events and southern African rainfall. *Geophysical Research Letters* **28,** 2225-2227.

Reason, C. J. C. (2002). Sensitivity of the southern African circulation to dipole sea-surface temperature patterns in the south Indian Ocean. *International Journal of Climatology* **22,** 377-393.

Reason, C. J. C., Allan, R. J., Lindesay, J. A., and Ansell, T. J. (2000). ENSO and climatic signals across the Indian Ocean Basin in the global context: part I, interannual composite patterns. *International Journal of Climatology* **20,** 1285-1327.

Reason, C. J. C., and Rouault, M. (2002). ENSO-like decadal variability and South African rainfall. *Geophysical Research Letters* **29,** 1638.

Reimer, P. J., Baillie, M. G. L., Bard, E., Bayliss, A., Beck, J. W., Bertrand, C., Blackwell, P. G., Buck, C. E., Burr, G., Cutler, K. B., Damon, P. E., Edwards, R. L., Fairbanks, R. G., Friedrich, M., Guilderson, T. P., Hughen, K. A., Kromer, B., McCormac, F. G., Manning, S., Bronk Ramsey, C., Reimer, R. W., Remmele, S., Southon, J. R., Stuiver, M., Talamo, S., Taylor, F. W., J., v. d. P., and Weyhenmeyer, C. E. (2004). INTCAL04 terrestrial radiocarbon age calibration, 0-26 cal kyr BP. *Radiocarbon* **46,** 1029-1058.

Reimold, W. U., Koeberl, C., Partridge, T. C., and Kerr, S. J. (1992). Pretoria Saltpan crater: Impact origin confirmed. *Geology* **20,** 1079-1082.

Rein, B., Lückge, A., Reinhardt, L., Sirocko, F., Wolf, A., and Dullo, W.-C. (2005). El Nino variability off Peru during the last 20,000 years. *Paleoceanography* **20,** doi:10.1029/2004PA001099.

Richter, T. O., Van der Gast, S., Koster, R., Vaars, A., Gieles, R., De Stigter, H. C., De Haas, H., and Van Weering, T. C. E. (2006). The Avaatech XRF Core Scanner: technical description and applications to NE Atlantic sediments. *In* New Techniques in Sediments Core Analysis (R. G. Rothwell, Ed.), pp. 39-51. Geological Society London, Special Publication, London.

Robinson, N., Cranwell, P. A., Finlay, B. J., and Eglinton, G. (1984). Lipids of aquatic organisms as potential contributors to lacustrine sediments. *Organic Geochemistry* **6,** 143-152.

Röhl, U., and Abrams, L. J. (2000). High-resolution, downhole, and nondestructive core measurements from sites 999 and 1001 in the Caribbean Sea: Application to the late Paleocene Thermal Maximum. *In* Proceedings of the Ocean Drilling Program, Scientific Results 165. (R. M. Leckie, H. Sigurdsson, G. D. Acton, and G. Draper, Eds.), pp. 191-203. Ocean Drilling Program, College Station, TX, USA.

Rommerskirchen, F., Eglinton, G., Dupont, L., and Rullkötter, J. (2006). Glacial/interglacial changes in southern Africa: Compound-specific $\delta^{13}C$ land plant biomarker and pollen records from southeast Atlantic continental margin sediments. *Geochemistry, Geophysics, Geosystems* **7,** 1-21.

Rommerskirchen, F., Eglinton, G., Dupont, L., Güntner, U., Wenzel, C., and Rullkötter, J. (2003). A north to south transect of Holocene southeast Atlantic continental margin sediments: Relationship between aerosol transport and compound-specific $\delta^{13}C$ land plant biomarker and pollen records. *Geochemistry, Geophysics, Geosystems* **4,** 1-29.

Rontani, J.-F., and Volkman, J. K. (2003). Phytol degradation products as biogeochemical tracers in aquatic environments. *Organic Geochemistry* **34,** 1-35.

Rontani, J.-F., and Volkman, J. K. (2005). Lipid characterization of coastal hypersaline cyanobacterial mats from the Camargue (France). *Organic Geochemistry* **36,** 251-272.

Rosell-Melé, A., Jansen, E., and Weinelt, M. (2002). Appraisal of a molecular approach to infer variations in surface ocean freshwater inputs into the North Atlantic during the last glacial. *Global and Planetary Change* **34,** 143-152.

Rosenfeld, W. D., and Silverman, S. R. (1959). Carbon isotope fractionation in bacterial production of methane. *Science* **130,** 1658-1659.

Rouault, M., and Richard, Y. (2005). Intensity and spatial extent of droughts in southern Africa. *Geophysical Research Letters* **32**.

Rullkötter, J. (1992). Geochemistry, Organic. *In* Encyclopedia of Physical Science and Technology. pp. 165-192. Academic Press.

Russell, J. M., Verschuren, D., and Eggermont, H. (2007). Spatial complexity of 'Little Ice Age' climate in East Africa: sedimentary records from two crater lake basins in western Uganda. *The Holocene* **17,** 183-193.

Saji, N. H., and Yamagata, T. (2003). Possible impacts of Indian Ocean Dipole mode events on global climate. *Climate Research* **25,** 151-169.

Saji, N. H., Goswami, B. N., Vinayachandran, P. N., and Yamagata, T. (1999). A dipole mode in the tropical Indian Ocean. *Nature* **401,** 360-363.

Sakata, S., Hayes, J. M., McTaggart, A. R., Evans, R. A., Leckrone, K. J., and Togasaki, R. K. (1997). Carbon isotopic fractionation associated with lipid biosynthesis by a cyanobacterium: Relevance for interpretation of biomarker records. *Geochimica et Cosmochimica Acta* **61,** 5379-5389.

Schefuß, E., Schouten, S., and Schneider, R. R. (2005). Climatic controls on central African hydrology during the past 20,000 years. *Nature* **437,** 1003-1006.

Schettler, G., and Albéric, P. (2008). Laghi di Monticchio (Southern Italy, Region Basilicata): genesis of sediments—a geochemical study. *Journal of Paleolimnology* **40,** 529-556.

Schidlowski, M., and Matzigkeit, U. (1984). Superheavy Organic Carbon from Hypersaline Microbial Mats. *Naturwissenschaften* **71,** 303-308.

Schouten, S., Hartgers, W. A., Lopez, J. F., Grimalt, J. O., and Sinninghe Damste, J. S. (2001). A molecular isotopic study of 13C-enriched organic matter in evaporitic deposits: recognition of CO2-limited ecosystems. *Organic Geochemistry* **32,** 277-286.

Schreck, C. J., and Semazzi, F. H. M. (2004). Variability of the recent climate of eastern Africa. *International Journal of Climatology* **24,** 681-701.

Schulz, H., von Rad, U., Erlenkeuser, H., and von Rad, U. (1998). Correlation between Arabian Sea and Greenland climate oscillations of the past 110,000 years. *Nature* **393,** 54-57.

Scott, L. (1999a). Palynological analysis of the Pretoria Saltpan (Tswaing crater) sediments and vegetation history in the Bushveld Savanna biome, South Africa. *In* Tswaing, investigations into the origin, age and palaeoenvironments of the Pretoria Saltpan. (T. C. Partridge, Ed.), pp. 143-166, Council of Geoscience (Geological Survey of South Africa), Pretoria.

Scott, L. (1999b). Vegetation history and climate in the Savanna biome South Africa since 190,000 ka: a comparison of pollen data from the Tswaing Crater (the Pretoria Saltpan) and Wonderkrater. *Quaternary International* **57-58,** 215-223.

Scott, L. (2002). Grassland development under glacial and interglacial conditions in southern Africa: review of pollen, phytolith and isotope evidence. *Palaeogeography, Palaeoclimatology, Palaeoecology* **177,** 47-57.

Scott, L., and Holmgren, K. (2003). Age interpretation of the Wonderkrater Spring sediments and vegetation change in the Savanna Biome, Limpopo province, South Africa. *South African Journal of Science* **99,** 484-488.

Scott, S. C., and Skilling, I. P. (1999). The role of tephrachronology in recognizing synchronous caldera-forming events at the Quaternary volcanoes Longonot and Suswa, south Kenya Rift. *In* Volcanoes in the Quaternary. (C. R. Firth, and W. J. McGuire, Eds.), pp. 47-67. Special Publications. Geological Society, London.

Shakun, J. D., Burns, S. J., Fleitmann, D., Kramers, J., Matter, A., and Al-Subary, A. (2007). A high-resolution, absolute-dated deglacial speleothem record of Indian Ocean climate from Socotra Island, Yemen. *Earth and Planetary Science Letters* **259,** 442–456.

Shiea, J., Brassel, S. C., and Ward, D. M. (1991). Comparative analysis of extractable lipids in hot spring microbial mats and their component photosynthetic bacteria. *Organic Geochemistry* **17,** 309-319.

Shiojima, K., and Ageta, H. (1990). Fern constituents: Two new triterpenoid hydrocarbons, hop-16-ene and isohop-22(29)-ene, isolated from *Davallia mariesii*. *Chemical and pharmaceutical Bulletin* **38**, 347-349.

Sifeddine, A., Bertrand, P., Lallier-Verges, E., and Patience, A. J. (1996). Lacustrine organic fluxes and palaeoclimatic variations during the last 15 ka: Lac du Bouchet (Massif Central, France). *Quaternary Science Reviews* **15,** 203.

Sinninghe Damsté, J. S., Rijpstra, W. I. C., Schouten, S., Fuerst, J. A., Jetten, M. S. M., and Strous, M. (2004). The occurrence of hopanoids in planctomycetes: Implications for the sedimentary biomarker record. *Organic Geochemistry* **35,** 561-566.

Spooner, N., Rieley, G., Collister, J. W., Lander, M., Cranwell, P. A., and Maxwell, J. R. (1994). Stable carbon isotopic correlation of individual biolipids in aquatic organisms and a lake bottom sediment. *Organic Geochemistry* **21,** 823-827.

Stager, J. C., Cumming, B. F., and Meeker, L. D. (2003). A 10,000-year high-resolution diatom record from Pilkington Bay, Lake Victoria, East Africa. *Quaternary Research* **59,** 172-181.

Stager, J. C., Mayewski, P. A., and Meeker, L. D. (2002). Cooling cycles, Heinrich event 1, and the desiccation of Lake Victoria. *Palaeogeography, Palaeoclimatology, Palaeoecology* **183,** 169-178.

Stauffer, R. E. (1987). A comparative analysis of iron, manganese, silica, phosphorus, and sulfur in the hypolimnia of calcareous lakes. *Water Research* **21,** 1009-1022.

Stern, J., Wang, Y., Gu, B., and Newman, J. (2007). Distribution and turnover of carbon in natural and constructed wetlands in the Florida Everglades. *Applied Geochemistry* **22,** 1936-1948.

Stokes, S., Haynes, G., Thomas, D. S. G., Horrocks, J. L., Higginson, M., and Malifa, M. (1998). Punctuated aridity in southern Africa during the last glacial cycle: The chronology of linear dune construction in the northeastern Kalahari. *Palaeogeography, Palaeoclimatology, Palaeoecology* **137,** 305-322.

Stokes, S., Thomas, D. S. G., and Washington, R. (1997). Multiple episodes of aridity in southern Africa since the last interglacial period. *Nature* **388,** 154.

Storzer, D., Koeberl, C., and Reimold, W. U. (1993). The age of the Pretoria Saltpan crater, South Africa. *Lunar and Planetary Science* **14,** 1365-1366.

Stott, L., Poulsen, C., Lund, S., and Thunell, R. (2002). Super ENSO and Global Climate Oscillations at Millennial Time Scales. *Science* **297,** 222-226.

Street-Perrott, F. A., Barker, P. A., Swain, D. L., Ficken, K. J., Wooller, M. J., Olago, D. O., and Huang, Y. (2007). Late Quaternary changes in ecosystems and carbon cycling on Mt. Kenya, East Africa: a landscape-ecological perspective based on multi-proxy lake-sediment influxes. *Quaternary Science Reviews* **26,** 1838–1860.

Street-Perrott, F. A., Ficken, K. J., Yongsong, H., and Eglinton, G. (2004). Late Quaternary changes in carbon cycling on Mt. Kenya, East Africa: an overview of the d13C record in lacustrine organic matter. *Quaternary Science Reviews* **23,** 861 - 879.

Stuut, J.-B. W., and Lamy, F. (2004). Climate variability at the southern boundaries of the Namib (southwestern Africa) and Atacama (northern Chile) coastal deserts during the last 120,000 yr. *Quaternary Research* **62,** 301-309.

Sun, Q., Chu, G., Liu, G., Li, S., and Wang, X. (2007). Calibration of alkenone unsaturation index with growth temperature for a lacustrine species, Chysotila lamellosa (Haptophyceae). *Organic Geochemistry* **38,** 1226-1234.

Talbot, M. R., and Kelts, K. (1986). Primary and diagenetic carbonates in the anoxic sediments of Lake Bosumtwi, Ghana. *Geology* **14,** 912-916.

Talbot, M. R., and Lærdal, T. (2000). The Late Pleistocene - Holocene palaeolimnology of Lake Victoria, East Africa, based upon elemental and isotopic analyses of sedimentary organic matter. *Journal of Paleolimnology* **23,** 141-164.

Talbot, M. R., Filippi, M. L., Jensen, N. B., and Tiercelin, J.-J. (2007). An abrupt change in the African monsoon at the end of the Younger Dryas. *Geochem. Geophys. Geosyst.* **8**.

Talling, J. F. (1966). The Annual Cycle of Stratification and Phytoplankton Growth in Lake Victoria (East Africa). *Internationale Revue der gesamten Hydrobiologie und Hydrographie* **51,** 545-621.

Talling, J. F. (1986). The seasonality of phytoplankton in African lakes. *Hydrobiologia* **138,** 139-160.

Talling, J. F., and Talling, I. B. (1965). The Chemical Compositions of African Lake Waters. *Internationale Revue der gesamten Hydrobiologie und Hydrographie* **50,** 421-463.

Talma, A. S., and Vogel, J. C. (1992). Late Quaternary paleotemperatures derived from a speleothem from Cango Caves, Cape Province, South Africa. *Quaternary Research* **37,** 203-213.

Taylor, G. H., Teichmüller, M., Davis, A., Diessel, C. F. K., Littke, R., and Robert, P. (1998). Organic Petrology. Borntraeger, Berlin, pp. 704.

Tchen, T. T., and Bloch, K. (1957). On the mechanism of enzymatic cyclization of squalene. *Journal of Biological Chemistry* **226,** 931-939.

Theissen, K. M., Zinniker, D. A., Moldowan, J. M., Dunbar, R. B., and Rowe, H. D. (2005). Pronounced occurrence of long-chain alkenones and dinosterol in a 25,000-year lipid molecular fossil record from Lake Titicaca, South America. *Geochimica et Cosmochimica Acta* **69,** 623-636.

Thiel, V., Jenisch, A., Landmann, G., Reimer, A., and Michaelis, W. (1997a). Unusual distributions of long-chain alkenones and tetrahymanol from the highly alkaline Lake Van, Turkey. *Geochimica et Cosmochimica Acta* **61,** 2053-2064.

Thiel, V., Merz-Preiß, M., Reitner, J., and Michaelis, W. (1997b). Biomarker studies on microbial carbonates: Extractable lipids of a Calcifying Cyanobacterial mat (Everglades, USA). *Facies* **36,** 163-172.

Thomas, D. S. G., and Shaw, P. A. (2002). Late Quaternary environmental change in central southern Africa: new data, synthesis, issues and prospects. *Quaternary Science Reviews* **21,** 783 - 797.

Thomas, D. S. G., Brook, G., Shaw, P., Bateman, M., Haberyan, K., Appleton, C., Nash, D., McLaren, S., and Davies, F. (2003). Late Pleistocene wetting and drying in the NW Kalahari: an integrated study from the Tsodilo Hills, Botswana. *Quaternary International* **104,** 53-67.

Thompson, L. G., Mosley-Thompson, E., Davis, M. E., Henderson, K. A., Brecher, H. H., Zagorodnov, V. S., Mashiotta, T. A., Lin, P.-N., Mikhalenko, V. N., Hardy, D. R., and Beer, J. (2002). Kilimanjaro Ice Core Records: Evidence of Holocene Climate Change in Tropical Africa. *Science* **298,** 589-593.

Thorpe, J. L. (2006). Records of late Quaternary climatic change from Tswaing crater lake, South Africa, and the Central Kenya Rift. PhD thesis, University College London, pp.396.

Tiercelin, J. J., Gibert, E., Umer, M., Bonnefille, R., Disnar, J. R., Lezine, A. M., Hureau-Mazaudier, D., Travi, Y., Keravis, D., and Lamb, H. F. (2008). High-resolution sedimentary record of the last deglaciation from a high-altitude lake in Ethiopia. *Quaternary Science Reviews* **27,** 449-467.

Tierney, J. E., and Russell, J. M. (2007). Abrupt climate change in southeast tropical Africa influenced by Indian monsoon variability and ITCZ migration. *Geophysical Research Letters* **34,** doi:10.1029/2007GL029508.

Tierney, J. E., Russell, J. M., Huang, Y., Damste, J. S. S., Hopmans, E. C., and Cohen, A. S. (2008). Northern Hemisphere Controls on Tropical Southeast African Climate During the Past 60,000 Years. *Science* **322,** 252-255.

Tissot, B. P., and Welte, D. H. (1984). Petroleum formation and occurrence. Springer-Verlag, Berlin, pp.699.

Tissot, B. P., Pelet, R., and Ungerer, Ph. (1987). Thermal History of Sedimentary Basins, Maturation Indices, and Kinetics of Oil and Gas Generation. *AAPG Bulletin* **71**, 1445-1466.

Tjallingii, R., Claussen, M., Stuut, J.-B. W., Fohlmeister, J., Jahn, A., Bickert, T., Lamy, F., and Rohl, U. (2008). Coherent high- and low-latitude control of the northwest African hydrological balance. *Nature Geoscience* **1,** 670-675.

Tjallingii, R., Röhl, U., Kölling, M., and Bickert, T. (2007). Influence of the water content on X-ray fluorescence core scanning measurements in soft marine sediments. *Geochemistry, Geophysics, Geosystems* **8**, Q02004, doi:10.1029/2006GC001393.

Tornabene, T. G., Langworthy, T. A., Holzer, G., and Oró, J. (1979). Squalenes, phytanes and other isoprenoids as major neutral lipids of methanogenic and thermoacidophilic "archaebacteria". *Journal of Molecular Evolution* **13,** 73-83.

Tulloch, A. (1976). Chemistry of waxes of higher plants. *In* Chemistry and Biochemistry of Natural Waxes. (P. E. Kolattukudy, Ed.), pp. 201-235. Elsevier, Amsterdam.

Tyson, P. D. (1986). Climatic Change and Variability in Southern Africa. Oxford University Press, Oxford, pp. 220.

Tyson, P. D. (1999). Late-Quaternary and Holocene palaeoclimates of southern Africa: A synthesis. *South African Journal of Geology* **102,** 335-349.

Tyson, P. D., and Preston-Whyte, R. A. (2000). The weather and climate of southern Africa. Oxford University Press Southern Africa, Cape Town, pp. 396.

Uemura, H., and Ishiwatari, R. (1995). Identification of unusual 17β(H)-moret-22(29)-ene in lake sediments. *Organic Geochemistry* **23**, 675-680.

Verschuren, D., Laird, K. R., and Cumming, B. F. (2000). Rainfall and drought in equatorial east Africa during the past 1,100 years. *Nature* **403,** 410.

Verschuren, D., Sinninghe Damsté, J. S., Moernaut, J., Kristen, I., Blaauw, M., Fagot, M., Haug, G. H. & CHALLACEA project members (submitted): Half-precessional dynamics of monsoon rainfall near the East African equator. *Nature*.

Vinther, B. M., Clausen, H. B., Johnsen, S. J., Rasmussen, S. O., Andersen, K. K., Buchardt, S. L., Dahl-Jensen, D., Seierstad, I. K., Siggaard-Andersen, M.-L., Steffensen, J. P., Svensson, A. M., Olsen, J., and Heinemeier, J. (2006). A synchronized dating of three Greenland ice cores throughout the Holocene. *Journal of Geophysical Research* **111,** doi:10.1029/2005JD006921.

Volkman, J. K. (1986). A review of sterol markers for marine and terrigenous organic matter. *Organic Geochemistry* **9,** 83-99.

Volkman, J. K. (2003). Sterols in microorganisms. *Applied Microbiology and Biotechnology* **60,** 495-506.

Volkman, J. K. (2005). Sterols and other triterpenoids: source specificity and evolution of biosynthetic pathways. *Organic Geochemistry* **36,** 139-159.

Volkman, J. K., Barrett, S. M., and Blackburn, S. I. (1999). Eustigmatophyte microalgae are potential sources of C29 sterols, C22-C28 n-alcohols and C28-C32 n-alkyl diols in freshwater environments. *Organic Geochemistry* **30,** 307-318.

Volkman, J. K., Burton, H. R., Everitt, D. A., and Allen, D. I. (1988). Pigment and lipid compositions of algal and bacterial communities in Ace Lake, Vestfold Hills, Antarctica. *Hydrobiologia* **165,** 41-57.

Walker, M. J. C., Björck, S., Lowe, J. J., Cwynar, L. C., Johnsen, S., Knudsen, K.-L., Wohlfarth, B., and group, I. (1999). Isotopic 'events' in the GRIP ice core: a stratotype for the Late Pleistocene. *Quaternary Science Reviews* **18,** 1143-1150.

Wang, G., Wang, T. G., Simoneit, B. R. T., Chen, Z., Zhang, L., and Xu, J. (2008). The distribution of molecular fossils derived from dinoflagellates in Paleogene lacustrine sediments (Bohai Bay Basin, China). *Organic Geochemistry* **39,** 1512-1521.

Wang, X., Auler, A. S., Edwards, R. L., Cheng, H., Cristalli, P. S., Smart, P. L., Richards, D. A., and Shen, C.-C. (2004). Wet periods in northeastern Brazil over the past 210 kyr linked to distant climate anomalies. *Nature* **432,** 740-743.

Wang, X., Auler, A. S., R. L. Edwards, Cheng, H., Ito, E., Wang, Y., Kong, X., and Solheid, M. (2007). Millennial-scale precipitation changes in southern Brazil over the past 90,000 years. *Geophysical Research Letters* **34,** doi:10.1029/2007GL031149.

Wang, X.-C., Chen, R. F., and Berry, A. (2003). Sources and preservation of organic matter in Plum Island salt marsh sediments (MA, USA): long-chain *n*-alkanes and stable carbon isotope compositions. *Estuarine, Coastal and Shelf Science* **58,** 917-928.

Wang, Y. J., Cheng, H., Edwards, R. L., An, Z. S., Wu, J. Y., Shen, C. C., and Dorale, J. A. (2001). A High-Resolution Absolute-Dated Late Pleistocene Monsoon Record from Hulu Cave, China. *Science* **294,** 2345-2348.

Wang, Y., Cheng, H., Edwards, R. L., He, Y., Kong, X., An, Z., Wu, J., Kelly, M. J., Dykoski, C. A., and Li, X. (2005). The Holocene Asian Monsoon: Links to Solar Changes and North Atlantic Climate. *Science* **308,** 854-857.

Washington, R., and Preston, A. (2006). Extreme wet years over southern Africa: Role of Indian Ocean sea surface temperatures. *Journal of Geophysical Research* **111,** doi:10.1029/2005JD006724.

Webster, P. J., Moore, A. M., Loschnigg, J. P., and Leben, R. R. (1999). Coupled ocean-atmosphere dynamics in the Indian Ocean during 1997-98. *Nature* **401,** 356-360.

Weldeab, S., Lea, D. W., Schneider, R. R., and Andersen, N. (2007). 155,000 Years of West African Monsoon and Ocean Thermal Evolution. *Science* **316,** 1303-1307.

Weldeab, S., Schneider, R. R., Kolling, M., and Wefer, G. (2005). Holocene African droughts relate to eastern equatorial Atlantic cooling. *Geology* **33,** 981-984.

Wersin, P., Höhener, P., Giovanoli, R., and Stumm, W. (1991). Early diagenetic influences on iron transformations in a freshwater lake sediment. *Chemical Geology* **90,** 233-252.

Wetzel, R. G. (1983). Limnology. Saunders College Publishing, New York, pp.767.

Whiticar, M. J., Faber, E., and Schoell, M. (1986). Biogenic methane formation in marine and freshwater environments: CO_2 reduction vs. acetate fermentation - Isotope evidence. *Geochimica et Cosmochimica Acta* **50,** 693-709.

Widgren, M. (2004). Towards a Historical Geography of Intensive Farming in Eastern Africa. *In* Islands of Intensive Agriculture in Eastern Africa. (M. Widgren, and J. E. G. Sutton, Eds.), pp. 1-18. James Currey Ltd, Oxford.

Wilkinson, P., Mitchell, J. G., Cattermole, P. J., and Downie, C. (1986). Volcanic chronology of the Meru-Kilimanjaro region, Northern Tanzania. *Journal of the Geological Society* **143,** 601-605.

Williams, L. A. J. (1970). Geochemistry and Petrogenesis of Kilimanjaro Volcanic Rocks of the Amboseli Area, Kenya. *Bulletin of Volcanology***,** 862-888.

Williams, M., Talbot, M., Aharon, P., Abdl Salaam, Y., Williams, F., and Inge Brendeland, K. (2006). Abrupt return of the summer monsoon 15,000 years ago: new supporting evidence from the lower White Nile valley and Lake Albert. *Quaternary Science Reviews* **25,** 2651.

Williamson, D., Jelinowska, A., Kissel, C., Tucholka, P., Gibert, E., Gasse, F., Massault, M., Taieb, M., Van Campo, E., and Wieckowski, K. (1998). Mineral-magnetic proxies of erosion/oxidation cycles in tropical maar-lake sediments (Lake Tritrivakely, Madagascar): paleoenvironmental implications. *Earth and Planetary Science Letters* **155,** 205-219.

Wooller, M. J., Swain, D. L., Ficken, K. J., Agnew, A. D. Q., Street-Perrott, F. A., and Eglinton, G. (2003). Late Quaternary vegetation changes around Lake Rutundu, Mount Kenya, East Africa: evidence from grass cuticles, pollen and stable carbon isotopes. *Journal of Quaternary Science* **18,** 3-15.

Wooller, M. J., Zazula, G. D., Edwards, M., Froese, D. G., Boone, R. D., Parker, C., and Bennett, B. (2007). Stable Carbon Isotope Compositions of Eastern Beringian Grasses and Sedges: Investigating Their Potential as Paleoenvironmental Indicators. *Arctic, Antarctic and Alpine Research* **39,** 318-331.

Xu, Y., and Jaffé, R. (2008). Biomarker-based paleo-record of environmental change for an eutrophic, tropical freshwater lake, Lake Valencia, Venezuela. *Journal of Paleolimnology* **40,** 179-194.

Yancheva, G., Nowaczyk, N. R., Mingram, J., Dulski, P., Schettler, G., Negendank, J. F. W., Liu, J., Sigman, D. M., Peterson, L. C., and Haug, G. H. (2007). Influence of the intertropical convergence zone on the East Asian monsoon. *Nature* **445,** 74-77.

Yuan, D., Cheng, H., Edwards, R. L., Dykoski, C. A., Kelly, M. J., Zhang, M., Qing, J., Lin, Y., Wang, Y., Wu, J., Dorale, J. A., An, Z., and Cai, Y. (2004). Timing, Duration, and Transitions of the Last Interglacial Asian Monsoon. *Science* **304,** 575-578.

Zachos, J., Pagani, M., Sloan, L., Thomas, E., and Billups, K. (2001). Trends, Rhythms, and Aberrations in Global Climate 65 Ma to Present. *Science* **292,** 686-693.

Zhang, R., and Delworth, T. L. (2005). Simulated Tropical Response to a Substantial Weakening of the Atlantic Thermohaline Circulation. *Journal of Climate* **18,** 1853-1860.

Zink, K.-G., Leythaeuser, D., Melkonian, M., and Schwark, L. (2001). Temperature dependency of long-chain alkenone distributions in Recent to fossil limnic sediments and in lake waters. *Geochimica et Cosmochimica Acta* **65,** 253-265.

Appendix A

Pilot study on the organic fraction of sediments from Lake Tswaing

INTRODUCTION

Within this section I will report on data which were not included in the two manuscripts about the studies on sediments from Lake Tswaing. They are, nevertheless, seen as an important part of this thesis, extending the studies on the nature of the organic matter described in chapter 3 and forming the basis for the detailed biomarker and stable carbon isotope study of chapter 4. Here I will present results from an initial screening of the complete composite profile (90 m uncorrected, 78 m corrected composite depth) for the biomarker composition of the bulk organic matter (OM). Main parts of this data report are documentations of identified and quantified biomarker compounds (see also App. B to H), chromatograms of selected samples and mass spectra of the most important compounds.

MATERIAL AND METHODS

The following section focuses on the detailed methodology of the biomarker analyses because of differences in the GC-MS settings in comparison to chapter 4. For a description of the study location, general lithology of the sediments, the age model and details about Rock-Eval pyrolysis the reader is referred to chapter 3.

Biomarker analyses

For biomarker analyses, the 90 m long sequence of lacustrine sediments was sampled in 21 intervals in a way to cover the maximum range of variability in TOC contents and lithology (Fig. A.1). From theses samples, 8 to 15 g of freeze-dried sediment were ground and extracted by flow-blending (Radke et al. 1978) using a mixture of dichloromethane and methanol (99/1, v/v) as a solvent. The extracts were separated by medium-pressure liquid chromatography (Radke et al. 1980) into fractions of aliphatic/alicyclic hydrocarbons, aromatic hydrocarbons and nitrogen, sulphur and oxygen (NSO) compounds. Further separation of the NSO compounds into a neutral NSO and a more polar fatty acid fraction was achieved following a modified method of McCarthy and Duthie (1962). Trimethylsilylation of the neutral fraction of NSO compounds was done with MSTFA (N-Methyl-N-(trimethylsilyl)trifluoroacetamide). Identification and quantification of individual compounds within the aliphatic fraction was

achieved using gas chromatography (GC) (for details on this technique see chapter 4) and gas chromatography-mass spectrometry (GC-MS), within the alcohol fraction GC-MS was used for identification and quantification. The MS-coupled GC "Agilent 6890" uses a Gerstel PTV injection system and a fused silica capillary column SGE BPX5 (50 m length, 0.22 mm ID, 0.25 µm FT). Helium was used as a carrier gas, and the temperature of the GC oven was programmed from 50 °C (1 min) to 310 °C at a rate of 3 °C/min, followed by an isothermal phase of 30 min. The injector temperature was programmed from 52 to 300 °C at a rate of 12 °C/sec. A MAT95XL mass spectrometer, operating in the electron impact ionisation mode (45 eV), was used for compound identification. Full scan mass spectra were recorded from *m/z* 50 to 600 (aliphatic hydrocarbons) or 650 (alcohols) at a scan rate of 1 scan/decade. Compound identifications are based on relative retention times, comparison of mass spectra to those reported in the literature, in the NIST mass spectral database, and on comparison with authentic standards.

RESULTS AND DISCUSSION

The amount of total extracted lipids varies in accordance with TOC and HI of the investigated samples (Fig. A.1), underlining the results from Rock-Eval pyrolysis and from organic petrology presented in more detail in chapter 3, which point to a noticeably higher autochthonous OM contribution to TOC-rich samples (Fig. A.1). This observation is supported by the biomarker analyses of the hydrocarbon and the neutral fraction of the lipids extracted from the sediments from Lake Tswaing as elaborated in the following.

Biomarker analyses show for samples with low TOC a higher relative contribution of odd-numbered long-chain *n*-alkanes ($nC_{25\text{-}33}$) and even-numbered long-chain *n*-alcohols ($nC_{26\text{-}32}$) which are characteristic for allochthonous input of land-plant OM (Eglinton and Hamilton 1963; Meyers 2003; Tulloch 1976) (Fig. A.2 and A.3). In TOC-rich samples, these compounds are also present but accompanied by autochthonous compounds such as specific steroidal alcohols (Fig. A.2). Below 60 m depth and between 35 and 20 m depth, TOC-rich samples are characterised by relatively high concentrations of dinosterol and isoarborinol. Dinosterol is known to be the dominant sterol in many dinoflagellates (Volkman 2003) and is frequently reported from lake sediments (e.g. Hanisch et al. 2003; Theissen et al. 2005; Xu and Jaffé 2008). It is sometimes (Hanisch et al. 2003) but not always (Xu and Jaffé 2008) associated with the occurrence of isoarborinol which is generally considered to be related to autochthonous productivity (Jaffé and Hausmann 1995; Xu and Jaffé 2008). Changes in biomarker concentrations over the profile allow the reconstruction of changes in autochthonous lake productivity. As the lake evolved over time, the microbial community of Lake Tswaing which included dinoflagellates, diatoms (identified in thin sections) and probably other algae was replaced by a community dominated by bacteria. This is indicated by decreasing isoarborinol

and dinosterol concentrations and increasing concentrations of tetrahymanol, its diagenetic product gammaceran-3-one (Thiel et al. 1997a) and moretene above 30 m depth (Fig. A.2) (Blumenberg et al. 2009; Hanisch et al. 2003; Kleemann et al. 1990; Uemura and Ishiwatari 1995) (for detailed argumentation about the bacterial sources for tetrahymanol and moretene see chapter 4). The especially low concentrations of steroidal alcohols between 60 and 40 m depth (samples 12, 14, 15, 16, 17 in Fig. A.2, and A.5 c) support results from Rock-Eval pyrolysis and organic petrology which indicate oxidation of OM (compare chapter 3) as these compounds are structurally altered during early diagenesis (Rullkötter 1992). The concomitant detection of the short-chain *n*-octadecanol (Fig. A.3) in these samples first appears contradictory as short-chain *n*-alkanols are often associated with autochthonous primary productivity (Volkman et al. 1999), and are reported to be preferentially biodegraded (Robinson et al. 1984). However, this compound is also detected in bacterial biomass (Albro 1976; Shiea et al. 1991) and may actually underscore the microbial influence on oxidation of the OM of sediments between 60 and 40 m depth. The absence of the – for primary OM characteristic – odd-over-even distribution in the *n*-alkanes can further suggest oxidation of primary OM in these samples (Fig. A.3). However, it can also be related to the presence of eroded, geologically older OM (Rullkötter 1992) which is supported by the observation of 'humps' within GC and GC-MS chromatograms of these samples (samples 12, 14, 15,16, 17, see Fig. A.4 c for one example).

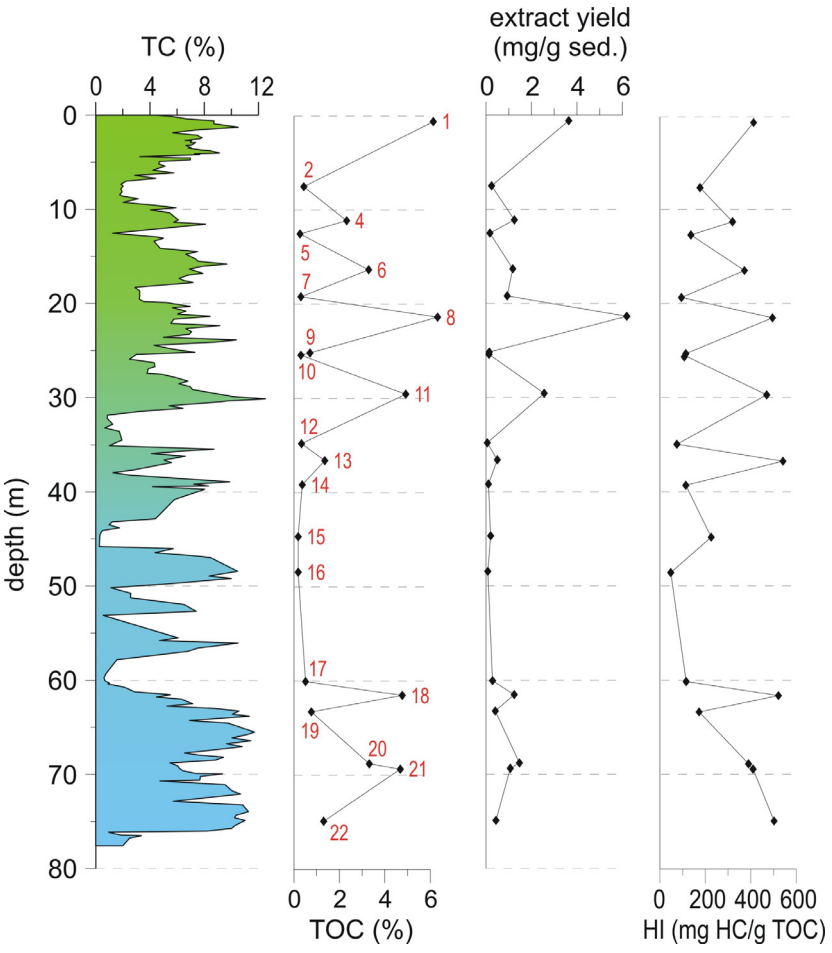

Figure A.1: Downcore profiles of total carbon (TC), TOC content, extract yields, hydrogen index (HI; higher values indicate higher amounts of hydrogen-enriched (autochthonous) OM, for detailed explanation see chapter 3); red numbers indicate sample no.; sampling occurred at minimal/ maximal TC concentrations, underlying colours indicate transition from deeper sediments, where major changes occur in total inorganic carbon (blue), to upper sediments, dominated by changes in organic carbon (green).

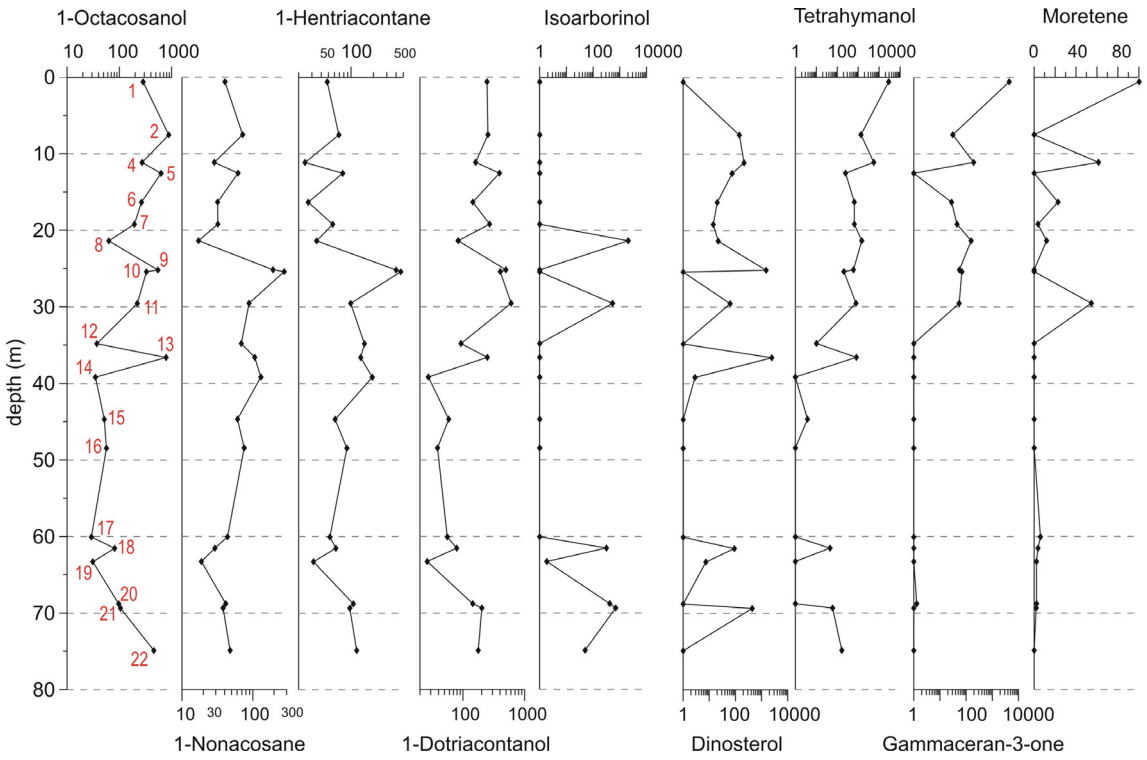

Figure A.2: Downcore profiles of selected biomarker concentrations (as µg/g TOC); red numbers indicate sample no.

The sediment samples from the Lake Tswaing profile contain besides many known biomarkers a suite of uncommon and also unknown compounds (pers. comm. Philippe Schaeffer, 2007); their analysis is beyond the scope of this study. Exemplary, I report here on the tentative identification of one norcholestene (Fig. A.4 f), one norcholestenol and two norcholestanol compounds (Fig. A.7 and App. C) from the extracted lipids of sample G002427(11); no norcholestane could be detected. Norcholesterols are rarely described from microorganisms, although they seem to be common in higher organisms (Volkman 2003). Norcholestadienols have been identified in few marine dinoflagellates (Goad and Withers 1982) and diatom species (Rampen et al. 2007). (Rampen et al. 2007) report on especially high concentrations of 24-norcholesta-5,22-dien-3β-ol in one polar marine diatom species and minor concentrations in dinoflagellates grown at temperatures of at least 15°C. Therefore, the latter group is a likely producer of norcholesterols in sediments from Lake Tswaing. This conclusion agrees with the observed co-occurrence of 24-norcholestane with fossils of dinoflagellates and dinocysts in tertiary lacustrine sediments from China (Wang et al. 2008). Norcholestanes are assumed to be diagenetically produced from norcholesterols. In sediments from Lake Tswaing diagenesis was obviously not strong enough to produce norcholestanes (as is to be expected for the relatively immature sediments from Lake Tswaing, see chapter 3); but early diagenesis might be responsible for the observed norcholestanols and norcholestene, although these compounds have to date not been reported from modern or ancient sediment samples, and their origin has to remain speculative.

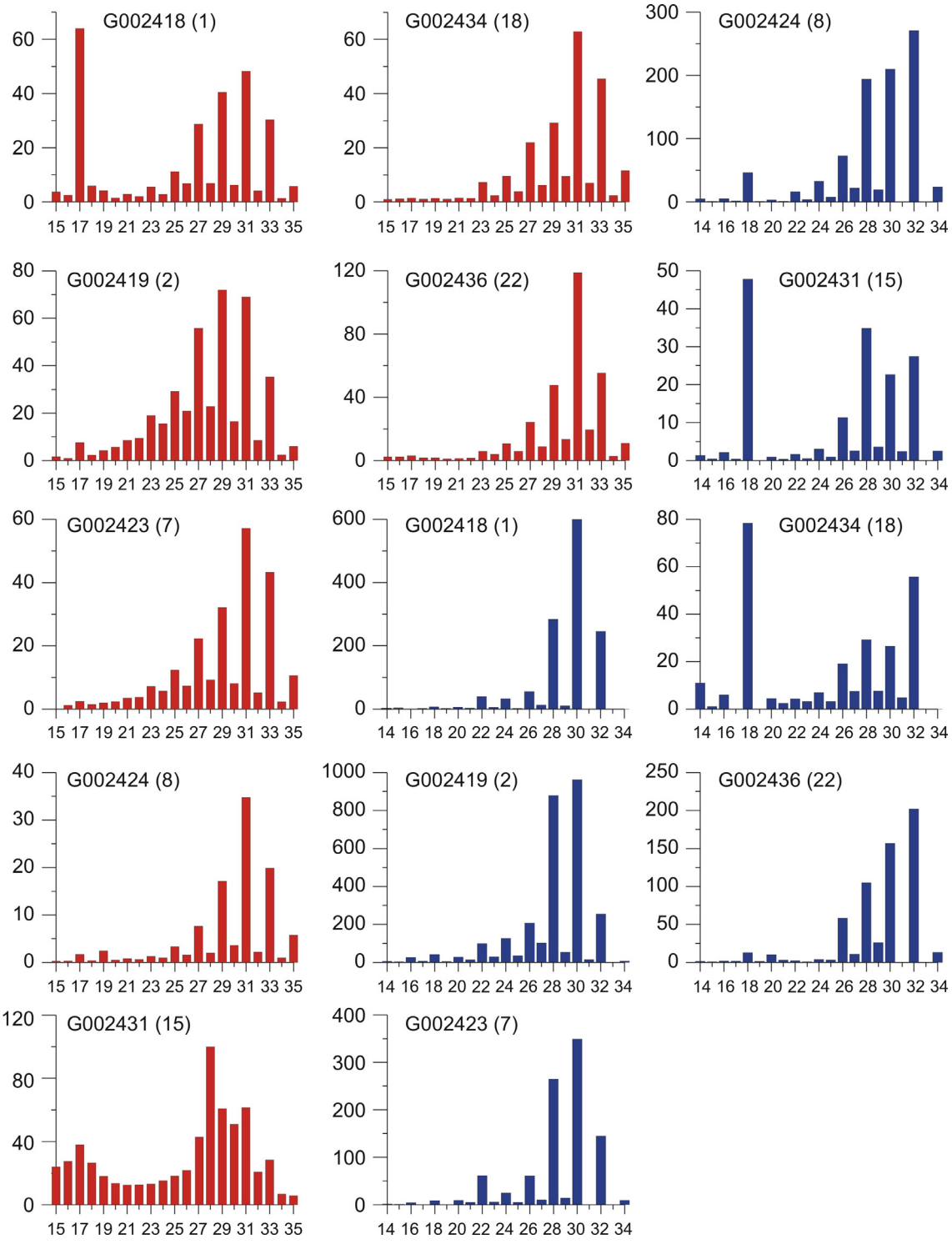

Figure A.3: *N*-alkane (red) and *n*-alkohol (blue) distribution of selected samples from the sediment profile from Lake Tswaing (x-axis indicates chain-length of *n*-alkanes/*n*-alkanols, y-axis indicates concentrations in µg/g TOC, 'G' refers to lab no., numbers in brackets indicate sample no., for quantification of all samples see App. D and E).

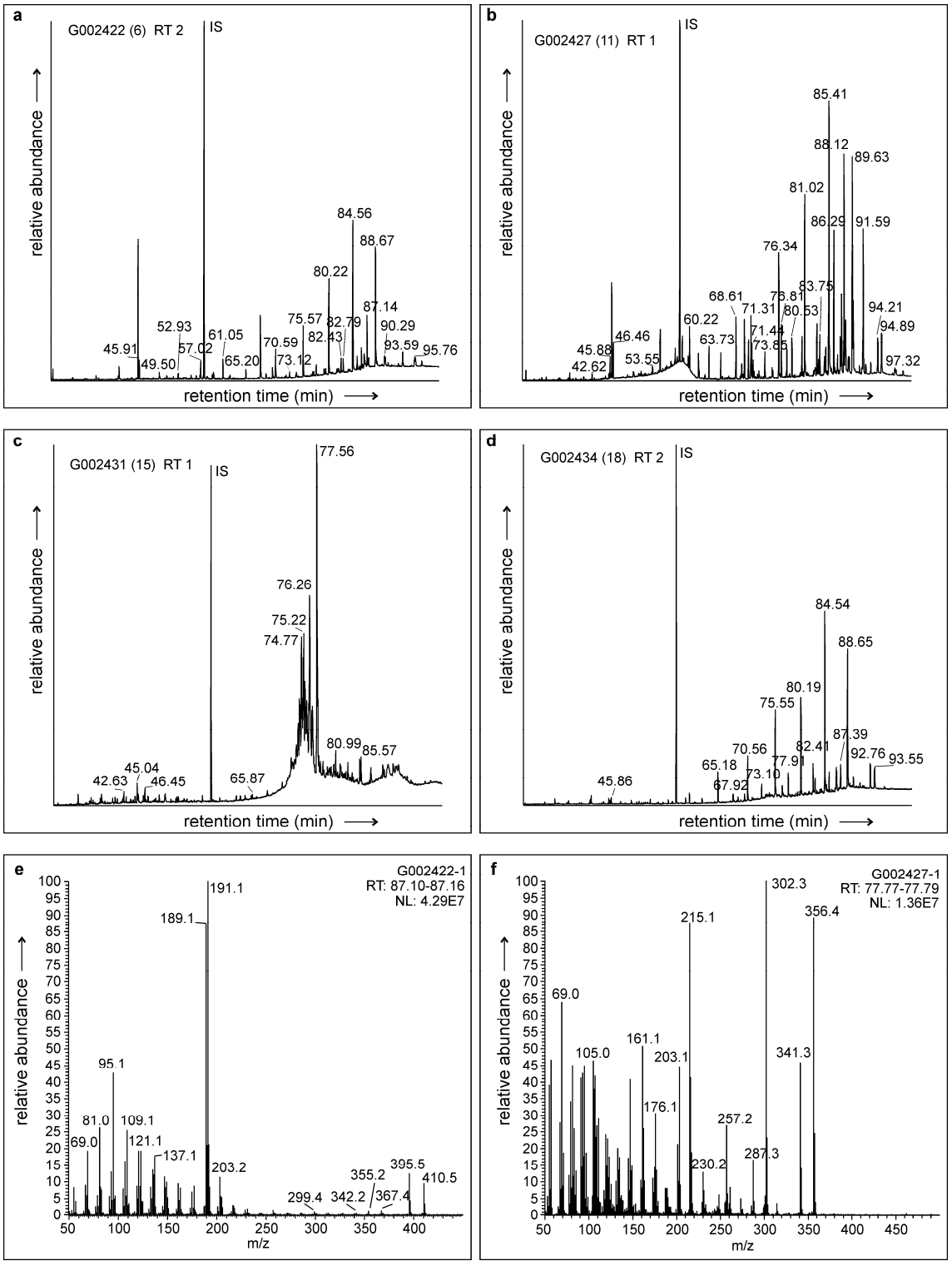

Figure A.4: a) – d) Exemplary TIC chromatograms of the aliphatic hydrocarbon fraction from the sediment profile of Lake Tswaing ('G' indicates lab no., sample no. in brackets, RT refers to column indicating the retention time of different sample runs in App. B, for attribution of compounds to respective retention times see also App. B, for quantification see App. D); e) mass spectrum of moretene, f) mass spectrum of 2-norcholestene detected in the aliphatic hydrocarbon fraction of sample G002427.

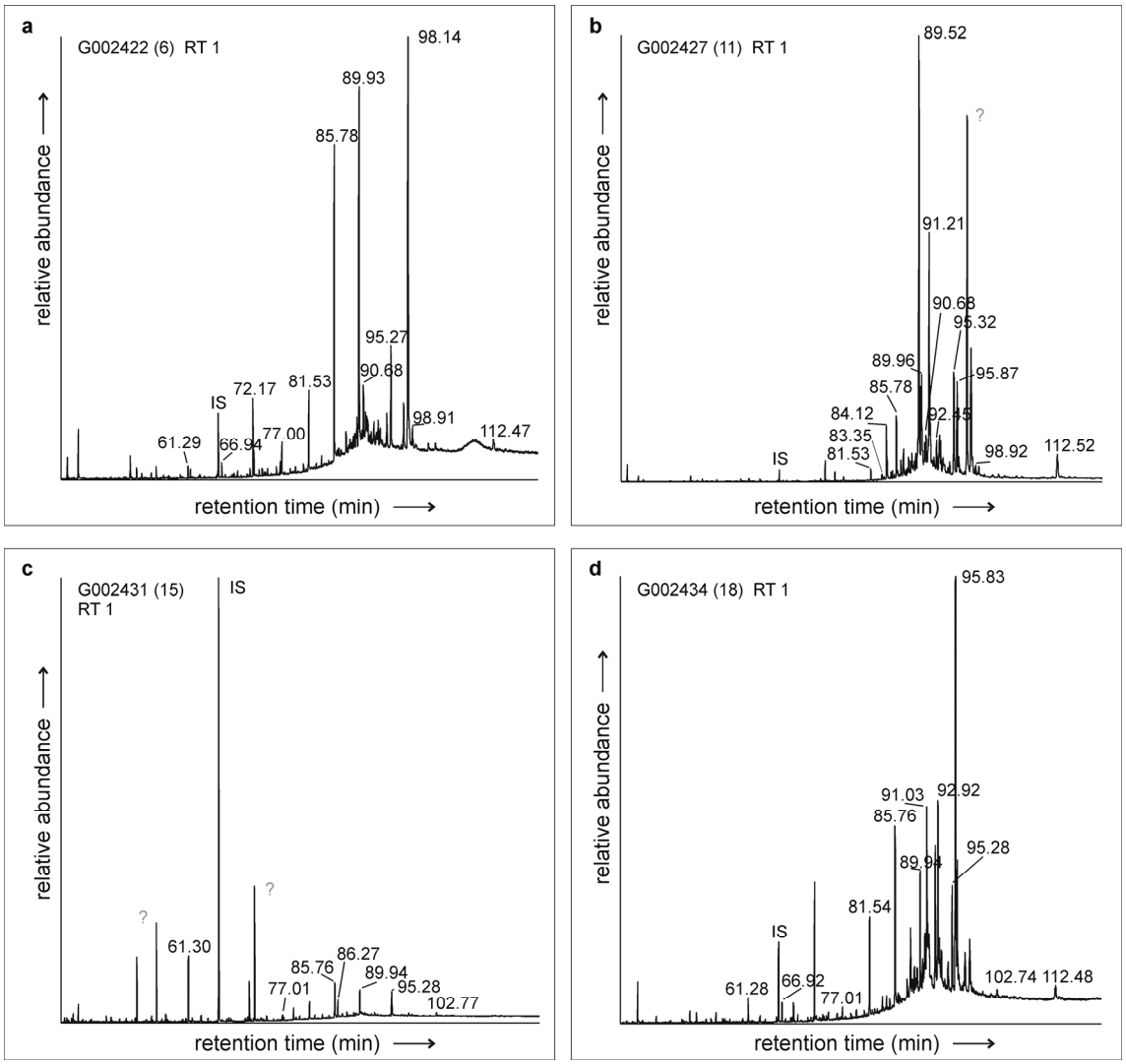

Figure A.5: a) – d) Exemplary TIC chromatograms of the neutral fraction of samples from the sediment profile from Lake Tswaing ('G' indicates lab no., sample no. in brackets, RT refers to retention time of sample runs indicated in App. C, for attribution of compounds to respective retention times see also App. C, for quantification see App. E).

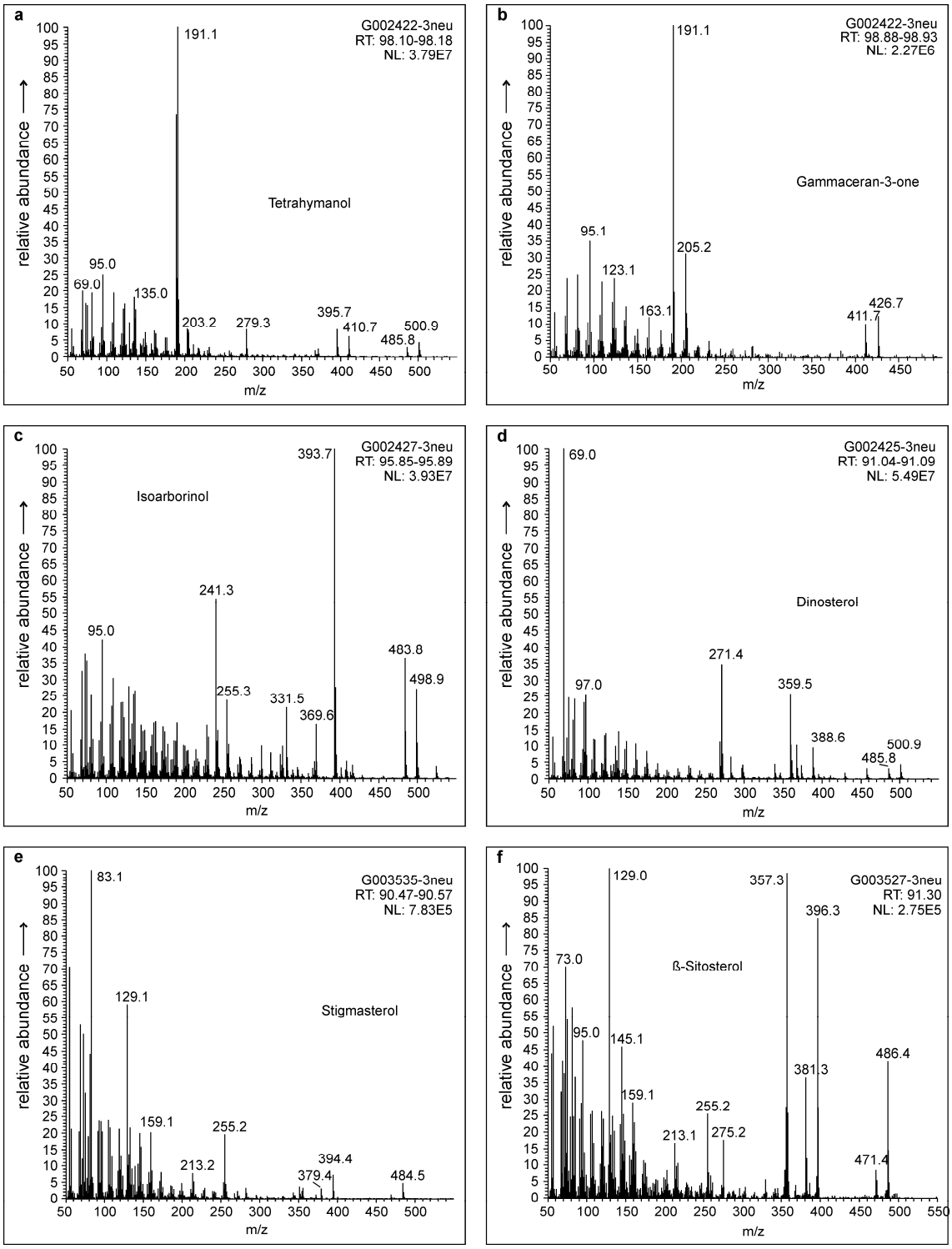

Figure A.6: a) – j) Mass spectra of major steroidal and terpenoidal neutral compounds from samples of the sediment profile from Lake Tswaing ('G' indicates lab no., RT refers to retention time of sample runs indicated in App. C, for information about sources and structures of the compounds refer to chapter 4 and App. H, for quantifications see App. E and G).

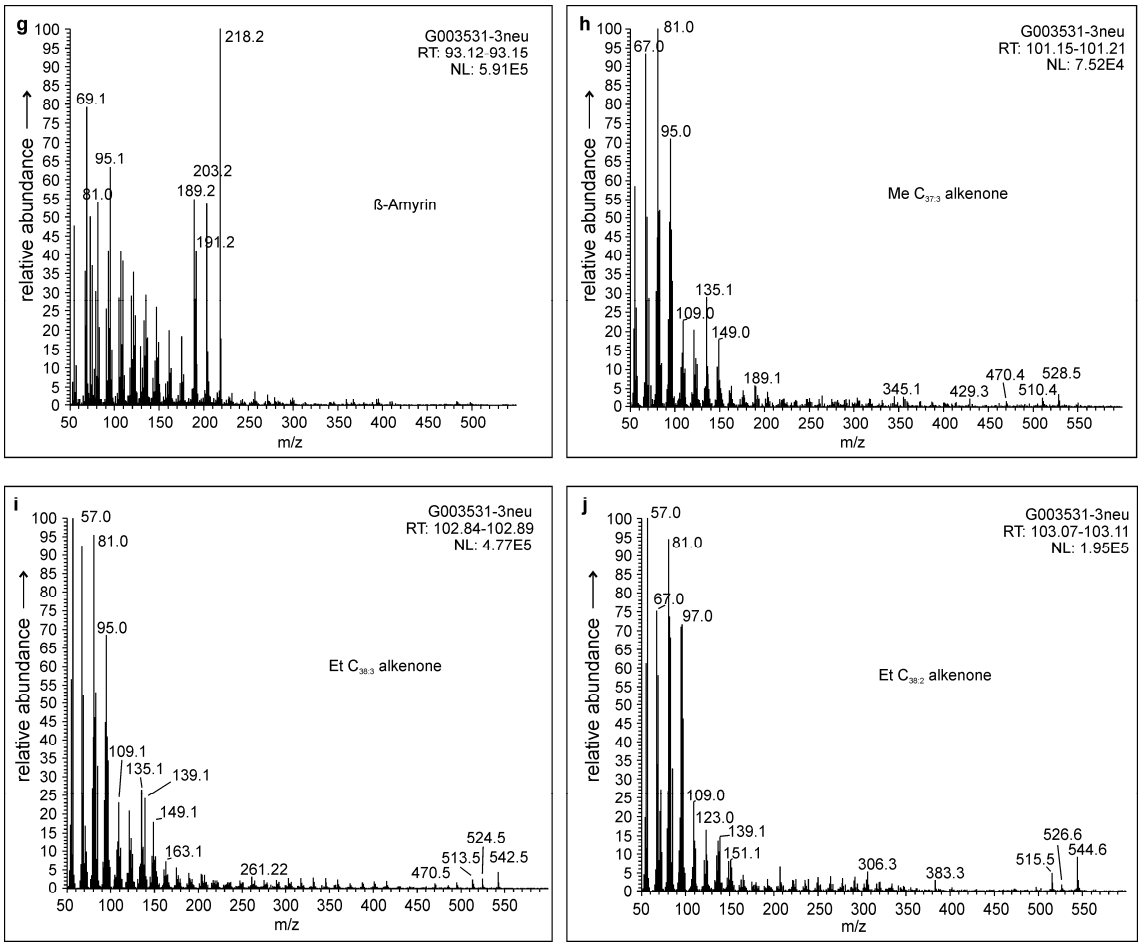

Figure A.6: continuation.

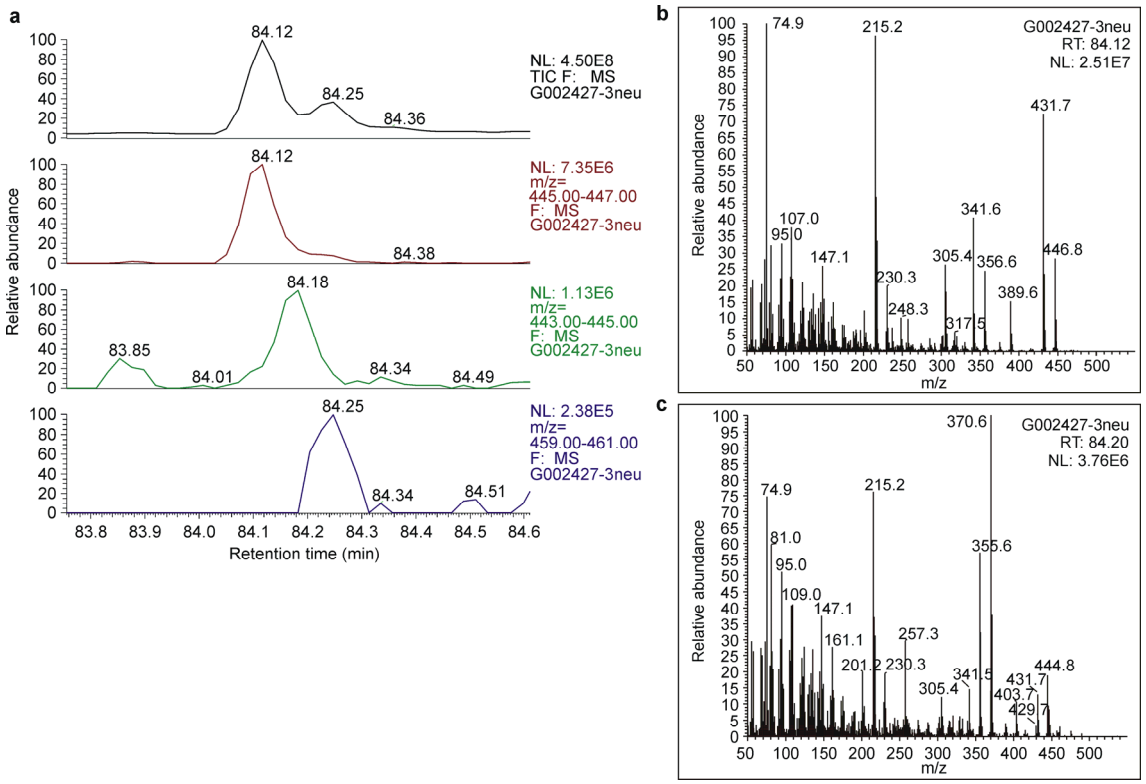

Figure A.7: a) Partial TIC chromatogram of the neutral fraction of sample G002427 with selected mass ranges 446 (red), 444 (green) and 460 (blue), indicating the subsequent elution of a norcholestanol (84.12) and a norcholestenol (84.18) before 5β-Cholestan-3β-ol (84.25); b) mass spectrum of the norcholestanol (84.12); c) mass spectrum of the tentatively identified norcholestenol (84.18).

App. B: Identification of aliphatic hydrocarbons in samples from the sediment profile from Lake Tswaing (M^+=molecular mass, RT=retention time, RT 1 and RT 2 refer to measurements of the initial sample set G002418 - G002438, RT 3 to the high-resolution sample set of manuscript 2: G003524 - G003537).

Compound	Formula	M^+	Fragments	RT 1 Mar 05	RT 2 Nov 05	RT 3 Jun 07
2,6,10-Trimethyltridecane	$C_{16}H_{34}$	226	183, 141, 113	36.81	36.32	
Branched alkane				37.07	36.53	
prob. branched Alkene		210	155, 125		37.80	
n-Pentadecane	$C_{15}H_{32}$	212	57, 71, 85	38.60	38.07	39.89
n-Hexadecane	$C_{16}H_{34}$	226	57, 71, 85	42.65	42.08	43.90
Branched Alkene	$C_{16}H_{32}$	224	196		44.40	
Branched Alkane		240	225, 197, 155	45.03	44.50	46.29
Branched Alkane			196, 168, 139	45.88	45.42	
n-Heptadecane	$C_{17}H_{36}$	240	57, 71, 85	46.57	45.91	47.67
prob. branched Alkane		282	267, 57		46.43	
prob. branched Alkane		268	225, 210, 195		48.44	
n-Octadecane	$C_{18}H_{38}$	254	57, 71, 85	50.10	49.50	51.28
Phytane (2,6,10,14-Tetramethylhexadecane)	$C_{20}H_{42}$	282	267, 197, 183	50.23	49.65	51.42
Phytene	$C_{20}H_{40}$	280	210, 196, 140	51.00	50.42	
Phytene	$C_{20}H_{40}$	280	210, 196, 140	51.04	50.46	
Phytene	$C_{20}H_{40}$	280	210, 196, 140	51.51	50.91	
prob. branched Alkane		356	239, 155		51.45	
4-Methyloktadecane	$C_{19}H_{40}$	268	253, 225, 85	52.28	51.66	
prob. Phytene	$C_{20}H_{40}$	282	267		51.84	
n-Nonadecane	$C_{19}H_{40}$	268	57, 71, 85	53.57	52.91	54.71
n-Icosane	$C_{20}H_{42}$	282	57, 71, 85	56.88	56.21	57.98
prob. branched Alkane		282	250, 235, 179, 97		56.92	
unknown compound			228, 131, 66	58.00	57.02	
a-Androstane (IS)	$C_{19}H_{32}$	260	245, 217, 203	58.60	57.61	59.75
Branched Alkene			69, 97		59.10	
n-Henicosane	$C_{21}H_{44}$	296	57, 71, 85	60.01	59.34	61.10
Tetracyclic Alkane	$C_{20}H_{34}$	274	259, 123	60.22		
2,6,10,14,18-Pentamethylnonadecane	$C_{24}H_{50}$	338	253, 225, 183	60.71	60.09	
Tetracyclic Alkane	$C_{21}H_{36}$	288	273, 245, 191	61.86	61.05	63.13
Tetracyclic Alkane	$C_{21}H_{36}$	288	273, 259, 135	61.94	61.17	
Tetracyclic Alkane	$C_{21}H_{36}$	288	273, 192,177		62.21	
n-Docosane	$C_{22}H_{46}$	310	57, 71, 85	63.01	62.33	64.08
Cyclic Alkane			201, 135, 134, 69		62.86	
Branched Alkane			57, 71, 85	63.73	63.09	
n-Tricosane	$C_{23}H_{48}$	324	57, 71, 85	65.91	65.20	66.96
Monounsaturated tetracyclic alkane	$C_{24}H_{40}$	328	313, 218, 203	68.27	67.45	
Monounsaturated tetracyclic alkane		328	313, 189, 177	68.46	67.64	
n-Tetracosane	$C_{24}H_{50}$	338	57, 71, 85	68.65	67.95	69.73
Monounsaturated tetracyclic alkane	$C_{24}H_{40}$	328	313, 205, 136	69.42	68.62	
Diunsaturated tetracyclic alkane	$C_{24}H_{38}$	326	311, 108, 95	69.57	68.75	
Diunsaturated tetracyclic alkane	$C_{24}H_{38}$	326	311, 204, 189	69.68	68.82	
Tetracyclic Alkane	$C_{24}H_{42}$	330	315, 287, 123	70.14	69.33	
Diunsaturated tetracyclic alkane	$C_{24}H_{38}$	326	311, 108, 95	70.87	70.02	72.19
n-Pentacosane	$C_{25}H_{52}$	352	57, 71, 85	71.34	70.59	72.38
Monounsaturated tetracyclic alkane	$C_{24}H_{40}$	328	313, 273, 136,95	71.44		72.77
Branched alkane			57, 71, 85	71.74	71.10	
unknown compound		342	149, 167, 279		71.70	
Branched Alkane			351, 323	72.91	72.17	
Branched Alkane			337, 71, 57	73.17	72.44	
Monounsaturated tetracyclic alkane	$C_{25}H_{42}$	342	327	73.82	72.97	
n-Hexacosane	$C_{26}H_{54}$	366	57, 71, 85	73.87	73.13	74.93
Diunsaturated tetracyclic alkane		326	311, 219, 173	74.78	73.84	
Branched Alkane				74.96	74.28	
Monounsaturated tetracyclic alkane	$C_{24}H_{40}$	328	313, 191, 95	75.28	74.36	76.62

Compound	Formula	M^+	Fragments	RT 1 Mar 05	RT 2 Nov 05	RT 3 Jun 07
Branched Alkane			337, 365	75.41	74.66	
Monounsaturated tetracyclic alkane	$C_{24}H_{40}$	328	313, 191, 95	75.55	74.66	76.90
n-Heptacosane	$C_{27}H_{56}$	380	57, 71, 85	76.38	75.57	77.24
unknown compound			69	76.81	76.13	
Branched Alkane			57, 71, 85	77.07	76.30	
Branched Alkane			57, 71, 85	77.26	76.49	
Branched Alkane			337, 379	77.47	76.72	
prob. Branched Alkane			281, 299, 252		76.80	
2-Norcholestene	$C_{26}H_{44}$	356	341, 302, 215	77.79	76.91	
Branched Alkane			57, 71, 85, 351	77.81	77.04	
Branched Alkane			57, 71, 85, 365	78.07	77.30	
Diunsaturated tetracyclic alkane	$C_{27}H_{44}$	368	352, 247, 145	78.58	77.70	
n-Octacosane	$C_{28}H_{58}$	394	57, 71, 85	78.73	77.94	79.82
unknown compound			69,81		78.30	
unknown compound			127, 140, 85		79.37	
x-Cholestene	$C_{27}H_{46}$	370	355, 257, 215	80.19	79.32	
2-Cholestene	$C_{27}H_{46}$	370	355, 316, 215	80.56	79.64	81.93
n-Nonacosane	$C_{29}H_{60}$	408	57, 71, 85	81.09	80.24	82.15
Trinorhopene	$C_{27}H_{44}$	368	353, 231, 191	82.62	81.69	
Diunsaturated tetracyclic alkane (steradiene)	$C_{28}H_{46}$	382	367, 298, 255	82.82	81.88	
24-Methyl-2-cholestene	$C_{28}H_{48}$	384	369, 330, 215, 145	82.94	82.07	
n-Triacontane	$C_{30}H_{62}$	422	57, 71, 85	83.24	82.43	84.39
22,29,30-Trinorhopane	$C_{27}H_{46}$	370	355, 191, 149	83.75	82.80	85.28
Triterpene	$C_{30}H_{52}$	412	397	84.60	83.71	
24-Ethyl-2-cholestene	$C_{29}H_{50}$	398	383, 344, 215	84.81	83.95	
n-Hentriacontane	$C_{31}H_{64}$	436	57, 71, 85	85.46	84.58	86.56
prob. Norhopane	$C_{29}H_{50}$	398	383, 191, 177		84.62	
Monounsaturated pentacyclic triterpene	$C_{30}H_{50}$	410	395, 367, 231	86.29	85.35	87.80
Monounsaturated pentacyclic triterpene	$C_{29}H_{50}$	398	383, 191, 177	86.75	85.82	
Triterpene		412	397,191,95		86.40	
n-Dotriacontane	$C_{32}H_{66}$	450	57, 71, 85	87.46	86.63	88.68
Moretene (17β(H)-moret-22(29)-ene)	$C_{30}H_{50}$	410	395, 367, 299, 203, 191, 189	88.25	87.16	89.90
x-Hopene	$C_{30}H_{50}$	410	395, 367, 191		87.40	
30-Norhopane	$C_{29}H_{50}$	398	383, 369, 191, 177	88.42	87.40	90.15
n-Tritriacontane	$C_{33}H_{68}$	464	57, 71, 85	89.65	88.69	91.03
Monounsaturated pentacyclic triterpene	$C_{30}H_{50}$	410	395, 243, 191	89.80	88.97	91.68
Diploptene (Hop-22(29)-ene)	$C_{30}H_{50}$	410	395, 299, 191, 189	91.59	90.33	93.68
Monounsaturated pentacyclic triterpene	$C_{30}H_{50}$	410	395, 367, 191, 189, 173	91.67	90.46	
n-Tetratriacontane	$C_{34}H_{70}$	478	57, 71, 85	92.04	90.95	
Pentacyclic triterpane	$C_{31}H_{54}$	426	369, 205, 191	94.21	92.81	
n-Pentatriacontane	$C_{35}H_{72}$	492	57, 71, 85	94.91	93.59	

App. C.1: Identification of (other than steroidal) neutral compounds in samples from the sediment profile from Lake Tswaing (TMS M+=molecular mass of the silylated compound, RT=retention time, RT 1 refers to measurements of the initial sample set G002418-G002438, RT 2 and 3 to the high-resolution sample set of manuscript 2: G003524-G003537).

Compound	TMS M+	Fragments	RT 1 May 05	RT 2 Jun 07	RT 3 Nov 07
1-Pentadecanol	300	285, 75	51.84		
1-Hexadecanol	314	299, 75	55.13	56.52	56.29
1-Heptadecanol (coelution)	328	313, 75	58.28	59.63	59.41
3,7,11,15-Tetramethyl-hexadecanol (Phytanol)		57, 355, 97, 125		61.39	61.16
1-Octadecanol	342	327, 75	61.28	62.63	62.40
3,7,11,15-Tetramethyl-hexadecenol (Phytol)		143,73	61.71	63.06	62.83
1-Nonadecanol	356	341, 75	64.16	65.48	
Androstanone (IS)	274		66.35	67.86	67.64
1-Icosanol	370	355, 75	66.94	68.24	68.01
4,8,12,16-Tetramethyl-heptadecan-4-olide (γ-lactone)	324	99, 114, 126, 151, 196, 254		68.83	68.62
1-Henicosanol	384	369, 75	69.61	70.89	70.66
1-Docosanol	398	383, 75	72.17	73.45	73.20
1-Tricosanol	412	397, 75	74.62	75.88	75.64
1-Tetracosanol	426	411, 75	77.01	78.25	78.01
1-Pentacosanol	440	425, 75	79.31	80.52	80.29
1-Hexacosanol	454	439, 75	81.54	82.76	82.50
1-Heptacosanol	468	453, 75	83.68	84.87	84.63
1-Octacosanol	482	467, 75	85.78	87.03	86.72
1-Nonacosanol	496	481, 75	87.80	89.10	88.72
1-Triacontanol	510	495, 75	89.94	91.56	90.72
1-Hentriacontanol	524	509, 75	92.39	93.97	92.68
1-Dotriacontanol	538	523, 75	95.28	97.34	94.48
1-Tritriacontanol	552	537, 75	98.69		
Gammacer-3-one	426	411, 205, 191	98.96	101.80	97.25
1-Tetratriacontanol	566	551, 75	102.74	105.64	98.10
1-Pentatriacontanol	580	565, 75	107.69		
Heptatriacontatrien-2-one (Me $C_{37:3}$ Alkenone)	528	67, 81, 95, 135, 149, 510			101.14
not identified		57, 71, 81, 97, 130, 147, 278, 369, 412, 426, 579		118.20	101.51
ßß-Dihomohopan-32-ol	528	191, 217, 307, 369, 513	112.52	116.95	102.44
probably ester		57, 69, 83, 97, 229, 257, 285, 550, 564			102.53
Octatriacontatrien-3-one (Et $C_{38:3}$ Alkenone)	542	57, 67, 81, 95, 135, 524		122.40	102.88
Octatriacontadien-3-one (Et $C_{38:3}$ Alkenone)	544	57, 67, 81, 95, 96, 109, 137, 292, 515		123.60	103.10
not identified		57, 71, 85, 130, 135, 149, 278, 369, 412, 426, 482, 496		118.07	110.15
1-Hexatriacontanol	594	579, 75	113.60	118.20	

App. C.2: Identification of steroidal neutral compounds in samples from the sediment profile from Lake Tswaing (TMS M^+= molecular mass of the silylated compound, RT=retention time, RT 1 refers to measurements of the initial sample set G002418-G002438, RT 2 and 3 to the high-resolution sample set of manuscript 2: G003524-G003537).

Steroidal alkohol	C no.	TMS M+	base peak	Fragments	RT 1 May 05	RT 2 Jun 07	RT 3 Nov 07
Cholestanol	C27	460		370, 355, 316, 215	80.30		
Norcholestanol	C26	446		431, 389, 356, 341, 305, 215, 75	83.35		
Norcholestanol	C26	446		431, 389, 356, 341, 305, 215, 75	84.12		
Norcholestenol (?) (partial coelution with neighbouring compounds)	C26	444		429, 370, 356, 215, 75	84.18		
5ß-Cholestan-3ß-ol	C27	460		370, 355, 257, 215	84.25	85.64	85.41
Cholestanol	C27	460		370, 355, 329,215	84.69	86.02	85.80
5ß-Cholestan-3a-ol	C27	460		370, 355, 257, 215		86.21	85.96
Cholest-5-en-3b-ol	C27	458	329	443, 368, 353, 129	86.28	87.65	86.94
5a(H)-Cholestan-3b-ol	C27	460	215	445, 403, 370, 355, 305	86.54	87.90	87.68
24-Methylcholestanol 5ß 3ß	C28	474		459, 369, 215	86.90		
Cholesta-dienol	C29	484		394, 379, 343, 318, 255, 229, 213, 83		88.56	88.34
24-Methyl-Cholesta-5,22-dienol (Brassicasterol)	C28	470	129	470, 455, 386, 380, 296, 253			89.02
C29 Stanol	C29	488		398, 383, 215, 257		89.69	89.35
24-Methylcholest-5-en-3b-ol	C28	472	343	457, 382, 367	88.25	89.96	89.65
24Methyl-5ß(H)-cholestan-3a-ol	C28	474	345	459, 384, 369	88.36	89.85	
24-Methyl-5a(H)-cholestan-3b-ol	C28	474	215	459, 417, 384, 369	88.73	90.28	
Stigmasterol (24-Ethylcholesta-5,22-dien-3ß-ol)	C29	484		394, 255, 129, 83		90.55	89.68
C29 Stenol (Coelution)	C29	486	69	471, 359, 353, 345, 271, 257	89.25	90.86	90.34
C29 Stenol	C29	486	135	471, 412, 396, 381, 353	89.47	91.08	
Dimethylcholest-5-en-3b-ol	C29	486		471, 283	89.50		
24-Methyl-Cholest-7-en-3ß-ol	C28	472		472, 457, 377, 351, 255			90.97
24-Ethyl-Cholesta-5,7,22-trien-3ß-ol	C29	482	377	83, 131, 211, 253, 351, 377, 392			91.05
Ergost-7ene-3ßol (24-Methyl-cholest-7-enol) (coelution)	C28	472	75	255,367,357		91.60	
ß-Sitosterol (24-Ethylcholest-5-en-3ß-ol)	C29	486	129	471, 396, 381, 357, 255, 129	90.35	92.08	91.35
24-Ethylcholesta-7,22-dien-3ß-ol (Stigmast-7,22-dien-3ß-ol)	C29	484		484, 469, 396, 343, 255	90.49	92.20	91.46
24-Ethylcholestan-5a(H)-3b-ol	C29	488	215	473, 431, 398, 383	90.67	92.44	91.56
4,24-Dimethylcholestanol	C29	488		473, 398, 359, 75, 271	90.75	92.48	
unsaturated Dinosterol	C30	498	69	368, 269, 139, 69		92.70	
Dinosterol (4,23,24-Trimethyl-5a(H)-cholest-22-en-3b-ol)	C30	500	69	388, 359, 271	91.06	92.89	
ß-Amyrine (Olean-12en-3ß-ol)	C30	500	218	189, 191, 203, 95, 69	91.23	93.06	92.17
17a-hopanol or Lupenol?	C30			410, 395, 191	91.27	93.15	92.14
C30 Stenol	C30	500	359	485, 271	91.33		
24-Ethyl-4-methylcholestenol	C30	500		367, 271	91.34		
17α-Hopanol or Lupenol?	C30		189	410, 395, 367, 341, 189, 191, 121, 69	91.42	93.31	
Germanicol (Olean-18-en-3ß-ol)	C30	498	189	498, 483, 408, 393, 279, 231, 204, 189, 177			92.36
24-Ethyl-Cholest-7-en-3ß-ol	C29	486	255	255, 485, 75, 213, 147, 269, 381		93.90	92.67
4,24-Dimethyl-Cholest-5-en-3ß-ol	C29	486	269	75, 95, 147, 161, 227, 255, 269, 381, 396, 471			92.88
a-Amyrin (Urs-12en-3ß-ol) + Lupeol (Lup-20(29)en-3ß-ol) (coelution)	C30	498	218	483, 189, 369, 393	92.46	94.48	93.04
a-Amyrin (Urs-12en-3ß-ol) + Lupeol (Lup-20(29)en-3ß-ol) (coelution)	C30			412, 397, 191	92.47		
4,23,24-Trimethylcholestanol	C30	502	373	487, 412, 397	92.93		
C30 Stenol	C30	500	189	485, 457, 410, 395, 371	93.15		
24-Methyl-Cycloartenol		422		422, 407, 379, 353, 73		95.91	94.00
Isoarborinol	C30	498	393	483, 241	95.87		
Tetrahymanol	C30	500	191	485, 410, 395, 279, 189	98.15	101.00	96.70
Diplopterol (17ß-21ß-Hopan-22-ol)	C30	500	131	191, 189, 485, 410, 395			96.73

App. D: Quantification of aliphatic hydrocarbons (µg/g TOC) and selected basic information on samples from the initial pilot study on the 90 m sediment profile from Lake Tswaing.

Depth (m)	2.2	9.56	13.22	14.62	18.49	21.36	24.16	28.05	28.29	32.45	39.14	40.95	43.52
Corr. depth (m)	0.6	7.52	11.13	12.53	16.33	19.2	21.36	25.165	25.405	29.545	34.795	36.605	39.175
Weighted sample (g)	4.5	10.01	5.01	10.1	4.89	6	5.03	10	10	5.02	10.05	5	8.08
Extract (mg/g Sed)	3.64	0.25	1.25	0.18	1.18	0.93	6.19	0.15	0.13	2.56	0.06	0.50	0.11
Compound / Sample	**1 G002418**	**2 G002419**	**4 G002420**	**5 G002421**	**6 G002422**	**7 G002423**	**8 G002424**	**9 G002425**	**10 G002426**	**11 G002427**	**12 G002428**	**13 G002429**	**14 G002430**
n **C_{15}**	3.69	1.68	0.69	2.46	1.41	0.00	0.28	5.97	6.44	3.16	0.00	0.00	0.00
n **C_{16}**	2.51	0.95	0.61	2.89	0.62	1.19	0.32	6.80	10.70	2.56	2.74	0.89	0.00
n **C_{17}**	64.01	7.61	5.95	8.18	3.93	2.48	1.71	10.40	155.54	10.14	6.22	3.67	5.85
n **C_{18}**	5.93	2.35	0.62	5.07	1.66	1.46	0.36	7.77	59.34	2.17	5.41	3.09	12.90
n **C_{19}**	4.15	4.29	1.31	10.28	2.00	1.98	2.42	8.40	91.11	3.37	5.04	5.57	22.95
n **C_{20}**	1.47	5.69	0.62	15.49	1.07	2.37	0.46	6.59	103.02	1.53	4.44	5.04	26.81
n **C_{21}**	2.93	8.51	1.36	29.46	2.55	3.50	0.78	9.67	155.64	3.18	5.38	10.71	29.06
n **C_{22}**	2.00	9.44	1.13	39.13	1.78	3.76	0.63	10.36	167.95	1.66	6.52	13.76	34.30
n **C_{23}**	5.46	19.06	4.51	54.47	4.61	7.17	1.29	25.19	206.51	8.57	9.47	31.16	43.29
n **C_{24}**	2.86	15.57	1.90	39.57	2.22	5.77	0.92	16.50	169.24	5.08	10.77	19.50	48.40
n **C_{25}**	11.27	29.11	8.29	53.30	8.71	12.34	3.31	53.88	228.88	21.62	18.33	48.30	59.51
n **C_{26}**	6.85	20.86	3.85	29.67	4.79	7.33	1.53	27.23	128.05	8.03	16.21	20.87	58.62
n **C_{27}**	28.71	55.77	17.69	62.22	22.49	22.28	7.60	110.37	250.11	51.16	34.68	77.84	80.61
n **C_{28}**	6.93	22.83	3.93	31.48	5.26	9.23	2.02	47.07	136.70	19.72	34.99	25.16	71.47
n **C_{29}**	40.49	71.92	28.62	61.91	31.84	32.10	17.11	192.43	277.57	88.59	68.77	106.54	129.96
n **C_{30}**	6.26	16.45	1.37	18.08	4.47	8.12	3.58	44.57	96.30	4.85	34.99	17.57	77.20
n **C_{31}**	48.15	68.96	24.27	77.52	26.82	57.16	34.76	400.01	461.94	98.94	151.16	134.85	192.38
n **C_{32}**	4.10	8.50	7.17	9.74	2.97	5.15	2.16	33.63	48.21	13.86	23.67	9.96	49.21
n **C_{33}**	30.32	35.21	22.47	49.77	29.60	43.24	19.88	276.22	257.18	147.39	100.90	62.96	105.03
n **C_{34}**	1.32	2.40	0.88	3.51	1.23	2.28	0.94	11.79	15.10	5.82	7.51	2.94	21.30
n **C_{35}**	5.78	5.93	4.69	10.51	6.57	10.61	5.72	56.76	54.88	32.18	29.05	12.60	27.87
S *n*-alkanes	290.80	417.62	142.43	616.33	166.96	240.14	107.92	1365.20	3086.93	535.70	579.57	614.28	1102.82
Phytane	5.60	4.53	0.50	1.61	0.35	0.62	0.16	3.59	6.52	2.12	3.31	1.30	6.09
Moretene	100.34	0.00	61.53	0.00	22.81	3.64	11.79	0.00	0.00	54.64	0.00	0.00	0.00

Depth (m)	51.93	55.91	67.94	69.5	71.475	81.27	81.86	87.53
Corr. depth (m)	44.675	48.435	60.055	61.535	63.27	68.785	69.355	74.885
Weighted sample (g)	7	9.01	4.4	5	5	5	5.05	5.07
Extract (mg/g Sed)	0.21	0.08	0.29	1.24	0.41	1.47	1.07	0.44
Compound / Sample	**15 G002431**	**16 G002432**	**17 G002433**	**18 G002434**	**19 G002435**	**20 G002436**	**21 G002437**	**22 G002438**
n C_{15}	24.02	20.91	4.34	1.01	4.91	1.16	1.10	2.27
n C_{16}	27.42	21.25	6.87	1.16	3.60	1.17	0.90	2.40
n C_{17}	37.81	20.69	9.01	1.42	3.29	1.64	1.41	3.16
n C_{18}	26.60	14.35	5.88	1.07	2.15	1.17	0.96	1.77
n C_{19}	18.04	14.04	6.52	1.39	1.79	1.72	1.91	1.83
n C_{20}	13.47	12.37	5.26	1.07	1.38	1.00	0.96	1.14
n C_{21}	12.53	11.46	4.91	1.51	1.50	1.93	1.46	1.27
n C_{22}	12.75	14.15	5.95	1.40	2.11	1.40	1.26	1.52
n C_{23}	13.23	15.24	9.17	7.33	2.69	11.12	7.94	5.86
n C_{24}	15.22	15.26	6.05	2.45	2.31	2.76	2.25	3.95
n C_{25}	18.24	19.30	9.52	9.58	4.08	13.20	8.90	10.77
n C_{26}	21.80	20.66	9.69	3.85	4.19	4.54	3.88	5.87
n C_{27}	42.86	41.75	19.30	21.93	14.76	25.17	19.12	24.32
n C_{28}	99.71	40.98	21.27	6.16	5.09	5.65	5.77	8.74
n C_{29}	60.84	75.55	43.98	29.20	18.80	41.53	38.08	47.78
n C_{30}	50.88	51.76	38.67	9.46	8.38	9.75	9.36	13.55
n C_{31}	61.37	88.01	52.27	62.84	31.53	107.47	96.35	118.91
n C_{32}	20.81	29.39	18.30	7.00	4.50	8.44	8.05	19.52
n C_{33}	28.36	43.02	29.17	45.48	18.02	59.64	54.73	55.36
n C_{34}	6.70	7.29	3.68	2.42	1.22	2.38	2.43	2.85
n C_{35}	5.72	7.18	6.65	11.63	3.23	13.19	12.30	10.93
S *n*-alkanes	637.61	595.39	321.95	229.73	141.56	316.73	279.54	344.91
Phytane	19.22	10.79	5.47	0.38	2.05	0.71	0.43	1.17
Moretene	0.00	0.00	5.98	3.63	2.19	2.30	1.92	0.00

App. E: Quantification of neutral (steroidal and *n*-alcohol) compounds (µg/g TOC) from samples from the initial pilot study on the 90 m sediment profile from Lake Tswaing.

Compound / Sample	1 G002418	2 G002419	4 G002420	5 G002421	6 G002422	7 G002423	8 G002424	9 G002425	10 G002426	11 G002427	12 G002428
1-Hexadecanol	4	26	5	28	4	5	2	2	19	2	2
1-Heptadecanol	2	6	1	6	0	1	1	0	12	1	0
1-Octadecanol	7	41	13	51	9	46	6	17	80	8	30
1-Nonadecanol	2	5	1	1	0	1	1	0	14	1	0
1-Icosanol	6	27	24	13	9	3	3	6	52	4	1
1-Henicosanol	3	13	7	16	5	1	1	2	41	1	0
1-Docosanol	39	98	81	99	61	16	3	28	202	3	2
1-Tricosanol	5	29	4	54	6	4	1	8	69	0	1
1-Tetracosanol	33	126	40	111	25	33	11	53	157	10	5
1-Pentacosanol	1	36	6	45	5	7	2	15	61	3	3
1-Hexacosanol	55	207	71	192	61	73	23	219	110	36	18
1-Heptacosanol	13	102	16	77	10	22	4	36	101	9	6
1-Octacosanol	284	880	272	627	265	194	63	546	329	220	37
1-Nonacosanol	10	53	30	56	14	19	0	42	44	74	6
Dimethylcholest-5-en-3b-ol	44	0	0	0	0	0	1347	0	0	2132	0
1-Triacontanol	600	962	482	699	349	210	108	347	243	324	34
Dinosterol	0	140	212	74	20	14	22	1476	0	62	0
1-Hentriacontanol	0	15	0	9	0	0	0	65	60	0	7
a-Amyrin(Urs-12en-3b-ol)+ Lupeol (Lup-20(29)en-3b-ol)	176	8	55	0	37	126	85	0	0	187	0
4,23,24-Trimethylcholestanol	0	0	11	0	0	17	34	85	0	157	0
1-Dotriacontanol	245	254	161	391	145	271	84	498	403	603	93
Isoarborinol	0	0	0	0	0	0	2065	0	0	534	0
Tetrahymanol	28658	1355	5583	248	653	656	1479	594	207	783	10
1-Tritriacontanol	0	0	0	0	0	0	0	0	0	0	2
Gammaceran-3-one	4427	31	194	0	28	45	155	55	69	54	0
1-Tetratriacontanol	0	7	5	17	9	23	0	52	52	18	8

Compound / Sample	13 G002429	14 G002430	15 G002431	16 G002432	17 G002433	18 G002434	19 G002435	20 G002436	21 G002437	22 G002438
1-Hexadecanol	6	2	11	4	6	1	5	1	2	4
1-Heptadecanol	1	0	0	1	0	1	1	2	2	1
1-Octadecanol	25	48	95	105	78	10	73	22	13	36
1-Nonadecanol	1	0	0	0	0	1	0	1	1	1
1-Icosanol	19	1	2	2	4	8	2	10	10	5
1-Henicosanol	11	0	1	0	2	3	0	3	3	1
1-Docosanol	136	2	0	4	4	2	2	2	2	4
1-Tricosanol	57	0	1	1	3	3	0	1	1	2
1-Tetracosanol	186	3	10	8	7	5	3	4	4	5
1-Pentacosanol	41	1	3	2	3	4	1	3	3	6
1-Hexacosanol	240	11	25	31	19	44	12	46	58	95
1-Heptacosanol	75	3	6	7	7	6	3	10	11	42
1-Octacosanol	782	35	51	57	29	82	31	97	105	456
1-Nonacosanol	69	4	7	7	8	9	5	11	26	31
Dimethylcholest-5-en-3β-ol	0	0	0	0	0	0	0	0	0	0
1-Triacontanol	1007	23	46	39	27	67	24	98	157	210
Dinosterol	2437	3	0	0	0	91	7	0	435	0
1-Hentriacontanol	0	2	6	4	5	0	0	0	0	28
α-Amyrin(Urs-12en-3β-ol)+ Lupeol (Lup-20(29)en-3β-ol)	0	0	0	0	0	119	25	0	158	0
4,23,24-Trimethylcholestanol	10440	7	0	0	0	118	14	61	154	49
1-Dotriacontanol	248	27	59	39	56	79	26	144	202	177
Isoarborinol	0	0	0	0	0	315	2	416	694	50
Tetrahymanol	816	0	4	0	0	45	0	0	59	165
1-Tritriacontanol	0	0	0	0	0	0	0	5	0	0
Gammaceran-3-one	0	0	0	0	0	0	0	1	0	0
1-Tetratriacontanol	118	3	12	2	0	4	1	12	13	5

App. F: Quantification of aliphatic hydrocarbons (µg/g TOC) and some basic information on samples from the high-resolution study section of manuscript 2.

Depth (m)	3.91	4.10	4.29	4.51	4.76	5.09	5.29	5.58	5.77	5.96	6.11	6.30	6.50
Corr. depth (m)	2.31	2.50	2.69	2.91	3.16	3.49	3.69	4.01	4.20	4.39	4.53	4.72	4.92
Est. age (yr BP)	4666	5046	5502	6005	6758	7518	8153	9318	10122	10926	11328	12132	12936
TOC (%)	6.0	5.6	5.5	5.5	5.2	3.1	2.3	6.3	3.3	0.8	2.8	0.8	0.5
Weighted sample (g)	7.3	7.5	7.9	7.7	8.0	10.0	10.0	8.0	10.0	15.0	10.0	15.0	10.0
Compound / Sample	**G003536**	**G003535**	**G003534**	**G003533**	**G003532**	**G003531**	**G003530**	**G003529**	**G003528**	**G003527**	**G003526**	**G003525**	**G003524**
$n\,C_{15}$	7	9	22	16	6	3	4	3	15	4	6	3	3
$n\,C_{16}$	1	3	3	4	2	1	2	1	4	3	4	2	3
$n\,C_{17}$	38	62	98	94	45	16	16	9	93	8	27	6	6
$n\,C_{18}$	3	6	11	7	7	5	4	2	5	3	6	4	4
$n\,C_{19}$	2	5	6	5	5	6	5	3	5	4	6	5	4
$n\,C_{20}$	1	2	3	2	2	3	2	2	2	4	3	4	4
$n\,C_{21}$	3	4	8	4	4	6	4	3	4	4	5	4	3
$n\,C_{22}$	2	3	5	3	3	5	3	3	2	4	4	4	3
$n\,C_{23}$	6	8	13	7	8	9	6	5	9	5	7	4	3
$n\,C_{24}$	3	5	7	4	5	6	4	3	3	4	5	3	2
$n\,C_{25}$	17	21	26	18	18	19	17	13	17	7	16	5	4
$n\,C_{26}$	7	9	10	6	7	8	7	5	5	4	7	4	3
$n\,C_{27}$	59	67	66	50	53	50	58	35	44	13	41	8	6
$n\,C_{28}$	11	13	15	11	11	12	11	7	8	5	10	4	3
$n\,C_{29}$	86	95	100	78	82	80	86	59	59	16	65	10	8
$n\,C_{30}$	12	15	15	13	11	12	9	10	12	5	9	5	3
$n\,C_{31}$	93	105	99	80	84	129	91	165	65	31	87	19	12
$n\,C_{32}$	7	8	9	6	5	7	5	10	4	4	6	4	0
$n\,C_{33}$	63	71	58	48	51	88	53	96	37	21	60	14	9
$n\,C_{34}$	0	0	0	0	0	3	0	0	0	0	0	0	0
$n\,C_{35}$	13	15	12	10	9	18	12	20	0	9	15	5	0
5a-Androstane (IS)	124	148	106	131	119	65	95	50	98	43	80	43	102
Phytane	1	5	12	9	6	10	96	4	37	2	14	3	3
Phytene	1	3	2	5	5	6	15	3	13	0	5	0	0
Moretene	93	126	91	107	88	31	34	8	65	0	31	0	0

App. G: Quantification of neutral (steroidal and *n*-alkanol) compounds (µg/g TOC) from samples of the high-resolution study section of manuscript 2.

Compound / Sample	G003536	G003535	G003534	G003533	G003532	G003531	G003530	G003529	G003528	G003527	G003526	G003525	G003524
1-Hexadecanol	0	6	9	9	11	9	6	4	7	11	8	8	0
1-Heptadecanol	0	0	3	4	3	3	0	1	4	0	3	0	1
3,7,11,15-Tetramethyl-hexadecanol (Phytanol)	0	4	6	11	25	38	47	15	14	4	21	0	0
1-Octadecanol	4	6	11	7	9	9	10	8	11	36	15	25	62
3,7,11,15-Tetramethyl-hexadecenol (Phytol)	2	12	11	26	42	15	14	4	30	0	22	0	0
Androstanone (IS)	18	19	18	19	19	26	35	16	25	68	29	69	162
1-Icosanol	6	23	45	31	24	12	3	8	5	4	5	1	2
4,8,12,16-Tetramethylhepta-decan-4-olide (γ-lactone)	0	2	0	4	5	3	4	2	6	0	2	0	0
1-Henicosanol	0	6	11	8	7	4	0	2	2	2	2	1	1
1-Docosanol	49	109	161	114	93	69	14	46	30	26	38	4	7
1-Tricosanol	4	7	9	6	6	7	1	4	3	5	4	0	0
1-Tetracosanol	17	40	47	34	34	40	11	27	19	29	22	5	7
1-Pentacosanol	3	8	5	5	5	8	3	6	3	9	5	1	0
1-Hexacosanol	56	98	71	72	76	79	37	44	33	59	48	12	16
1-Heptacosanol	12	21	11	11	10	15	6	7	5	12	0	3	6
5β-Cholestan-3β-ol	32	48	13	18	10	16	6	5	19	3	12	0	0
Cholestanol	0	0	0	0	0	4	2	0	4	3	2	0	0
5β-Cholestan-3α-ol	10	15	0	3	0	7	0	3	7	0	6	0	0
1-Octacosanol	518	571	320	418	423	358	223	140	138	131	223	44	64
Cholest-5-en-3β-ol	43	104	34	43	17	22	4	5	22	9	14	4	0
5α(H)-Cholestan-3β-ol	82	110	48	61	49	50	16	17	47	16	41	4	0
Cholesta-dienol	55	103	0	19	0	4	5	0	10	0	4	0	0
24-Methyl-Cholesta-5,22-dienol (Brassicasterol)	37	71	73	45	0	0	0	0	0	0	0	0	0
1-Nonacosanol	71	55	21	28	22	24	14	8	0	10	11	3	0
C29 Stanol	93	78	48	66	49	53	21	16	24	6	29	0	0
24-Methylcholest-5-en-3β-ol	186	263	75	86	49	0	0	0	45	4	15	0	0
24Methyl-5β(H)-cholestan-3α-ol	0	0	0	0	0	18	11	13	23	8	0	0	0
24-Methyl-5α(H)-cholestan-3β-ol	0	78	43	60	58	42	27	16	44	10	30	3	0
Stigmasterol (24-Ethylcholesta-5,22-dien-3β-ol)	228	377	85	140	75	55	32	25	85	14	39	0	0
C29 Stenol (coelution)	173	141	92	110	94	52	40	19	100	10	35	0	0
1-Triacontanol	767	729	455	616	626	588	367	169	177	114	333	55	43

Compound / Sample	G003536	G003535	G003534	G003533	G003532	G003531	G003530	G003529	G003528	G003527	G003526	G003525	G003524
Ergost-7ene-3β-ol (24-Methyl-cholest-7-enol) (coelution)	374	582	154	234	137	57	23	27	82	6	46	0	0
β-Sitosterol (24-Ethyl-cholest-5-en-3β-ol)	48	93	76	78	39	46	20	32	16	40	29	13	0
24-Ethylcholesta-7,22-dien-3β-ol (Stigmast-7,22-dien-3β-ol)	816	1040	135	295	237	56	33	38	117	4	42	0	0
24-Ethylcholestan-5a(H)-3β-ol	170	148	87	113	115	101	49	42	0	41	58	11	0
unsaturated Dinosterol	0	0	34	69	64	0	0	0	226	12	22	0	0
Dinosterol	0	0	0	98	79	25	11	0	459	7	37	0	0
β-Amyrine (Olean-12en-3β-ol)	0	0	0	0	0	24	6	44	0	5	16	0	0
17α-hopanol and/or Lupenol (?)	151	71	151	0	0	0	0	0	0	0	0	0	0
C30 Stenol	80	0	104	0	0	0	11	16	0	0	0	0	0
1-Hentriacontanol	0	0	0	0	0	0	0	0	0	0	0	2	0
Hentriacontanol + 24-Ethyl-Cholest-7-en-3β-ol (coelution)	581	705	161	301	271	103	57	37	184	12	75	0	0
α-Amyrin (Urs-12en-3β-ol) + Lupeol (Lup-20(29)en-3β-ol) (coelution)	0	37	57	39	43	77	39	179	27	17	41	0	0
24-Methyl-Cycloartenol	458	398	154	156	123	33	38	15	67	3	21	0	0
1-Dotriacontanol	256	262	104	142	133	195	56	86	46	82	88	25	23
Tetrahymanol	7750	6160	5116	4698	4321	824	248	381	2636	6	1277	21	183
Gammaceran-3-one	588	654	373	565	450	59	21	28	264	2	73	0	6
1-Tetratriacontanol	0	0	8	0	0	33	9	14	8	48	21	14	6
Σ C27 Sterols	168	276	95	126	75	100	27	29	99	31	75	8	0
Σ C28 Sterols	597	995	344	425	243	117	61	56	194	28	92	3	0
Σ C29 Sterols	2165	2685	683	1123	878	469	258	208	536	127	312	24	0
Σ Sterols	2930	3956	1122	1673	1197	686	346	293	829	186	479	36	0
Σ Hopanols	8126	6267	5358	4905	4506	995	333	616	3349	46	1393	21	183
Σ terr. Sterols	277	507	218	257	156	202	97	281	128	76	126	13	0
Σ Tetrahymanol+Gammaceran-3-one	8338	6814	5489	5263	4771	883	268	409	2900	8	1349	21	190
Σ C_{28} + C_{30} alkanol	1285	1301	775	1033	1049	946	590	309	315	246	556	99	107
Σ *n*-alkanols	1763	1942	1292	1503	1484	1455	759	572	491	581	825	202	239
Ratio Tetrahy+G/*n*-alkanols	5	4	4	4	3	1	0	1	6	0	2	0	1
Me $C_{37:3}$ alkenone	0	0	0	0	0	35	0	78	0	0	21	0	0
Et $C_{38:3}$ alkenone	0	0	0	0	0	249	0	409	0	0	121	0	0
Et $C_{38:2}$ alkenone	0	0	0	0	0	91	0	434	0	0	55	0	0

Appendix H

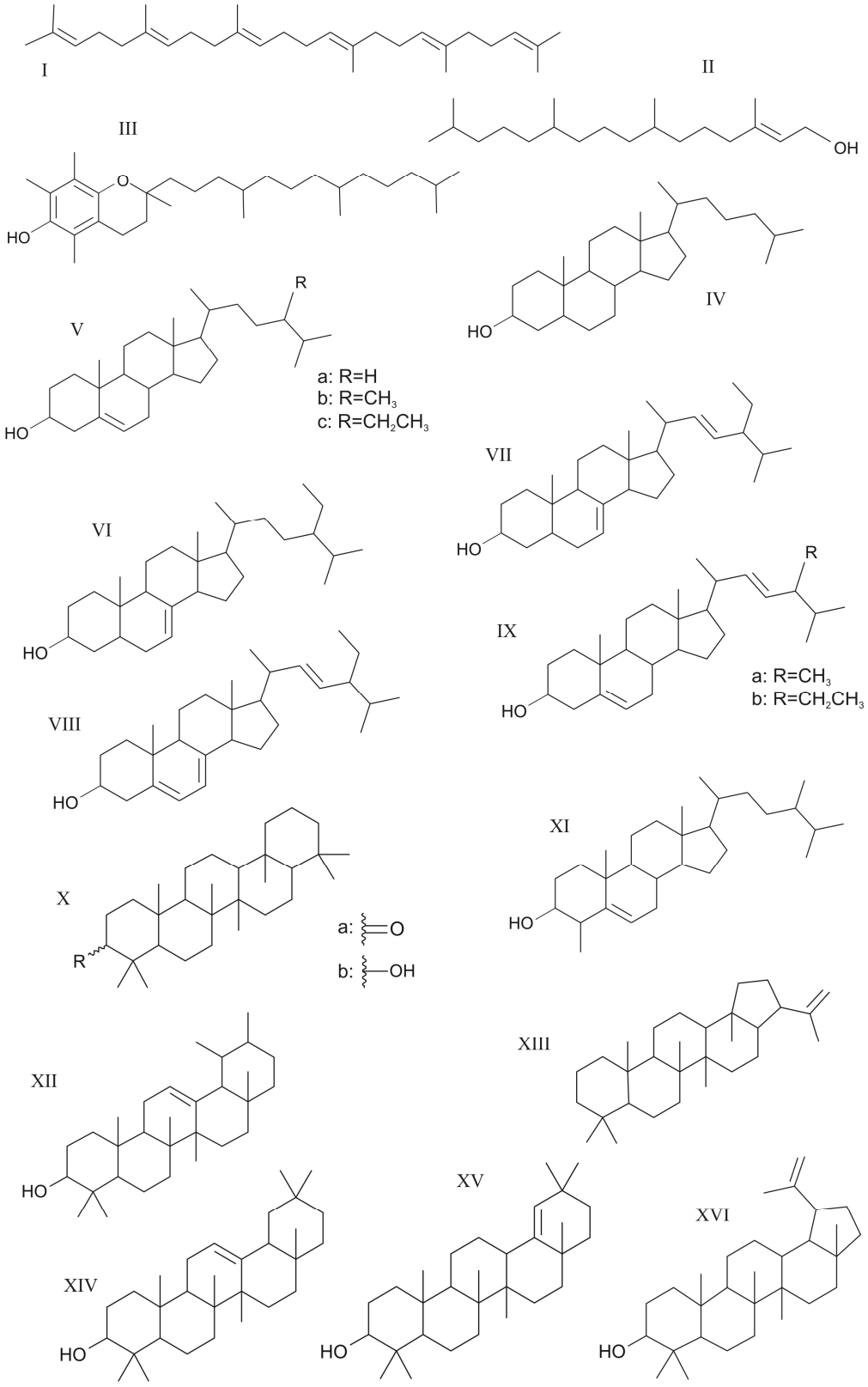

App. H: Structures of steroidal and terpenoidal neutral compounds found in organisms and sediments from the Tswaing impact crater.